Synthesis and Properties of *tert*-butyl Trioxatriangulene Superstructures: Solid State and Intermolecular Dynamics

Dissertation

zur

Erlangung der naturwissenschaftlichen Doktorwürde
(Dr. sc. nat.)

vorgelegt der

Mathematisch-naturwissenschaftlichen Fakultät

der

Universität Zürich

von

James R. Noyes

aus U.S.A.

Promotionskomitee:

Prof. Dr. Jay S. Siegel (Vorsitz)

Prof. Dr. John A. Robinson

Prof. Dr. Stefan Bienz

Zürich, 2009

Table of Contents

List of Figures:

List of Tables:

List of Schemes:

Acknowledgements

Prof. Dr. Jay S. Siegel

Prof. Dr. Kim K. Baldridge

Prof. Dr. John A. Robinson

Prof. Dr. Stefan Bienz

PD Dr. Anthony Linden

PD Dr. Nathaniel S. Finney

Prof. Dr. Hans-Beat Bürgi

UNIZH NMR Service

UNIZH MS Service

Fabia Gozzo and Antonio Cervellino at the Paul Scherrer Institut

All Siegel & Baldridge Group members past and present

JAMES R. NOYES

Institute of Organic Chemistry, Universität Zürich, Zürich, Switzerland
Winterthurerstrasse 190, CH-8057
jrnoyes@oci.uzh.ch

Education:

Universität Zürich, Zürich, Switzerland
Ph.D. Organic Chemistry, 2009
Advisor: Prof. Dr. Jay S. Siegel
Thesis title: "Synthesis and Properties of *tert*-butyl Trioxatriangulene Superstructures"
Illinois State University, Normal, Illinois, U.S.A.
M.S. Chemistry, 2002
Advisor: Prof. Dr. Cheryl Stevenson
Thesis title: "Condensation Products of C_{60} Anion Radicals and a Route to Endohedral Fullerenes"
Iowa State University, Ames, Iowa, U.S.A.
B.S. Zoology (emphasis in molecular biology), 1993

Professional Experience:

Research Assistant, Universität Zürich, Organisch-chemisches Institüt, 2003-2008
- Coordinated and executed organic research experiments on a variety of molecular systems: Prof. Dr. Jay S. Siegel, Advisor.

Laboratory Assistant, Universität Zürich, Organisch-chemisches Institüt, 2004-2006
- Coordinated laboratory materials, conducted lab sessions, and evaluated lab reports for general chemistry laboratories for 1 year: Prof. Dr. Andreas J. Rippert and Dr. Khaled AbouHadeed, Instructors.

Research Assistant, Illinois State University, Normal, Illinois, 2000-2002
- Coordinated and executed physical organic research experiments on a variety of molecular systems: Prof. Dr. Cheryl Stevenson, Advisor.

Laboratory Assistant, Illinois State University, Normal, Illinois, 1999-2002
- Coordinated laboratory materials, conducted lab sessions, and evaluated lab reports for physical and general chemistry laboratories for 2.5 years: Prof. Dr. Jean Standard and Prof. Dr. Jim Webb, Instructors.

Secondary Education Science Teacher, Peace Corps, Ghana, West Africa, 1995-1997
- Instructed 75 students in the core and elective portions of the national science curriculum including Biology, Chemistry, and Physics for 30 periods per week for six school terms attaining a 30% pass rate from 0%.

Research Assistant, Iowa State University, Ames, Iowa, 1989-1991
- Coordinated and developed neurobiological experiments as part of a National Institute of Health grant to study aspects of neuron death: Prof. Dr. Dennis Emery, Advisor.

Publications:

Noyes, J.R.; Linden, A.; Siegel J.S. "Synthesis and Properties of *tert*-butyl Trioxatriangulene Suprastructures", manuscript in preparation.

Noyes, J.R.; Linden, A.; Siegel J.S. "Solid-state Rotational Dynamics of a Phenylene Rotator in a Crystalline *tert*-butyl Trioxatriangulene Assembly", manuscript in preparation.

Noyes, J.R.; Linden, A.; Siegel J.S. "Crystal Design: Defined Trioxatriangulene Bridges Direct Crystal Order of *tert*-butyl Trioxatriangulene Assemblies", manuscript in preparation.

Stevenson, C.D.; Noyes, J.R.; Reiter, R.C. "Condensation Products from the Anionic Radicals of C_{60} and the Common Solvent: Hexamethylphosphoramide" *J. Phys. Chem. B,* **2002**, *106*, 10369-10373.

Publications:

Stevenson, C.D.; Noyes, J.R.; Reiter, R.C. "Mass Spectral Evidence of Alkali Metal Insertion into C_{60}-Cyclooctatetraene Complexes: $M^{+}@C_{60}$-$C_8H_8^{\cdot 3-}$" *J. Org. Chem.* **2002**, *67*, 8648-8652.

Stevenson, C.D.; Noyes, J.R.; Reiter, R.C. "Endohedral Alkali Metal Fullerene Complexes" *J. Am. Chem. Soc.* **2000**, *122,* 12905-12906.

Presentations:

"Synthesis and Properties of Trioxatricornan Suprastructures"; Noyes, J.R. Linden, A. and Siegel, J.S.; poster presented at the 2007 Gordon Research Conference on Physical Organic Chemistry – Summer 2007 – Plymouth, New Hampshire, U.S.A.

"Trioxatriangulene Derivatives as Building Blocks"; Noyes, J.R. Linden, A. and Siegel, J.S.; oral presentation given at the Swiss Chemical Society Meeting – Fall 2006 – Zürich, Switzerland

"Trioxatricornan Derivatives: Reactivity and Building Blocks" and "Synthesis and Properties of Trioxatricornan Suprastructures"; Noyes, J.R. Linden, A. and Siegel, J.S.; poster presented at the Dorothy Crowfoot Hodgkin Symposium – Spring 2006 and 2007 – Zürich, Switzerland

"Synthesis and Dynamics of Triangulene Derivatives"; Noyes, J.R. and Siegel, J.S.; oral presentation given at the UNIZH Organish-chemisches Institüt Doktorandentag – Summer 2005 – Zürich, Switzerland

"Endohedral Alkali Metal Fullerene Complexes"; Noyes, J.R. Reiter, R.C. and Stevenson, C.D.; poster presented at the ISU/IWU Chapter of Sigma Xi Initiation Banquet – Spring 2001 – Normal, Illinois, U.S.A.

"Endohedral Alkali Metal Fullerene Complexes"; Noyes, J.R. Reiter, R.C. and Stevenson, C.D.; oral presentation given at the Illinois State University Graduate Research Symposium – Spring 2001 – Normal, Illinois, U.S.A.

"Endohedral Alkali Metal Fullerene Complexes"; Noyes, J.R. Reiter, R.C. and Stevenson, C.D.; poster presented at the AAAS Annual Meeting and Science Innovation Exposition – Spring 2001 – San Francisco, California, U.S.A.

Awards:

Abbott Laboratories Research Fellowship – 2001

Graduate Student Research and Professional Advancement Awards – Illinois State University – 2001

John B. Balinsky Award for excellence in undergraduate research – Department of Zoology, Iowa State University – 1991

Professional Affiliations:

American Chemical Society

American Association for the Advancement of Science

Sigma Xi – Honorary Scientific Research Society – 2001

Swiss Chemical Society

ABSTRACT OF THE DISSERTATION

Synthesis and Properties of *tert*-butyl Trioxatriangulene Superstructures:

Solid State and Intermolecular Dynamics

by

James R. Noyes

Doctor of Philosophy in Chemistry

University of Zürich, 2009

Prof. Dr. Jay S. Siegel, Chair

The structural transmission of molecular components to specified solid-state and dynamic characteristics is growing area of research. Supramolecular chemistry is the study of molecular systems and the intermolecular interactions in the systems. Supramolecular chemistry also requires the availability of modifiable building blocks that can be obtained in large quantities. This dissertation is divided into four areas: 1) The synthesis of *tert*-butyl trioxatriangulene building blocks. 2) The synthesis of the *tert*-butyl trioxatriangulene superstructures. 3) The solid-state characteristics of the *tert*-butyl trioxatriangulene superstructures. 4) The physical properties of the *tert*-butyl trioxatriangulene superstructures.

The triangulene skeleton serves as an attractive base molecule for this investigation. Many triangulene derivatives exist and the *tert*-butyl trioxatriangulene derivative will be used in this investigation. The polycyclic aromatic *tert*-butyl trioxatriangulene **3.32** (TOTA) is utilized as the base molecule is this project due to the facile modification at the central position, large surface area and solubility. Starting with the well-known *tert*-butyl trioxatriangulene cation, six molecular building blocks were synthesized that could be further used to generate larger superstructures.

The prediction of solid-state properties has been an important area of research. A series of seven superstructures were synthesized to investigate the solid-state properties. The series is unique

because the relative topology is constant with a *tert*-butyl trioxatriangulene moiety at each end of the superstructure connected by a linear, molecular axis. The variation of the series of *tert*-butyl trioxatriangulene structures is in the length of the central axis that varies by approximately 400 %, whilst the molecular weight only varies by 20 %.

Various physical aspects of the *tert*-butyl trioxatriangulene superstutures were investigated. Single crystals were obtained for two of the *tert*-butyl trioxatriangulene species. In the case of **4.2** and **4.3**, with approximately similar axis lengths, it was found that both species crystallized in a cubic space group. A complete powder diffraction analysis of the *tert*-butyl trioxatriangulene series was also attempted with a synchrotron radiation source.

Dynamic investigations are another component of this discussion. The *tert*-butyl trioxatriangulene species with a single phenyl unit **4.2**, **4.4** and **4.6** were of interest to explore rotational dynamics of the central phenyl ring. The original synthetic methodology was established to create a void that may allow "free" rotation of the central phenyl ring. Thermal ellipsoid analysis of the single crystal structure of **4.2** determined a barrier to rotation for the central phenyl ring to be less than 1 kcal/mol. This dynamic result is supported by preliminary evidence from solid-state ^{2}H NMR experiments.

Photophysical measurements were also done with the *tert*-butyl trioxatriangulene series. Incorporation of well-known fluorophores into molecular superstructures is an important area of research. In general, as the axis length of the series increased there was a *red-shift* in the absorption and emission spectra. Also, the incorporation of well-known fluorophores resulted in the expected characteristic spectra of the fluorophore in the *tert*-butyl trioxatriangulene scaffold. The photophysical dynamics of the *tert*-butyl trioxatriangulene series were also investigated in terms of quantum yields and lifetimes.

ZUSAMMENFASSUNG

Synthese und Eigenschaften von *tert*-butyl Trioxatriangulen Derivaten:
Festkörper- und Intermolekulare Dynamiken

von

James Noyes

Dr. sc. nat.

Universität Zürich, 2009

Prof. Dr. Jay S. Siegel, Vorsitz

Die strukturelle Übertragung von molekularen Komponenten zu spezifischen Festphasen und dynamischen Charakteristiken ist ein wachsender Bereich der Forschung. Die Supramolekulare Chemie ist die Untersuchung der molekularen Systeme und der intermolekularen Wechselwirkungen in den Systemen. Außerdem benötigt die Supramolekulare Chemie auch die Verfügbarkeit von modifizierbaren Bausteinen, die in großen Mengen erhalten werden können. Diese Dissertation ist unterteilt in vier Bereiche: 1) Die Synthese von *tert*-butyl Trioxatriangulen-Bausteinen. 2) Die Synthese von *tert*-butyl Trioxatriangulen Superstrukturen. 3) Die Festphasen-Eigenschaften der *tert*-butyl Trioxatriangulen Superstrukturen. 4) Physikalische Eigenschaften der *tert*-butyl Trioxatriangulen Superstrukturen.

Das Triangulen Skelett dient als attraktives Basismolekül für diese Untersuchungen. Es existieren viele Trioxatriangulen Derivate und das *tert*-butyl Trioxatriangulen Derivat wird für diese Untersuchungen verwendet. Das polyzyklische, aromatische *tert*-butyl Trioxatriangulen **3.32** (TOTA) wird als Basismolekül in diesem Projekt eingesetzt, aufgrund seiner einfachen Modifikation an der zentralen Position, der großen Oberfläche und der Löslichkeit. Beginnend mit dem gut bekannten *tert*-butyl Trioxatriangulen Kation wurden sechs molekulare Bausteine synthetisiert, die dann zu größeren Superstrukturen weiter verwendet werden konnten.

Die Vorhersage der Festphasen-Eigenschaften ist ein wichtiges Gebiet in der Forschung geworden. Eine Serie von sieben Superstrukturen wurde synthetisiert um die Festphasen-Eigenschaften zu untersuchen. Diese Serie ist einmalig, da die relative Topologie konstant mit einem *tert*-butyl Trioxatriangulen Rest an jedem Ende der Superstrukturen verbunden durch eine lineare molekulare Achse ist. Die Variation der Serien der *tert*-butyl Trioxatriangulen-Strukturen ist die Länge der zentralen Achse, die dabei ungefähr 400% variiert bei einer Massenvariation von nur 20%.

Verschiedenartige physikalische Aspekte der *tert*-butyl Trioxatriangulen Superstrukturen wurden untersucht. Ein-Kristalle wurden für zwei der *tert*-butyl Trioxatriangulen Spezies erhalten. In Fall von **4.2** und **4.3**, mit einer ungefähr gleichen Achsen-Länge, wurde gefunden, dass beide Spezies in einer kubischen Raumgruppe kristallisieren. Es wurde auch eine komplette Debye-Scherrer (Pulveraufnahme) Analyse der *tert*-butyl Trioxatriangulen-Serie mit einer Synchrotron-Strahlen-Quelle durchgeführt.

Dynamische Untersuchungen sind ein weiterer Teil dieser Erörterung. Die *tert*-butyl Trioxatriangulen-Spezies mit einer einzelnen Phenyl-Einheit **4.2**, **4.4** und **4.6** waren von Interesse um die Rotation-Dynamik des zentralen Phenylringes zu ermitteln. Die original-synthetische Methodik wurde eingeführt um eine Fehlstelle zu kreieren, die möglicherweise ein Verfolgen der „freien“ Rotation um den zentralen Phenylring erlaubt. Thermal-ellipsoid-Analysen der Einkristallstrukturen von **4.2** ergaben eine Rotationsbarriere für den zentralen Phenylring von weniger als 1 kcal/mol. Dieses dynamische Ergebnis wird unterstützt durch den einleitenden Beleg von den Festphasen ^{2}H-NMR Experimenten.

Photophysikalische Messungen wurden ebenfalls mit *tert*-butyl Trioxatriangulen-Serien gemacht. In Verbindung mit bekannten Fluorophoren in die molekulare Superstruktur hinein ist auch ein wichtiges Gebiet der Forschung. Im Allgemeinen, wenn die Achsenlänge der Serien anstieg gab es eine Rotverschiebung im Absorptions- und Emissionsspektren. Auch in Verbindung

mit bekannten Fluorophoren resultierten die erwarteten charakteristischen Spektren der Fluorophoren in dem *tert*-butyl Trioxatriangulen-Gerüst. Die photophysikalischen Dynamiken der *tert*-butyl Trioxatriangulen-Serien wurden ebenfalls in Hinblick auf Quantität und Lebensdauer ermittelt.

Chapter 1. Organic Molecules in the Condensed Phase:

Transmission of Molecular Structure to Long-range Order

1.1 Overview

For more than the past 100 years, chemical research has principally been focused on synthetic methodology and building ever more complex molecules, some mimicking the most complex structures found in nature. In the last quarter of the twentieth century there has been a new focus in chemical research. This new focus uses current synthetic methodology to create chemical structures that aid in the understanding of noncovalent molecular interactions, often referred to as supramolecular chemistry.[1]

Noncovalent interactions, attractive and repulsive, play a significant role in determining molecular organization, ranging from the complex three-dimensional folding of large biological molecules to the binding geometry in host-guest complexes. Furthermore, many of the functional properties of molecules are a result of the molecular organization instilled by interactions of this type. Therefore, a fundamental understanding of noncovalent interactions is critical to identifying, predicting, and utilizing the relationship between structure and function (Figure 1.1).

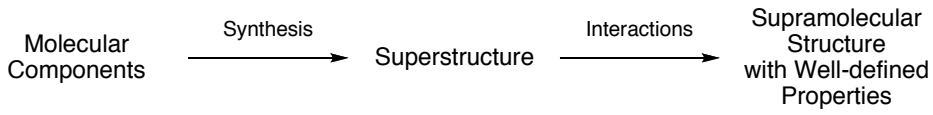

Figure 1.1 Schematic of molecular organization.

Attractive noncovalent interactions can be intermolecular or intramolecular, but are generally weaker than the covalent bonds commonly encountered in organic chemistry. Energetically, noncovalent interactions range from < 1 kcal/mol for dispersion forces to *ca*. 75 kcal/mol for ionic interactions (Table 1.1). Some of the prototypical examples of noncovalent interactions are ionic interactions, hydrogen bonding, dipole-dipole interactions, and dispersion forces.[2]

Table 1.1 Energies of Noncovalent Interactions

Interaction	Approximate Energy (kcal/mol)
Ion-ion	50 – 75
Ion-dipole	10 – 50
Dipole-dipole	< 1 – 10
Hydrogen bonding	< 1 – 30
π-π	< 1 – 10
van der Waals	< 1[a]

[a] Variable depending on molecular surface area

Ionic interactions are purely electrostatic interactions between two oppositely charged species, and are governed by Coulomb's Law (Equation 1.1).[3] In terms of

$$F = k\frac{Q_1 Q_2}{r^2} \quad (1.1)$$

atomic interactions, an ionic bond forms when the difference in electronegativity between the two atoms is large enough that one atom almost completely removes an electron from the other atom; however, there are no purely ionic bonds, as sharing of electrons always occurs to some extent. Ionic compounds generally have high melting and boiling points, due to the significant amount of energy required to overcome the interaction between the charged ions.

Whereas ionic bonding involves the electrostatic interaction between charged species, hydrogen bonding occurs between the partial positive charge (δ+) of a hydrogen atom and a highly electronegative atom (δ-). Hydrogen bonding is one of the most common and energetically significant of the weak interactions. It most frequently occurs when a hydrogen atom is bound to a strongly electronegative atom and another electronegative atom is present in the system. The single point interaction of the hydrogen bonds produces well-defined geometries.[4] The electrostatic forces between the donor hydrogen atom and the electronegative acceptor determine the magnitude of a hydrogen bond.[5]

Hydrogen bonding is responsible for the unique properties of water and also provides an intermolecular force that produces commonly occurring eight-membered

rings holding together adjacent base pair strands in the DNA double helix (Figure 1.2). In nature, hydrogen bonding produces selectivity and specificity in bioprocesses. This attractive force is commonly described with the notation X–H•••Y, where X and Y are the two electronegative atoms, both interacting with the electron deficient hydrogen atom. In comparison to hydrogen bonding, the other weak interactions are not nearly as well understood.

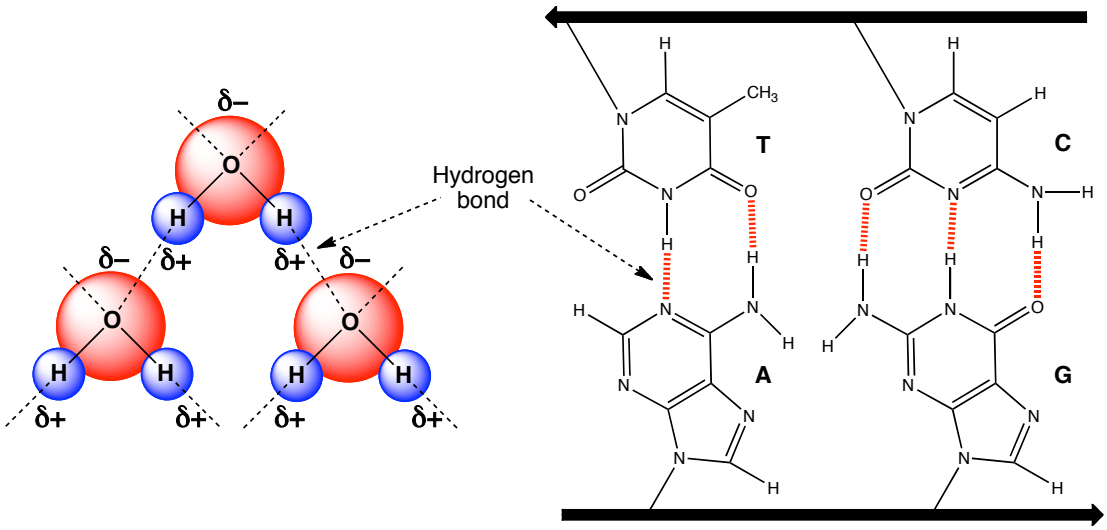

Figure 1.2 Illustration of hydrogen bonding between water molecules and DNA base pairs.

Dipole-dipole interactions occur between two molecules with permanent dipoles. They are similar to ionic interactions, but weaker in magnitude because only partial charges are involved. The difference between hydrogen bonding and dipole-dipole interactions is that, in hydrogen bonding, the hydrogen is partially transferred from one molecule to the other.[6]

Dispersion forces involve the interactions between transient dipoles. These interactions are generally weaker than dipole-dipole interactions or hydrogen bonding. Transient dipoles of this type can be induced by proximity to another dipole or can simply result from an instantaneous uneven distribution of electrons.

Dispersion forces become more significant in larger molecular systems due to their increased polarizability. Dispersion is the only attractive force between the noble gases, and is the reason they can be obtained in the condensed form.

One of the themes of this thesis is exploring noncovalent interactions, attractive and repulsive, of large, rigid molecular systems, in the solution phase and the solid phase. Interactions in these systems can involve a wide array of functional groups, multiple points of contact, and play a significant role in determining molecular geometries and molecular aggregations in the condensed forms.

1.1.1 Benzene in the Solid State: A Noncovalent Molecular Crystal

Benzene in the solid state offers the prototypical example of weak, noncovalent interactions and the transfer of the weak, noncovalent interactions to the supramolecular order. The regions of benzene directly above and below the plane of the ring have high electron densities. In contrast, the periphery of the ring is electron deficient, due to the polarized C–H bonds. The contrasting arrangement established a quadrupole in benzene (Figure 1.3).[7] This environment fits the criteria described above for noncovalent polar interactions, although the symmetry of benzene excludes the existence of a dipole.

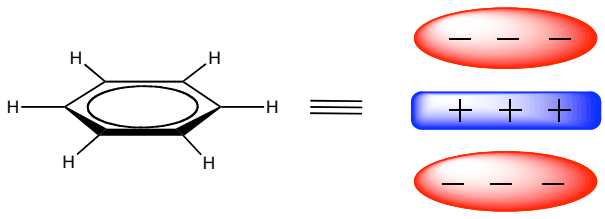

Figure 1.3 Schematic of the alignment of the quadrupole moment in benzene.

The herringbone structure of crystalline benzene, in which the electron deficient edge of one molecule is directed into the electron rich face of an adjacent one, provides evidence for the existence of this type of interaction in π systems (Figure 1.4).[8] The term used here to describe this intermolecular attraction is polar-π

interaction. The stacking motif in crystalline benzene not only enables favourable electrostatic interactions, but also deters repulsive face-to-face and edge-to-edge interactions. Similar investigations have found that the orientations of benzene in solution,[9,10] as well as in the gas phase,[11,12,13] are best modeled with polar-π and dispersion interactions.

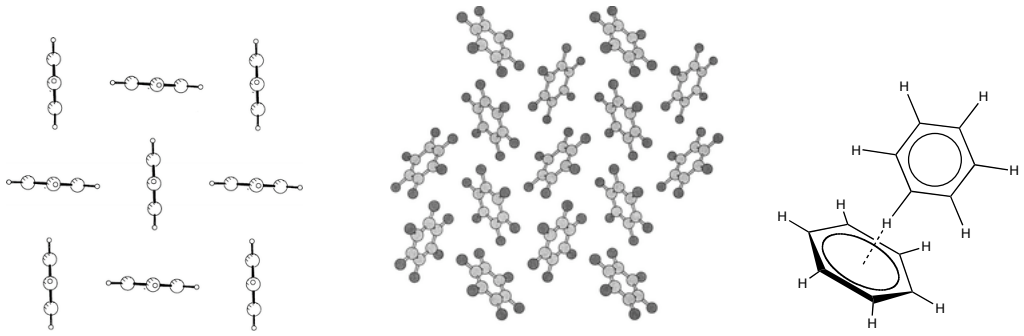

Figure 1.4 Section through the unit cell of the crystal structure of benzene by neutron diffraction at -135 °C and illustration of interaction.[14]

A similar molecular order is observed for larger flat polyaromatic systems such as naphthalene. The crystal structure of these aromatic systems is directed in part by the avoided repulsion of C–H•••H–C contacts, rather than the C–H•••π attraction.[15] Gavezzotti modeled this type of system and based on stack *versus* glide ratio[16] was able to make predictions about some aromatic hydrocarbons yet unknown.[17]

In 1960, Patrick and Prosser reported a 1:1 complex of benzene and hexafluorobenzene in the solid-state.[18] When equal amounts of the two liquids were combined at room temperature, a binary complex was formed as a solid. The interaction was originally attributed to charge-transfer, but no charge-transfer band was found in the UV spectrum. Neutron diffraction experiments showed the complex to consist of alternating layers of benzene and hexafluorobenzene (Figure 1.5).[19] X-

ray structures of other binary mixtures of hexafluorobenzene and methylated benzenes showed similar packing structures (Figure 1.6).[20]

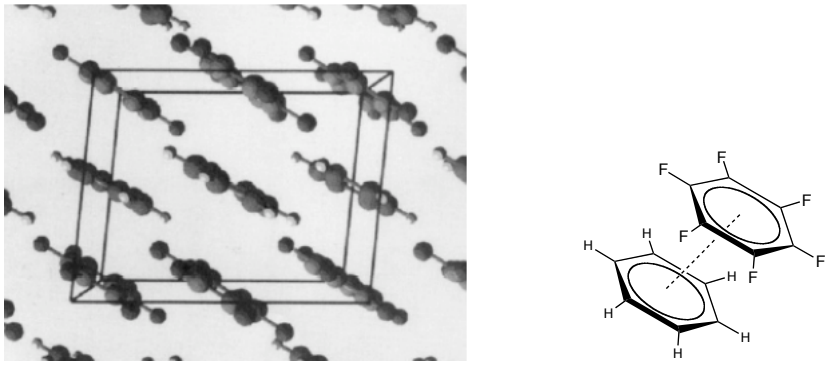

Figure 1.5 Section through the unit cell of solid C_6H_6/C_6F_6, at low temperature viewed along the *b* crystalline axis, as revealed by neutron and synchrotron diffraction experiments.[19]

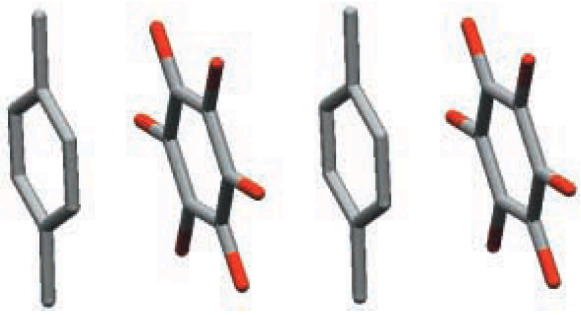

Figure 1.6 Illustration of the X-ray structure of solid *p*-xylene/hexafluorobenzene, indicating face-to-face stacking.[20]

The formation of alternating stacks of benzene and hexafluorbenzene was rationalized in terms of the quadrupole moment and van der Waals surfaces of the two molecules. In the case of benzene, the quadrupole moment is large and negative ($-$ 29.0 x 10^{-40} C m^2). The quadrupole moment of hexafluorobenzene is large and positive due to the high electronegativity of the fluorine atoms (31.7 x 10^{-40} C m^2).[21] The observed alignment of benzene and hexafluorobenzene maximizes the interaction energy because a positive quadrupole moment is found parallel and adjacent to a negative quadrupole moment (Figure 1.7). These interactions are also responsible for

tightly packed crystals as indicated by the high packing coefficient, 0.748. This arrangement enables favorable face-to-face stacking of the rings, and, in addition, the C–H bonds of benzene molecules are directed towards the C–F bonds of hexafluorobenzene molecules in the adjacent layers.

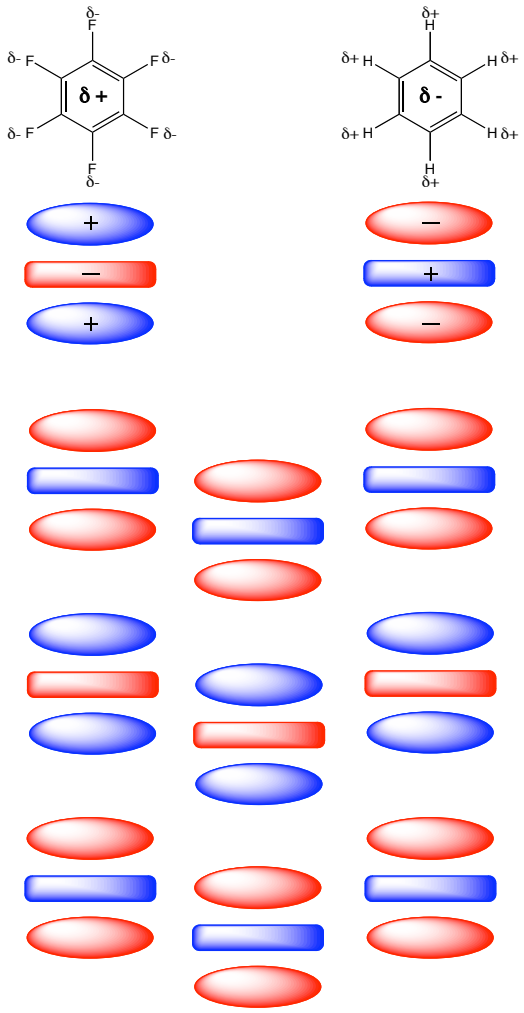

Figure 1.7 A schematic illustration of the alignment of the quadrupole moments in the binary mixture of benzene and hexafluorobenzene.[5]

A recent attempt to exploit the interactions between benzene and hexfluorobenzene in an extended network to generate mixed crystals was shown by Siegel and co-workers (Figure 1.8).[22] By using the phenyl/perfluorophenyl compounds they were able to control the order of the crystal structure through predictable noncovalent interactions.

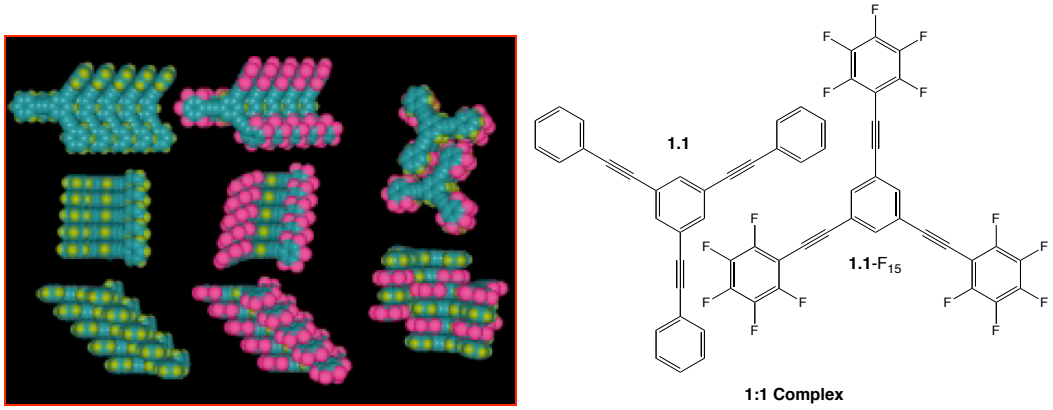

Figure 1.8 Three views of the *sym*-triphenethynylbenzene crystals and an illustration of the molecules: The first column is compound **1.1**, the second column is compound **1.1**-F_{15} and the third column is the 1:1 complex.

It has been demonstrated that polar-π interactions are manifested in the crystal structures of benzene and the binary mixture of benzene and hexafluorobenzene, plus extended systems with the phenyl/perfluorophenyl moieties. In these three cases, molecule orientations maximize favorable electrostatic interactions and minimize unfavorable ones, which is consistent with what was predicted.

1.2 Elementary Solid State Characteristics

1.2.1 Introduction

The design of solid-state material, or crystals, has many applications in chemistry, physics and emerging technologies. The assembly of a molecular crystal may be controlled by chemical and geometric factors. As demonstrated with the previous benzene examples, knowledge of the fundamental properties of a molecule, or system, may enable researchers to design and build molecular structures with the desired extended properties.

1.2.2 Basic Concepts of Crystallinity

Solids can be divided into two categories: crystalline solids and amorphous solids.[23] A crystalline solid possesses rigid and long-range order. In such a solid,

atoms, molecules, or groups of molecules occupy specific positions; the center of each of the positions is termed a lattice point. The crystal structure consists of a three dimensional geometrical order of these lattice points. Amorphous solids such as rubber, glass and plastic lack well-defined arrangement and long-range molecular order although they can posses a lattice order. A crystal's structure and symmetry play a role in determining many of its properties, such as, electronic band structure or optical properties.[24]

The fundamental repeating unit by translational displacement of the arrangement of atoms or molecules in a crystalline solid is the unit cell. Crystalline solids can be described in terms of seven types of primitive unit cells (Figure 1.9), which possess unique rotational symmetry elements (Table 1.2). The cubic unit cell is the simplest and highest symmetric unit cell. The geometry of the cubic unit cell is particularly simple, since all sides and all angles are equal, and has four threefold axes in a tetrahedral array. The location of the lattice points determines the type of unit cell that can be a simple cubic cell (scc), a body-centered cubic cell (bcc), or a face-centered cubic cell (fcc) (Figure 1.9).

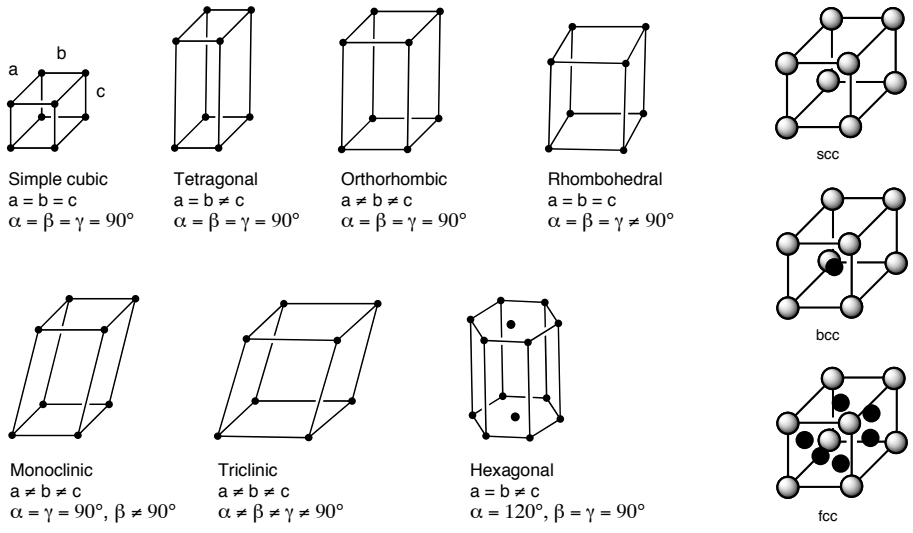

Figure 1.9 The seven types of unit cells and the three types of cubic cells. Angle α is defined by edges *b* and *c*, angle β by edges *a* and *c*, and angle γ by edges *a* and *b*.

Table 1.2 Seven Crystal Systems and Symmetries

System	Essential Symmetries
Triclinic	None
Monoclinic	One C_2 axis
Orthorhombic	Three perpendicular C_2 axes
Rhombohedral	One C_3 axis
Tetragonal	One C_4 axis
Hexagonal	One C_6 axis
Cubic	Four C_3 axes in a tetrahedral arrangement

If the apex of the cell represents an atom or molecule, the volume can be appreciable larger and the atom or molecule is in direct contact with it neighbors. The forces responsible for the stability of any crystal can be attractive ionic forces, covalent bonds, van der Waals forces, hydrogen bonds, or some combination of these forces.

The packing coefficient, or percentage of the unit cell space occupied by the molecular sphere, is an important crystal property (Equation 1.2).[25] Furthermore, the ordered intermolecular arrangement determines the density of the crystal and molecules in the solid state tend to maximize the space in the unit cell.

$$Packing\,coefficient = \frac{Molecular\,Volume\,inside\,the\,unit\,cell}{Volume\,of\ the\,unit\,cell} x100\% \qquad (1.2)$$

The types of attractive forces that hold the component atoms or molecules together determine the structure and properties of crystals. Crystals are classified in one of four types: ionic, covalent, molecular or metallic.[26]

Ionic crystals have two important factors: the charges on the species present and the difference in radii between anions and cations. For example, the prototypical example of this crystal is an alkali metal halide crystal, *e.g.* NaCl. In this case, the number of anions surrounding a cation must equal the number of cations surrounding an anion in order to maximize attraction and minimize repulsion.

In covalent crystals, atoms are held together entirely by covalent bonds. Covalent bonds in a definite spatial orientation link atoms in a network extending throughout the crystal. The stereochemical demand of valence overrides the problem of packing spheres, as in ionic solids, and elaborated and extensive structures may be formed. Two well-known examples are the two allotropes of carbon: graphite and diamond.

The structure of diamond is based on a face-centered cubic lattice. There are eight carbons atoms at the corners of the cube, six carbon atoms in the face centers, and four more carbons within the unit cell. Each tetrahedral sp^3-hybridized carbon atom is bonded to four other atoms (Figure 1.10). The strong covalent bonds in three dimensions contribute to diamond's unusual hardness. In graphite, carbon atoms are arranged in six-membered rings (Figure 1.10). Each atom is covalently bonded to three other atoms. The layers are held together by the weak van der Waals forces. The covalent bonds in graphite account for its hardness; however, because the layers can slide over one another, graphite is slippery to touch and often used as a lubricant.

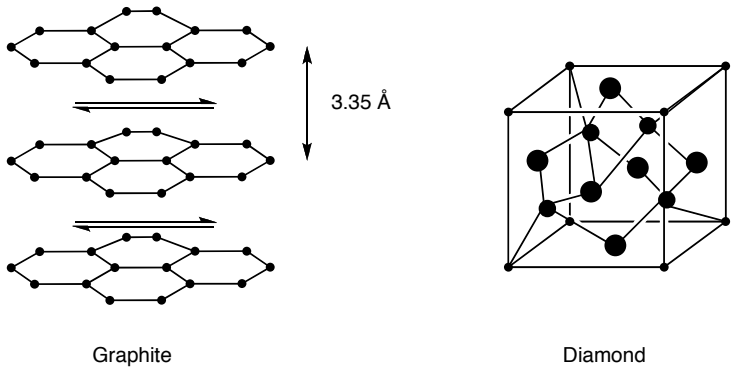

Figure 1.10 Two allotropes of carbon: Graphite sheets and cubic lattice of diamond.

In a molecular crystal, molecules occupy lattice points and the attractive forces between them are principally van der Waals forces and/or hydrogen bonding. The observed crystal structure is nature's solution to the problem of condensing

objects of various shapes into an aggregate of minimum energy. Predicting the structure is very difficult and rarely possible due to the many factors. In solid I_2 there are only dispersion forces, whereas, in solid SO_2, the predominant attractive forces are dipole-dipole interactions. Intermolecular hydrogen bonding is mainly responsible for maintaining the three-dimensional ice lattice. In general, molecules in molecular crystals are packed together as closely as their size and shape allow. Because van der Waals forces and hydrogen bonding are generally weak, the stability of molecular crystals is considerably lower than that of ionic and covalent crystals.

Kitaigorodskii was one of the first to investigate molecular packing in the solid state. In his Principle of Close Packing[27] he stated the fact that organic molecules in crystals are closely packed and tend to fill space as tightly as possible. As tightly as possible may be quantified by the packing coefficient of molecular crystals being 0.7 – 0.8 and is achieved when the "bumps" of one molecule fit into the "hollows" of the adjacent molecule: contact maximized and volume per molecule minimized (Figure 1.11).

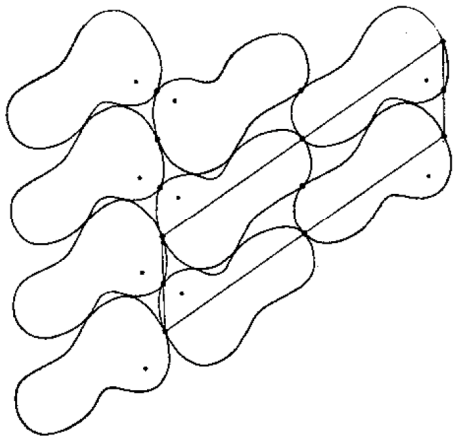

Figure 1.11 Kitaigorskii's illustration of the Principle of Close Packing.

The last type of crystal is the metallic crystals and is the simplest to consider since an atom of the same metal occupies every lattice point in a crystal. In most cases, metallic crystals are body-centered cubic, face-centered cubic, or hexagonal

close packed. In metals, the bonding electrons are highly delocalized over the entire crystal. The cohesive force of resulting from delocalization is responsible for the strength of metals plus accounts for the fact that they are good conductors of heat and electricity.

1.3 Encoding the Solid State in Hydrogen Bonding Networks

1.3.1 Introduction

The hydrogen bond plays a key role in biology, physics and chemistry. This weak interaction is also partly responsible for inspiring an area of solid-state research. Often referred to as crystal engineering, it is the design and synthesis of molecular solid-state structures with desired properties, based on an understanding and exploitation of intermolecular interactions. The stability of the crystal results from a balance between attractive and repulsive forces, and major structural consequences sometimes result from minor differences in total energy.

The two main strategies currently in use for crystal engineering are based on hydrogen bonding[28] and coordination complexation.[29] These may be described with key concepts such as the supramolecular synthon and the secondary building unit. The supramolecular synthons, defined by Desiraju,[30] are "structural units within supermolecules that can be formed and/or assembled by known or conceivable synthetic operations involving intermolecular interactions". Hydrogen bonding networks provide one of the strongest noncovalent examples in the design of supramolecular architectures, or solid-state materials (Figure 1.12).

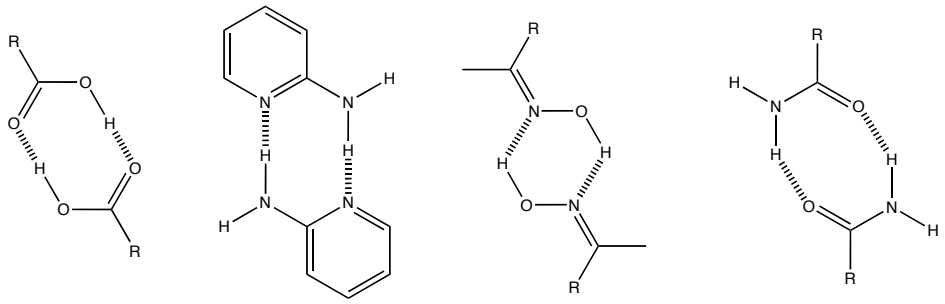

Figure 1.12 Some common examples of self-complementary hydrogen bonding in the solid state.

1.3.2 Intermolecular Interactions in the Solid State: Hydrogen Bonding

As the field of crystallography rapidly solved many more structures, which are available through the Cambridge Structural Database (CSD),[31] researchers began to observe clearly intermolecular interactions, such as hydrogen bonding, in the crystal lattice. The growing CSD led to the obvious interest in describing and engineering these interactions into the supramolecular structures.

In the solid state, hydrogen bond patterns are usually well defined and often involve infinite chains or arrays. Hydrogen bond interactions in organized systems may be utilized in the following manner: (1) the organization of reactive molecules in solid state, (2) the design of polar crystals, the design of molecular handles for chiral resolution by crystallization, (3) the self-assembly of supramolecular species, (4) the organization of molecules for biomimetic chemistry, (5) the formation of molecular films composed of synthetic layered structures.

The chemical groups that participate in hydrogen bonds are given in Table 1.3, with the ability as a donor or acceptor decreasing down the table and energy for the hydrogen bond ranging from *ca*. 20 kcal/mol to 1 kcal/mol.[32] The X•••A and H•••A distance are generally less than the sum of the van der Waals radii, Table 1.4.[33]

Table 1.3 Chemical Functional Groups in Hydrogen Bonds

Donors	Acceptors
O — H	O⋯P
O — H	O═C
N — H	O═C
O — H	O — H
C — H	O⋯C

Table 1.4 Experimentally Observed XH•••A Hydrogen Bond Distances

Type of bond	H•••A distances (Å)
OH•••O	1.44 – 2.10
NH•••O=C	1.58 – 2.05
NH•••O	1.60 – 2.40
NH•••N	1.73 – 2.23

With regard to structural correlation of the hydrogen bond, the points discussed here will be on the order of molecular packing, the role of hydrogen bonding in molecular assemblies, and the patterns and motifs of hydrogen bonds. The general consequences of hydrogen bonding in packing patterns rather than the specific packing geometries will be the focus of this section.

1.3.3 C–H•••O and C–H•••N Interactions in Molecular Packing

Representative crystal structures and patterns of C–H•••O,N interactions have been examined with proton donors in three different hybridization states that include C(*sp*) –H, C(sp^2) –H, and C(sp^3) –H. The acetylenic C≡C–H•••O interaction is the first example that has been established in a variety of crystal structures.[34] For example, the crystal structure of *o*-bromo-benzoylacetylene shows C≡C–H•••O contacts in which the molecules are interlinked by twofold screw symmetry (Figure 1.13).

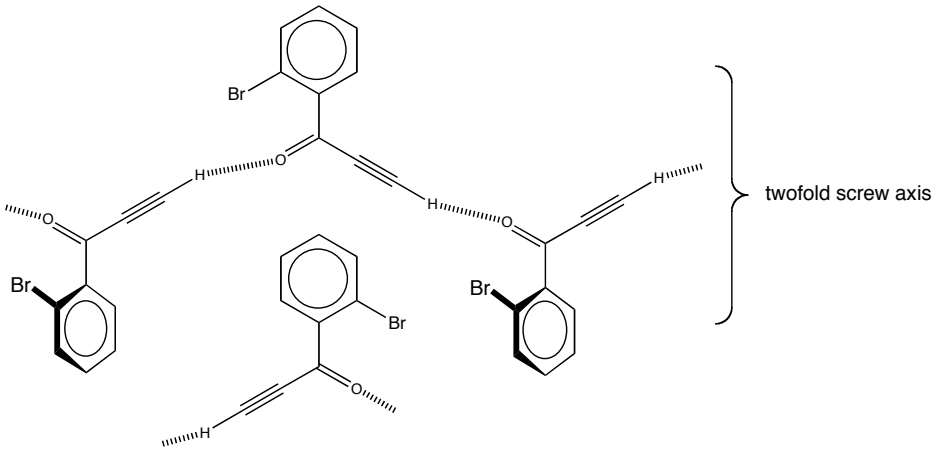

Figure 1.13 Illustrated molecular packing for *o*-bromo-benzoylacetylene.

The crystal packing of quinones and carboxylic acids have been described in terms of C(sp^2)–H•••O interactions, with each molecule participating in several C–H•••O interactions. The crystal structure of 1,4-benzoquinone incorporates a dimer motif, which through further C–H•••O contacts along a translational axis, leading to a ribbon.[35] Additional C–H•••O contacts of 3.4 Å in benzoquinone are formed across twofold screw axes in a triangular pattern linking adjacent ribbons, forming a layer structure (Figure 1.14). Support for the role played by C–H•••O interactions resulting in the layer structure was provided by the molecular arrangement in a 1:1 complex between substituted quinones and in the case of tetrafluoro-*p*-benzoquinone there was no layer observed.[36]

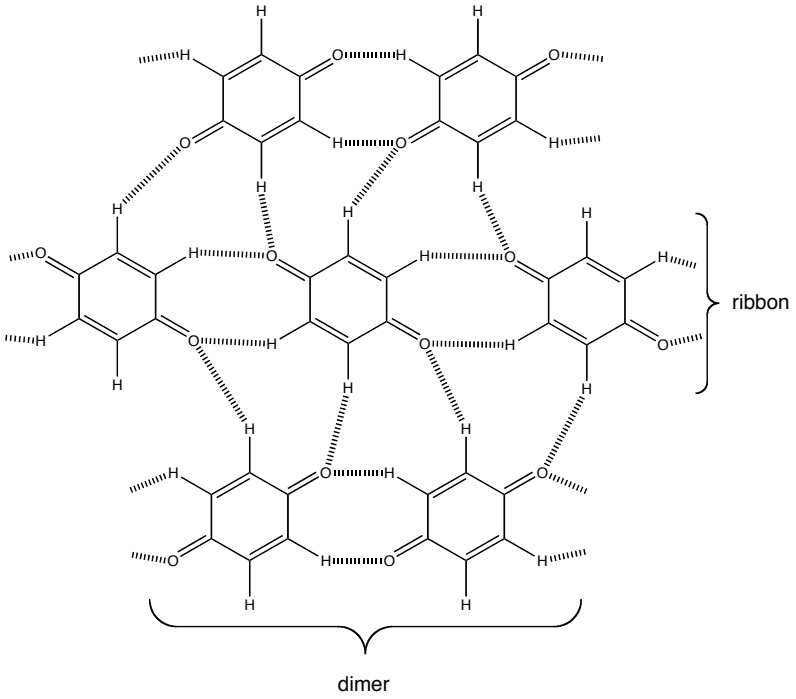

Figure 1.14 Illustration of benzoquinone layer structure in the solid state. The C–H•••O contacts are shown.

Pyrazine carboxamide crystallizes in four forms: α, β, γ and δ.[37] In the β form, the cyclic hydrogen-bonded pairs N–H•••O are interlinked along the translation axis by N–H•••O and C–H•••N contacts (Figure 1.15).[38]

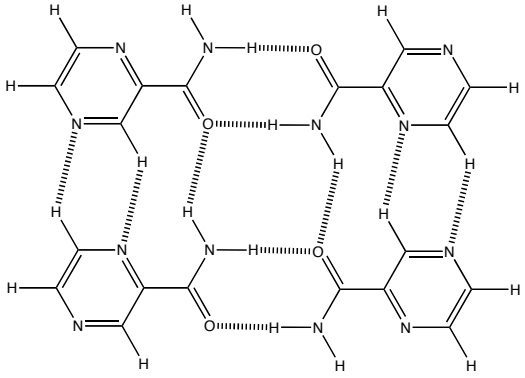

Figure 1.15 Illustration of pyrazine carboxamide in the solid state.

A C(sp^3)–H•••O interaction involving acetamide as C–H donor can be inferred by comparison of the isomorphous crystal structures of acetamide-barbital and urea-barbital (Figure 1.16).[39] In a similar fashion, the crystal structure of acetic acid contains infinite chains "linked" by C–H•••O interactions (Figure 1.16).[40]

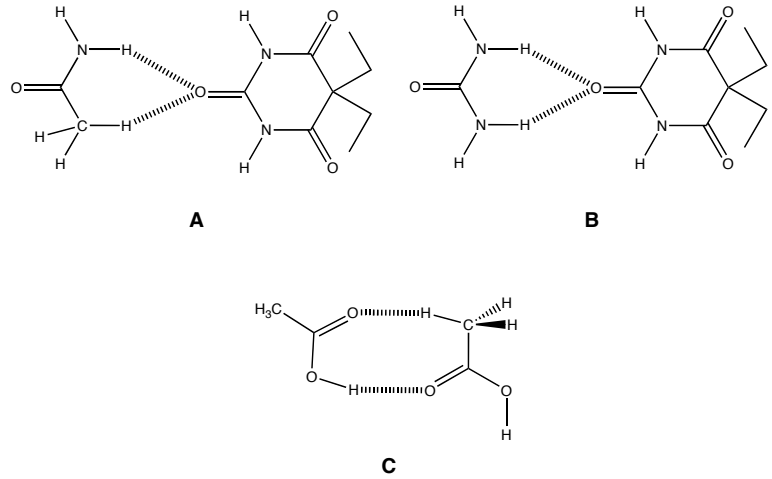

Figure 1.16 Illustrations of acetamide-barbital (A), urea-barbital (B), and acetic acid (C) complexes in the solid state.

1.3.4 Characterizing the Patterns of Hydrogen Bonds in the Solid State

The Cambridge Structural Database (CSD) has been utilized in a number of studies aimed at obtaining geometric features of a wide variety of hydrogen bond networks.[31,41] The formation of hydrogen bonds in crystals has been found to lead to characteristic one-, two- and three-dimensional molecular patterns.[42] The characteristic hydrogen-bond patterns may be utilized in predicting crystal packing or in designing crystals with predetermined structural properties.

The work of Etter[43] and others[44] began to direct attention on the hydrogen-bond patterns and the ability of hydrogen bonds to control order in molecular crystallization. This molecular interaction control arises largely because of the strength and directionality of the hydrogen bonds. Moreover, this early focus of Etter further revealed that reliable hydrogen-bonding motifs formed by elementary functional groups are frequently encountered in the crystal structure of simple molecules.[6]

Several rules of hydrogen-bond recognition and pattern definition have been outlined; however, the pattern rules are restricted to organic crystals composed of neutral molecules with sterically accessible hydrogen-bonding groups.[43] Also, the

observed hydrogen-bond interactions should be perturbed minimally by competing steric or ionic interactions. The framework of hydrogen bonds may belong to four pattern types (Figure 1.17): A, B, C, and D.

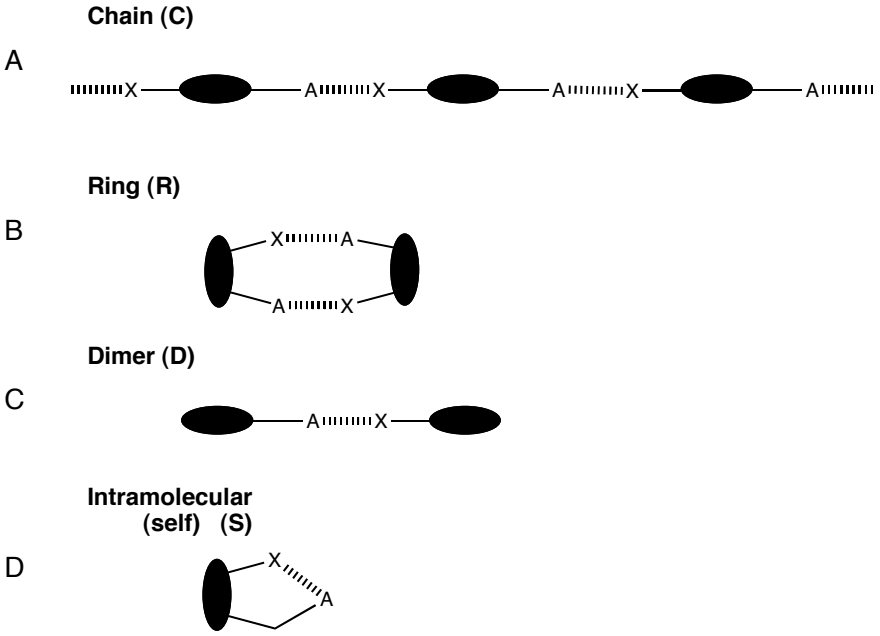

Figure 1.17 The four basic motifs of hydrogen bonds in the solid state.

The basic motifs in the hydrogen-bonding scheme reveal some obvious characteristics. Intermolecular hydrogen bonds are involved in the first of the three types and the fourth is an intramolecular hydrogen bond. Combinations of the patterns may exist although the greater pattern can always be deconvoluted to the fundamental patterns or types. The deconvolution of the patterns considers that certain functional group types prefer certain hydrogen bond patterns. The remainder of the molecule will be organized into the hydrogen bond directed supramolecular assembly and is a subset of the crystal structure.

In addition, Etter developed and established notation to clarify the number of donors (*d*), the number of acceptors (*a*), and the size or degree of the pattern (G) specified as the total number of atoms (*n*) in that pattern.[43] First the number and type

of hydrogen bond motifs must be identified. For motifs generated from intermolecular hydrogen bonds, the designators are C (chain or catemer), R (ring) and D (dimer or other finite set), while S denotes an intramolecular hydrogen bond. The numbers of donors (*d*) and acceptors (*a*) used in each motif are assigned as subscripts and superscripts, respectively, and the size or degree of the motif (corresponding to the number of atoms in the repeat unit) is indicated in parentheses. This hydrogen-bonding motif notation is illustrated as $G_b^a(n)$ and some graph set examples are given in Figure 1.18. Higher order networks N_i resulting from a combination of these motifs may also be assigned that have two or more types of hydrogen bonds.

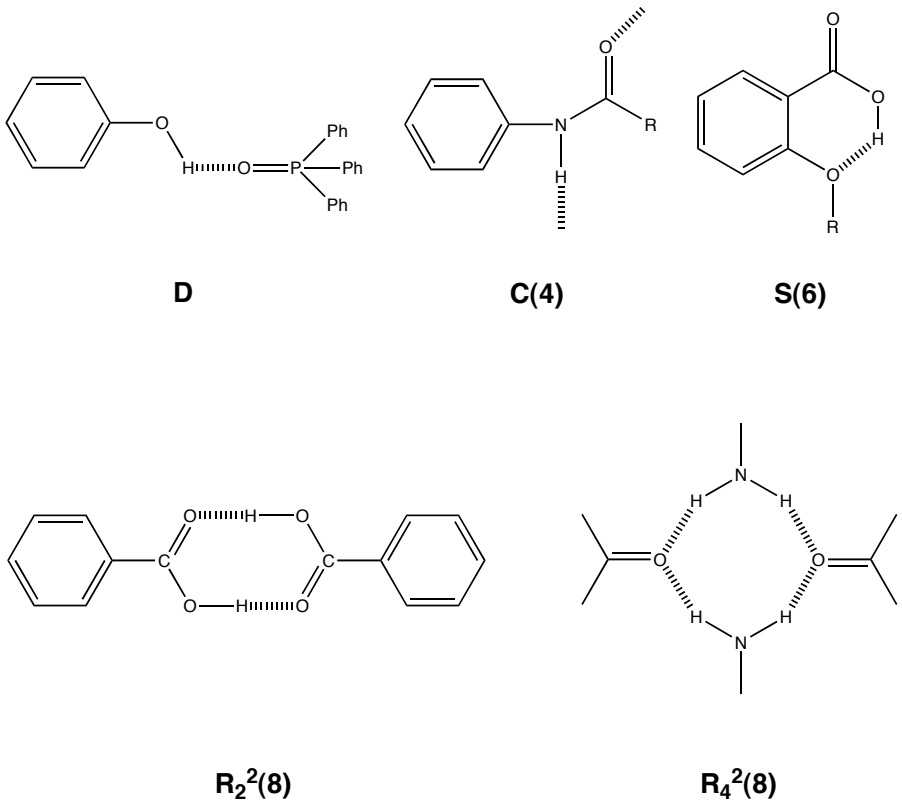

Figure 1.18 Examples of hydrogen-bonding graph set representations.

Furthermore, Etter found preferred modes of hydrogen bonding were developed from intermolecular contacts found in the CSD. The correlations between hydrogen-bond functional groups and the aggregate hydrogen-bonded patterns have

been presented in some general empirical rules.[43] Previously, graph sets illustrated connectivity or configuration of a set of hydrogen-bonded molecules. The first three general rules apply to functional groups in neutral organic molecules. These hydrogen-bonding rules include:

1. All good proton donors and acceptors are used in hydrogen bonding.[45]
2. Six-membered ring intramolecular hydrogen bonds form in preference to intermolecular hydrogen bonds.[46]
3. The best proton donors and acceptors remaining after intramolecular hydrogen-bond formation will form intermolecular hydrogen bonds (Figure 1.19).[47]

Additional rules have been described for specific classes of functional groups that include nitroanilines,[48] diarylureas,[49] carboxylic acid cocrystals with 2-aminopyrimidine,[47] and nucleotide base cocrystals.[50]

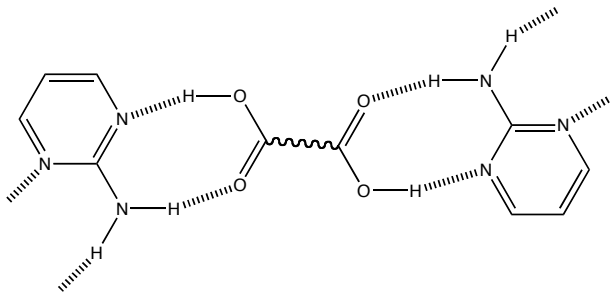

Figure 1.19 Cocrystal of best donors (acidic protons) are paired with the best acceptors (nitrogen atoms).[47]

The examination of hydrogen bonding networks was an endeavor to understand how noncovalent interactions compete with and cooperates with other forces in the solid state. This study by Etter to describe patterns illustrates the potential for supermoleculer design that is utilized in contemporary research to correlate a molecular component to the larger superstructure.

1.4 Molecular Voids in the Solid State

1.4.1 Introduction

As previously shown, ordered materials in the solid state are often organized by noncovalent interactions, *i.e*. hydrogen bonds, in a close crystal packing. Also of interest to solid-state investigations is the void or spaces, or channels, which may be generated in solid-state structures. These molecular voids have been shown to trap small molecules or volatile gases, which has been demonstrated with metal organic frameworks (MOFs).[29a] By generating new solid-state structures it may be possible to design unique, functional components or motifs to further expand the list of solid-state structures.

1.4.2 Clathrates

Clathrate structures, or inclusion compounds, are solids made of a principle host molecule that produces the lattice and a guest molecule. The host-guest compounds are necessary for the ordered solid material; if one is absent then the material will not be stable. In general, the host is responsible for the overall repeating patterns in the solid structure and the guest is necessary to fill voids created by the host. As with supramolecular structures, the interactions are of a weak nature and molecular components are not covalently bonded to each other.

Clathrates are sometimes categorized with regard to the form found in the solid state.[51] For instance, *cryptato-clathrates* (E) involve cages with the molecular guest in the center and *tubulato-clathrates* (C) contain simple channels for the guest molecules (Scheme 1.1). Different cavities produce different dynamic properties of the clathrates. Synthetic clathrates can be categorized with respect to the type of lattice formed, either by weak or strong interactions.

Scheme 1.1

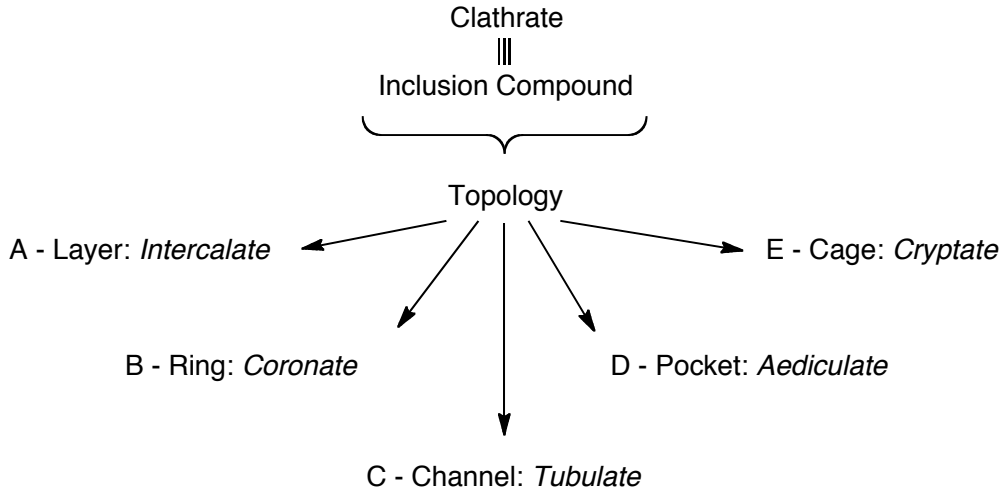

1.4.3 Urea/Thiourea Clathrates

Urea and thiourea are some of the most well studied synthetic clathrate systems. The robust nature of the urea/thiourea clathrates is due in part to the good donor ability of the acidic amine NH_2 and the good acceptor ability of the oxygen or sulfur atoms found in the molecules.[52]

The urea molecules form a helix around a channel, with an internal diameter of *ca.* 6 Å, where the guest molecule resides (Figure 1.20). All intermolecular interactions of the urea molecules are maximized leaving an "inert" channel that does not allow the guest molecules to chemically interact with the urea molecules. Therefore the channels are 'smooth' and only van der Waals forces retain the guest molecule. In general, the guest molecules include long chain alkanes with minimal branching; molecules such as benzene or cyclohexane may be excluded due to their size. The nature of the channel also results in a non-stoichiometric relation in that there is not a fixed ratio between the repeating unit and the guest molecule.

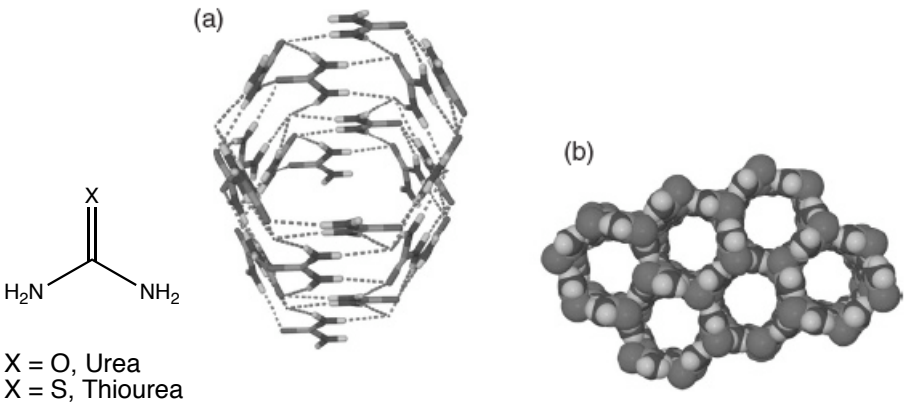

Figure 1.20 (a) The structure of a urea channel with a high degree of hydrogen bonding. (b) The honeycomb arrangement produced by urea channels.

Thiourea clatherates usually have slightly larger channels that can accommodate larger, or branched, molecules or allows greater movement of the molecules (Figure 1.21).[53] This difference in size between urea and thiourea could be utilized for separation purposes based on size, or branching, of the molecules. Thus the void, or enclosed space, could also be utilized to impose stereospecific or regiospecific interactions between molecules during reactive conditions.

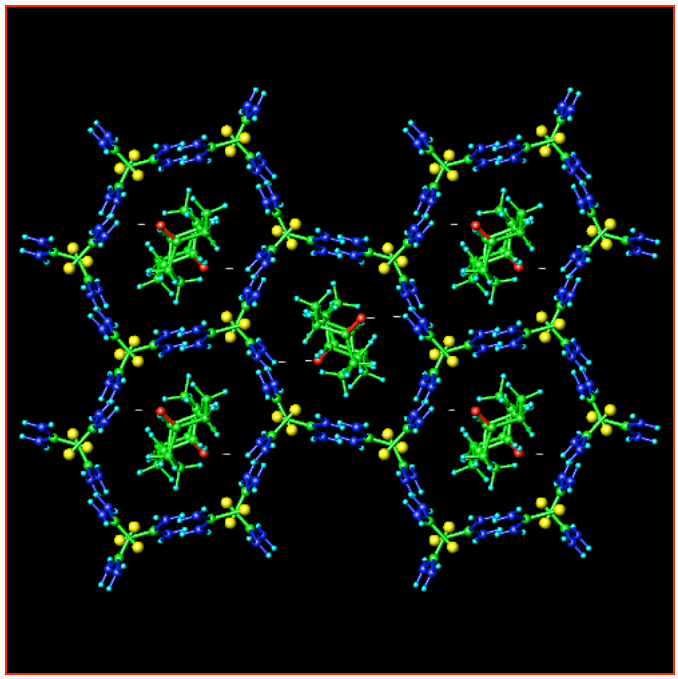

Figure 1.21 Section of the unit cell of the thiourea inclusion compound with cyclooctanone. Cell has been transformed to have the channel axis running along the crystallographic *a* axis.[53]

1.4.4 Trimesic Acid (TMA) Clathrates

Trimesic Acid (TMA), or 1,3,5-benzenetricarboxylic acid, are carboxylic acids that are well-known to self-associate and form a dimer, or more commonly a staggered conformation resulting in ribbons (Figure 1.22). TMA has been found to prevent clathrate formation and increasing the packing density whereby the 'chicken wire' network may be triply concantenated in each hole, which leads to an infinite interpenetration of independent networks.[54] TMA·H_2O forms a rectangular cavity joined by hydrogen bonding and can accommodate neutral guests. Trimesic Acid can also crystallize in the presence of large species and prevent interpenetration to form *ca*. 14 Å hexagonal channels (Figure 1.23).[55]

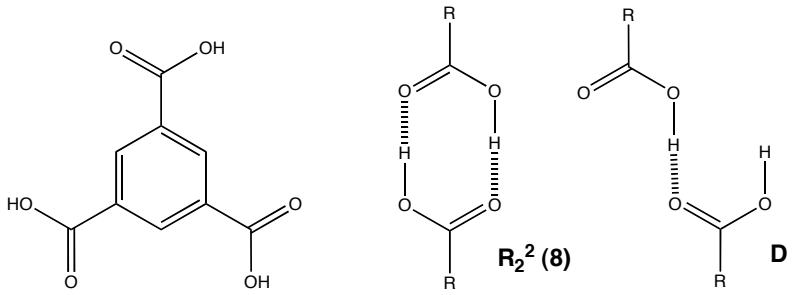

Figure 1.22 Trimesic Acid: dimeric hydrogen bonding and staggered hydrogen bonding pattern.

In an effort to prevent interpenetration and investigate some new host-guest trimesic acid compounds, Zimmerman and co-workers chose several aromatic guest compounds because of their rigidity and ability to stack in columns in the solid state.[56] In this study, pyrene obtained the best results (Figure 1.23) whereas the potentially better fitting molecule, coronene, was not soluble enough to cocrystallize. Also, smaller molecules did not prove to be as robust as pyrene in forming clathrates. Of the five variations of TMA, surprisingly, only one produced the desired clathrate, suggesting there may be limits to our understanding of rational design in crystal engineering.

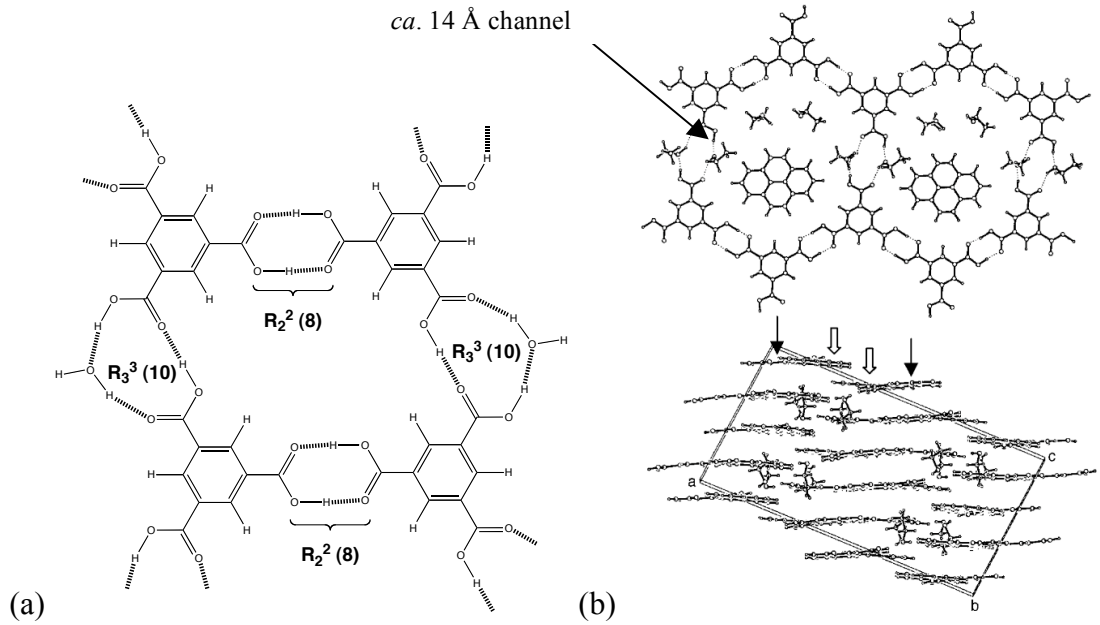

Figure 1.23 (a) Illustration of the rectangular channel formed by TMA·H_2O.[57] (b) Sections through the hexagonal channels formed by TMA due to a guest species, pyrene.[56]

1.5 Conclusions

Noncovalent interactions are present in a wide array of systems and their energetic contributions vary greatly between systems. Hydrogen bonding is one of the most identifiable noncovalent interactions responsible many molecular organization and recognition events. In the solid state, benzene demonstrates a fundamental example of noncovalent interactions, which can be subtly altered to induce different molecular arrangements. The work of Etter and others was instrumental in bringing to light the seemingly enormous array of functionalities that were responsible, in part, for the arrangement of solid-state structures. Their work also highlighted certain molecular moieties that may be exploited for design purposes. With the fundamental understanding these noncovalent interactions and others, the design and tuning of new molecular materials with unique structure/function properties may be realized.

1.6 References:

[1] Lehn, J.-M. *Supramolecular Chemistry*; VCH: Weinheim, 1995.

[2] Chang, R. Intermolecular Forces and Liquids and Solids. *Chemistry*, 2nd ed.; Random House: New York, 1984; pp 258-264.

[3] Giancoli, D.C. Electric Charge and Electric Field. *Physics*, 2nd ed.; Prentice-Hall: New Jersey, 1985; pp 357-361.

[4] Hobza, P.; Havlas, Z. *Chem. Rev*. **2000**, *100*, 4253-4264.

[5] Hunter, C.A.; Lawson, K.R.; Perkins, J.; Urch, C.J. *J. Chem. Soc., Perkin Trans. 2,* **2001**, 651-669.

[6] Steiner, T. *Angew. Chem. Int. Ed*. **2002**, *41*, 48-76.

[7] Williams, J.H. *Acc. Chem. Res*. **1993**, *26*, 593-598.

[8] (a) Cox, E.G. *Proc. R. Soc. A,* **1932**, *135*, 491-498. (b) Cox, E.G.; Cruikshank, D.W.J.; Smith, J.C. *Proc. R. Soc. A,* **1958**, *247*, 1-21.

[9] Lowden, L.J.; Chandler, D. *J. Chem. Phys*. **1974**, *61*, 5228-5241.

[10] Shi, X.; Bartell, L.S. *J. Phys. Chem*. **1988**, *92*, 5667-5673.

[11] Hobza, P.; Selze, H.L.; Schlag, E.W. *J. Am. Chem. Soc*. **1994**, *116*, 3500-3506.

[12] Janda, K.C.; Hemminger, J.C.; Winn, J.S.; Novick, S.E.; Harris, S.J.; Klemperer, W. *J. Chem. Phys*. **1975**, *63*, 1419-1421.

[13] Steed, J.M.; Dixon, T.A.; Klemperer, W. *J. Chem. Phys*. **1979**, *70*, 4940-4946.

[14] Bacon, G.E.; Curry, N.A.; Wilson, S.A. *Proc. R. Soc. A,* **1964**, *279*, 98-110.

[15] Desiraju, G.R.; Gavezzotti, A. *Acta Cryst*. **1989**, *B45*, 473-482.

[16] The stack orientation describes the non-favourable parallel molecular arrangement and the glide orientation describes the favourable parallel molecular arrangement.

[17] Gavezzotti, A. *Acc. Chem. Res*. **1994**, *27*, 309-314.

[18] Patrick, C.R.; Prosser, G.S. *Nature*, **1960**, *187*, 1021.

[19] Williams, J.H.; Cockcroft, J.K.; Fitch, A.N. *Angew. Chem. Int. Ed. Engl.* **1992**, *31*, 1655-1657.

[20] Dahl, T. *Acta Chem. Scan. A.* **1975**, *29,* 170-174.

[21] Battaglia, M.R.; Buckingham, A.D.; Williams, J.H. *Chemical Physics Letters*, **1981**, *78*, 421-423.

[22] Ponzini, F.; Zagha, R.; Hardcastle, K.; Siegel, J.S. *Angew. Chem. Int. Ed.* **2000**, *39*, 2323-2325.

[23] Chang, R. Intermolecular Forces and Liquids and Solids. *Chemistry*, 2nd ed.; Random House: New York, 1984; pp 270-280.

[24] Ladd, M.F.C. *Symmetry in Molecules and Crystals*; Wiley: New York, 1989.

[25] Dunitz, J.D.; Gavezzotti, A. *Angew. Chem. Int. Ed*. **2005**, *44*, 1766-1787.

[26] Mullin, J.W. Solid state bonding. *Crystallization*, 4th ed.; Butterworth-Heinemann: Oxford, 2001; pp 15-16.

[27] Kitaigorodskii, A.I. *Organic Chemical Crystallography*. Consultants Bureau: New York, 1961.

[28] For recent reviews, see: (a) Desiraju, G.R. *Angew. Chem. Int. Ed.* **2007**, *46*, 8342-8356. (b) Wuest, J.D. *Chem. Commun*. **2005**, 5830-5837.

[29] For examples, see: (a) Eddaoudi, M.; Moler, D. B.; Li, H.; Chen, B.; Reineke, T. M.; O'Keeffe, M.; Yaghi, O. M. *Acc. Chem. Res*. **2001**, *34*, 319-330. (b) Hosseini, M.W. *Acc. Chem. Res*. **2005**, *38*, 313-323. (c) Hill, R. J.; Long, D.-L.; Champness, N. R.; Hubberstey, P.; Schröder, M. *Acc. Chem. Res*. **2005**, *38*, 335-350.

[30] Desiraju, G.R. *Angew. Chem. Int. Ed. Engl*. **1995**, *34*, 2311-2327.

[31] (a) Allen, F.H.; Bellard, S.; Brice, M.D.; Cartwright, B.A.; Doubleday, A.; Higgs, H.; Hummelink, T.; Hummelink-Peters, B.G.; Kennard, O.; Motherwell, W.D.S.;

Rodgers J.R.; Watson, D.G. *Acta Cryst*. **1979**, *B35*, 2331-2339. (b) Allen, F.H.; Kennard, O.; Taylor, R. *Acc. Chem. Res*. **1983**, *16*, 146-153.

[32] Desiraju, G.R.; Steiner, T. *The Weak Hydrogen Bond in Structural Chemistry and Biology*; Oxford University Press, 1999.

[33] Jeffery, G.A. *An Introduction to Hydrogen Bonding*; Oxford University Press: Oxford, 1997.

[34] (a) Ferguson, G.; Tyrrell, J. *J. Chem. Comm. (London)*, **1965**, 195-197. (b) Ferguson, G.; Islam, K.M.S. *J. Chem Soc. B*, **1966**, 593-600.

[35] (a) Bernstein, J.; Cohen, M.D.; Leiserowitz, L. *The Chemistry of the Quinonoid Compounds*, Vol. 1, Part 1; Patai, S., Ed.; Wiley: New York, 1974; pp 37-110. (b) Trotter, J. *Acta Cryst*. **1960**, *13*, 86-95.

[36] (a) Sakurai, T.; Okunuki, M. *Acta Cryst*. **1971**, *B27*, 1445. (b) Sakurai, T. *Acta Cryst*. **1965**, *19*, 320. (c) Shipley, G.G.; Wallwork, S.C. *Acta Cryst*. **1967**, *22*, 593. (d) Meresse, A.; Courseilile, C.; Chanh, N.B. *Acta Cryst*. **1974**, *B30*, 524.

[37] Tamura, C.; Kuwano, H.; Sasada, Y. *Acta Cryst*. **1961**, *14*, 693.

[38] RØ, G.; Sørum, H. *Acta Cryst*. **1972**, *B28*, 991.

[39] Berkovitch-Yellin, Z.; Leiserowitz, L. *Acta Cryst.* **1984**, *B40*, 159-165.

[40] Jönsson, G.G. *Acta Cryst*. **1971**, *B27*, 893.

[41] (a) Sarma, J.A.R.P.; Desiraju, G.R. *Acc. Chem. Res*. **1986**, *19*, 222-228. (b) Murray-Rust, P.; Glusker, J.P. *J. Am. Chem. Soc*. **1984**, *106*, 1018-1025. (c) Kroon, J.; Kanters, J.A.; van Duijneveldt-van De Rijdt, J.G.C.M.; van Duijneveldt, F.B.; Vliegenthart, J.H. *J. Mol. Struct*. **1975**, *24*, 109-129. (d) Brown, I.D. *Acta Cryst*. **1976**, *A32*, 24-31. (e) Ceccarelli, C.; Jeffery, G.A.; Taylor, R. *J. Mol. Struct*. **1981**, *70*, 255-271. (f) Taylor, R.; Kennard, O.; Versichel, W.J. *J. Am. Chem. Soc*. **1984**, *106*, 244-248. (g) Jeffrey, G.A.; Mitra, J. *J. Am. Chem. Soc*. **1984**, *106*, 5546-5553.

[42] (a) Leiserowitz, L. *Acta Cryst.* **1976**, *B32*, 775-802. (b) Leiserowitz, L.; Tuval, M. *Acta Cryst*. **1978**, *B34*, 1230-1247. (c) Hagler, A.T.; Leiserowitz, L. *J. Am. Chem. Soc*. **1978**, *100*, 5879-5887. (d) Leiserowitz, L.; Hagler, A.T. *Proc. R. Soc. A*, **1983**, *338*, 133-175. (e) Leiserowitz, L.; Schmidt, G.M.J. *J. Chem. Soc. A*, **1969**, 2372-2382. (f) Jeffrey, G.A.; Takagi, S. *Acc. Chem. Res*. **1978**, *11*, 264-270.

[43] Etter, M.C. *Acc. Chem. Res.* **1990**, *23*, 120-126.

[44] Taylor, R.; Kennard, O. *Acc. Chem. Res.* **1984**, *17*, 320-326.

[45] Donohue, J. *J. Phys. Chem*. **1952**, *56*, 502-510.

[46] Etter, M.C.; Urbañczyk-Lipkowska, Z.; Fish, P.A.; Panunto, T.W.; Baures, P.W.; Frye, J.S. *J. Crystallogr. Spectrosc. Res*. **1988**, *18*, 311-325.

[47] Etter, M.C.; Adsmond, D.A. *J. Chem. Soc., Chem. Commun*. **1990**, 589-591.

[48] Panunto, T.W.; Urbañczyk-Lipkowska, Z.; Johnson, R.; Etter, M.C. *J. Am. Chem. Soc*. **1987**, *109*, 7786-7797.

[49] Etter, M.C.; Panunto, T.W. *J. Am. Chem. Soc*. **1988**, *110*, 5896-5897.

[50] Tamura, C.; Sato, S.; Hata, T. *Bull. Chem. Soc. Jpn*. **1973**, *46*, 2388-2394.

[51] Weber, E.; Josel, H.-P. *J. Inclusion Phenom*. **1983**, *1*, 79-85.

[52] Harris, K.D.M. Urea inclusion compounds. In *Encyclopedia of Supramolecular Chemistry*; Steed, J.W.; Atwood, J.L., Eds.; Marcel Dekker: New York, NY, 2004; pp 1538-1549.

[53] Maris, T.; Henson, M.J.; Heyes, S.J.; Prout, K. *Chem. Mater*. **2001**, *13*, 2483-2492.

[54] Duchamp, D.J.; Marsh, R.E. *Acta Cryst*. **1969**, *B25*, 5-19.

[55] Herbstein, F.H.; Kapon, M.; Reisner, G.M. *J. Inclusion Phenom. Macrocyclic Chem.* **1987**, *5*, 211-214.

[56] Kolotuchin, S.V.;Thiessen, P.A.; Fenlon, E.E.; Wilson, S.R.; Loweth, C.J.; Zimmerman, S.C. *Chem. Eur. J*. **1999**, *5*, 2537-2547.

[57] Herbstein, F.H.; Marsh, R.E. *Acta Cryst*. **1977**, *B33*, 2358-2367.

Chapter 2. Molecular Rotation: Single Bonds to Molecular Machines

2.1 Introduction

In general, molecular motions may be grouped by type: rotary, threading, allosteric, or linear. This chapter will primarily focus on rotary molecular motion in an array of molecular systems. One fundamental type of rotation occurs about a carbon-carbon bond and when one considers the backbone assembly of a polymeric structure, *i.e*. a protein, the significance of the single bond models and dynamics may seem of great importance for scientific study.

Classic examples in conformational analysis, such as ethane or biphenyl, provide the elementary basis of the discussion of molecular rotary motion. In recent years, researchers have synthesized more complicated systems with the aim to investigate and control rotational barriers influenced by sterics or crystal packing. Although the emerging field of molecular machines is still in its infancy, and consequently, the construction of useful molecular devices will require a strong foundation in the basic concepts of molecular motion.

2.1.1 Conformational Rotation in Basic Hydrocarbon Compounds

The ethane molecule provides the prototypical case of bond rotation, or torsional strain. The eclipsed conformation of ethane is 2.9 kcal/mol higher in energy than the staggered conformation and the potential energy varies with the angle of rotation in a sinusoidal manner.[1] The torsional strain is readily reproduced by *ab initio* molecular orbital calculations and often referred to as "Pitzer Strain".[2] Generally, the strain was thought to be due to steric effects but this of secondary importance. The cause for this energy barrier can be rationalized in terms of quantum mechanical hyperconjugation. The staggered conformation provides a more favourable interaction between the filled and empty σ orbitals (Figure 2.1).[3]

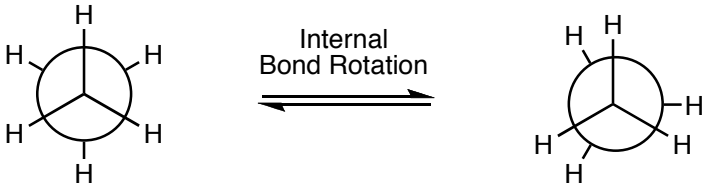

Figure 2.1 Newman projections of staggered and eclipsed conformations of ethane.

The biphenyl molecule, which has a rotational barrier of 2 kcal/mol,[4] is another fundamental example of conformational analysis. The molecule is planar in the solid state at room temperature, reportedly due to packing effects as opposed to a geometric preference (Figure 2.2).[5] In contrast, biphenyl is twisted in the gas phase, with a dihedral angle close to 45°.[6] This angle is a result of competition between the repulsion of the *ortho* hydrogens, which favors a perpendicular geometry, and the delocalization of π electrons, which is maximized in a planar structure.

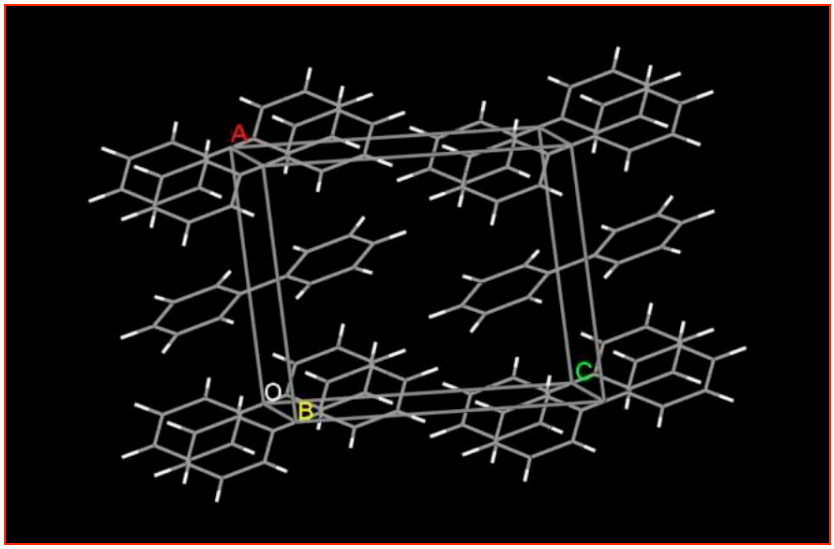

Figure 2.2 Section through the unit cell of biphenyl in the solid state.[5]

In calculations conducted by Grein, the optimized conformation of unsubstituted biphenyl has a dihedral angle of 46°.[7] This geometry is stabilized by 3 kcal/mol relative to the coplanar conformation and 1.5 kcal/mol relative to the perpendicular one.

If one of the *ortho* hydrogens of the biphenyl is replaced by a bulkier substituent, an increase in the dihedral angle relative to unsubstituted biphenyl is expected. If one *ortho* hydrogen on each ring is replaced by a bulkier substituent, a double minimum potential is anticipated, with *syn*-diagonal (τ_{syn}) and *anti*-diagonal (τ_{anti}) conformations (Figure 2.3). The *anti*-diagonal geometry is presumed lowest in energy because steric interactions are minimized and conjugation is partially maintained.[8]

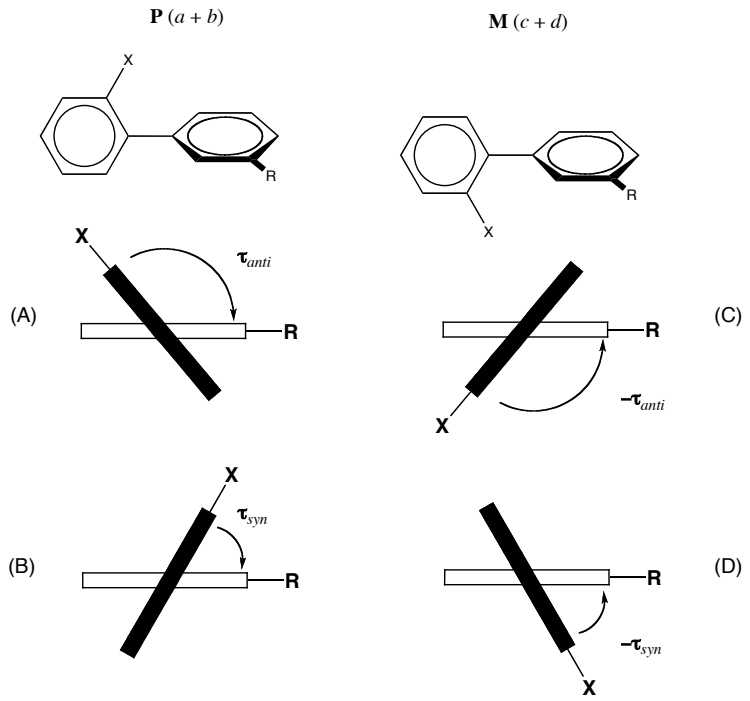

Figure 2.3 *Syn*-diagonal and *anti*-diagonal conformations of disubstituted biphenyls with both *P* and *M* helicity.

Several disubstituted biphenyls have been studied both experimentally and computationally. For example, according to the crystal structure, 2,2'-difluorobiphenyl has a dihedral angle of 57.6°.[9] This result is somewhat surprising because the angle is smaller than 90°, corresponding to a *syn*-diagonal conformation. The value calculated by Grein (58°) is in close agreement with the crystal structure.[7] This conformation is stabilized by 11 kcal/mol relative to the coplanar conformation

with both fluorines on the same side. There is a significant decrease in the energy barrier when both fluorine substituents are in the *meta* position.

Diphenylacetylene, also known as tolan, is the last fundamental molecule considered. In tolan, the space between adjacent rings is much larger than in biphenyl, and, as a result, interactions between substituents on the phenyl groups are considerably less significant (Figure 2.4). There are three primary scenarios to consider in predicting the geometry of diphenylacetylene. First, the *p* orbitals of both phenyl rings could overlap with the same set of *p* orbitals in the alkyne, leading to a planar geometry. Second, the molecule could act like two adjacent phenylacetylene units. In this case, the *p* orbitals of one phenyl ring would overlap with one set of *p* orbitals of the alkyne and the π system of the other ring interacts with the other *p* orbitals of the alkyne. This would favor a perpendicular geometry. A third possibility is that there is no strong preference for either geometry, leading to essentially free bond rotation.

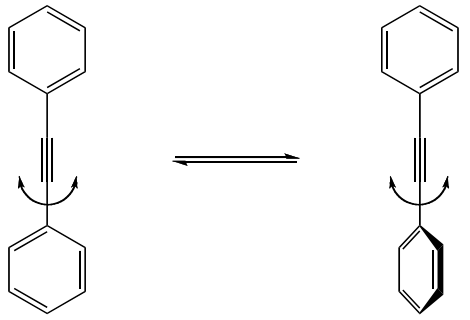

Figure 2.4 Rotational process in diphenylacetylene.

Early calculations using a wide range of methodologies (CNDO and INDO) were conducted by Liberles and Matlosz, who predicted barrier values of ~ 1 kcal/mol, favoring the perpendicular form.[10] More recently, Xu and Cooksy using *ab initio* B98/cc-pVDZ level calculations coincidentally found agreement with the experimental value of 202 cm^{-1}, or 0.58 kcal/mol.[11] This value is quite small, and can be interpreted as nearly free rotation. The crystal structure of tolan shows a planar

structure with D_{2h} symmetry.[12] However, as in biphenyl, this may be the result of a packing effect rather than a reflection of the preferred geometry.

The absorbance spectra of diphenylacetylene were compared to the spectra of phenylacetylene as well as *cis*- and *trans*-stilbene.[10] Tolan did not have absorbances in the same region as phenylacetylene, however there was significant peak overlap with the stilbenes. Tolan is therefore generally thought to be planar in solution because the UV spectrum more closely resembled stilbene rather than two independent phenylacetylene units. Calculations indicated a very small rotational barrier in tolan, only slightly favoring the planar species. In a later experimental study, Ito and co-workers[13] measured the torsional motion in tolan in a supersonic free jet and obtained a value (202 cm^{-1} or *ca*. 0.58 kcal/mol) and inside the previously reported experimental value.

2.2 Sterically Congested Alkynes

Although tolan shows a very small rotational barrier, the work of Toyota and co-workers looked to isolate rotational isomers of aryl alkynes by inducing transalkyne steric interactions.[14] In their initial work, the rotational barriers of bis(triptycyl)ethynes were investigated. The threefold symmetry of triptycene makes this system similar to ethane, but more closely related to 2-butyne. Whereas the rotational barrier in ethane is 2.9 kcal/mol, the barrier in butyne was found to be 4 cm^{-1}(*ca*. 0.011 kcal/mol).[15] The alkyne spacer increases the distance between the terminal methyls to about 4 Å, effectively eliminating all steric interactions. Consequently, Toyota and co-workers determined that *peri* substituents would be necessary in order to induce a measurable barrier (Figure 2.5). Therefore, substituents

were added in the 1 and 4 positions of each triptycene unit, leading to derivatives **2.1a-c** and **2.2a-d**.

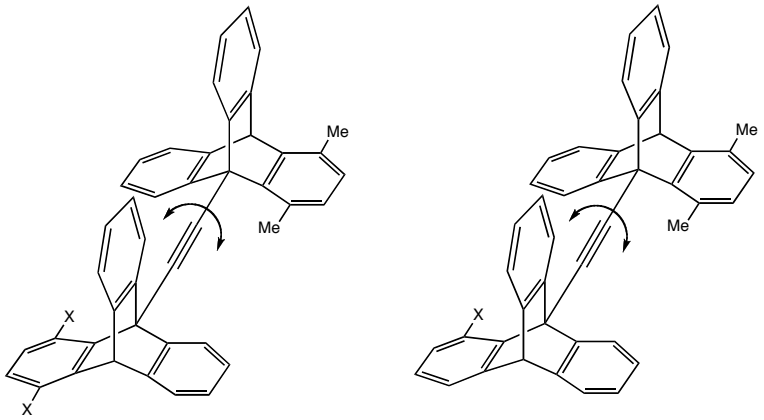

2.1 **2.2**

Figure 2.5 The introduction of *peri* substituents, indicated with X, were expected to lead to measurable rotational barriers for ditriptycyl ethynes.

Rotational barriers for a series of derivatives were measured using variable temperature ^{1}H NMR, and ranged from 9 to 17 kcal/mol, with good linear correlation between the barrier height and van der Waals radius of the substituent (Table 2.1).[16]

Table 2.1. van der Waals Radii and Rotational Barriers for **2.1a-c** and **2.2a-d**

Compound	X	Radius (Å)	Rotational Barrier (kcal/mol)
2.1a	H	1.20	10.1
2.1b	OMe	1.52	12.7
2.1c	Me	1.80	15.4
2.2a	F	1.47	11.6
2.2b	Cl	1.75	14.7
2.2c	Br	1.85	16.7
2.2d	I	1.98	17.3

In an effort to increase the barrier, the substituents were changed to different aryl and arylethynyl groups.[17] Whereas the barrier for a simple phenyl substituent was nearly equivalent to a methyl group at 15.7 kcal/mol, phenethynyl and naphthethynyl substituents increased the barrier to 17.5 and 17.8 kcal/mol, respectively. A particularly noteworthy result is that when the substituent X was changed to mesityl, the barrier was found to be 18.8 kcal/mol. The authors state that the rigidity of the mesityl substituent relative to the ethynyl groups leads to the barrier increase,

suggesting that both steric bulk and flexibility must be considered when attempting to hinder rotation.

In the subsequent series, an ethyne linker was connected to two terphenyl groups.[18] In this case, tolyl groups were used as the flanking rings. Bromination followed by reaction with sodium methoxide produced **2.3**, the desired desymmetrized compound for variable temperature ^{1}H NMR spectroscopy.

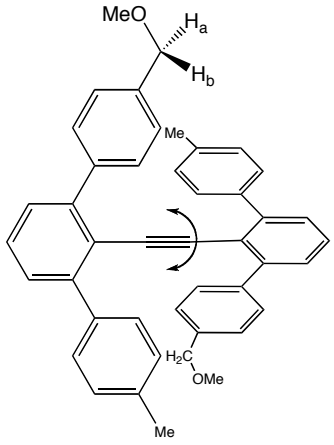

2.3

Unfortunately, it was not possible to determine the barrier for **2.3**. Throughout the investigated temperature range, the methylene protons adjacent to methoxy showed only a sharp singlet, suggesting fast rotation about the triple bond and a barrier of less than 8 kcal/mol. This result is attributed to the flexibility of both the alkyne and the terphenyl system.

In a further study, the authors utilized two anthracene moieties bridged by ethyne.[19] In this case, for the diisopropylphenyl derivative, the rotational barrier of the acetylene bond (sp^2)C-C≡C-C(sp^2) was 18.0 kcal/mol using variable temperature ^{1}H NMR and line shape analysis. A DFT calculation for the parent compound, di(9-anthryl)ethyne, without substituents gave a barrier of less than 1 kcal/mol. Therefore, the barrier can be appropriately attributed to the steric interactions between *peri* substituents (Figure 2.6).

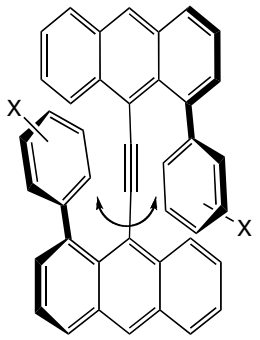

Figure 2.6 Steric interactions between *peri* substituents in dianthracenylethyne derivatives.

In light of the significant barrier increase from phenyl to mesityl in the triptycene systems, mixed terphenyl **2.4** was prepared with one mesityl and one *p*-tolyl ring on each side of the diphenylethyne core.[20] Although the rotational barrier was too low to be measured when all four rings were *p*-tolyl, in the case of **2.4**, a barrier of 12.1 kcal/mol was determined by variable temperature ^{1}H NMR and line shape analysis.

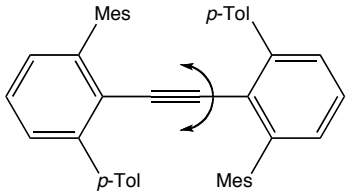

2.4

The work of Toyota and co-workers toward the isolation of rotational isomers of alkynes demonstrates the necessity of significant steric interactions in order to induce barriers to rotation observable by variable temperature NMR. In two cases, adding a mesityl substituent provided enough steric bulk to hinder rotation. In the most hindered systems, the maximum barrier was almost 19 kcal/mol.[20]

2.3 A Molecular Turnstile – Phenylene Rotator

Bedard and Moore synthesized a hexa(phenylacetylene) macrocyclic frame with a diethynylene bridge, which they referred to as a molecular turnstile.[21] This

molecule consists of a rigid macrocyclic framework containing an internal spindle with alkyne spacers. The size of the substituents attached to this spindle was varied and the barrier to rotation of the interior *p*-phenylene group was determined by variable temperature ^{1}H NMR. As the size of the substituents was increased, the barrier to rotation also increased due to steric interactions between these groups and the rigid framework. In the simplest case, **2.5**, where R is hydrogen, the barrier was too small to measure by NMR, as expected from the tolan experiments. It was expected that during variable temperature ^{1}H NMR, the benzylic protons in compound **2.6** and **2.7** are diastereotopic in the absence of rotation, and enantiotopic under free rotation conditions (Scheme 2.1). ^{1}H NMR of **2.7** revealed the benzylic protons appearing as an AB pattern (up to 150 °C), which indicated no rotation on the NMR time scale. In the case of **2.6**, the benzylic protons appeared as an AB system only at low temperature, and coalescence was observed at about 0 °C. In the case of **2.6**, the barrier was determined to be 13.4 kcal/mol. In compound **2.7** the rotational barrier was not observed and conformationally locked.

Scheme 2.1

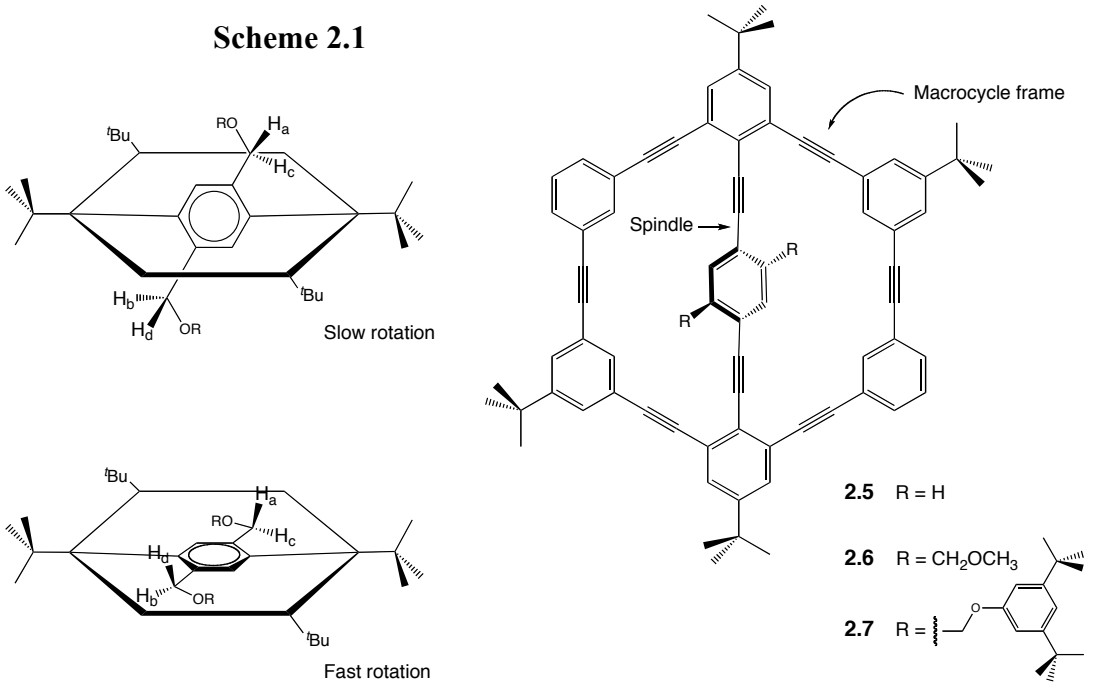

In this study, the authors demonstrated that the nearly free rotation of a pair of isoenergetic rotational isomers corresponds to a double-well energy surface so that the system has conformational bistability. Furthermore the two degenerate conformations of **2.6** could be identified by low temperature ^{1}H NMR. Although there was no specific control of the rotation of the central spindle, this study laid the groundwork for the design of controllable molecular rotors.

2.3.1 Allosteric Binding in a Molecular Turnstile

In the turnstile synthesized by Shinkai and co-workers, the anion binding properties of the compound were investigated.[22] The authors observed that **2.8** was capable of allosteric binding. When the first anion binds to the turnstile, the central spindle is forced to rotate, leaving the turnstile in an open state. This in turn presumably elicits cooperative binding of another anion to the second binding site (Figure 2.7).

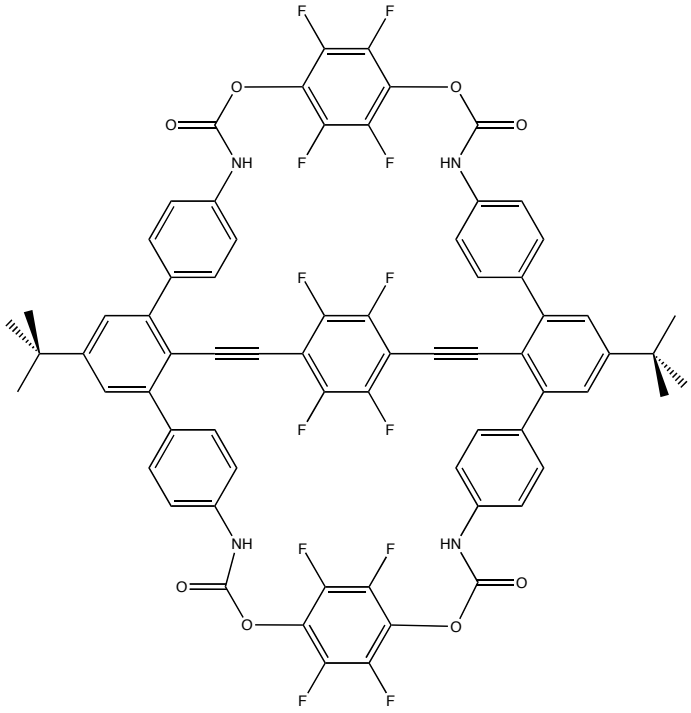

2.8

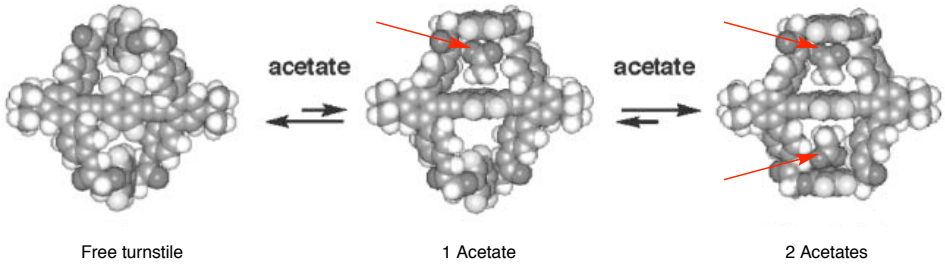

Figure 2.7 Schematic of proposed mechanism for allosteric binding of an acetate anion by **2.8**. Arrow indicates the acetate anion.

NMR titrations were performed on **2.8** in a mixture of deuterated THF-d_8 and DMSO-d_6. Anions examined included bromide, chloride, acetate, hydrogensulfate, and dibenzylphosphinate. ^{1}H and ^{19}F NMR measurements in the presence of several of the anions showed the ^{1}H signal from the amide nitrogen and the ^{19}F signal both moved downfield with increasing anion concentration.

Job plots ($\Delta\delta_{NH}$ *versus* guest concentration) were conducted to observe complexation events and gave a maximum value at 0.33, corresponding to a 1:2 host-guest complex. Furthermore, a Hill Plot demonstrated that binding between **2.8** and

acetate took place cooperatively. Association constants could be estimated from a plot of the change in chemical shift ($\Delta\delta$) versus the concentration of guest anion (M^{-1}), and these values correlated with the basicity of the guest anion. Most of the anions tested satisfied the condition of homotropic allosterism, in which the second association constant must be more than 0.25 times the first one ($K_2 > 0.25\ K_1$). Of the anions tested, chloride was a notable exception. The first binding constant was of the same order of magnitude as for other anions; however, the significantly lower second association constant did not satisfy the requirements for allosteric binding, as it was less than 0.25 times the first one. The authors state that it may be the smaller size of the chloride ion that prevents allosteric binding, as the smaller anion is not large enough to rotate the spindle and open the second binding site. The radius of the chloride ion is reported to be 1.67 Å, whereas a bromide ion is 1.82 Å. Shinkai and co-workers conclude that they have prepared a new dynamic host capable of allosteric anion binding through the motion of a turnstile.

2.4 Molecular Gyroscopes

A molecular gyroscope emulates its comparative structure by possessing a rotating mass in a rigid frame. Structurally, these molecular devices are related to their macroscopic relative by being endowed with an internal environment free from physical obstruction, *i.e*. another molecule or a solvent molecule. If the central unit is polar or has polar substituents, then external stimuli could be applied to influence the internal dynamics and thus creating a distinctive device.

Whereas the previous examples where studied in the solution phase, Garcia-Garibay and co-workers worked towards the synthesis and arrangement of a series of

phenylene rotors in a close-packed crystalline molecular assembly. Their intention was to control the rotary motion of this assembly using crystal engineering.[23]

The rotary processes found in macroscopic machines, such as clocks and automobile engines, require sufficient free space within the high-density apparatus, and a crystalline assembly requires a similar cavity. In a molecular rotor, the collective framework is referred to as a rotor, in which the stationary portion is called the stator and the rotating spindle is called the rotator (Figure 2.8).[24] Dynamic properties of the aryl alkyne rotors were observed by variable temperature solid-state NMR[25] and dielectric spectroscopy.[26]

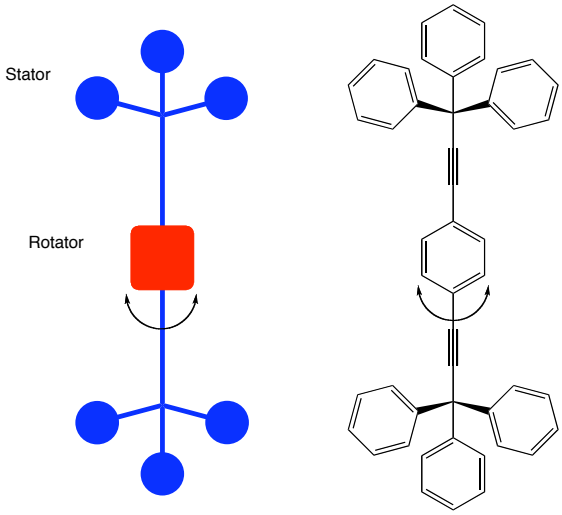

Figure 2.8 Illustration and chemical structure of a molecular rotor prepared by the Garcia-Garibay group. The stationary frame is referred to as the stator and the central component is termed the rotator.

In order to allocate enough free space for motion in the solid-state assembly, the authors proposed using crystal engineering to modify the packing density while still providing a durable crystal lattice.[27] The size of the stator is an important design component because it determines the density of the crystal packing. Bulkier stators generally reduce the crystal packing density and increase the cavity size by limiting

interactions with adjacent molecules. As a result, increasing the stator size should reduce the barrier to rotation (Figure 2.9).

The size of the stator, as well as the nature of the crystal packing, is critical in determining the rotational barrier. For example, flexible trityl and rigid triptycyl stators were utilized. The trityl based rotor had a barrier of 12.8 kcal/mol in the solid state at ambient temperature and a $k_{rot} < 10^4$ s^{-1}.[28] In comparison, the barrier in the triptycene-based rotor was too high to be measured in the solid state, even though solution phase NMR spectroscopy shows free rotation of the central spindle.[29] The trityl stator creates more free space than the triptycyl stator for the central spindle, presumably due to less dense packing, which prevents interdigitation.

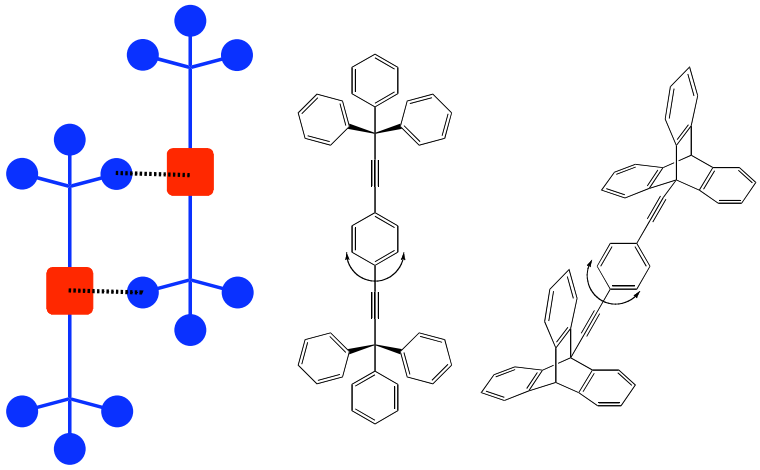

Figure 2.9 Interdigitation of adjacent rotors prevents free movement of the rotator. The rotational barrier in the solid state for the trityl rotor was 12.8 kcal/mol, but the barrier was too high to be measured in the triptycyl derivative.

The Garcia-Garibay group also synthesized molecular rotors containing dipolar rotator groups.[30] Whereas the rotator in the original system was a benzene ring, polarity is introduced by replacing one of the hydrogens on benzene with a fluoro-, amino-, or nitro- substituent, as seen in **2.9a-c**. The crystal structure and rotational barrier of **2.9a** is nearly identical to the parent compound. Dielectric spectroscopy measurements on the three-dimensional crystal lattice indicate rapid

thermal motion of the rotors and no interaction between adjacent rotators. These results suggest that an oscillating electric field might facilitate motion of the rotor in the crystal lattice.

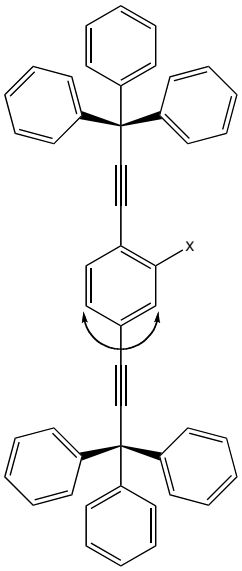

Compound	Substituent
2.9a	F
2.9b	NH_2
2.9c	NO_2

The Garcia-Garibay group also constructed more cylindrical rotators *versus* the flattened phenylene rotor in the previous studies. A flattened rotator, such as the phenylene unit, tends to have relatively high energy barriers with rotational potentials characterized by two energy minima connected by angular displacements of 180°. In contrast, more cylindrical groups with higher rotational symmetry order (C_n, $n > 2$) with have energy profiles with n minima, lower barriers, 360°/n angular displacements, and n states that may be potentially addressed with external stimuli if a permanent dipole is introduced into the structure. Following ^{13}C CPMAS measurements, the analysis suggests that the dimantane rotor **2.10**, with a barrier of 4.1 kcal/mol, rotates *ca*. 20 000 times faster than the phenylenes at 300 K.[31]

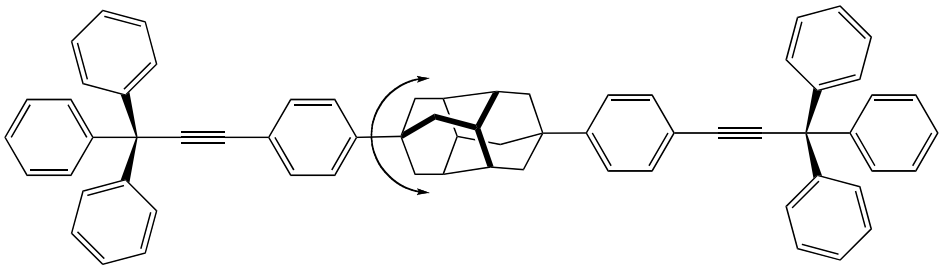

2.10

It could be speculated that if several of these rotors were placed in proximity to each other in the solid state, it would be possible to construct a responsive crystalline molecular machine capable of correlated motion. The ability to design a molecular assembly that responds to a stimulus in order to carry out a specific function is a critical step towards the development of molecular machines.

2.5 Bond Rotation and Metal Complexation

2.5.1 A Molecular "Brake"

Kelly and co-workers reported the synthesis of what they referred to as a molecular "brake", in which response to an external chemical stimulus leads to hindered rotation of a previously free rotor.[32] In this case, the chemical stimulus is the addition of mercury cation, which causes the 2,2'-bipyridine moiety to lock into a single conformation (Figure 2.10). The goal was to demonstrate that this conformational change (noncoplanar to coplanar) could stop rotation of the adjacent 9-triptycene unit and that the change could be reversed by the removal of mercury.

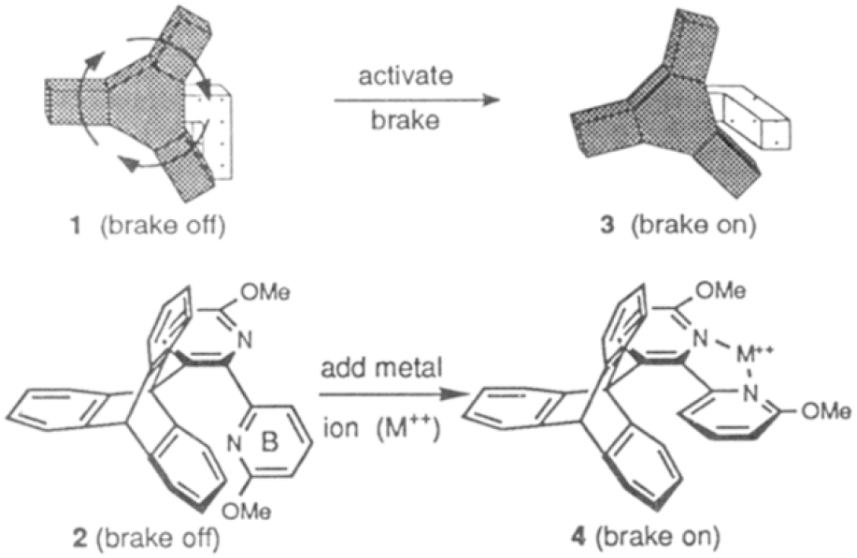

Figure 2.10 Schematic of the activation (with Hg^{2+}) and deactivation (with EDTA) of a molecular "brake".

The dynamic processes in the molecule were monitored by variable temperature NMR spectroscopy in the presence and absence of mercury cation. At 303 K rapid rotation is observed on the ^{1}H NMR timescale. As a result, only four sets of resonance signals are observed for the aromatic protons of the 9-triptylcyl ring system. As the temperature is lowered to 193 K, the twelve aromatic protons are nonequivalent. With the addition of the metal cation, the unit is locked leading to the methoxy group resonance being shifted downfield and the proton resonance of the 9-triptycyl systems are broadened. At 243 K, the single bond rotation between the 9-triptycyl and the bipyridine is slow rendering some of the aromatic protons of the 9-triptycl nonequivalent. This indicates a slowing, or "braking" of the rotation. Addition of EDTA results in the removal of the mercury and rotation of the triptycene unit is no longer hindered, demonstrating that the change is reversible.

In their molecular "brake", Kelly and co-workers demonstrate a response to a stimulus that leads to a change in the physical properties of the system. This is a significant proof of principle in terms of a reversible chemical stimulus leading to a change in the dynamics of a system.

2.5.2 Rotation in Metal-Arene Complexes

In a related system of metal persubstituted arenes complexes, Kilway and Siegel investigated rotational dynamics in metal-arene complexes.[33] In previous work, Mislow and co-workers, metal complexation with tricarbonyl chromium was shown to desymmetrize hexaethylbenzene by making the two faces of the π system nonequivalent **2.12**, which made it possible to determine the rotational barrier of the ethyl groups.[34] It was not clear, however, if the two interconversion pathways of the metal and the ethyl group were independent.

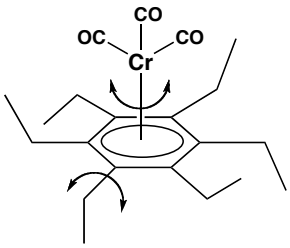

2.12

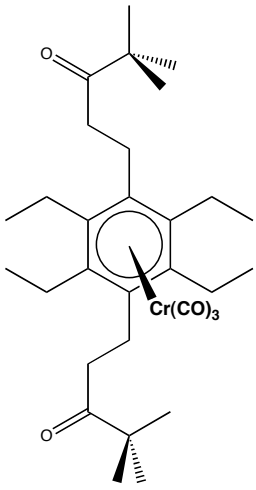

2.13

Kilway and Siegel synthesized a system in which the rotational barriers of the ethyl groups and the chromium tripod could be determined independently.[33] In **2.13**, rotation of the tricarbonyl group makes the three C—O groups equivalent, but the ketone carbons remain nonequivalent. Ethyl group rotation is required to make these sites equivalent. At room temperature, the ^{13}C NMR shows one ketone signal and one C—O signal. Cooling the sample to –60 °C splits the ketone into two signals, while the tricarbonyl groups remain equivalent, indicating that ethyl group rotation was static. Decoalescence at –60 °C corresponds to a rotational barrier of 11.8 kcal/mol. Further cooling of the sample to –90 °C splits the carbonyl signal into two peaks with

a 2:1 ratio, indicating that the tripod motion was static. The barrier for this process is found to be 9.5 kcal/mol. The ethyl group barrier was determined again in the uncomplexed arene to give a barrier of 11.3 kcal/mol.

From this work, Kilway and Siegel concluded that tri-carbonyl chromium does not significantly influence the measured barrier, and it provides a valid reference point for a rotational barrier determination. Additionally, they propose that the proximal alkyl groups may gate, cogwheel-like, the motion of the tripod.

Kilway and Siegel studied the effect of metal complexation on the barrier to rotation of the ethyl groups in several related systems to further demonstrate the utility of this method, and indicate the small influence metal complexation has on the measured barrier.[35] In **2.14-2.16**, ethyl group barriers were determined in the free ligands and metal complexes. As expected, there was only a small perturbation of the barrier due to metal complexation. These results also point to the possibility of correlation between tripod and ethyl group rotation.

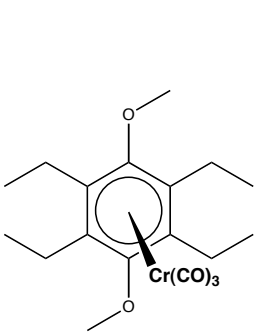

2.14

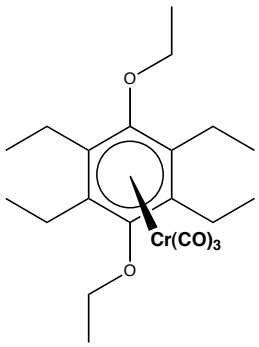

2.15

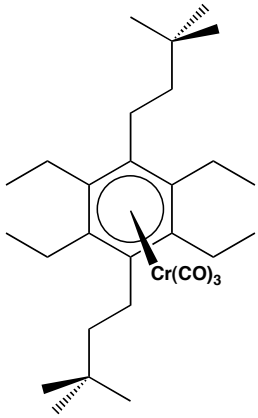

2.16

In order to investigate the prospect of correlated motion, the metal in **2.13** was changed from chromium to molybdenum to give **2.14**.[33] Comparing the crystal structures of the chromium and molybdenum complexes shows that the molybdenum-arene bond is 1.88 Å, which is 0.16 Å longer than the chromium-arene bond. Once

again, the barriers were determined by variable temperature ^{1}H NMR. The barrier to ethyl group rotation in the molybdenum complex was 11.4 kcal/mol, nearly the same value found in the free ligand. The tripod rotational barrier was 6.7 kcal/mol, almost 3 kcal/mol less than the barrier for the chromium tripod.

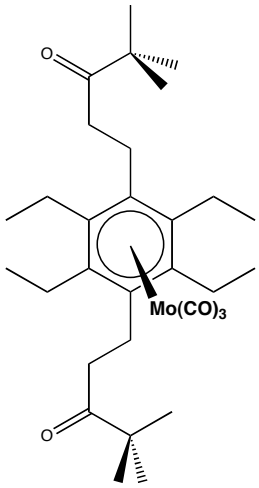

2.17

The barrier decrease from chromium to molybdenum suggests that the longer bond reduces steric interactions and therefore also reduces the rotational barrier. The significant barrier change relative to the chromium complex further supports the idea of correlation between the ethyl group and tripod motions.

2.6 Molecular Motors and Machines

2.6.1 Towards a Unidirectional Molecular Motor

Internal rotations are interesting physical properties to study; however, harnessing molecular motion is difficult to achieve. The ability to control molecular motion should enable the construction of useful molecular assemblies with practical functions. Unidirectional chemical motion was reported in 1999 by Kelly and co-workers in *Nature* with their triptycene-helicene system, using a chemical reaction to rotate 120°; however, not full rotation.[36] In the same issue of *Nature*, Feringa and co-

workers reported a significant advance in the design of a different type of molecular machine.[37] They prepared the first unidirectional molecular motor, using the photoisomerization of a carbon-carbon double bond bridging two chiral elements.

Light is an attractive option to initiate or control molecular rotation. It has been shown been shown that light can make a photochemical transformation in a molecule leading to a change in chirality;[38] this potentially makes it possible to access unique properties associated with the different stereoisomers. The importance of chiroptical switches is further emphasized because chirality controls many natural chemical processes, such as molecular recognition, transport, information storage, catalysis, assembly and replication.

The direction of movement leading to geometrical isomerization is controlled by the wavelength of light used and the chirality of the molecule. The concerted action of two chiral elements in a single physical event leads to unique handedness of the molecule. In the two tetrahydrophenanthrenes, each one can have left-handed (*M*) or right-handed (*P*) helicity. Including the *cis*-*trans* isomerization of the double bond, the cycle contains four distinct stereoismers. Light is used to induce *cis* and *trans* isomerization whereas irreversible helicity inversion is caused thermally, without affecting the *cis* or *trans* configuration (Figure 2.11).

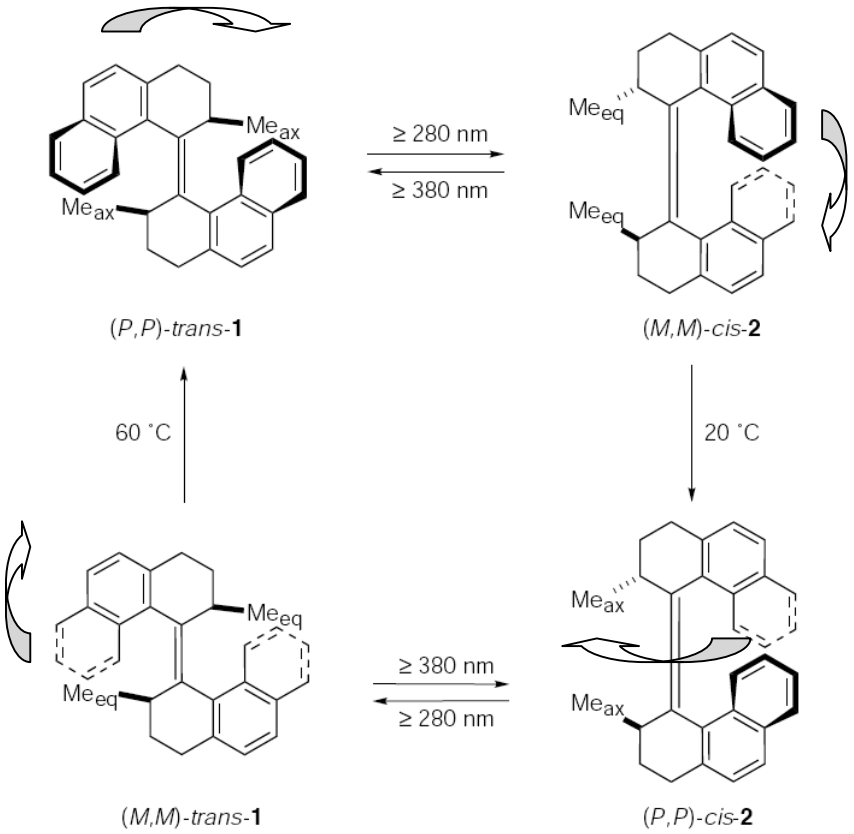

Figure 2.11 Schematic of the photochemical and thermal isomerization of a molecular motor.[37]

In the first step of the cycle, irradiation at 280 nm at 218 K converts the (*P*,*P*)-*trans* isomer to the (*M*,*M*)-*cis* isomer. The solution is then warmed to 293 K, at which point there is irreversible conversion to the (*P*,*P*)-*cis* isomer. Subsequent irradiation at 280 nm produces the (*M*,*M*)-*trans* isomer. Further increasing the temperature to 333 K irreversibly converts back to the starting (*P*,*P*)-*trans* isomer. In the four-step cycle, light and temperature are used to induce unidirectional motion. This motion is dictated by the stereogenic centers on each tetrahydrophenanthrene unit. In the first *trans*-*cis* isomerization, the axial methyl groups in the (*P*,*P*)-*trans* conformation are forced equatorial in the (*M*,*M*)-*cis* isomer. This strain is released in the next step, as the methyl groups are once again axial in the (*P*,*P*)-*cis* isomer. The subsequent light driven isomerization again forces the methyl groups equatorial, and the following step

returns them to their starting most stable configuration, in which the methyl groups are axial.

In the second-generation molecular motor synthesized by Feringa and co-workers, there are distinct upper and lower parts to the assembly, and only one stereogenic center.[39] However, one stereocenter is sufficient to drive unidirectional motion. Additional modifications were made to reduce the barrier to the thermal isomerizations. In newly synthesized **2.18** and **2.19**, rotational barriers are reduced to 24.7 kcal/mol and 22.7 kcal/mol, respectively, compared to the original barrier of 26.2 kcal/mol. The utility of these systems, make it possible to attach one side to a surface in order to make a mounted unidirectional molecular rotor.

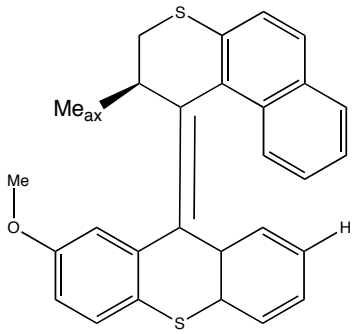

2.18

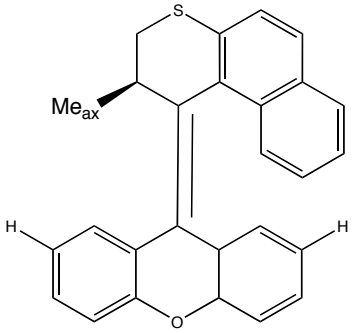

2.19

Related work by the Feringa group strived to control the rate of single bond rotation in a similar photochemical bistable system.[40] It was believed that isomerization of **2.20** to the *trans* isomer would reduce the biaryl rotational barrier by decreasing steric interactions. However, results showed that the barrier is actually higher for the *trans* isomer. A plausible explanation is interaction between the *ortho* methyl groups and the adjacent ring methylenes, an interaction that is avoided in the *cis* conformation. The authors propose that the naphthalene unit easily bends away to enable passage of the rotor, plus, *cis* and *trans* isomer assumptions may not hold for helical shaped, crowded alkenes.

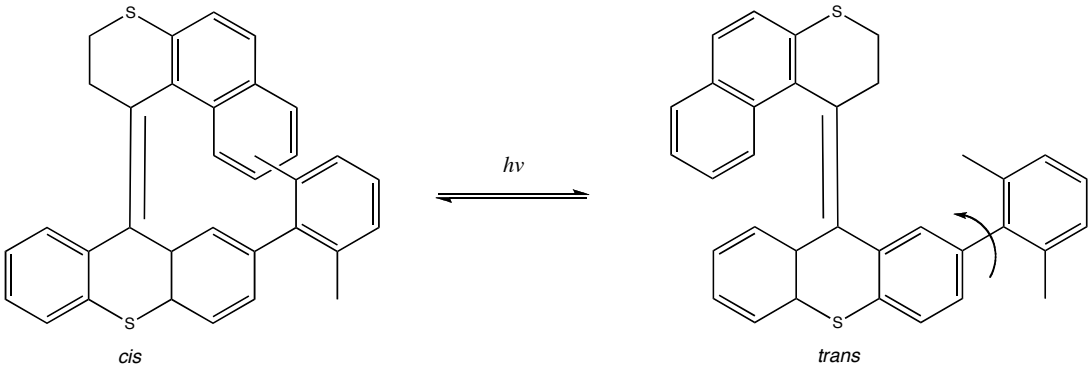

2.20

In summary, this work demonstrates the ability to induce light-driven, repetitive unidirectional motion in an artificial molecular machine. Chemical modifications led to changes in the rate of rotation and slight modifications of the structure should allow it to be attached to surfaces or other molecules. Feringa and co-workers have demonstrated a molecular model with the ability to harness internal rotation.

2.6.2 Molecular Motion and Electronic Devices

In a related effort to integrate rotational devices into electronic devices, Mayor and co-workers synthesized macrocyclic aryl alkynes, **2.21** and **2.22**, with the goal of developing potential electronic devices.[41] The macrocycles prepared by the Mayor group contain three components: a molecular rod, a molecular handle and ethynyl-linked phenyl rings with protected terminal thiol groups at each end to eventually permit immobilization between gold contacts. Initially, two derivatives were investigated, one containing one nitro group on the central ring and the other containing two nitro groups.

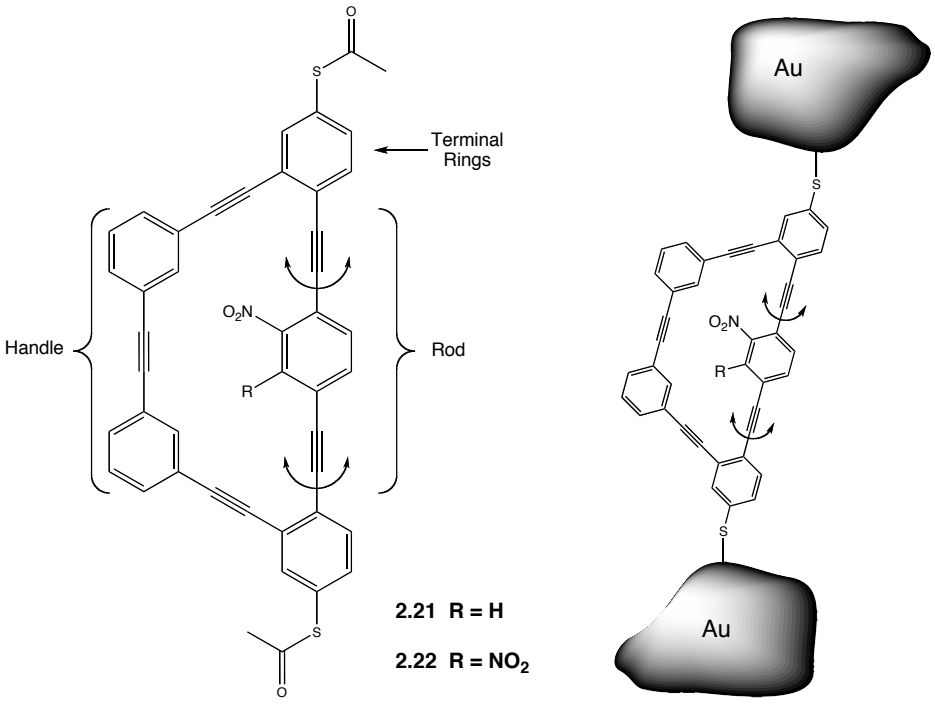

In an earlier study Mayor and co-workers demonstrated another example of using ethynyl linked phenyl rings to construct a molecular electronic device, or a single-molecule diode.[42] Tour and co-workers also previously prepared, a bisphenethynyl molecular compound with a nitroamine redox center on the central ring.[43] A self-assembled monolayer (SAM) of this compound was formed between gold electrodes (Figure 2.12). The authors observed negative differential resistance (NDR) behavior with **2.23**. NDR behavior indicates that, in a particular voltage range, current is a decreasing function of voltage. In a control experiment, a compound lacking substituents on the central ring was tested in the same manner, but, in this case, NDR behavior was not observed.

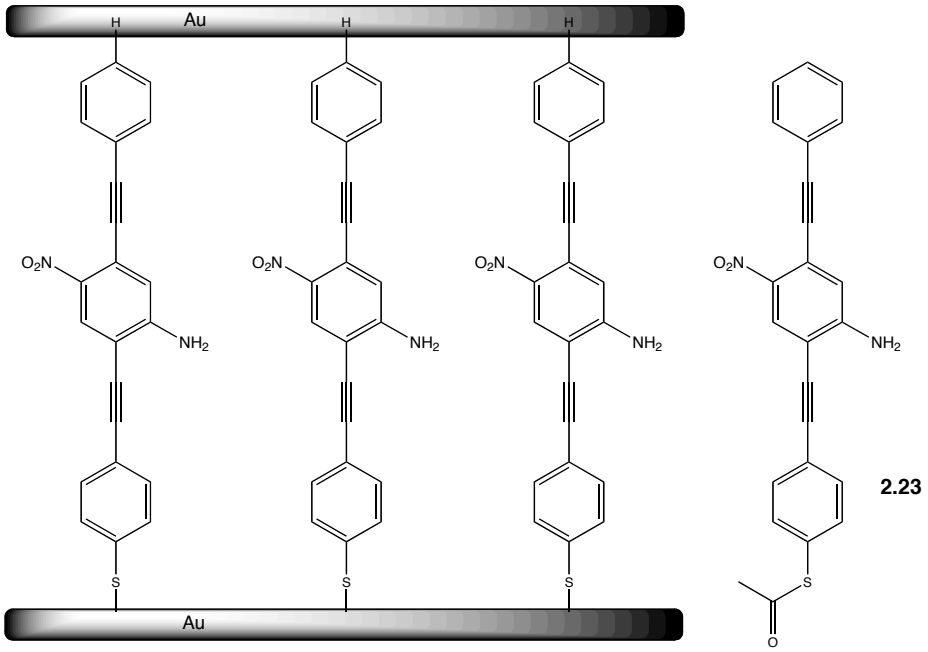

Figure 2.12 Compound **2.23** free and sandwiched in a gold junction.

The authors rationalize the NDR behavior of **2.23** based on a two-step reduction process that modifies charge transport through the molecule. As the voltage increases, a one-electron reduction takes place, which supplies a charge carrier for the conductive state. A further increase in voltage results in a second reduction to the dianion, which blocks the current, establishing the insulating state. The fact that NDR behavior was not observed in the absence of the nitro group indicates the importance of this functionality in facilitating the flow of current.

DFT computational investigations were conducted on these systems by Stokbro and co-workers to elucidate the basis of the NDR behavior.[44] Their work suggested that an intermolecular interaction between a nitro group and the phenyl ring of the neighboring molecule in the self-assembled monolayer is the cause for the NDR behavior. This assertion is further supported by the fact that the NDR was not observed in single molecule experiments.

Based on Tour's results, Mayor and co-workers decided to investigate a single macrocyclic structure containing both the central bis(phenylethynyl) core and the

neighboring phenyl group. In this manner, the intermolecular interaction postulated by Stokbro and co-workers becomes an intramolecular interaction, and the conducting properties of the macrocycle can be investigated in single-molecule experiments.

Mayor and co-workers synthesized macrocycles **2.21** and **2.22** based on previously established acetylene scaffolding strategies. Whereas **2.21** has one nitro group in close proximity to an adjacent phenyl ring, there are two such interactions in the case of **2.22**. The authors point out that the "handle" bridging the two terminal rings consists of the poorly conjugated *meta*-diethynyl unit. Therefore, the current is still expected to travel predominantly through the central rod.

Mayor and co-workers attempted to grow crystals of *tert*-butyl protected dithiol **2.24** in order to investigate the structural relationship between the rod and handle. In efforts to increase the solubility of the compounds, a sample was dissolved in toluene and gently heated, which caused the solution to change from yellow to orange. The suspected decomposition product was determined from single crystal X-ray analysis to be isatogen **2.25**. A crystal structure was obtained, indicating that an intramolecular rearrangement between the nitro group and acetylene took place to form the heterocycle isatogen derivative (Figure 2.13).

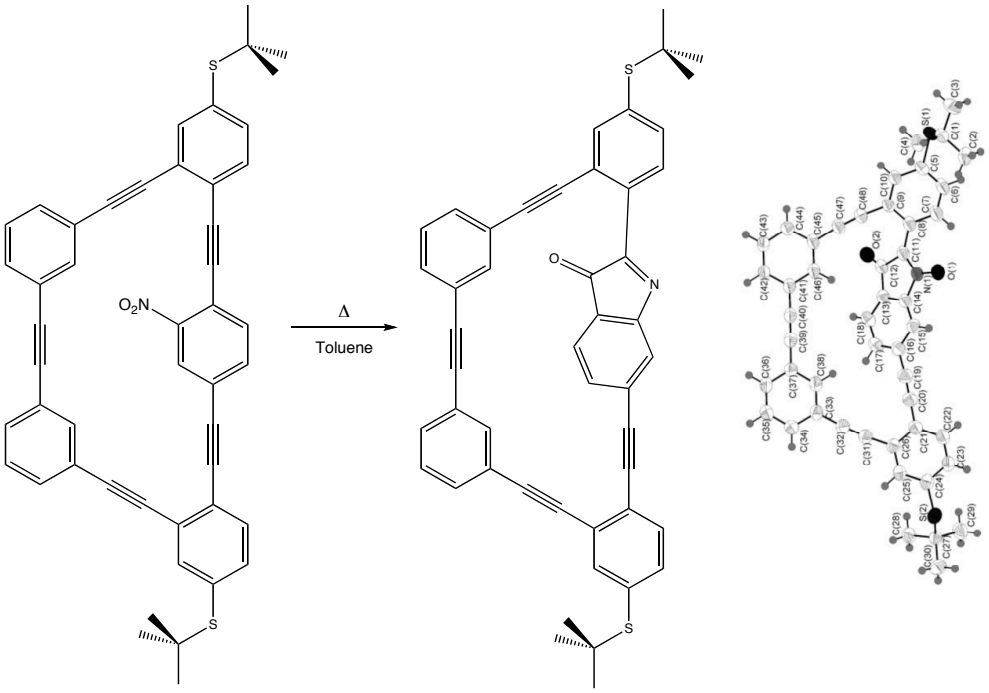

Figure 2.13 Intramolecular rearrangement of **2.24** and crystal structure of rearrangement product **2.25**.

The authors state that the rearrangement indicates the delicate thermal stability of the *ortho*-nitro phenyl ethynyl substructure. Even without heating, the yellow solution of the original macrocycle turned orange within several weeks. Mayor and co-workers state that this rearrangement should also be considered as a means for tuning the electronic properties.

Mayor has demonstrated a successful synthesis of a prototype for a single molecule electronic device. Investigations of the conductance properties of this molecule and related derivatives are ongoing.[45] This work serves as another example of potential applications of an aryl alkyne rotor integrated into an electrical device.

2.6.3 Surface Mounted Molecular Rotors

Previous examples have shown rotors in solution and solid phase but Michl and co-workers were able to demonstrate rotation of a polar and dipolar rotor mounted on a gold surface, with the axle parallel to the surface (Figure 2.14).[46]

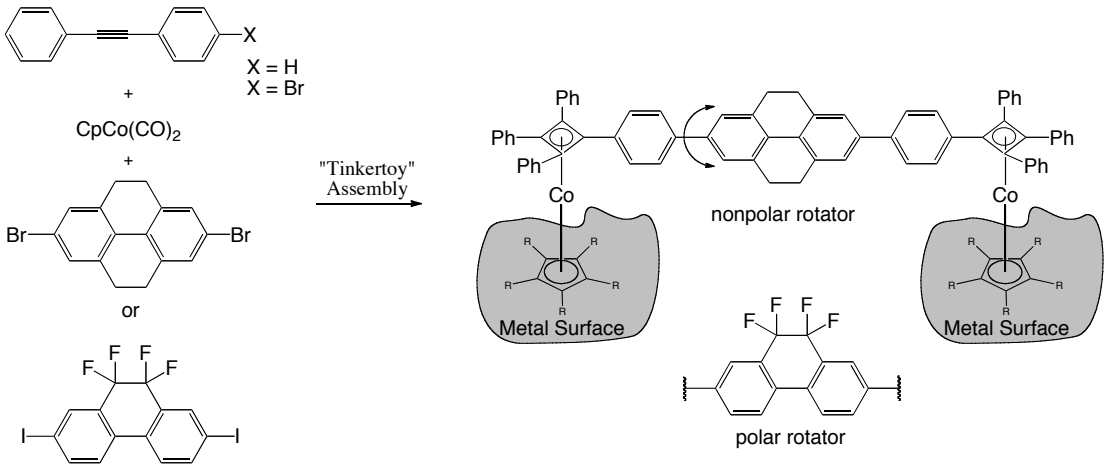

Figure 2.14 "Tinkertoy"[47] assembly of altitudinal molecular rotor with nonpolar and polar rotator.

After the rotors were absorbed on a gold surface, STM imaging was used to characterize the structure and monitor molecular dynamics. In order to detect whether the rotators in the surface-mounted rotor were turning, the STM tip was used to measure the work function between the tip and the surface. Conclusions were that one-third of the surface-mounted rotors are free to flip in the direction of their dipole in response to an external electric field and turning rapidly and randomly at room temperature. The other two-thirds of the rotors appear to be in a blocked state but over time can change to a free state, or from a free state to a blocked state. This work represents an advance in surface-mounted rotors and the prospect to construct closely packed surface-mounted devices that could exhibit correlated motion as a result of an external stimuli (magnetic, electric, or physical).

2.7 Conclusions

Bond rotation is one of the most basic dynamic parameters for the understanding of molecular systems. The initial determination of the rotational profiles of ethane and biphenyl provides the basis for the conformational analysis in a wide array of complex molecules. As the example of tolan shows, rotational barriers in aryl alkynes are quite low. However, by varying certain parameters, the rotational barriers could be modulated in the congested aryl alkynes prepared by Toyota as well as the turnstile systems synthesized by Moore (Table 2.2). The turnstile system of Shinkai and co-workers is structurally quite similar to the molecules synthesized by the Moore group; however, in Shinkai's system, the researchers observed a response in the turnstile molecule due to an external stimulus. The transition from the observation of physical properties to the investigation of response to a stimulus is an important step towards the rational design of functional molecular devices.

The final three examples all aim to take advantage of bond rotation in order to accomplish mechanical or electrical work. The work of Garcia-Garibay in pursuit of a responsive crystalline molecular assembly and the efforts by Feringa towards the design of a molecular motor both enter the realm of rational design. The work of Mayor is primarily interested in the conductance properties of aryl alkynes and the possibility of bond rotation inducing on-off switching events. Lastly, the Michl group was able to assembly a more complex rotor device and mount it to a metal surface. Their work also expanded some to the experimental techniques to describe the rotator movement and some the difficulties with such a dynamic process in a surface-mounted device.

The field of molecular machines is in its infancy, and efforts towards the rational design of functional molecular assemblies are critical to its development.

However, this area of research must first rely on fundamental studies of simple molecular systems before progressing towards the construction of complex assemblies. A strong foundation in the fundamental factors influencing molecular motion is essential to realizing true molecular machines.

Table 2.2 'Freely' Rotating Nonmetallic Rotors

Molecular System	Barrier to rotation (kcal/mol)	Ref.
Ethane	2.9	1
Biphenyl	2.0	4
Diphenylacetylene	0.58	11
Toyota alkynes	10.1-18.1	14-20
Bedard/Moore turnstile	13.4	21
Garcia-Garibay rotors	4.1-12.8	28-31
Feringa systems	22.7-26.2	37-39

2.10 References:

[1] (a) Smith, L.G. *J. Chem. Phys.* **1949**, *17,* 139-167. (b) Weiss, S.; Leroi, G.E. *J. Chem. Phys.* **1968**, *48,* 962-967. (c) Hirota, E.; Saito, S.; Endo, Y. *J. Chem. Phys.* **1979**, *71,* 1183-1187.

[2] Pitzer, R.M. *Acc. Chem. Res.* **1983**, *16*, 207-210.

[3] Pophristic, V.; Goodman, L. *Nature,* **2001**, *411,* 565-568.

[4] Katon, J.E.; Lippincott, E.R. *Spectrochim. Acta.* **1959**, *15,* 627-650.

[5] Charbonneau, G.-P.; Delugeard, Y. *Acta. Crystallogr. B,* **1976**, *32,* 1420-1423.

[6] (a) Almenningen, A.; Bastiansen, O.; Fernholt, L.; Cyvin, B.N.; Cyvin, S.J.; Samdal, S. *J. Mol. Struct.* **1985**, *128*, 59-76. (b) Almenningen, A.; Bastiansen, O.; Fernholt, L.; Gundersen, S.; Kloster-Jensen, E.;Cyvin, B.N.; Cyvin, S.J.; Samdal, S. Shancke, A. *J. Mol. Struct.* **1985**, *128*, 77-93. (c) Almenningen, A.; Bastiansen, O.; Fernholt, L.; Gundersen, S.; Samdal, S. Shancke, A. *J. Mol. Struct.* **1985**, *128*, 95-114.

[7] Grein, F. *J. Phys. Chem. A,* **2002**, *106,* 3823-3827.

[8] Leroux, F. *ChemBioChem*, **2004**, *5*, 644-649.

[9] Aldridge, B.; DeLuca, G.; Edgar, M.; Emsley, J.W.; Furby, M.I.C.; Webster, M. *Liquid Cryst.* **1998**, *24,* 569-581.

[10] Liberles, A.; Matlosz, B. *J. Org. Chem.* **1971**, *36,* 2710-2713.

[11] Xu, D.; Cooksy, A.L. *J. Mol. Struct.-THEOCHEM*, **2007**, *815*, 119-125.

[12] Robertson, J.M.; Woodward, I. *Proc. R. Soc. A,* **1938**, *164,* 436-446.

[13] Okuyama, K.; Hasegawa, T.; Ito, M.; Mikami, N. *J. Phys Chem.* **1984**, *88*, 1711-1716.

[14] Toyota, S.; Yamamori, T.; Asakura, M.; Oki, M. *Bull. Chem. Soc. Jpn.* **2000**, *73,* 205-213.

[15] (a) Papoušek, D. *J. Mol. Spectrosc*. **1968**, *28,* 161-190. (b) Olson, W.B.; Papoušek, D. *J. Mol. Spectrosc*. **1971**, *37,* 527-534.

[16] Toyota, S.; Yamamori, T.; Makino, T.; Oki, M. *Bull. Chem. Soc. Jpn*. **2000**, *73*, 2591-2597.

[17] Toyota, S.; Yamamori, T.; Makino, T. *Tetrahedron* **2001**, *57,* 3521-3528.

[18] Toyota, S.; Iida, T.; Kunizane, C.; Tanifuji, N.; Yoshida, Y. *Org. Biomol. Chem*. **2003**, *1,* 2298-2302.

[19] Toyota, S.; Makino, T. *Tetrahedron Lett*. **2003**, *44,* 7775-7778.

[20] Toyota, S.; Yanagihara, T.; Yoshida, Y.; Goichi, M. *Bull. Chem. Soc. Jpn.* **2005**, *78,* 1351-1353.

[21] Bedard, T.C.; Moore, J.S. *J. Am. Chem. Soc*. **1995**, *117,* 10662-10671.

[22] Hirata, O.; Takeuchi, M.; Shinkai, S. *Chem. Commun*. **2005**, 3805-3807.

[23] Garcia-Garibay, M.A. *Proc. Natl. Acad. Sci. U.S.A*. **2005**, *102*, 10771-10776.

[24] Khuong, T.-A.V.; Nuñez, J.E.; Godinez, C.E.; Garcia-Garibay, M.A. *Acc. Chem. Res*. **2006**, *39,* 413-422.

[25] Pines, A.; Gibby, M.G.; Waugh, J.S. *J. Chem. Phys*. **1973**, *59,* 569-590.

[26] Clarke, L.I.; Horinek, D.; Kottas, G.S.; Varaska, N.; Magnera, T.F., Hinderer, T.P.; Horansky, R.D.; Michl, J.; Price, J.C. *Nanotechnology*, **2002**, *13*, 533-540.

[27] Dominguez, Z.; Dang, H.; Strouse, M.J.; Garcia-Garibay, M.A. *J. Am. Chem. Soc*. **2002**, *124,* 2398-2399.

[28] Dominguez, Z.; Dang, H.; Strouse, M.J.; Garcia-Garibay, M.A. *J. Am. Chem. Soc*. **2002**, *124,* 7719-7727.

[29] Godinez, C.E.; Zepeda, G.; Garcia-Garibay, M.A. *J. Am. Chem. Soc*. **2002**, *124,* 4701-4707.

[30] Dominguez, Z.; Khoung, T.-A.V.; Dang, H.; Sanrame, C.N.; Nuñez, J.E.; Garcia-Garibay, M.A. *J. Am. Chem. Soc*. **2003**, *125,* 8827-8837.

[31] Karlen, S.; Ortiz, R.; Chapman, O.; Garcia-Garibay, M.A. *J. Am. Chem. Soc*. **2005**, *127*, 6554-6555.

[32] Kelly, T.R.; Bowyer, M.C.; Bhaskar, K.V.; Bebbington, D.; Garcia, A.; Lang, F.; Kim, M.H.; Jette, M.P. *J. Am. Chem. Soc.* **1994**, *116,* 3657-3658.

[33] (a) Kilway, K.V.; Siegel, J.S. *J. Am. Chem Soc.* **1991**, *113,* 2332-2333. (b) Kilway, K.V.; Siegel, J.S. *Organometallics* **1992**, *11,* 1426-1427.

[34] Iverson, D.J.; Hunter, G.; Blount, J.F.; Damewood, J.R., Jr.; Mislow, K. *J. Am. Chem. Soc*. **1981**, *103,* 6073-6083.

[35] Kilway, K.V.; Siegel, J.S. *J. Am. Chem. Soc*. **1992**, *114,* 255-261.

[36] Kelly, T.R.; De Silva, H.; Silva, R.A. *Nature*, **1999**, *401*, 150-152.

[37] Koumura, N.; Zijlstra, R.W.J.; van Delden, R.A.; Harada, N.; Feringa, B.L. *Nature*, **1999**, *401*, 152-155.

[38] Feringa, B.L; Jager, W.F.; de Lange, B. *J. Am. Chem. Soc*. **1991**, *113*, 5468-5470.

[39] Koumura, N.; Geertsema, E.M.; Meetsma, A.; Feringa, B.L. *J. Am. Chem. Soc.* **2000**, *122,* 12005-12006.

[40] Schoevaars, A.M.; Kruizinga, W.; Zijlstra, R.W.J.; Veldman, N.; Spek, A.L.; Feringa, B.L. *J. Org. Chem*. **1997**, *62,* 4943-4948.

[41] Błaszczyk, A.; Chadim, M.; von Hänisch, C.; Mayor, M. *Eur. J. Org. Chem.* **2006**, 3809-3825.

[42] Elbing, M.; Ochs, R.; Koentopp, M.; Fischer, M.; von Hänisch, C.; Weigend, F.; Evers, F.; Weber, H.B.; Mayor, M. *Proc. Natl. Acad. Sci. U.S.A*. **2005**, *102*, 8815-8820.

[43] (a) Chen, J.; Reed, M.A.; Rawlett, A.M.; Tour, J.M. *Science*, **1999**, *286,* 1550-1552. (b) Donhauser, Z.J.; Mantooth, B.A.; Kelly, K.F.; Bumm, L.A.; Monnell, J.D.; Stapleton, J.J.; Price, Jr., D.W.; Rawlett, A.M.; Allara, D.L.; Tour, J.M.; Weiss, P.S. *Science*, **2001**, *292*, 2303-2307.

[44] Taylor, J.; Brandbyge, M.; Stokbro, K. *Phys Rev. B*, **2003**, *68,* 121101-1-121101-4.

[45] Błaszczyk, A.; Fischer, M.; von Hänisch, C.; Mayor, M. *Eur. J. Org. Chem.* **2007**, 2630-2642.

[46] Zheng, X.; Mulcahy, M.E.; Horinek, D.; Galeotti, F.; Magnera, T.F.; Michl, J. *J. Am. Chem. Soc.* **2004**, *126*, 4550-4542.

[47] Tinkertoy is a trademark of Playskool, Inc., Pawtucket, RI 02862, and designates a toy construction set of wooden sticks insertable into connectors. This assembly concept was put forth by authors in ref. 46 for the construction of nanosize structures.

Chapter 3. Centrally Substituted *tert*-butyl Trioxatriangulene Building Blocks

3.1 Introduction

Bowl-shaped molecules stimulate interest due to their intriguing structural properties. Many researchers have made use of these "molecular bowls": serving as enzyme models,[1] providing a new basis for mesophases of liquid crystals,[2] facilitating the formation of highly reactive species[3] and acting as synthetic targets *en route* to novel structures like planar methane.[4] The molecular bowl morphology endows the structure with a concave and a convex surface.

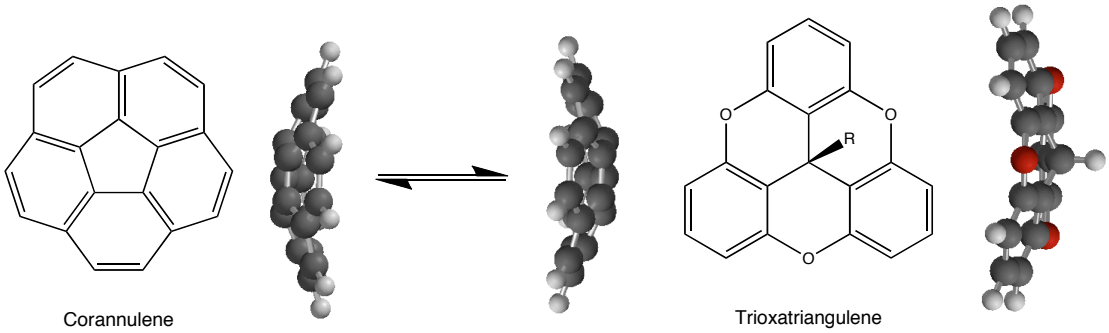

Figure 3.1 Flexible molecular bowl (corannulene) and a rigid molecular bowl (trioxatriangulene).

One can separate "molecular bowls" into two classes, those that can invert (flexible bowls) and those that cannot (rigid bowls) (Figure 3.1): bowl inversion exchanges these two surfaces. The interest outlined here is the investigation of molecular bowls that do not invert and do have high axial symmetry. The dibenzopyrene skeleton, called triangulene,[5] serves as the conceptual foundation upon which the design of these molecular bowls is based. The skeleton of triangulene consists of six benzene rings annulated in a triangle (Figure 3.2). Figure 3.3 illustrates the size of the oxa-bridged derivative with a volume of 291 $Å^3$ and an overall surface area of 283 $Å^2$.

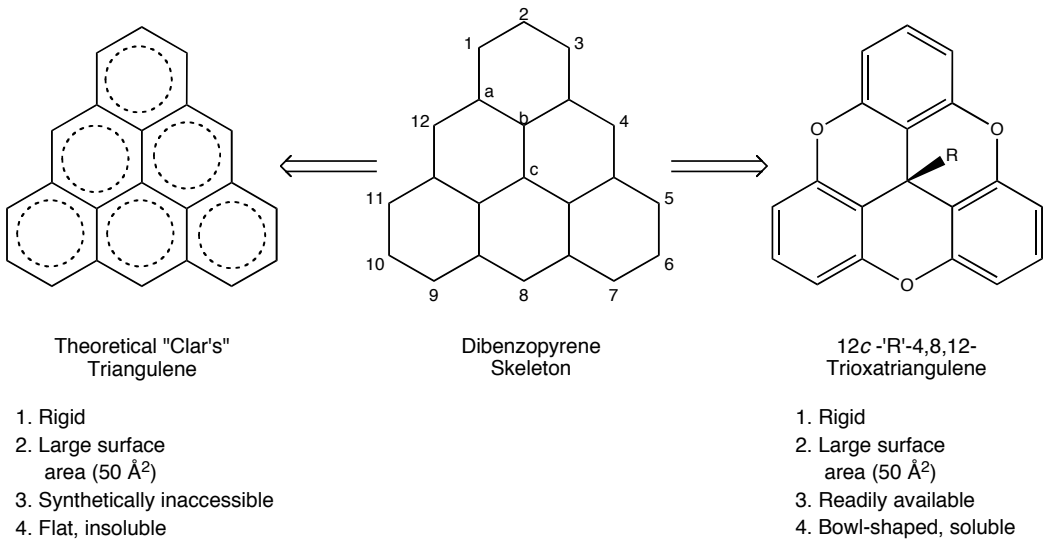

Figure 3.2 Triangulene nomenclature and design of a molecular building block.

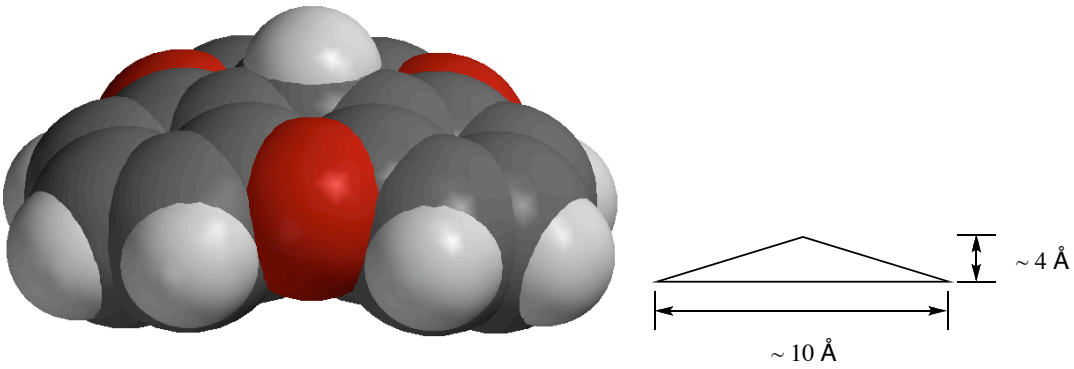

Figure 3.3 Space-filling model and van der Waals approximation of the trioxatriangulene molecule.

This dibenzopyrene skeleton was termed triangulene by Clar[5] and is predicted by Hückel MO theory to be a biradical.[6] Several derivatives of triangulene, with one or more sp^2 atoms replaced by sp^3 carbons or heteroatoms,[7] have appeared in the literature. The dibenzopyrene skeleton also suffices as a starting templete for a molecular building block due to its favourable characteristics.

Modifications of the oxygen bridged triangulene by addition of functionality to the central carbon and substitution onto the periphery have been investigated.[8] Addition of H to the central carbon results in the compound called trioxatriangulene, or also trioxatricornan,[9] and the parent hydrocarbon is then referred to as the

triangulene, or also tricornan. The triangular shape and the upward arch of the sides of the tricorn hats,[10] worn by gentlemen of the 17th and 18th centuries, makes an apparent resemblance with these centrally reduced triangulenes.

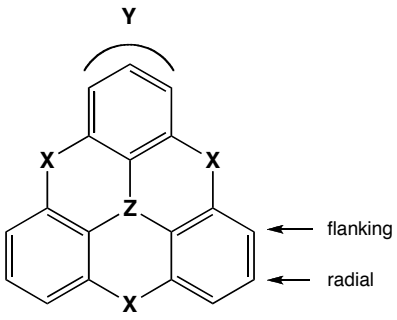

X (bridge)	**Z** (center)	**Y** (outer)
CO	CH, CCH_3	H
CMe_2	COH, C^+	CH_3, $C(CH_3)_3$
O	P	NH_2, $N(CH_2CH_3)_2$
$N(CH_2CH_3)_2$	N	Br
		$Si(CH_3)_3$

Figure 3.4 Some of the derivatives of triangulene. Effects of variation: **X** – mediates π electronics, **Z** – controls solubility, and **Y** – controls symmetry.

The triangulene skeleton has three variable regions, **X** for atoms 4, 8, 12 (the bridge); **Y** for atoms 1-3, 5-7, 9-11 (the rim); **Z** for atom 12*c* (the center) (Figure 3.4). Derivatives of triangulene principally consist of substitutions at the **X** and **Z** positions. The *ortho*-linking, or **X** position, modifications include ketones, dimethyl methylenes, and oxygens.[11] In this bridging region the electronic demands of the molecule can be regulated. Region **Y** encompasses the radial and flanking positions on the aromatic rings. In this region bridging arms and/or functionality can be attached to the molecule. Substitution in region **Y** also modifies the symmetry; radial substitution on each ring results in C_{3v} symmetry, whereas substitution of one flanking position from each ring results in C_3 or C_1 symmetry. Region **Z** stems directly from the 12*c* central atom and conversion of central atom from an sp^2 to an sp^3 hybridized atom transforms the planar triangulene structure into a rigid molecular bowl. This region can be extended to change the solubility of the molecule, or to attach it to a solid support.[12]

3.2 Synthesis

3.2.1 Introduction

The most easily accessible triangulene is the 4,8,12-trioxadibenzo[*cd*,*mn*]pyrene cation **3.1**, reported by Martin and Smith, which is obtained in just two steps starting from commercially available 1,3-dimethoxybenzene (Scheme 3.1).[13] With a central sp^3 hybridized atom, it is one of the simplest hydrocarbon derivatives of triangulene. The worked contained herein utilizes the triangulene with oxygen in the **X** positions (Figure 3.4).

3.2.2 Synthesis of the Trioxatricornan Cation 3.1

The initial anionic intermediate is formed through deprotonation of the 2 position of 1,3-dimethoxybenzene by ortholithiation with *t*-butyllithium in tetrahydrofuran. The solvent is exchanged for benzene and the triaryl carbinol forms with the addition of ethyl chloroformate. The extremely hindered *tris*(di-*ortho*-methoxyphenyl)methanol can be purified by recrystallization from ethyl acetate. To form the desired Martin's salt **3.1**, the triarylcarbinol is heated at 205 °C for 30 minutes in pyridinium hydrochloride. The resulting carbocation **3.1** precipitates from water with the addition of tetrafluoroboric acid.

Scheme 3.1

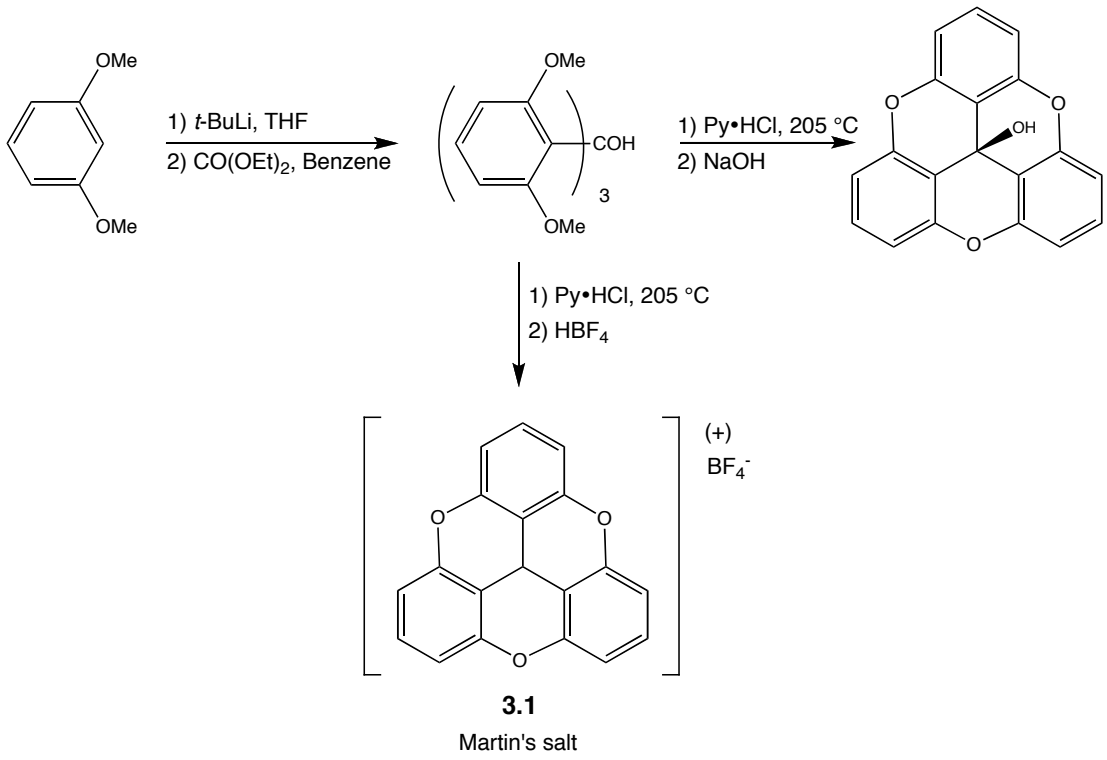

3.1
Martin's salt

3.2.3 Modifications of the Trioxatricornan Center (Z)

Functionality appended onto region **Z**, which is centered at the convex side of the molecule, disrupts the planarity of **3.1**, converting the central (12*c*) carbon from an sp^2 (planar) to an sp^3 (pyramidal) carbon. This molecular transformation serves to alter the solubility of the molecule or attach it to a solid support. Extending lipophilic functional groups off of spherical macrocages has previously been shown to enhance drastically the solubility of the macrocage, in organic solvents.[14] Similiarly, appending hydrophilic functional groups onto the molecule in a cyclophane construct has yielded water-soluble macrocages.[15] Similar effects were expected to occur by substitution at region **Z**.

Modification of region **Z** in **3.1** is based on nucleophilic reactions at carbon 12*c* of Martin's salt **3.1** (Scheme 3.2). Precedence for this chemistry comes from studies on the trityl cation that alkylates weakly acidic compounds such as acetone and acetonitrile in the presence of a hindered base.[16] Furthermore, triphenylmethanol

reacts with trimethyl aluminum to form triphenylethane.[17] Indeed, stabilized carbocations are known to react with nucleophilic organometallic reagents in general.[18]

In an earlier study, acetone has been shown to nucleophilic attack **3.1** when the two are refluxed together in the presence of triethylamine yielding **3.2**. Also, reagents such as methyllithium, vinyl grignard and allyl grignard react with compound **3.1** in dry tetrahydrofuran to place a methyl **3.3** (73 %), vinyl **3.4** (68 %), or allyl **3.5** (75 %) group, respectively, at the 12*c* position (Scheme 3.2).[9] The reaction with methyl lithium was found to be particularly facile and provides a model molecule **3.3**, on which further modifications of region **Y** could be performed.

Scheme 3.2

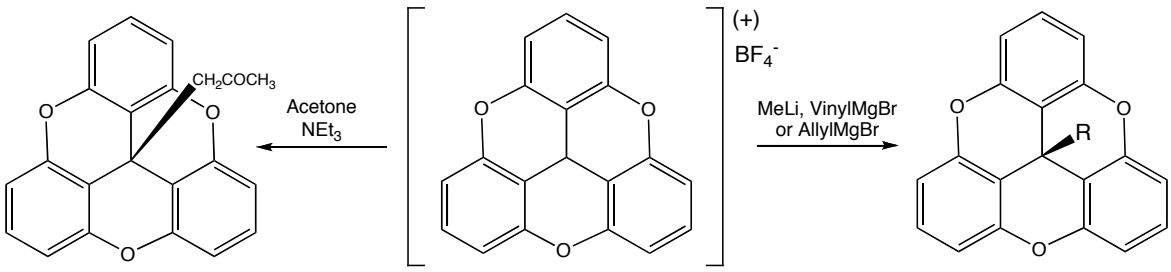

3.2

3.1
Martin's salt

3.3 R = Me
3.4 R = vinyl
3.5 R = allyl

As previously stated, the general scheme for placing a desired alkyl group, or functionality, on the central (12*c*) carbon uses nucleophilic addition. With Martin's salt **3.1** as the starting point, an obvious choice for bond formation to the central carbon is alkylation by addition of an anion. This quenching of the cation of trioxatricornan was the method of choice for formation of the 12*c*-methyl, -ethyl, -isopropyl, -adamantyl, -benzyl, -allyl, -vinyl, -phenyl, -ethynyl, and -iodo substitutions.[9] Separation of the inorganic salt byproduct by extraction with water was facile and thus many compounds were readily available.

It was also reported that the nucleophilic addition approach to the synthesis yielded a surprise in four cases. The anionic synthetic equivalent of the acetyl group, made from *n*-butyllithium and 2-methyl-1,3-dithiane, was added to Martin's salt **3.1** under appropriate conditions with no adddition on the central carbon 12*c*. Other anions chosen, such as *t*-buytllithium, potassium *t*-butoxide, and potassium 1-adamantoxide also failed to add to Martin's salt **3.1**. In each of these cases, steric repulsion was assumed to be the overriding reason for the results. The steric argument was given support by the observation that none of the CPK models of trioxatricornan with these bulky substituents could be constructed.[19]

Extension of a molecular bowl, derived from Martin's salt **3.1**, included the synthesis of several *para*-substituted benzylic derivatives. Several difficulties were reported in an attempt to form the Grignard from the *p*-methoxybenzyl chloride and subsequently producing very high yields of the Wurtz coupled dibenzyl type product.[20] An effort was made to reverse the reaction by forming the anion of Martin's salt **3.1** and adding in the *p*-methoxybenzyl chloride. The trioxatricornan anion **3.7** was formed by first creating the hydride from Martin's salt **3.1** with sodium borohydride, then deprotonating this position with *n*-buytllithium (Scheme 3.3). The desired 12*c*-(4-methoxybenzyl) trioxatricornan **3.8** was formed but in very low yields. A more efficient route to create the desired *p*-substituted benzyl trioxatricornan was subsequently pursued.

Scheme 3.3

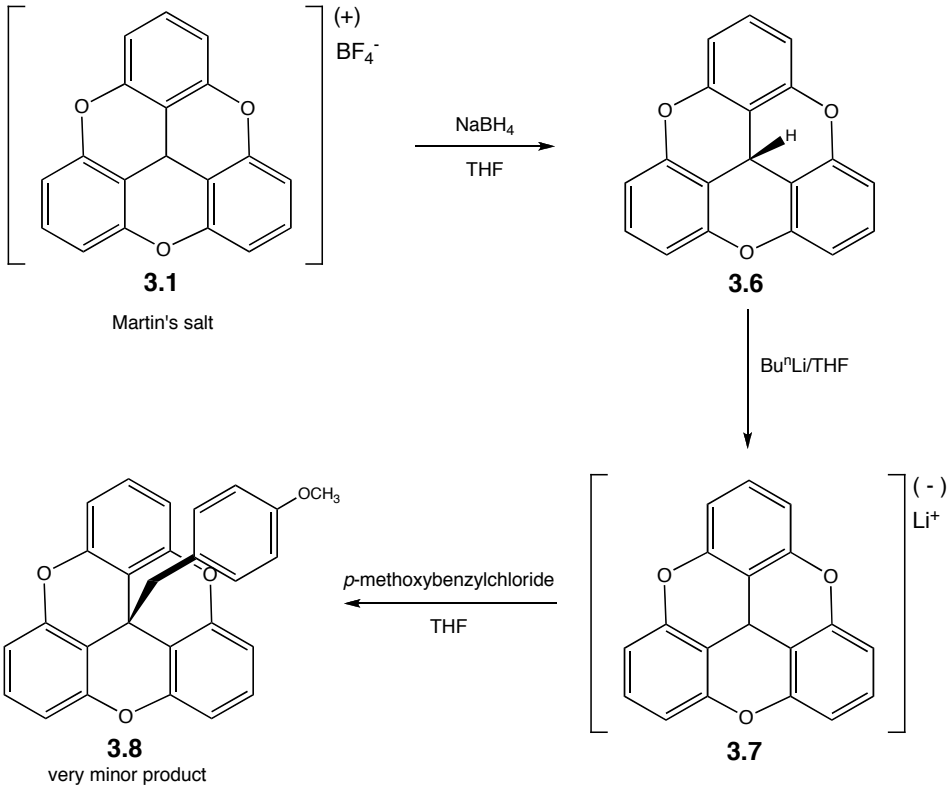

Having explored both the cationic and anionic reactivity of the trioxatricornan, the radical character was described as the next reasonable approach.[20] Chromium mediated couplings of carbon-halogen compounds are well known and assumed to have substantial radical-like character.[21] In order to attempt this reaction, 12*c*-iodo-trioxatricornan was required. 12*c*-Iodo-trioxatricornan **3.9** was formed by quenching the closure of the triarylmethanol in pyridinium hydrochloride with saturated potassium iodide instead of $HBF_4 \bullet OEt_2$ (Scheme 3.4).

Scheme 3.4

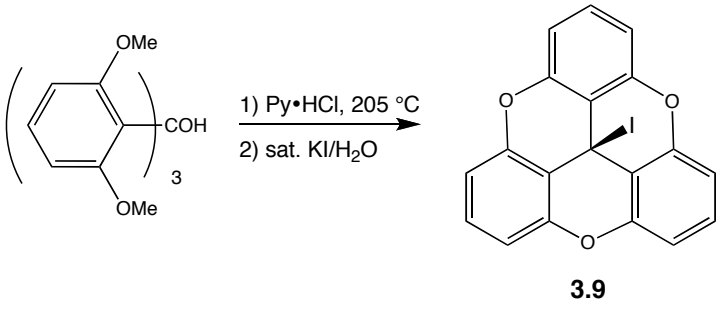

The chromium mediated coupling occurred when a third of an equivalent of the iodo-trioxatricornan **3.9** was added to chromium(II) chloride. One third of an equivalent of *p*-bromobenzyl bromide was then added to the mixture. After stirring for two days, the desired product 12*c*-(4-bromobenzyl)-4,8,12-trioxatricornan was obtained. Similar methodology was employed for the creation of the methoxy substituted benzyl trioxatricornan, but the reaction did not succeed with the *p*-nitrile, the *p*-nitro, or the *p*-acetyl benzyl halides. Creating the latter products required an extended route by mixing the anion of the *p*-bromobenzyl compound with *N*-acylaziridine.

These methods considerably extended the list of known substitutions at the **Z** position of trioxatricornan (Figure 3.5).[20] Specifically, the central carbon 12*c* of trioxatricornan, which is sp^3 hybridized, is bound to the *s* orbital of hydrogen; the sp^3 orbitals of methyl, ethyl (a primary carbon), isopropyl (a secondary carbon), and 1-adamantyl (a tertiary carbon); the allylic orbital of 3-propenyl, the α carbonyl orbital of acetone, and the benzylic orbital of phenylmethyl; the sp^2 orbitals of ethenyl and phenyl; and the *sp* orbital of the ethynyl.

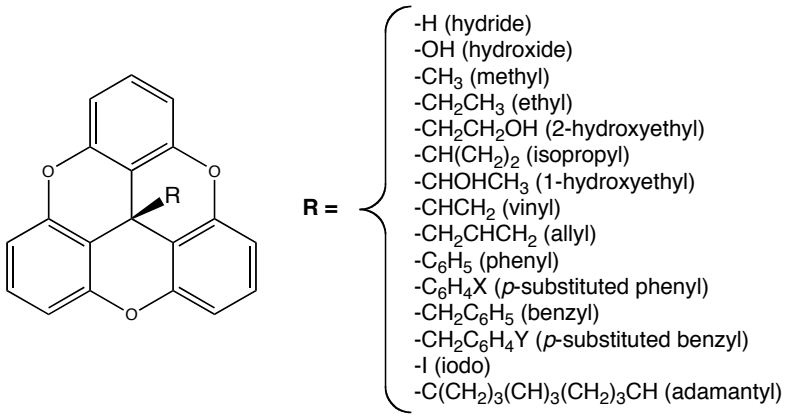

Figure 3.5 Substitutions at the central carbon of trioxatricornan.

3.2.4 Modifications of the Trioxatricornan Rim (Y)

With the methyl adduct **3.3**, there are many different pathways for incorporation of appendages. Appendages could be used to affix cage-forming arms onto the perimeter of the trioxatricornan[22] or attachment to a surface.

3.2.4.1 Electrophilic Aromatic Substitution at the Trioxatricornan Rim of 3.3

It was reported that incorporation of three dissymmetrically disposed "amino-handles" on **3.3** was achieved by electrophilic nitration, followed by catalytic hydrogenation of the tri-nitrated molecules (Scheme 3.5).[9] The two regioisomeric tri-amines, of C_1 (**3.10**) and C_3 (**3.11**) symmetry, resulting from substitution at one flanking site on each benzene ring, were obtained in approximately a statistical ratio of 3:1 with a total yield of 36 %, based on **3.3**.

Another route into chiral molecules involved the electrophilic bromination of **3.3** (Scheme 3.5). Bromination of **3.3** in neat glacial acetic acid produced the C_1/C_3 (**3.12**, **3.13**) mixture with only a small amount of over brominated product, in a 95 % yield of the isomeric mixture. [23] Crystallization from acetone yielded the less soluble C_1 isomer **3.12** in a 42 % yield. The C_3 isomer **3.13** was recovered from the filtrate, or *ca*. 60-70 % yield in C_3 isomer.

Scheme 3.5

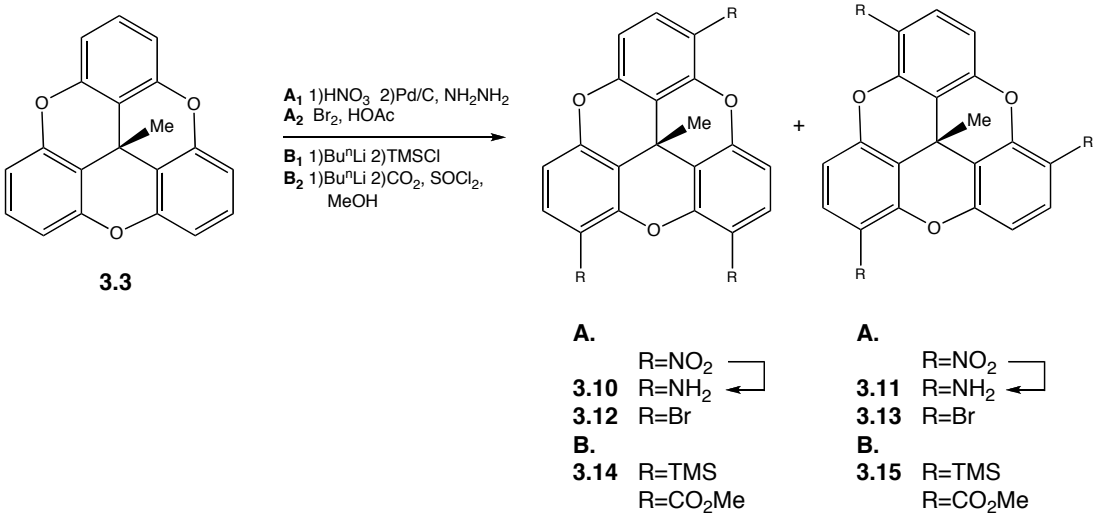

3.2.4.2 Ortholithiation at the Trioxatricornan Rim of 3.3

A second approach to incorporate "linking-sites", involved the deprotonation of **3.3**, under ortholithiation conditions, followed by electrophilic quench. [24] This type of reaction has considerable precedence, and many heteroatom-directed ortholithiations have been reported in the literature, oxygen being among the most common directing group.[25] In 1944 Gilman and Gorsich showed that dibenzofuran, which contains no highly acidic hydrogens, reacts with *n*-butyllithium in diethyl ether to yield 4-dibenzofuryllithium (Reaction 1).[26] In a related study, Gilman also reported that diphenyl ether can be deprotonated in the 2-position or bis-deprotonated in the 2,2'-positions when treated with excess *n*-butyllithium.[27]

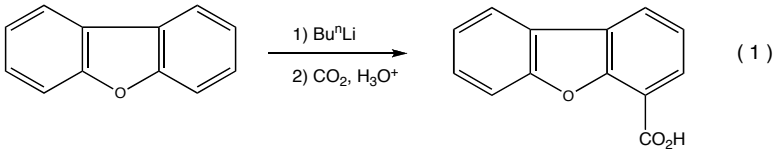

(1)

Treatment of **3.3** with excess *n*-butyllithium in tetrahydrofuran followed by quench with chlorotrimethylsilane, resulted in only one deprotonation per aromatic unit and the directing power of the oxygens limits the number of regioisomeric products to the C_1, **3.14**, and C_3, **3.15**, isomers, which were obtained in *ca*. 80 % yield (Scheme 3.5). Treatment of the trimethylsilane-mixture **3.14** and **3.15** with bromine, in a subsequent step, yielded the corresponding tribromides **3.12,** isolated in 51 % yield, based on **3.3**.

Carbon dioxide quench of the tri-deprotonated **3.3** gave a low yield of the corresponding mixture of C_1 and C_3 acids. The lower yield, compared to the chlorotrimethylsilane quench, was likely due to competing polymerization reactions where an initially formed carboxylic acid reacts with unquenched aryllithiate to tie together two molecules *via* a ketone (Reactions 2 and 3).[28] It was further reported that there was the formation of an insoluble material from the CO_2 quench, which was

assumed to be polymeric material. For separation and analysis, the crude acid mixture was converted into the corresponding methyl esters.

$$C_6H_5Li + CO_2 \longrightarrow C_6H_5CO_2Li \quad (2)$$

$$C_6H_5CO_2Li + C_6H_5Li \longrightarrow [\text{Intermediate}] \xrightarrow{H_2O} (C_6H_5)_2CO \quad (3)$$

3.2.4.3 Symmetry Analysis of Trioxatricornan 3.3 and the C_3-symmetric Trioxatricornan Derivative 3.11

A symmetry analysis of *cent*-methyltrioxatricornan **3.3** and reveals that; H_3 and H_5 are enantiotopic (related by transverse plane, σ) and H_3 and H_7 are homotopic (related by a three-fold axis, C_3) (Figure 3.6). The enantioiotopic *trios*, H_3, H_7, H_{11} and H_1, H_5, H_9, are also related by a three-fold axis. The absolute configuration of these unusual dissymmetric molecules can be further elaborated.

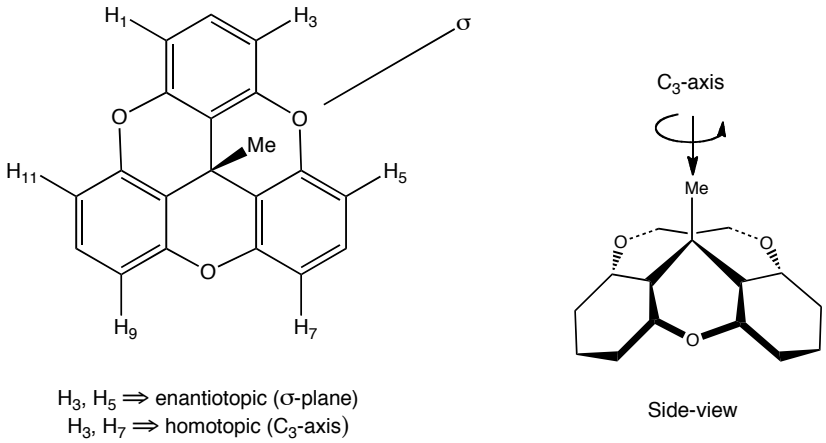

Figure 3.6 Symmetry analysis of *cent*-methyltrioxatricornan **3.3**.

An analogous system to the trioxatricornan **3.3** may be the crown-shaped cyclophane cyclotriveratrylene, CTV or hexamethoxytribenzocyclononene (Figure 3.7). According to the Cahn Ingold Prelog (CIP) system of molecular chirality,[29] the helical C_3 isomers of the crown-shaped CTV are classified as conformers, and they are therefore designated according to the helicity rules with *M* and *P*.[30]

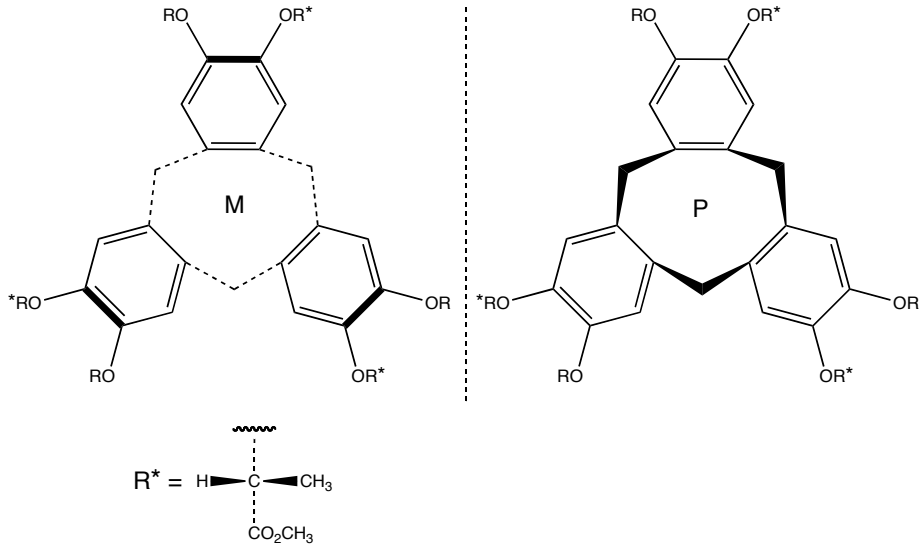

Figure 3.7 Classification of the cyclotriveratrylene conformers.

The tri-substituted trioxatricornan isomers **3.10** and **3.11** are not conformers, and a different set of CIP rules should be used in this system. In this case the central 'chiral centre' contains one three-fold axis as its only symmetry (C_3). By connecting the next-neighbor atom in a cyclic sequence with three like bridges that have no transverse symmetry plane a precise description of the stereochemical relationship can be established.

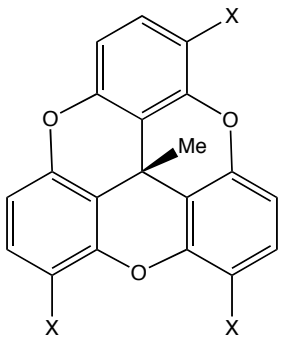

C_1 isomer

3.10

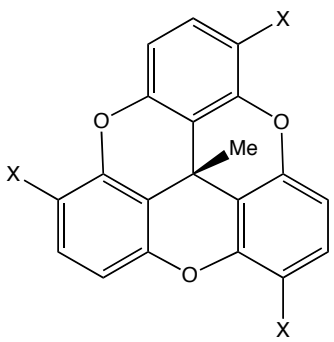

C_3 isomer

3.11

The CIP rules classifies the central carbon, 12*c*, in trioxatricornan **3.3** as an asymmetric center, and the configurations are assigned with *R* and *S* depending on the priority of substitution around the central carbon (Figure 3.8). The substituent of lowest priority, the methyl group, is turned away from the observer, and one of the

neighboring aromatic carbons is arbitrarily assigned the highest priority, a_1. The carbon of priority two, a_2, is assigned by determining which one of the two carbons has the shortest outward path to a_1, following the outward path of highest priority, which is the shortest path past the substituent of high priority. The absolute configuration of trioxatricornan **3.11a** is assigned the *R-enantiomer* and trioxatricornan **3.11b** is assigned the *S-enantiomer*.

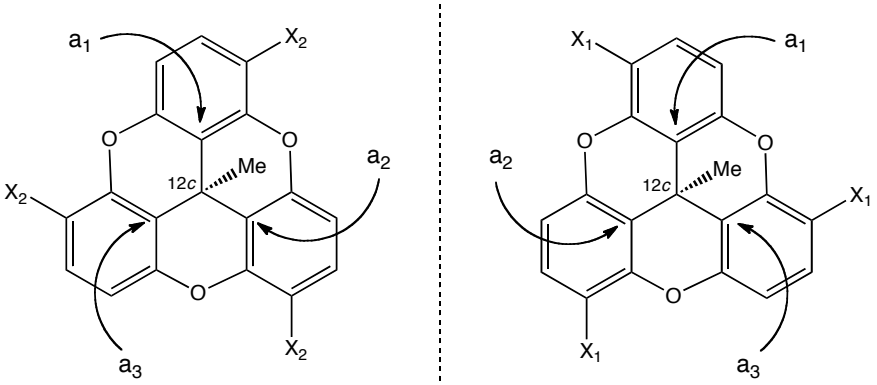

X > H ⇒ R-*enantiomer* **3.11a**

X > H ⇒ S-*enantiomer* **3.11b**

Figure 3.8 Absolute configuration of the C_3-symmetric derivatives **3.11** of *cent*-methyltrioxatricornan **3.3**.

3.2.4.4 Nucleophilic Aromatic Substitution at the Trioxatricornan Rim of 3.3

Initially, it was presumed that two pathways, electrophilic substitution and ortholithiation, were restricted to mixtures of C_3 and C_1 isomers, leaving the all-radial C_{3v} isomer unattainable. However, following the methodology taken for the synthesis of 3,5-dimethoxyaniline,[11] the crude mixture of tribromides **3.12**, **3.13** was mixed with sodium amide resulting in a triple cine-substitution.[31] This resulted in the formation of the C_{3v} symmetric 2,6,10-triamino-12*c*-methyltrioxatricornan **3.17** as the sole regioisomer, in 37 % yield, based on **3.3** (Scheme 3.6). The production of only one regioisomer, from a proposed benzyne intermediate, is a manifestation of the weaker basicity of the site *ortho* to the oxygen. This was also seen in the

ortholithiations previously presented. Similarly, dimethylamide reacts *via* a cine-substitution to yield the C_{3v} symmetric 2,6,10-tris(dimethylamino)-*cent*-methyltrioxatricornan **3.18**.[32]

Scheme 3.6

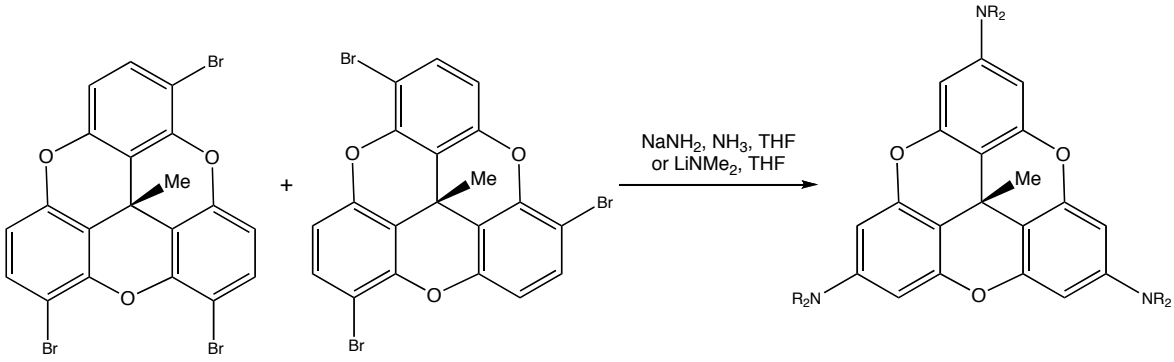

3.12 **3.13** **3.17** R = H, **3.18** R = Me

The spectroscopic results for the three "triamines" **3.17** (C_{3v}), **3.11** (C_3), and **3.10** (C_1) and the parent molecule *cent*-methyltrioxatricornan (**3.3**) clearly revealed the symmetry, of the parent trioxatricornan, and the pattern of substitution in the three triamines. The $^{13}C\{^1H\}$ NMR data was especially revealing; **3.17** and **3.3** (C_{3v}) have four aromatic carbon resonances, since the three aromatic rings are related by a three-fold axis and the carbons within each ring are half related by a mirrorplane that passes through the center to the corners of the triangle. In **3.11** (C_3) the mirror plane has been removed, resulting in six aromatic resonances, and in **3.10** (C_1), the three-fold axis was removed, resulting in eighteen aromatic carbon signals.

3.2.5 Modifications to the Appendage of the Trioxatricornan Rim (Y)

The amines derivatives serve as handles onto which bridging arms, *i.e.* macrocage formation, could be appended. Tosylation of the triamine, **3.17**, gave an entry point into alkylation chemistry at nitrogen, which was the synthetic procedure selected for appendage cage forming arms (Scheme 3.7).

Alkylation of **3.19** was affected by heating a mixture of the tosylated "triamine", alkylating agent, and potassium carbonate in dimethylformamide or acetone for 24 hours. The versatility of this alkylation scheme for introduction of extended functionality was shown by the successful synthesis of molecules with terminal alkyl -amines, -acetylenes, -hydroxides, -bromides, -carboxylate. The elaboration of these molecules into macrocages was reported.[8]

Scheme 3.7

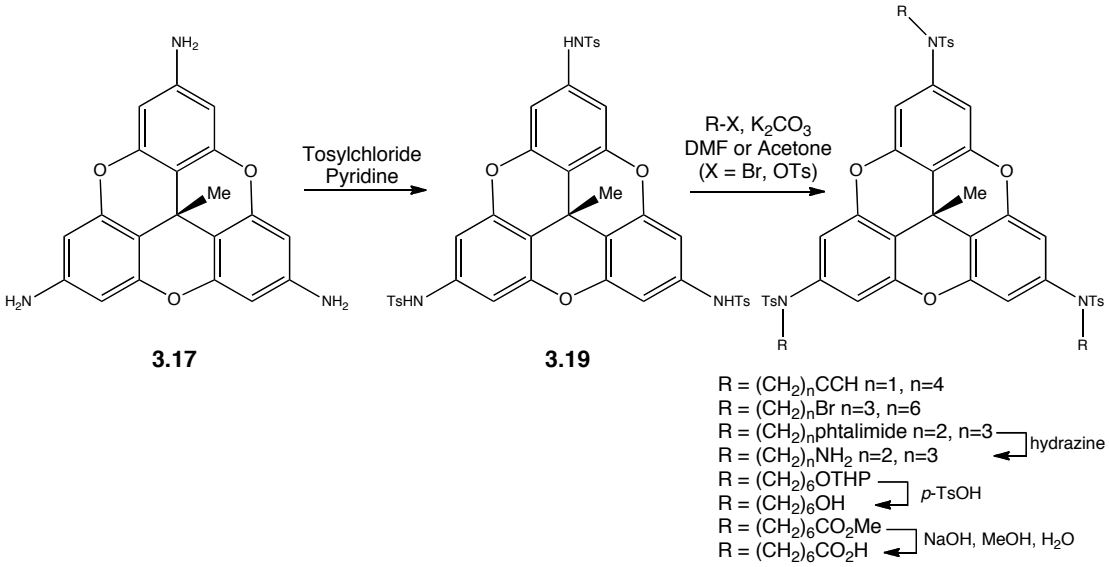

3.2.6 Synthesis of *tert*-butyl Trioxatriangulene – Rim (Y)

In order to improve the solubility of trioxatriangulene, Peters[33] outlined a synthesis of the *tert*-butyl functionalized trioxatriangulene starting from 2,6-dimethoxyphenol. The *tert*-butyl group was chosen as the preferred group since it would be expected to improve the solubility of the trioxatriangulene derivatives, plus it gives a singlet resonance peak in the ^{1}H spectra and its lack of benzylic hydrogens makes it chemically inert. The pseudo *para* (or radial) position was also the preferred site so that the symmetry of the molecule (C_{3v}) would be disrupted to a minimum degree.

Following the general scheme of Martin and Smith,[13] the 3,5-dimethoxybenzene precursor was prepared with the *tert*-butyl functionality in the *para* position. Initially, generating the *tert*-butyl group from the carboxylic acid was considered but a more favourable route involved starting with 3,5-dimethoxyphenol, adding the *tert*-butyl group[34] and subsequently cleaving of the phenylic hydroxyl group was pursued (Scheme 3.8).

Scheme 3.8

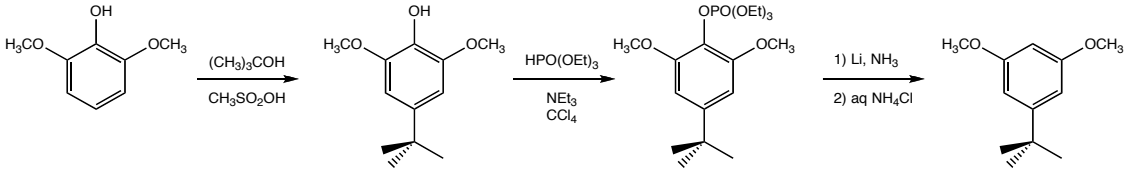

After bromination, three methods where investigated to lithiate the aryl species followed by a ketone electrophile to make the *tris*-carbinol. Direct lithiation, prior to the bromination, reportedly worked in only 56 % so bromination followed by the lithiation with *n*-butyllithium was found to be the preferred method (Scheme 3.9). Martin and Smith[13] reported the use of diethyl carbonate yielding 31 % of the carbinol. The use of phosgene[35] reported the best yield of 72 % and a simple quench with CO_2 yielded 20 % of the carbinol.[13]

Scheme 3.9

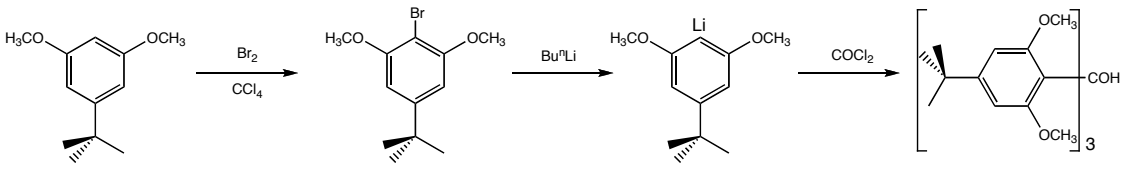

The conversion of the carbinol to the precursor of the *tert*-butyl trioxatriangulene cation was carried out in pyridine hydrochloride at a slightly lower temperature than reported with the parent trioxatriangulene[13] (Scheme 3.10). Also, a large excess of the pyridine hydrochloride was necessary to obtain good yields.

Finally, the treatment with trifluoromethanesulfonic acid results in the stable salt, 2,6,10-tri-*tert*-butylsesquixanthydryl triflate.

Scheme 3.10

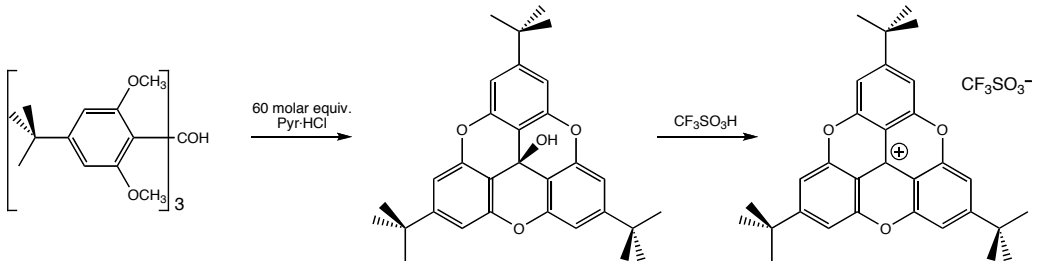

3.2.7 Conclusions

In sections **3.2.3** to **3.2.5**, Siegel, Lofthagen, and VernonClark utilized the concept of a molecular building block serving as a structural support for construction of polycyclic macrocages. In their case, the trioxatricornan building block was developed and substitution in two discreet regions was investigated. The central region **Z** serves to disrupt the planarity and alter the solubility of the molecule. The outer region **Y** serves to append functionality that is used for attachment of cage forming functionality and demonstrating routes into both chiral and achiral substituted derivatives.

The last section covered the synthesis of the *tert*-butyl trioxatriangulene cation. This trixoatriangulene derivative is an additional molecular building block with improved solubility and increased steric bulk that will be utilized in this study.

3.3 Physical Properties

The physical properties of triarylmethanols and triarylmethyl derivatives have been extensively studied for many years. Interest in these compounds has stemmed from the relatively high stability of their corresponding carbocations and free radicals.

3.3.1 Triarylmethanols and Triarylmethyl Cations

Triarylmethanols are generally considered to ionize in acid media *via* protonation followed by loss of water rather than the typical Bronsted-Lowry manner. Compounds ionizing in this manner have been termed secondary bases by Gold (Figure 3.9).[36]

$$Ar_3COH + HX \rightleftharpoons Ar_3COH_2^+X^- \rightleftharpoons Ar_3C^+X^- + H_2O$$

$$pK_{R^+} = pH + \log\frac{\left[Ar_3C^+X^-\right]}{\left[Ar_3COH\right]}$$

Figure 3.9 Acid equilibrium for triarylmethanols and pK_{R+} equation.

Martin and Smith[37] prepared 12*c*-hydroxy-4,8,12-trioxadibenzo[*cd*,*mn*] pryrene **3.20** which was found to have a pK_{R+} of 9.25. This is much more basic than the analogous tris(*p*-methoxyphenyl) methanol **3.21**, which has a pK_{R+} of only 0.82.[37] The increased stability was interpreted as being due to the ability of all the aromatic rings in **3.20** to exist in a coplanar configuration upon ionization and thus, maximize charge delocalization into the rings. Non-bridged species such as **3.21** must adopt a "propeller" conformation due to steric interactions between the *ortho* hydrogens.[38] The alternative conformation in **3.21** would likely be expected to reduce the degree of delocalization of the positive charge.

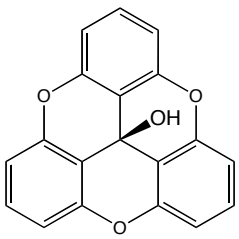

3.20

pK_{R+} **9.25**

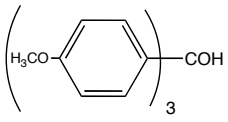

3.21

0.82

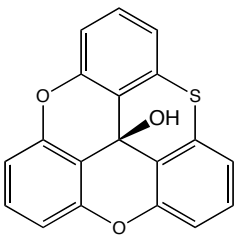

3.22

10.07

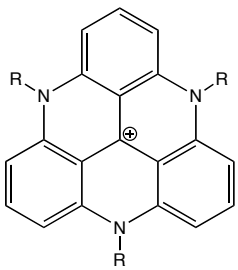

3.23

> 20
R = Me
R = *n*-Pr

Yamaye synthesized 4-thiasesquixanthdrol **3.22** which was found to have a pK_{R+} of 10.07 and was thus at the time the strongest base of this type known.[39] More recently, triazatriangulenium salts **3.23** have been prepared and found to have pK_{R+} values greater than 20.[40]

Based on Yamaye findings, the greater pK_{R+} of this methanol compared to **3.20** could be accounted for by the greater electron releasing ability of sulfur *versus* oxygen. The increased strain on the central sp^3 hybridized carbon in **3.22** produced by the replacement of oxygen with the larger sulfur atom may also be factor. Due to these factors it would be of interest to synthesize the trithiatriangulene system. One would expect that sulfur in each bridging **X** position would further stabilize the carbocation and the sulfur atoms should introduce more strain to force the central carbon into planar sp^2 hybridization. Additionally, oxidation of one or more of the sulfide bridges to the sulfoxide or sulfone state would be a convenient method of further varying the system to explore the relation between structure and physical property.

The ^{13}C NMR spectra of stable carbocations is also a powerful probe of the structure and charge density of the triarylmethyl cations. It was demonstrated that the chemical shifts of the central carbon in *para* substituted triarylmethyl cations correlates well with the charge density on the central carbon as calculated by CNDO method.[41] Olah *et al*. also correlated the chemical shift of the *para* carbon with its calculated charge density in a wide variety of neutral and cationic benzenes.[42] HMO calculated charge densities and ^{13}C chemical shifts reaffirm the conclusions of Martin and Smith[37] that the positive charge in the trioxatriangulene is extensively delocalized.

Table 3.1 Summary of TOTA Physical Characteristics

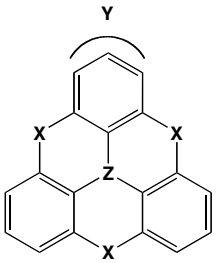

X	Y	Z	pK_R^+	λ_{max} (log ε)	Ref.
O	H	COH	9.05	280 (3.86) 288 (3.95)	37
O, O, N-Me O, O, N-^{n}Pr N-Me	H	C^+	23.7 14.5 19.4	519 (4.17) 539 (3.99) 556 (4.17)	40
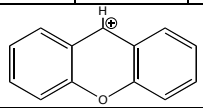			- 0.84	254 (4.55)	40

3.3.2 Hexaarylethanes

Triarylmethyl radicals and their dimers have been of considerable interest since Gomberg first prepared them in 1900.[43] After much debate Gomberg's dimer of the triphenylmethyl radical was assumed to be hexaphenylethane **3.24**.[44] This mode of dimerization of triarylmethyl radicals was accepted for over fifty years despite some now obvious discrepancies. Lankamp, Nauta, and MacLean reinvestigated the structures of these dimers because of the very large inhibitory effect of *para* alkyl substituents on dimer formation.[45] They concluded from the UV and ^{1}H NMR spectra that substituted methyl dimers, which readily dissociate into free radicals have a cyclohexadiene structure such as **3.25**. Staub confirmed this by synthesizing Gomberg's dimer from α-^{13}C triphenylchloromethane.[46] The ^{13}C NMR spectrum of the dimer included peaks at δ 62.4 (α-C) and δ 137.1 (α'-C).[47] Further evidence for structure **3.25** was provided by the ^{1}H NMR of the *para* deuterated dimer[46] and ^{1}H NMR decoupling.[48]

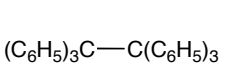

3.24

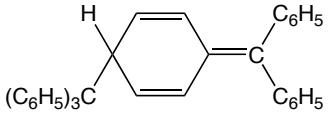

3.25

Although most triarylmethyl dimers exist in the cyclohexadiene form, some true hexaarylethanes are known. The "cross clamped" ethane **3.26** has the expected

ABCD splitting pattern in the ^{1}H NMR spectrum.[49] The "back clamped" ethane **3.27** was prepared by Schlenk[50] in 1910 and was shown to be a true hexaarylethane by Staab[51] by the ^{1}H and ^{13}C NMR spectra. Sabacky and Smith[52] prepared the trioxatriangulene dimer **3.28** that was found to be almost totally insoluble in organic solvents. Müller obtained a resolved ESR spectrum of the trioxatriangulene radical indicating the radical, rather than the dimer, is strongly favoured thermodynamically due to the high degree of delocalization of unpaired electron allowed by the essentially planar trioxatriangulene radical.[53] The insolubility of **3.28** made it impossible to characterize it by UV or NMR spectroscopy.

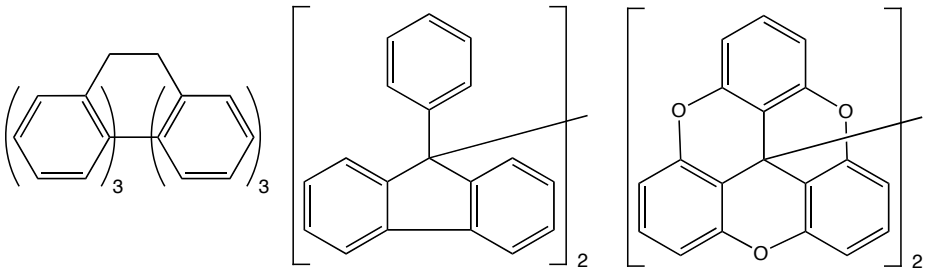

3.26 **3.27** **3.28**

The molecular structures of two hexaarylethanes have been determined by X-ray crystallography. Mislow and co-workers reported the molecular structure of 9,9'-bitriptycyl **3.29** and compared it to the structure calculated by empirical force field methods.[54] The molecular structure of hexakis(2,6-di-*tert*-butyl-4-biphenylyl)-ethane **3.30** has been reported by Rieker.[55] This dimer is especially interesting since it is the only known hexaarylethane that is neither "back clamped" nor "cross clamped". Mislow's[56] empirical force field calculations indicate that here should be a high degree of steric strain between the trityl moieties as indicated by a long C_{ethane}—C_{ethane} bond (1.64 Å for **3.24**). The C_{ethane}—C_{ethane} bonds of **3.29** (1.56 Å) and **3.30** (1.46 Å) are shorter than those predicted by Mislow's calculations (1.59 Å for **3.29** and 1.64 Å for **3.24**).[57]

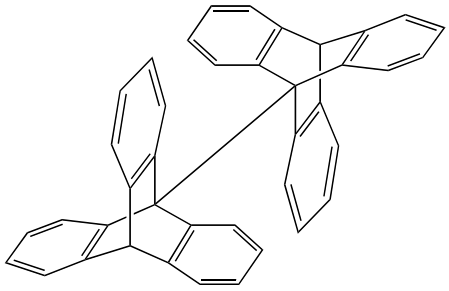

3.29

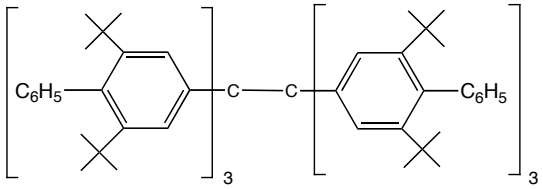

3.30

Peters reported making 2-*tert*-butyl-trioxatriangulene dimer **3.31** and found the X-ray structure revealed the C_{ethane}—C_{ethane} to be unusually long (1.63 Å).[33] This was explained by interaction of the σ orbitals and adjacent *p* orbitals that weakens the C_{ethane}–C_{ethane} bond while strengthening the C_{ethane}–C_{phenyl} bonds. The overall geometry suggests through-bond interactions account for the observed long C_{ethane}–C_{ethane} bond and the short C_{ethane}–C_{phenyl} bonds. However, later studies by Siegel and co-workers have challenged the explanation that through-bond coupling accounts for changes in bond length.[58]

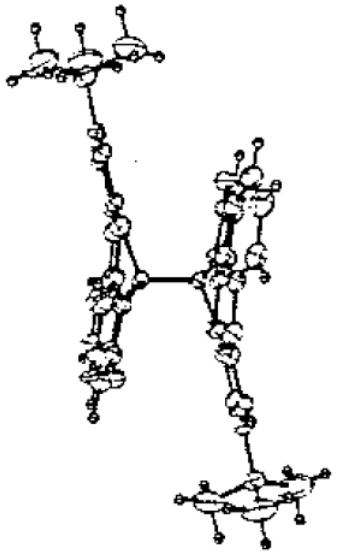

3.31

3.4 Current Work

3.4.1 Introduction

The previous sections have shown some of the synthetic details and physical properties concerning trioxatriangulenes derivatives. The current work is to explore the synthesis of centrally substituted *tert*-butyl trioxatriangulenes that will be utilitzed as building blocks in larger molecular structures. The polycyclic aromatic *tert*-butyl trioxatriangulene **3.32** (TOTA) is utilized as the base molecule is this project due to the facile modification at the central position, large surface area and solubility.

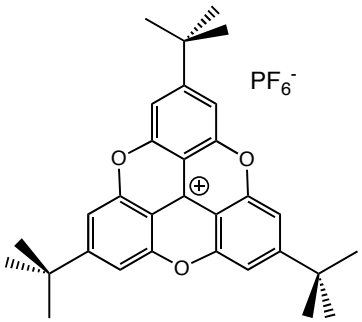

3.32

3.4.2 Retrosynthesis

The retrosynthesis of the building blocks will principally use nucleophilic addition of an organometallic species. In the retrosynthesis, the TOTA building block comes from functional group attachment to the center carbon, either an ethynylene or phenylene moiety (Figure 3.10). The trioxatriangulene cation species is generated from a triaryl species. At this point there are two possible routes that can lead to either an ether linkage or an amine linkage of the aryl bridge **X** of the cation species. The triaryl species comes from a commercially available phenylene starting material.

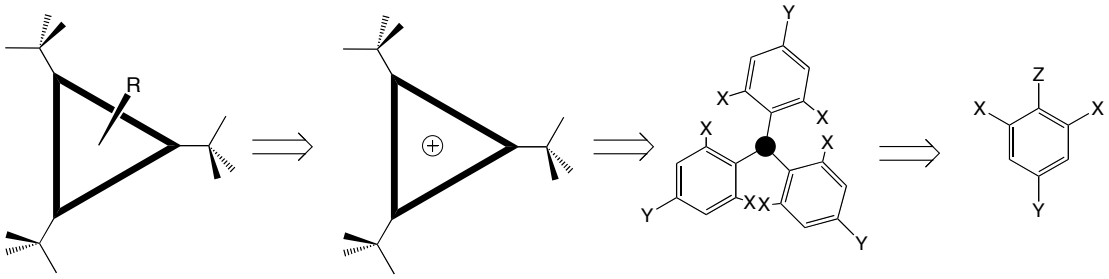

Figure 3.10 Proposed disconnection for the retrosynthesis of center substituted *tert*-butyl TOTA.

3.4.3 Synthesis

Initially, several centrally substituted trioxatriangulene species were generated. Afterwards, possible phenyl or ethynyl building blocks species were also generated. In order for the building blocks to be useful, functionality for cross-coupling methodology or conversion to an organometallic species would be required to elaborate the molecular structure. Synthetic protocol will also have to be robust generating grams quantities of the building block.

3.4.4 Synthesis of *tert*-butyl Trioxatriangulene Cation

The eight-step synthesis of the *tert*-butyl trioxatriangulene (TOTA) cation **3.32** begins with commercially available 2,6-dimethoxyphenol.[59] The synthesis begins by generating the *tert*-butyl derivative **3.33** under Friedel-Crafts conditions. Without isolating the material, the *tert*-butyl derivative **3.33** was then converted to diethyl phosphate compound **3.34**. Reduction of the phosphate **3.34** with metallic lithium in liquid ammonia gave compound **3.35** in quantitative yield. Bromination of compound **3.35** resulted in almost quantitative yield of the bromo-phenylene **3.36**. Compound **3.36** was then lithiated with *t*-butyllithium and after stirring for one hour, diethyl carbonate was added to the mixture. This mixture was then refluxed for 48 hours. The tris-carbinol **3.37** was then treated with refluxing hydrochloric acid resulting in the isolation of the crude xanthol **3.38** and subsequently mixed with pyridine hydrochloride at 150 ºC to give compound **3.39**. Finally, aqueous HPF_6 was added to

a solution of compound **3.39** in diethyl ether to generate the intensely orange coloured *tert*-butyl trioxatriangulene salt **3.32** in quantitative yield. Overall, the trioxatriangulene salt **3.32** (TOTA-PF_6) starting material was generated in 20 % yield and gram quantities (Scheme 3.11).

Scheme 3.11

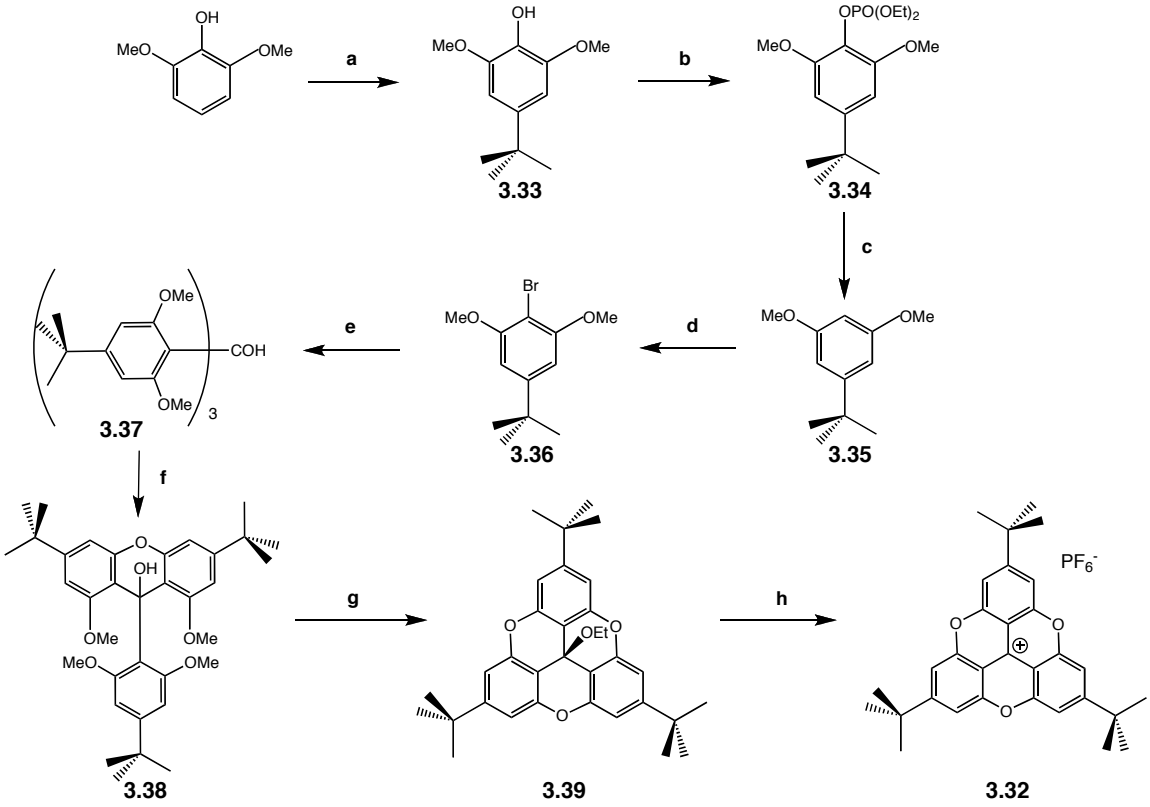

a. CH_3SO_3H, Bu^tOH b. $HPO(OEt)_2$, Et_3N, CCl_4, 104 g, 76% c. Li, NH_3, aq. NH_4Cl, 95 g, 98% d. Br_2, CCl_4, 104 g, 95% e. Bu^tLi, $(EtO)_2CO$, THF/Toluene, 3.4 g, 57% f. HCl, H_2O, Reflux g. Py·HCl, EtOH, 3.5 g, 52% h. aq. HPF_6, Et_2O, 4.0 g, 95%

3.4.5 Synthesis of the *tert*-butyl Trioxatriangulene

A solution of the *tert*-butyl trioxatriangulene cation **3.32** in dimethoxyethane was reduced when sodium borohydride was added and experimentally observed by an immediate solution colour change from yellow to white (Scheme 3.12).[60] Crystals suitable for single crystal X-ray analysis were obtained by recrystallization from ethyl acetate.

Scheme 3.12

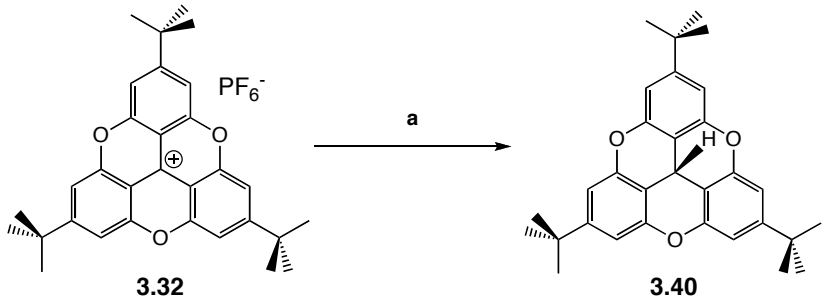

3.32 **3.40**

a. $NaBH_4$, DME, 91%

3.4.6 Synthesis of Methylene *tert*-butyl Trioxatriangulene

A solution of *tert*-butyl trioxatriangulene cation **3.32** in tetrahydrofuran was prepared and a methyllithium solution was added to give the methyl adduct **3.41** in 90% yield (Scheme 3.13). Originally, a catalytic amount copper iodide was added but later trials demonstrated that copper iodide was not necessary. Crystals suitable for single crystal X-ray analysis were obtained by slow evaporation from a dichloromethane/hexane solution.

Scheme 3.13

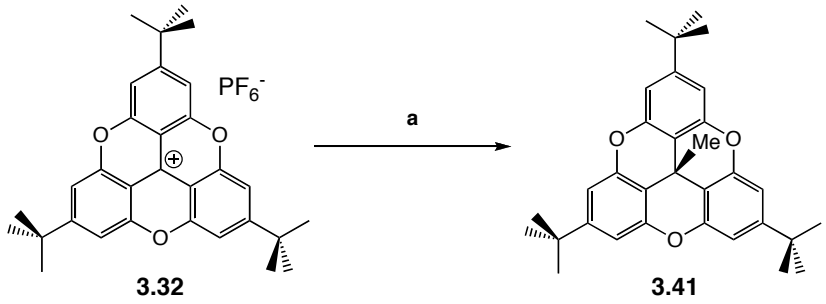

3.32 **3.41**

a. MeLi, CuI, THF, 98%

3.4.7 Synthesis of the Ethynylene *tert*-butyl Trioxatriangulene Building Block

A solution of the organolithium ethynyltrimethylsilane species was prepared by treating ethynyltrimethylsilane with *n*-butyllithium in THF. The *tert*-butyl trioxatriangulene cation **3.32** was then added to the ethynyltrimethylsilane solution

that resulted in product **3.42**. The next step followed standard deprotection protocol, and under basic conditions, to obtain the desired building block **3.43** in good yield (Scheme 3.14). Because this building block was functionalized with a terminal alkyne, Sonogashira coupling methodology[61] could be employed to expand the molecular structure.

Scheme 3.14

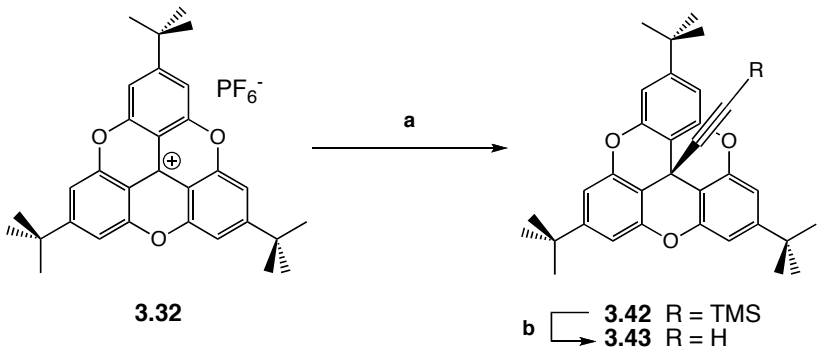

a. Ethynyltrimethylsilane, Bu^nLi, THF, 98% b. K_2CO_3, MeOH, THF, 98 %

3.4.8 Synthesis of Arylethynylene *tert*-butyl Trioxatriangulene Derivatives

Two other ethynylene derivatives were prepared to explore the methodology in making various trioxatriangulene structures. Phenylacetylene and 3-ethynylpyridine derivatives were prepared by organometallic methods. The organolithium phenylacetylene or ethynylpyridine species was first prepared by addition of *n*-butyllithium and the trioxatriangulene cation **3.32** was added to the solution (Schemes 3.15 and 3.16). Both procedures resulted in good yield of the desired product.

Scheme 3.15

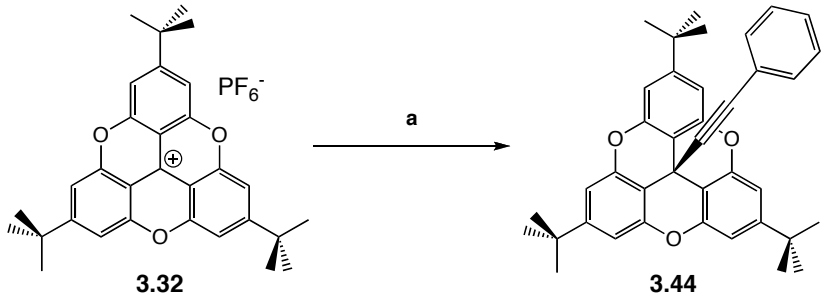

3.32 **3.44**

a. Phenylethynylene, Bu^{n}Li, THF, 80%

Scheme 3.16

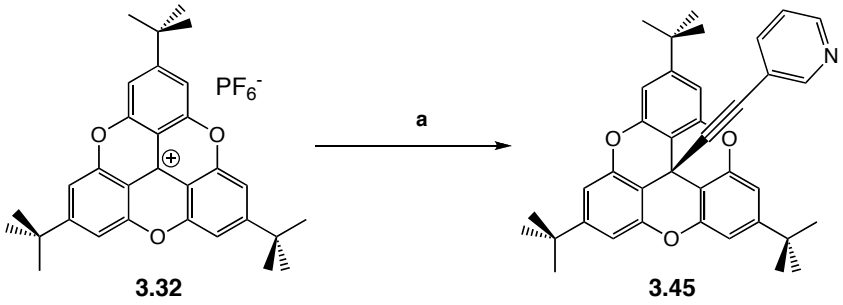

3.32 **3.45**

a. 3-Ethynylpyridine, Bu^{n}Li, THF, 58%

3.4.9 Synthesis of the 4-Bromophenylene *tert*-butyl Trioxatriangulene Building Block

A solution of the organolithium bromobenzene species was prepared by treating 1,4-dibromobenzene with one equivalent of *n*-butyllithium in THF. The *tert*-butyl trioxatriangulene cation **3.32** in THF was then cannulated into the organolithium bromobenzene solution. The desired building block **3.46** was obtained in good yield (Scheme 3.17). This product would constitute another fundamental building block that could be utilized in cross-coupling methodology to synthesize larger molecular structures. After several trails, conditions were optimized to increase the yield that used three equivalents of the 1,4-dibromobenzene and a 0.1 M reaction mixture.

Scheme 3.17

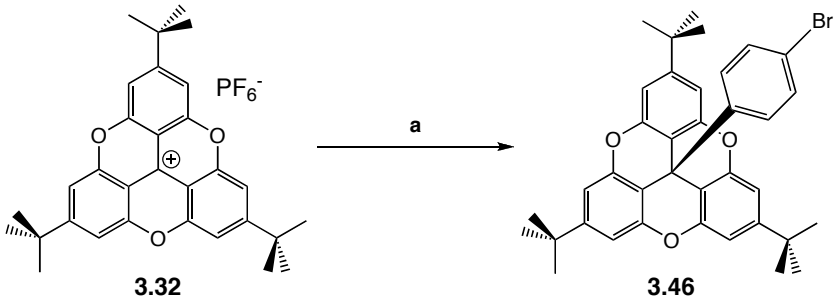

3.32 **3.46**

a. 1,4-Dibromobenzene, Bu^{n}Li, THF, 90%

3.4.10 Synthesis of the 4-Iodophenylene *tert*-butyl Trioxatriangulene Building Block

A solution of the organolithium iodobenzene species was prepared by treating 1,4-diiodobenzene with one equivalent of *n*-butyllithium in THF. The *tert*-butyl trioxatriangulene cation **3.32** in THF was then cannulated into the organolithium iodobenzene solution. The desired building block **3.47** was obtained in good yield (Scheme 3.18). Again, this product would constitute another fundamental building block that could be utilized in cross-coupling methodology to synthesize larger molecular structures. As stated with the bromophenyl synthesis, conditions were optimized to increase the yield that used three equivalents of the 1,4-diiodobenzene and a 0.1 M reaction mixture.

Scheme 3.18

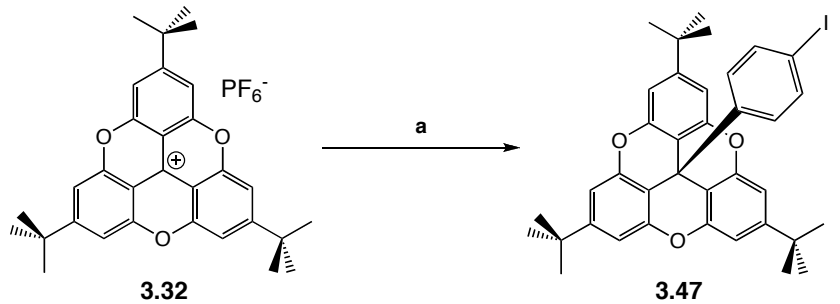

3.32 **3.47**

a. 1,4-Diiodobenzene, Bu^{n}Li, THF, 98 %

3.4.11 Synthesis of the 4-Trifluoromethanesulfonate Phenylene *tert*-butyl Trioxatriangulene Building Block

A solution of the organolithium anisole species was prepared by treating 4-bromoanisole with one equivalent of *n*-butyllithium in THF. The *tert*-butyl trioxatriangulene cation **3.32** in THF was then cannulated into the organolithium anisole solution to obtain the initial product **3.48**. After several attempts at deprotection, 16 equivalents of BBr_3 were required to fully deprotect **3.48**.[62] With the addition of base and triflic anhydride, the desired triflate **3.50** was obtained in good yield (Scheme 3.19).[63] This product would constitute another fundamental building block that could be utilized in cross-coupling methodology[64] to synthesize larger molecular structures.

Scheme 3.19

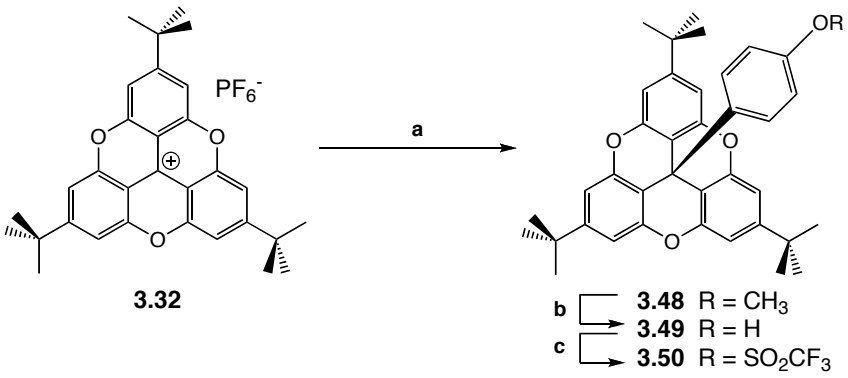

a. 4-Bromoanisole, Bu^nLi, THF, 98% b. BBr_3, CH_2Cl_2, 70% c. $(CF_3SO_2)_2O$, CH_2Cl_2, Pyr, 65%

3.4.12 Synthesis of the 4-Boronic Ester Phenylene *tert*-butyl Trioxatriangulene Building Block

A solution of the organolithium iodobenzene species was prepared by treating 1,4-diiodobenzene with one equivalent of *n*-butyllithium in THF. The *tert*-butyl trioxatriangulene cation **3.32** in THF was then cannulated into the organolithium iodobenzene solution to prepare the initial species. The desired building block **3.47**

was obtained in good yield (Scheme 3.20). Palladium cross-coupling methodology was then employed to prepare the boronic ester **3.51** in 40% yield.[65] This was done in moderate yield. This product would constitute another fundamental building block that could be utilized in cross-coupling methodology[66] to synthesize larger molecular structures.

Scheme 3.20

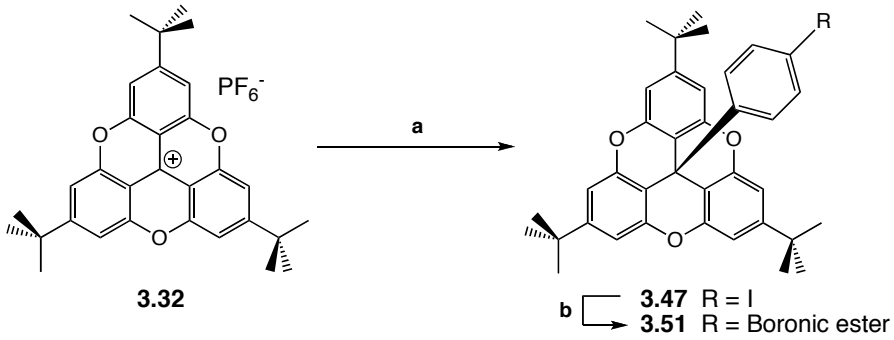

a. 1,4-Diiodobenzene, Bu^nLi, THF, 98 % b. $(Me_4C_2O_2)B\text{-}B(O_2C_2Me_4)$, $PdCl_2(dppf)$, KOAc, DMSO, 40%

3.4.13 Synthesis of the 4-Trimethyl Stannane Phenylene *tert*-butyl Trioxatriangulene Building Block

A solution of the organolithium iodobenzene species was prepared by treating 1,4-diiodobenzene with one equivalent of *n*-butyllithium in THF. The *tert*-butyl trioxatriangulene cation **3.32** in THF was then cannulated into the organolithium iodobenzene solution to prepare the initial species. The desired building block **3.47** was obtained in good yield (Scheme 3.21). Palladium cross-coupling methodology was utilized to couple with hexamethylditin and the iodophenyl trioxatriangulene derivative.[67] This building block **3.52** could further be utilized for Stille coupling methodology to prepare further superstructures.[64]

Scheme 3.21

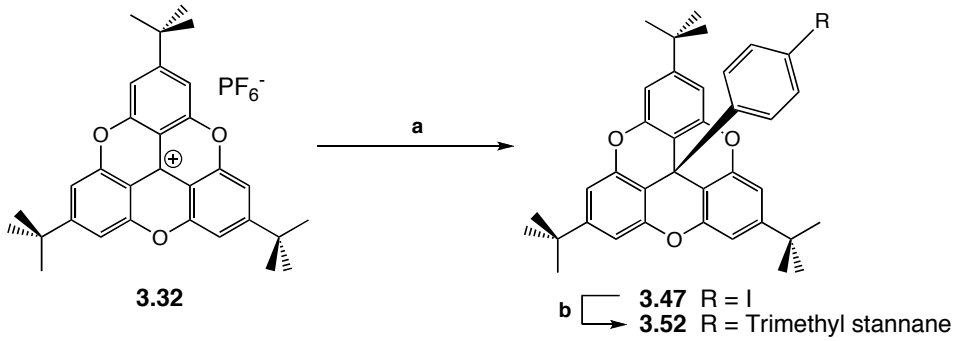

a. 1,4-Diiodobenzene, Bu^nLi, THF, 98 % b. Me_3Sn-$SnMe_3$, $Pd(PPh_3)_4$, THF, 40%

Table 3.2 Preparation of *tert*-butyl Trioxatriangulene Derivatives

Compound	Substituent (-R)	Reagents[a]	Conditions	Yield (%)
3.40	-H	$NaBH_4$, DME	1 h, Reflux	91
3.41	$-CH_3$	MeLi, CuLi, THF	1 h, -78 °C	98
3.43	-C≡C-H	1.EthynyleneTMS, Bu^nLi, THF 2.K_2CO_3, MeOH, THF	1. 1.5 h, -78 °C 2. 16 h, RT	96
3.44	-C≡C-Ph	Phenylethynylene, Bu^nLi, THF	1.5 h, -78 °C	80
3.45	-C≡C-Pyr	3-EthynlenePyr, Bu^nLi, THF	1.5 h, -78 °C	58
3.46	-Ph-Br	1,4-DBB, Bu^nLi, THF	1.5 h, -78 °C	90
3.47	-Ph-I	1,4-DIB, Bu^nLi, THF	1.5 h, -78 °C	98
3.50	-Ph-OSO_2CF_3	1,4-BrAnisole, Bu^nLi, THF 2. BBr_3, CH_2Cl_2 3. $(CF_3SO_2)_2O$, CH_2Cl_2, Pyr	1. 1.5 h, -78 °C 2. 16 h, -78 °C→ RT 3. 16 h, -78 °C→ RT	45
3.51	-Ph-$B(O_2C_2Me_4)$	1. 1,4-DIB, Bu^nLi, THF 2. $(Me_4C_2O_2)B$-$B(O_2C_2Me_4)$, $PdCl_2(dppf)$, KOAc, DMSO	1. 1.5 h, -78 °C 2. 16 h, 80 °C	40
3.52	-Ph-$SnMe_3$	1. 1,4-DIB, Bu^nLi, THF 2. Me_3Sn-$SnMe_3$, $Pd(PPh_3)_4$, THF	1. 1.5 h, -78 °C 2. 16 h, 80 °C	40

[a] 1,4-DBB = 1,4-Dibromobenzene and 1,4-DIB = 1,4-Diiodobenzene

3.4.14 Crystal Structure Properties of *tert*-butyl Trioxatriangulene Derivatives

Single crystal X-ray structures were obtained for compounds **3.32**, **3.40**, **3.41**, **3.44**, and **3.45**. The *tert*-butyl trioxatriangulene derivatives molecular packing, basic unit cell and molecular structures were investigated.

3.4.15 Crystal Structure of the *tert*-butyl Trioxatriangulene Cation 3.32

Following slow evaporation in dichloromethane, crystals of **3.32** suitable for X-ray diffraction were obtained. The asymmetric unit contains two trioxatriangulene cations, two hexafluorophosphate anions and one molecule of dichloromethane. The crystal structure of TOTA cation **3.32** shows the planar nature of the molecule (Figure 3.11). It was found to occupy $P2_1/c$ space group, a monoclinic crystal system. The packing of this molecule occurs as dimers with a planar distance of 3.41 Å and oriented *anti* (180°) to minimize direct interactions of the *tert*-butyl groups (Figure 3.12).

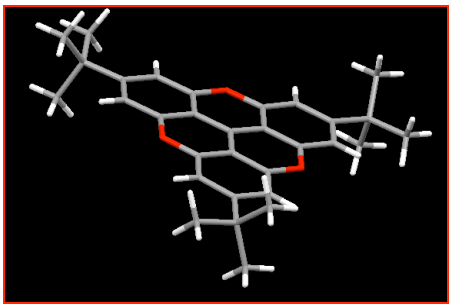

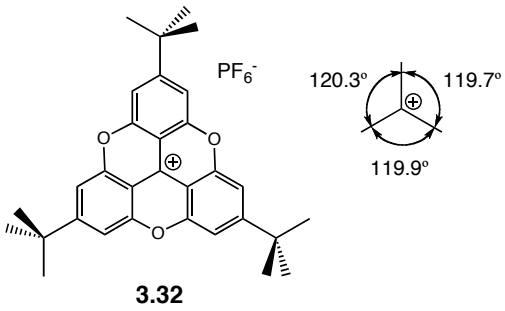

3.32

Figure 3.11 X-ray crystal structure of **3.32**. Bond angles around the central carbon are also represented.

(a) 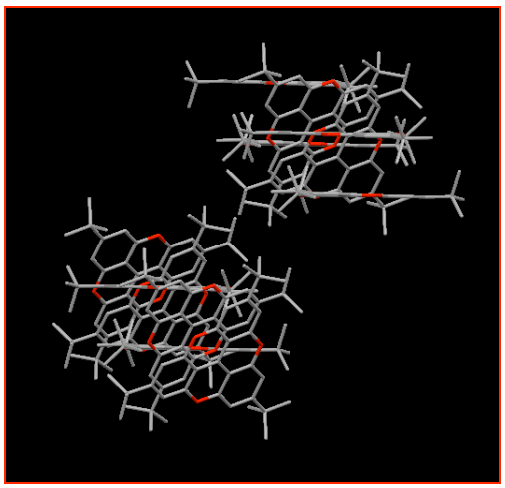 (b) 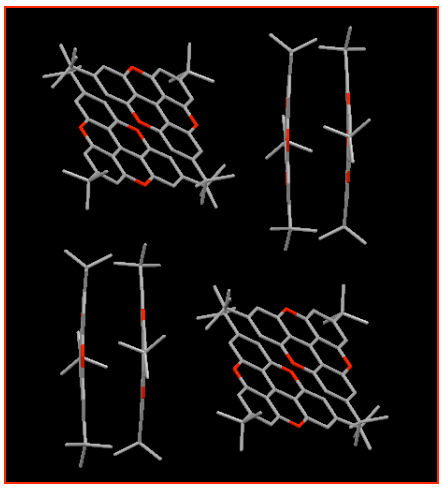

(c) 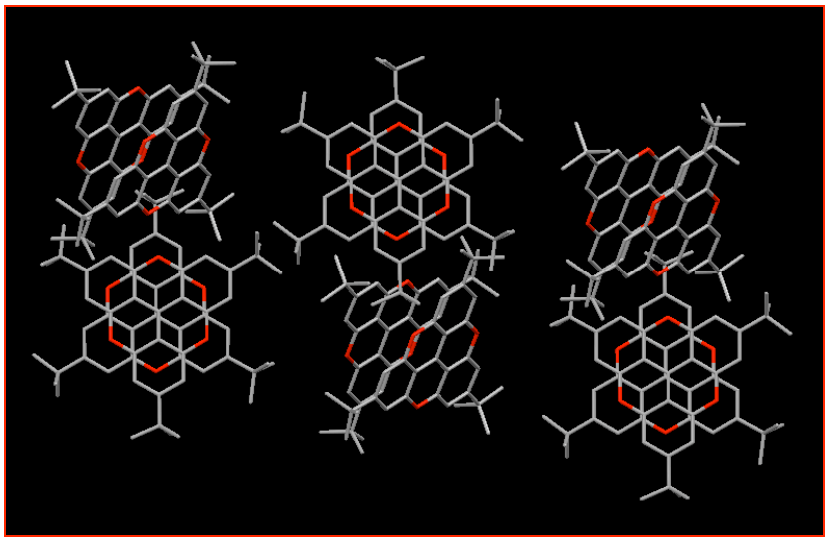

(d) 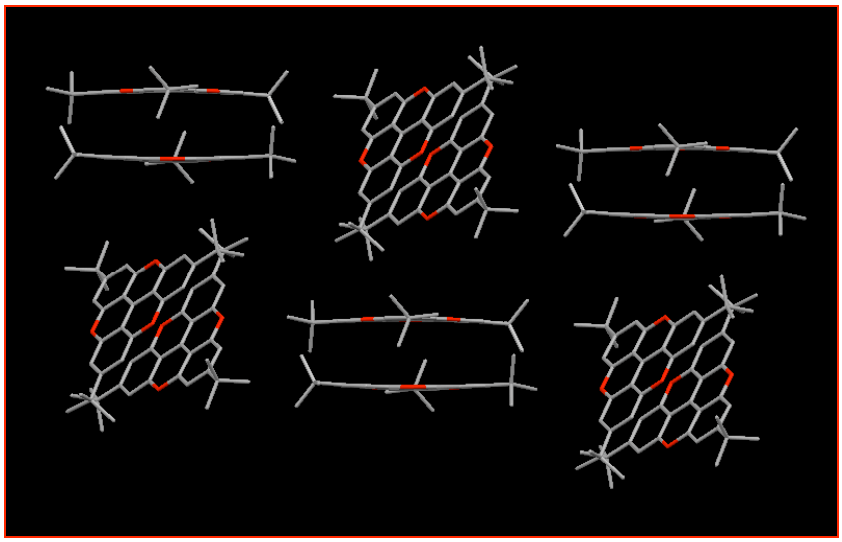

Figure 3.12 Section through the unit cell of **3.32**. (a) End view (b) View (a) reoriented *z – 90* (c) View (a) reoriented *x – 90* (d) View (a) reoriented *y – 90*. Hydrogens, PF_6 and CH_2Cl_2 have been omitted for clarity.

3.4.16 Crystal Structure of the *tert*-butyl Trioxatriangulene 3.40

Following recystallization in ethyl acetate, crystals of **3.40** suitable for single crystal X-ray diffraction were obtained. The crystal structure of *tert*-butyl trioxatriangulene **3.40** sits on a C_3 axis and shows the rigid molecular bowl shape of the molecule (Figure 3.13). The central carbon is tetrahedral (109.0°). The depth of the molecular bowl was measured and found to be 1.32 Å (C_q to a plane made by the *pseudo-para* carbons of the trioxatriangulene). It was found to crystallize in a high symmetry space group *I*4-*bar*3*d*, a cubic crystal system (Figure 3.14).

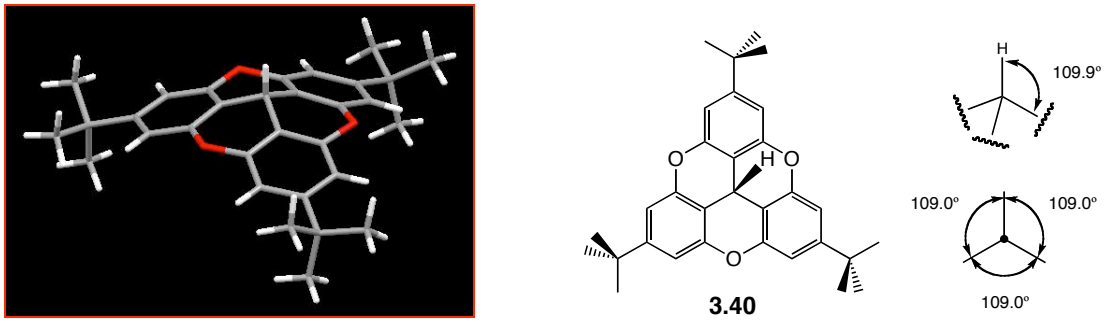

Figure 3.13 X-ray crystal structure of **3.40**. Bond angles around the central carbon are also represented.

(a) 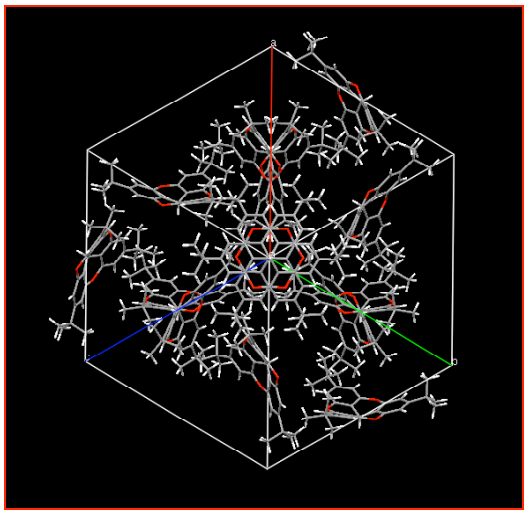 (b) 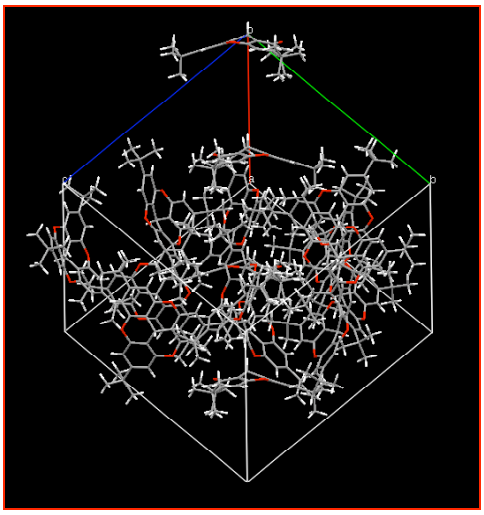

(c) 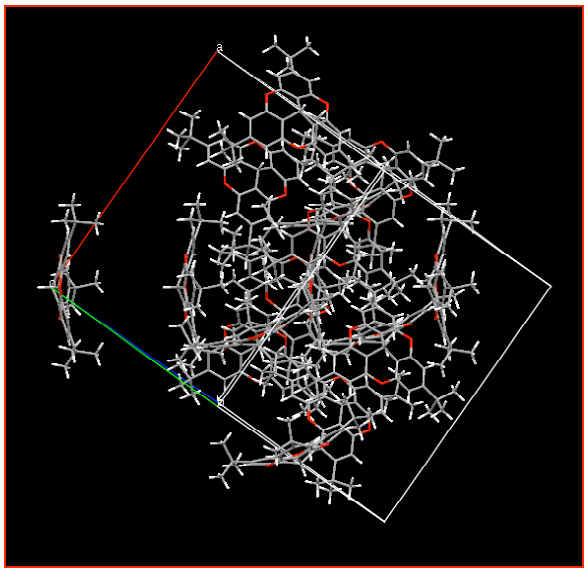

(d) 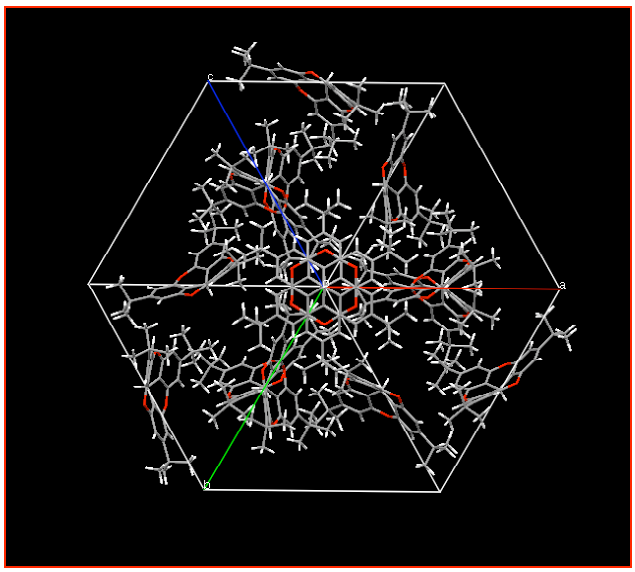

Figure 3.14 Section through the unit cell of **3.40**. (a) End view of six-fold axis (b) View (a) reoriented *x* – *90* (c) View (a) reoriented *y* – *90* (d) View (a) reoriented *z* – *90*.

3.4.17 Crystal Structure of the Methylene *tert*-butyl Trioxatriangulene 3.41

Following slow evaporation in dichloromethane/hexane, crystals of **3.41** suitable for single crystal X-ray diffraction were obtained. The molecule sits across a crystallographic mirror plane. The crystal structure of methylated *tert*-butyl trioxatriangulene **3.41** shows the rigid molecular bowl shape of the molecule (Figure 3.15). The central carbon is nearly regular tetrahedral. The depth of the molecular bowl was measured and found to be 1.28 Å (C_q to a plane made by the *pseudo-para* carbons of the trioxatriangulene). It was found to crystallize in the space group *Pnma*, possess an orthorhombic crystal system and pack in opposing layers (Figure 3.16).

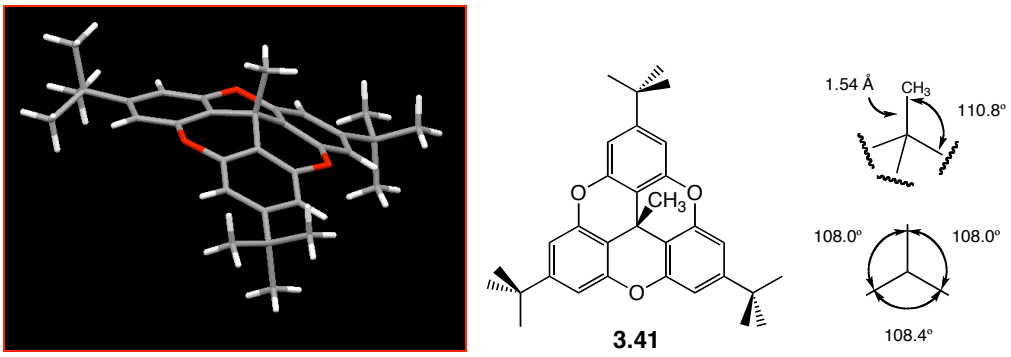

Figure 3.15 X-ray crystal structure of **3.41**. Bond angles around the central carbon are also represented and the bond distance between the central quaternary carbon and the methyl carbon.

(a)

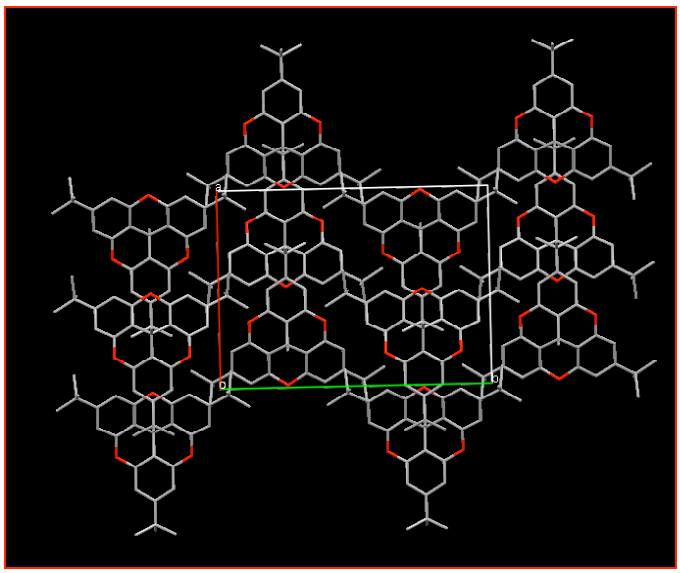

(b)

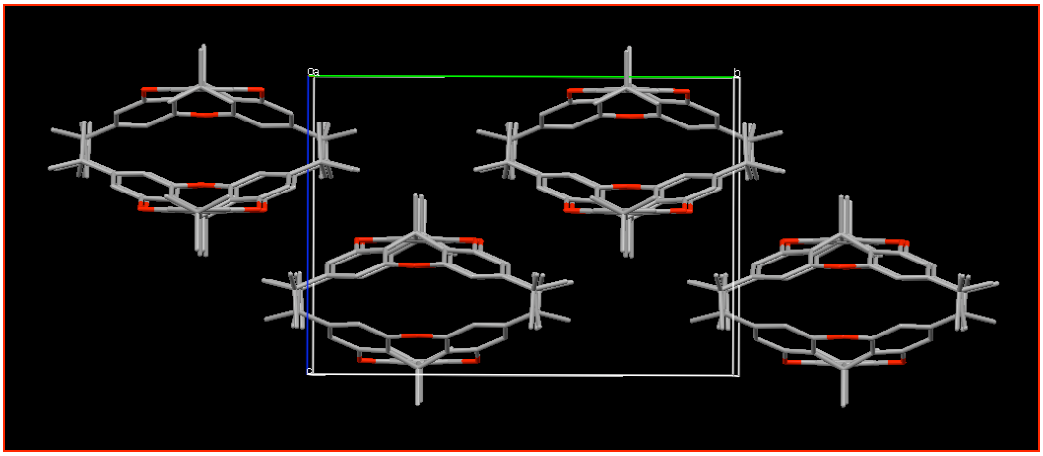

(c)

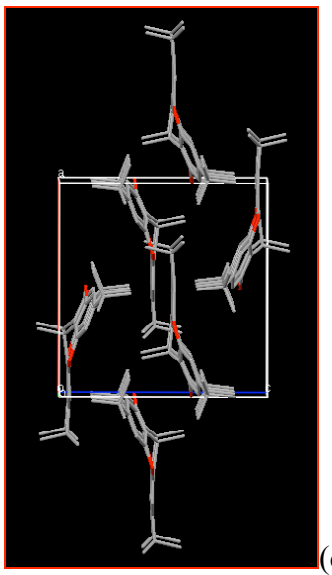

(d)

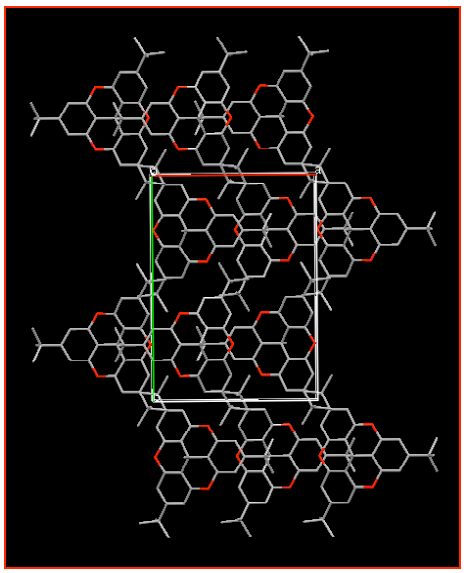

Figure 3.16 Section through the unit cell of **3.41**. (a) End view along *c* axis (b) View (a) reoriented *x* – *90* (c) View (a) reoriented *y* – *90* (d) View (a) reoriented *z* – *90*. Hydrogens have been omitted for clarity.

3.4.18 Crystal Structure of the Ethynylphenylene *tert*-butyl Trioxatriangulene 3.44

Following slow evaporation in hexane, crystals of **3.44** suitable for single crystal X-ray diffraction were obtained. The crystal structure of ethynylphenyl *tert*-butyl trioxatriangulene **3.44** shows the rigid molecular bowl shape of the molecule (Figure 3.17). The central carbon is nearly tetrahedral. The depth of the molecular bowl was measured and found to be 1.44 Å (C_q to a plane made by the *pseudo-para* carbons of the trioxatriangulene). The acetylenic bonds are slightly bent (∠176.9° and ∠177.5°). It was found occupy $P2_1/n$ space group, a monoclinic crystal system (Figure 3.18).

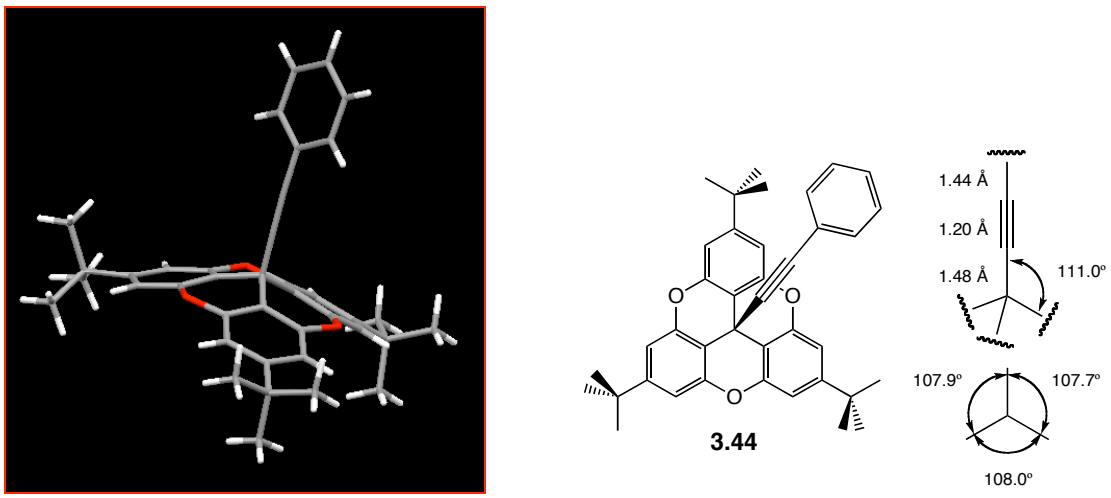

Figure 3.17 X-ray crystal structure of **3.44**. Bond angles around the central carbon are also represented and the bond distances from the central quaternary carbon to the phenyl adduct.

(a)

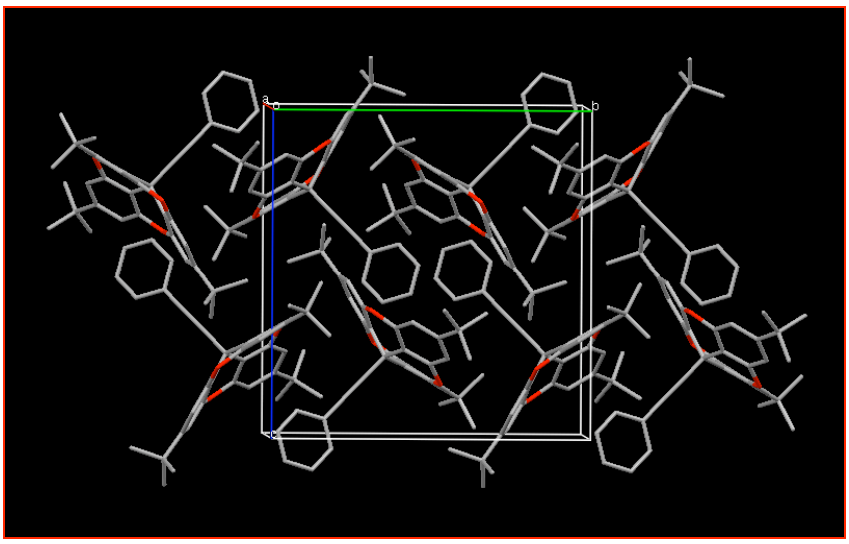

(b)

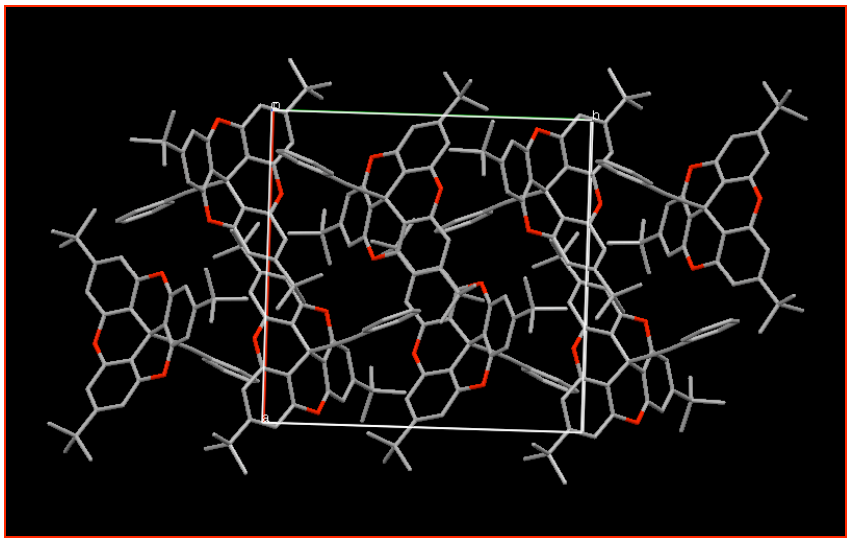

(c)

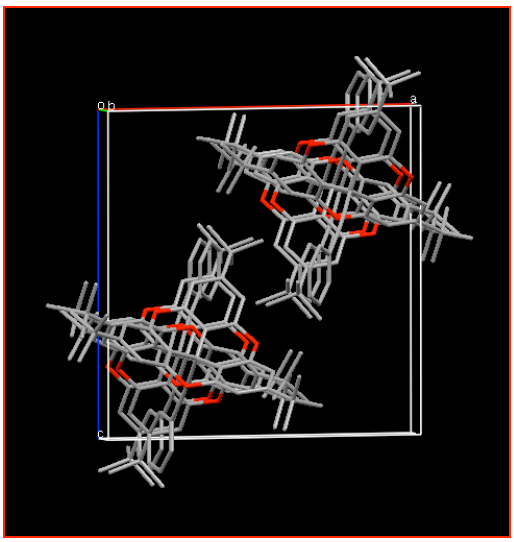

(d)

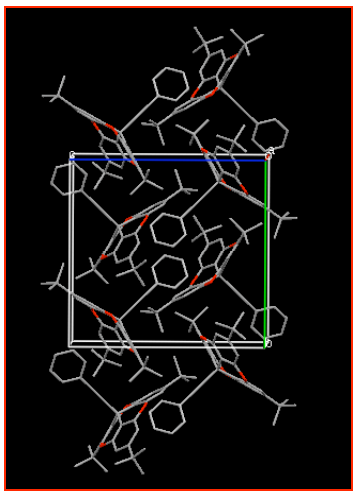

Figure 3.18 Section through the unit cell of **3.44**. (a) End view along *a* axis (b) View (a) reoriented *x* – *90* (c) View (a) reoriented *y* – *90* (d) View (a) reoriented *z* – *90*. Hydrogens have been omitted for clarity.

3.4.19 Crystal Structure of the Ethynylpyridylene *tert*-butyl Trioxatriangulene 3.45

Following slow evaporation in hexane/ethyl acetate, crystals of **3.45** suitable for single crystal X-ray diffraction were obtained. The crystal structure of ethynylpyridyl *tert*-butyl trioxatriangulene **3.45** shows the rigid molecular bowl shape of the molecule (Figure 3.19). The central carbon is nearly tetrahedral. The depth of the molecular bowl was measured and found to be 1.44 Å (C_q to a plane made by the *pseudo-para* carbons of the trioxatriangulene). The acetylenic bonds are slightly bent (∠177.7° and ∠177.8°). It was found occupy $P2_1/n$ space group and possess a monoclinic crystal system (Figure 3.20). The structure is isostructural with that of the previous phenyl analogue (Figure 3.17).

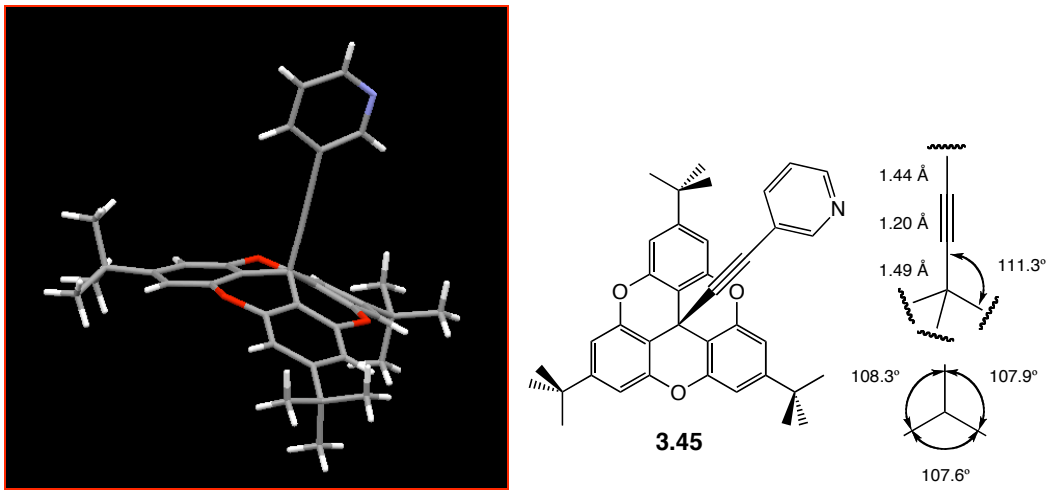

Figure 3.19 X-ray crystal structure of **3.45**. Bond angles around the central carbon are also represented and the bond distances from the central quaternary carbon to the pyridyl adduct.

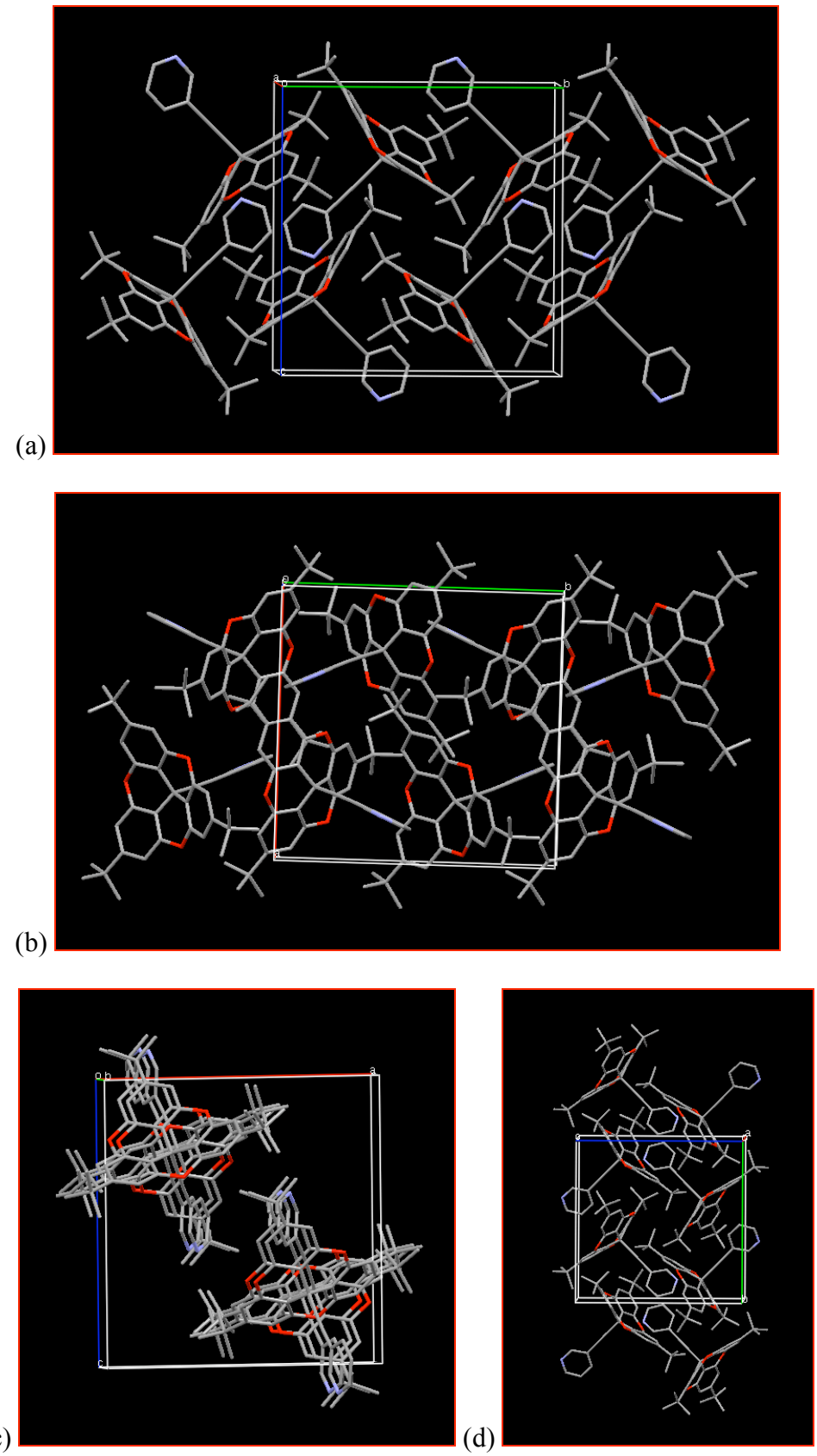

Figure 3.20 Section through the unit cell of **3.45**. (a) End view along *a* axis (b) View (a) reoriented *x – 90* (c) View (a) reoriented *y – 90* (d) View (a) reoriented *z – 90*. Hydrogens have been omitted for clarity.

Table 3.3 Summary of the *tert*-butyl TOTA Solid-state Characteristics

Molecule	Formula	MW	Bowl Depth (Å (X-ray))	Crystal System – Space Group	Z	Packing Coefficient
3.32	$C_{31}H_{33}O_3$	453	---	Monoclinic - $P2_1/c$	8	0.85
3.40	$C_{31}H_{34}O_3$	454	1.32	Cubic - *I*4-*bar*-3*d*	16	0.84
3.41	$C_{32}H_{36}O_3$	468	1.28	Orthorhombic - P*nma*	4	0.83
3.44	$C_{39}H_{38}O_3$	554	1.44	Monoclinic - $P2_1/n$	4	0.84
3.45	$C_{39}H_{37}NO_3$	555	1.44	Monoclinic - $P2_1/n$	4	0.84

3.5 Conclusions

This chapter has established a synthetic methodology for the preparation several *tert*-butyl trioxatriangulene building blocks on a large scale (0.75-1.0 g). The facile preparation of these building blocks is important for the preparation of larger structures to explore solid-state characteristics and voids created by the bulky *tert*-butyl TOTA moieties in the superstructures. Also, this synthetic methodology could easily be applied to generate other derivatives, such as: (1) asymmetric species that may respond to an external stimulus, (2) steric species that may influence solid-state dynamics, (3) species for multiple points of attachment to generate more complex structures. These additional derivatives, endowed with specific chemical or physical properties, could further be used to explore the transfer functionality or structure to superstructures.

3.6 References:

[1] (a) Singh, S.; Singh, H. *Indian J. Chem., Sect. B: Org. Chem. Incl. Med. Chem.* **1990**, *29B*, 601-602. (b) West, Jr., A.P.; Van Engen, D.; Pascal, Jr., R.A. *J. Am. Chem. Soc.* **1989**, *111*, 6846-6847. (c) Song, Q.; Ho, D.M.; Pascal, Jr., R.A. *J. Org. Chem*. **2007**, *72*, 4449-4453.

[2] Wang, L.; Sun, Z.; Pei, X.; Zhu, Y. *Chem. Phys.* **1990**, *142*, 335-343.

[3] Goto, K.; Kawashima, T. *J. Synth. Org. Chem, Jpn*. **2005**, *63*, 1157-1170.

[4] Dodziuk, H. *J. Mol. Struct.* **1990**, *239*, 167-172.

[5] Clar, E.; Stewart, D.G. *J. Am. Chem. Soc.* **1953**, *75*, 2667-2672.

[6] Inoue, J.; Fukui, K.; Kubo, T.; Nakazawa, S.; Sato, K.; Shiomi, D.; Morita, Y.; Yamamoto, K.; Takui, T.; Nakasuji, K. *J. Am. Chem. Soc*. **2001**, *123*, 12702-12703.

[7] (a) Martin, J.C.; Smith, R.G. *J. Am. Chem. Soc.* **1964**, *86*, 2252-2256. (b) Weiß, R.; Korczyn, J. *Monatsh. Chem.* **1925**, *45*, 207-214. (c) Hellwinkel, D.; Aulmich, G.; Melan, M. *Chem. Ber.* **1981**, *114*, 86-108. (d) Hellwinkel, D.; Melan, M. *Chem. Ber.* **1974**, *107*, 616-626. (e) Hellwinkel, D.; Melan, M. *Chem. Ber.* **1971**, *104*, 1001-1016.

[8] Lofthagen, M.; Siegel, J.S. *J. Org. Chem*. **1995**, *60*, 2885-2890.

[9] Lofthagen, M.; VernonClark, R.; Baldridge, K.K.; Siegel, J.S. *J. Org. Chem*. **1992**, *57*, 61-69.

[10] Tricorn: "A hat with the brim turned up on three sides." [< Lat. *tricornis*, three-horned.] *The American Heritage Dictionary*, 3rd Ed., Houghton Mifflin Company, 1994.

[11] (a) Weiß, R.; Korczyn, J. *Monatsh.* **1925**, *45*, 207-214. (b) Hellwinkel, D.; Mulmich, G.; Melan, M. *Chem. Ber.* **1981**, *114*, 86-108. (c) Hellwinkel, D.; Melan, M. *Chem. Ber.* **1974**, *107*, 616-626. (d) Hellwinkel, D.; Melan, M. *Chem. Ber.* **1971**,

104, 1001-1016. (e) Figuly, G.D.; Loop, C.K.; Martin, J.C. *J. Am. Chem. Soc.* **1989**, *111*, 654-658.

[12] Pirkle, W.H.; House, D.W. *J. Org. Chem.* **1979**, *44*, 1957-1960.

[13] Martin, J.C.; Smith, R.G. *J. Am. Chem. Soc.* **1964**, *86*, 2252-2256.

[14] Sherman, J.C.; Knobler, C.B.; Cram, D.J. *J. Am. Chem. Soc.* **1991**, *113*, 2194-2204.

[15] (a) Diederich, F. *Angew. Chem. Int. Ed. Engl.* **1988**, *27*, 362-386. (b) Petti, M.A.; Shepodd, T.J.; Dougherty, D.A. *Tetrahedron Lett.* **1986**, *27*, 807-810.

[16] Bidan, G.; Cauquis, G.; Genies, M. *Tetrahedron* **1979**, *35*, 177-180.

[17] Harney, D.W.; Meisters, A.; Mole, T. *Aust. J. Chem*. **1974**, *27*, 1639-1653.

[18] (a) Top, S.; Jaouen, G. *J. Org. Chem.* **1981**, *46*, 78-82. (b) Semmelhack, M.F. *Annals New York Academy of Sciences,* **1977**, *295*, 36-51. (c) Nicholas, K.M.; Mulvaney, M.; Bayer, M. *J. Am. Chem. Soc.* **1980**, *102*, 2508-2510.

[19] The authors note (ref. 9) failure to form a CPK model does not preclude the actual molecule from existence. Indeed, the tris(di-*ortho*-methoxy)triphenyl methanol, intermediate in the synthesis of Martin's Salt, itself cannot be formed from CPK models. However, they are a reasonable indicator of steric repulsion.

[20] VernonClark, R.N. Synthesis, Analysis, and Calculational Comparison, using Semiempirical and Molecular Mechanical Methods, of Centrally Substituted Trioxatricornan Structures: Investigation of Through-Bond Interactions. Ph.D. Dissertation, University of California, San Diego, CA, 1992.

[21] Bowie, W.T.; Feldman, M.R. *J. Am. Chem. Soc.* **1977**, *99*, 4721-4726.

[22] Prior to this study, the sole change in region **Y** was the replacement of *tert*-butyl for H in positions 2, 6, and 10. The substitution was first reported by Peters that began with the synthesis with *tert*-butyl-2,6-dimethoxybenzene. See: Peters, N. J. Synthesis

and Properties of Ortho-Bridged Triarylmethyl Compounds. Ph.D. Dissertation, University of Illinois, Urbana-Champaign, IL, 1980.

[23] Benkeser, R.A.; Hickner, R.A.; Hoke, D.I.; Thomas, O.H. *J. Am. Chem. Soc.* **1958**, *80*, 5289-5294.

[24] Gilman, H.; Young, R.V. *J. Am. Chem. Soc.* **1934**, *56*, 1415-1416.

[25] (a) Gschwend, H.W.; Rodriguez, H.R. *Org. Reactions*, **1979**, *26*, 43-92. (b) Gilman, H.; Morton, J.W.,Jr.; *Org. Reactions*, **1956**, *8*, 258-289. (c) Wakefield, B.J. *Organolithium Methods*; Academic Press: San Diego, CA, 1988, pp 1-189.

[26] Gilman, H.; Gorsich, R.D. *J. Org. Chem.* **1957**, *22*, 687-689.

[27] Langham, W.; Brewster, R.Q.; Gilman, H. *J. Am. Chem. Soc.* **1941**, *63*, 545-549.

[28] (a) Gilman, H.; van Ess, P.R. J. Am. Chem. Soc. 1933, 55, 1258-1261. (b) Jorgenson, M.J. *Org. Reactions*, **1970**, *18*, 2-64.

[29] Cahn, R.S.; Ingold, C.; Prelog, V. *Angew. Chem. Int. Ed. Engl.* **1966**, *5*, 385-415.

[30] Gabard, J.; Collet, A. *J. Chem. Soc., Chem. Commun*. **1981**, 1137-1139.

[31] Hoffman, R.W. *Dehydrobenzene and Cycloalkynes*; Academic Press: New York, 1967.

[32] Lofthagen, M.; VernonClark, R.; Baldridge, K.K.; Siegel, J.S. *J. Org. Chem*. **1992**, *57*, 61-69.

[33] Peters, N. J. Synthesis and Properties of Ortho-Bridged Triarylmethyl Compounds. Ph.D. Dissertation, University of Illinois, Urbana-Champaign, IL, 1980.

[34] Dominianni, S.J.; Ryan, C.W.; DeArmitt, C.W. *J. Org. Chem*. **1977**, *42*, 344-346.

[35] (a) Glaser, F.; Schäfer, W. *Angew. Chem*. **1959**, *71*, 372. (b) Jacot-Guillarmod, A. *Helv. Chim. Acta*. **1958**, *41*, 474.

[36] Gold, V.; Hawes, B.M.V. *J. Chem. Soc.* **1951**, 2102-2111.

[37] Martin, J.C.; Smith, R.G. *J. Am. Chem. Soc.* **1964**, *86*, 2252-2256.

[38] (a) Gust, D.; Mislow, K. *J. Am. Chem. Soc.* **1973**, *95*, 1535-1547. (b) Mislow, K. *Acc. Chem. Res.* **1976**, *9*, 26-33.

[39] Yamaye, M. Ortho-bridged Triarylmethyl Derivatives. Ph.D. Dissertation, University of Illinois, Urbana-Champaign, Urbana, IL, 1971.

[40] (a) Laursen, B.W.; Krebs, F.C. *Angew. Chem. Int. Ed*. **2000**, *39*, 3432-3434. (b) Laursen, B.W.; Krebs, F.C. *Chem. Eur. J.* **2001**, *7*, 1773-1783. (c) Reynisson, J.; Wilbrandt, R.; Brinck, V.; Laursen, B.W.; Nørgaard, K.; Narrit, N.; Brouwer. A.M. *Photochem. Photobiol. Sci*. **2002**, *1*, 763-773.

[41] Ray, G.J.; Kurland, R.J.; Colter, A.K. *Tetrahedron*, **1971**, *27*, 735-752.

[42] Olah, G.A.; Westerman, P.W.; Forsyth, D.A. *J. Am. Chem. Soc.* **1975**, *97*, 3419-3427.

[43] (a) Gomberg, M. *J. Am. Chem. Soc.* **1900**, *22*, 757-771. (b) Gomberg, M. *Chem. Ber.* **1900**, *33*, 3150-3163.

[44] McBride, J.M. *Tetrahedron* **1974**, *30*, 2009-2022.

[45] Lankamp, H.; Nauta, W.Th.; MacLean, C. *Tetrahedron Lett.* **1968**, 9, 249-254.

[46] Staab, H.A.; Brettschneider, H.; Brunner, H. *Chem. Ber.* **1970**, *103*, 1101-1106.

[47] The chemical shifts have been converted to the δ scale, ppm downfield of tetramethylsilane, using δ $CHCl_3$ = 77.0.

[48] Smith. W.B. *J. Chem. Ed.* **1970**, *47*, 535-536.

[49] Wittig, G.; Schoch, W. *Justus Liebigs Ann. Chem.* **1971**, *749*, 38-48.

[50] Schlenk, W.; Herzenstein, A.; Weickel, T. *Chem. Ber.* **1910**, *43*, 1753-1758.

[51] Staab, H.A.; Rao, K.; Brunner, H. *Chem. Ber.* **1971**, *104*, 2634-2636.

[52] Sabacky, M.J.; Johnson, Jr., C.S., Jr.; Smith, R.G.; Gutowsky, H.S.; Martin, J.C. *J. Am. Chem. Soc.* **1967**, *89*, 2054-2058.

[53] Müller, E.; Moosmayer, A.; Rieker, A.; Scheffler, K. *Tetrahedron Lett.* **1967**, 8, 3877-3880.

[54] Ardebili, M.H.P.; Dougherty, D.A.; Mislow, K.; Schwartz, L.H.; White, J.G. *J. Am. Chem. Soc.* **1978**, *100*, 7994-7997.

[55] Stein, M.; Winter, W.; Rieker, A. *Angew. Chem. Int. Ed. Engl.* **1978**, *17*, 692-694; *Angew. Chem.* **1978**, *90*, 737-738.

[56] (a) Hounshell, W.D.; Dougherty, D.A.; Hummel, J.P.; Mislow, K. *J. Am. Chem. Soc.* **1977**, *99*, 1916-1924. (b) Osawa, E.; Onuki, Y.; Mislow, K. *J. Am. Chem. Soc*. **1981**, *103*, 7475-7479.

[57] Mislow's calculations were further supported in a subsequent study: Kahr, B.; Van Engen, D.; Mislow, K. *J. Am. Chem. Soc*. **1986**, *108*, 8305-8307.

[58] (a) Kahr, B.; Mitchell, C.A.; Chance, J.M.; VernonClark, R.; Gantzel, P.; Baldridge, K.K.; Siegel, J.S. *J. Am. Chem. Soc*. **1995**, *117*, 4479-4482. (b) Baldridge, K.K.; Battersby, T.R.; VernonClark, R.; Siegel, J.S. *J. Am. Chem. Soc*. **1997**, *119*, 7048-7054. (c) Baldridge, K.K.; Kasahara, Y.; Ogawa, K.; Siegel, J.S.; Tanaka, K.; Toda, F. *J. Am. Chem. Soc*. **1998**, *120*, 6167-6168.

[59] (a) Peters, N. J. Synthesis and Properties of Ortho-Bridged Triarylmethyl Compounds. Ph.D. Dissertation, University of Illinois, Urbana-Champaign, IL, 1980. (b) Faldt, A.; Krebs, F.C.; Thorup, N. *J. Chem. Soc., Perkin Trans. 2*, **1997**, 2219-2227.

[60] Bell, H.M.; Brown, H.C. *J. Am.Chem. Soc*. **1966**, *88*, 1473-1477

[61] (a) Sonogashira, K.; Tohda, Y.; Hagihara, N. *Tetrahedron Lett*. **1975**, *16*, 4467-4470. (b) Venkataramana, G.; Sankararaman, S. *Org. Lett*. **2006**, *8*, 2739-2742.

[62] Yang, Y.; Escobedo, J.O.; Wong, A.; Schowalter, C.M.; Touchy, M.C.; Jiao, L.; Crowe, W.E.; Fronczek, F.R.; Strongin, R.M. *J. Org. Chem*. **2005**, *70*, 6907-6912.

[63] Stang, P.J.; Dueber, T.E. *Organic Syntheses*; Wiley & Sons: New York, 1988; Collect. Vol. 6, p. 757.

[64] Scott, W.J.; Crisp, G.T.; Stille, J.K. *Organic Syntheses*; Wiley & Sons: New York, 1993; Collect. Vol. 8, p. 97.

[65] Ishiyama, T.; Murata, M.; Miyaura, N. *J. Org. Chem*. **1995**, *60*, 7508-7510.

[66] Goodson, F.E.; Wallow, T.I.; Novak, B.M. *Organic Syntheses*; Wiley & Sons: New York, 2004; Collect. Vol. 10, p. 501.

[67] Li, D.; Zhao, B.; LaVoie, E.J. *J. Org. Chem.* **2000**, *65*, 2802-2805.

Chapter 4. *tert*-Butyl Trioxatriangulene Superstructures: Ordered Solid State and Molecular Dynamics

4.1 Project Design

For much of the last half of the 20th century, the design of ordered organic molecules for the solid-state structure and function has intrigued chemists. The molecular crystal has been described as the perfect supermolecule, according to Dunitz "a supermolecule *par excellence*".[1] The idea of a designable order in the crystal began with experiments in organic solid-state photochemistry,[2] studies in the packing of molecular crystals[3] and the decoding of hydrogen-bond networks in the solid state.[4] Furthermore, crystal design has seen an evolution of sophisticated materials endowed with unique structures or properties.

The goal of this thesis is to develop a design principle for ordered crystals that translates structure to function. In general, attractive and repulsive interactions, plus structural aspects, are used to order the molecules in a well-defined manner within a crystal, *i.e.* engineer the crystal. Much of this chemistry is based on analogies with the macroscopic world. One might speculate that the trioxatriangulene superstructure, with a narrow centered and bulky ends, is analogous to a Lincoln Logs™ construction set;[5] pieces made of cylindrical wood logs notched in a manner that allows for an ideal geometric fit to construct larger structures (Figure 4.1).

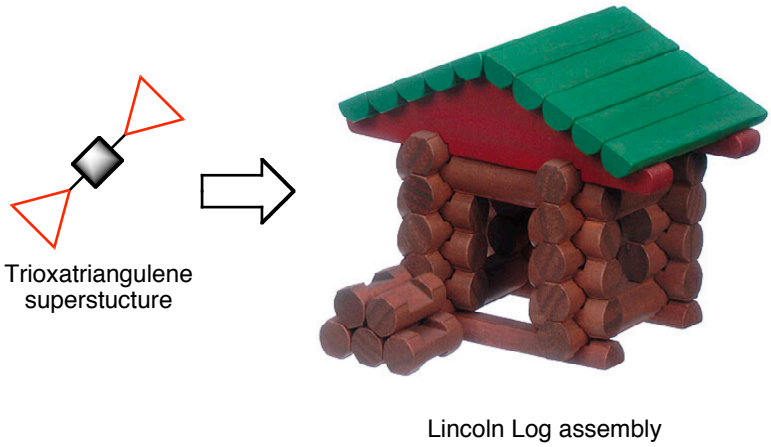

Figure 4.1 Proposed molecular component that may emulate the ordered arrangement as seen in a Lincoln Log™ assembly.

Besides structural features, electronic and dynamic function in the solid-state are also of interest. The incorporation of an interesting chromophore or bond rotation in a well-defined structure is an area of investigation. The bond rotation in aryl alkynes, such as diphenylacetylene, is one of the simplest structures of interest. Experimental and computational methods have shown the barrier in diphenylacetylene in the gas phase to be quite low, *ca*. 0.5 kcal/mol.[6] In order to dramatically increase the barrier in the aryl alkyne systems, steric interactions had to be introduced, as seen in the work of Moore[7] and Toyota.[8] Whereas significant steric interactions resulted in a drastic barrier increase in the solution phase, it is postulated that very subtle solid-state perturbations could also lead to interesting molecular dynamics.

The design and transfer of easily modifiable building blocks for the construction of larger superstructures endowed with desired functions remains a challenge.[9] This project will make use of bulky substituents to make unique solid-state geometric structures and precisely modulate the internal dynamic environment of the target molecule. The molecular building block in the larger superstructure will also be investigated with respect to long-range order, molecular characteristics and component synthesis (Figure 4.2).

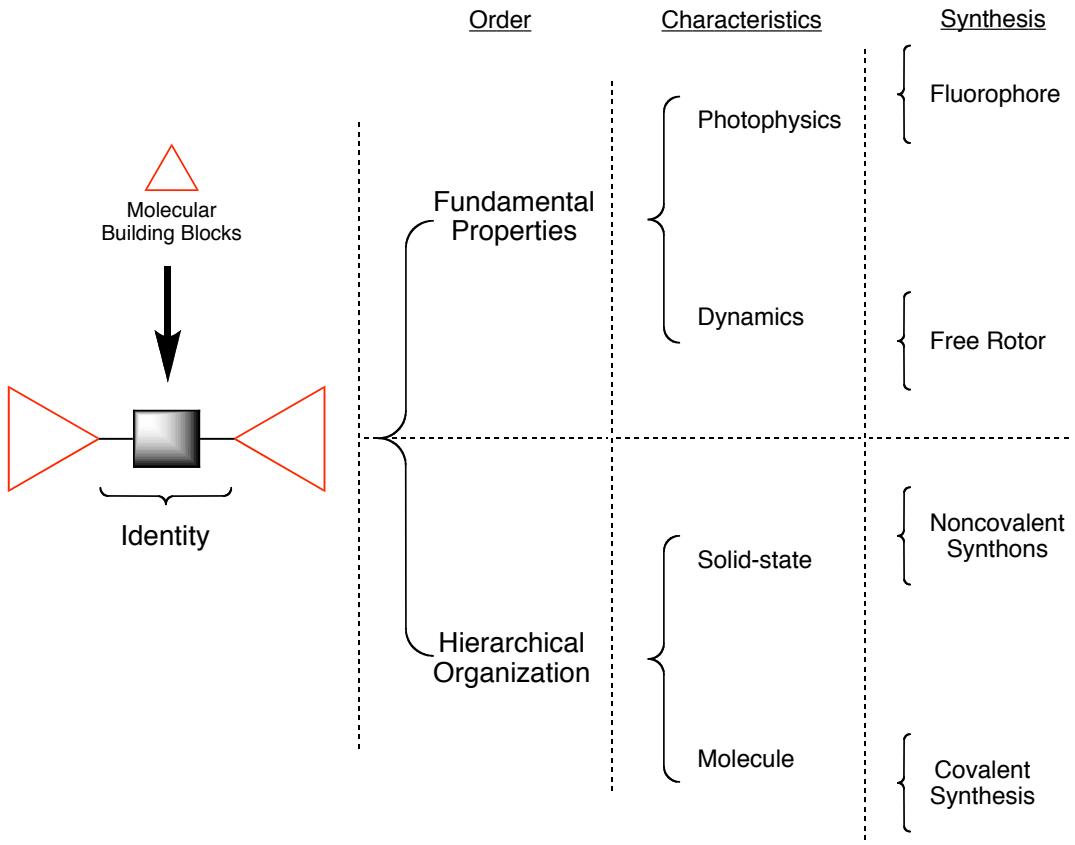

Figure 4.2 Schematic illustration of project design.

4.1.1 Experimental Design

The polycyclic *tert*-butyl trioxatriangulene cation **3.32** (TOTA), represented here as a red triangle, is utilized as the base molecule in this project due to the facile modification at the central position, large surface area and solubility in organic solvents. In Figure 4.3, the space-filling model demonstrates the bulkiness of the 68-atom TOTA building block with a surface area of 512 $Å^2$ and a volume of 525 $Å^3$.

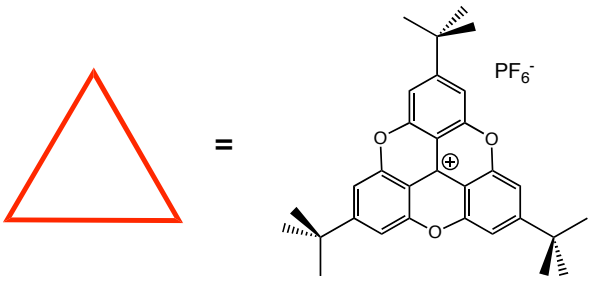

3.32

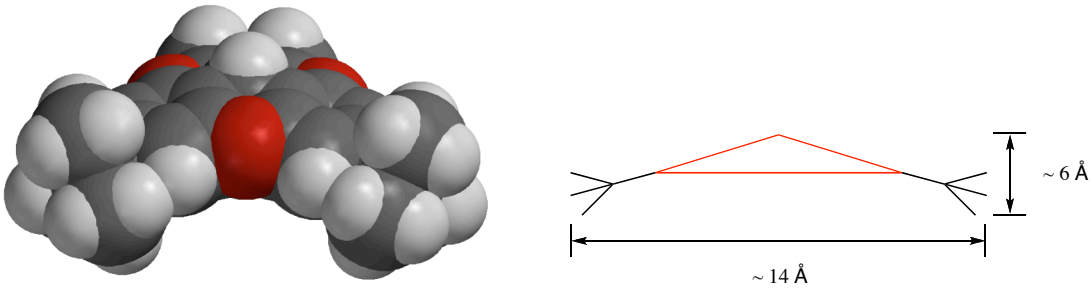

Figure 4.3 Space-filling model and van der Waals physical dimensions of the reduced *tert*-butyl TOTA molecule.

Nucleophilic addition to the central position provides the molecular base for the generation of many superstructures. The central position has been functionalized to generate two elementary building blocks that are used to build well-defined superstructures. Additionally the importance of the elementary building blocks is that it allows the aryl/alkyne axis to be easily modifiable with respect to structure (Figure 4.4).

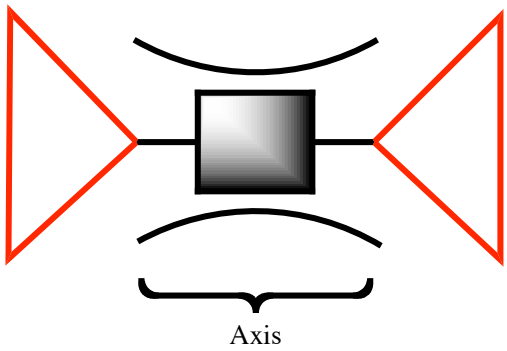

Figure 4.4 Illustration of TOTA superstructure with a modifiable central axis environment.

4.2 Trioxatriangulene Building Blocks

The trioxatriangulene molecule has been utilized in a number of investigations. Besides a basic building block for larger structures, such as macrocycles,[10] it has been used to investigate the stability of charged species, plus interesting electronic derivatives and solid-state materials.[11]

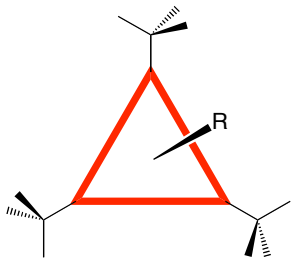

Figure 4.5 *tert*-butyl Trioxatriangulene building block.

4.2.1 *tert*-butyl Trioxatriangulene Building Block Retrosynthesis

In considering the retrosynthesis of the building block, the first disconnection from functional group attachment to the center carbon, is either a terminal ethynylene or a halogenated phenylene moiety (Figure 4.6). The trioxatriangulene cation species is generated from a triaryl species. At this point there are two possible routes that can lead to either an ether linkage or an amine linkage of the trioxatriangulene bridge **X**. In the last disconnect, the triaryl species comes from a commercially available phenylene starting material.

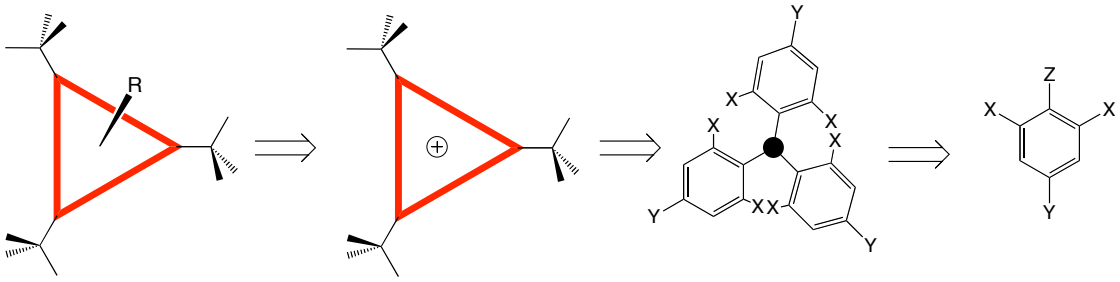

Figure 4.6 Proposed disconnection for the retrosynthesis of the *tert*-butyl TOTA building block.

4.2.2 Synthesis of *tert*-butyl Trioxatriangulene Cation

The eight-step synthesis of the *tert*-butyl trioxatriangulene (TOTA) salt **3.32** begins with commercially available 2,6-dimethoxyphenol (Scheme 4.1).[12] The *tert*-butyl trioxatriangulene salt starting material **3.32** (TOTA-PF_6) is generated with an overall yield of 20 % and in 1-2 gram quantities. The detailed scheme for this synthesis is shown in Chapter 3 (Scheme 3.11).

Scheme 4.1

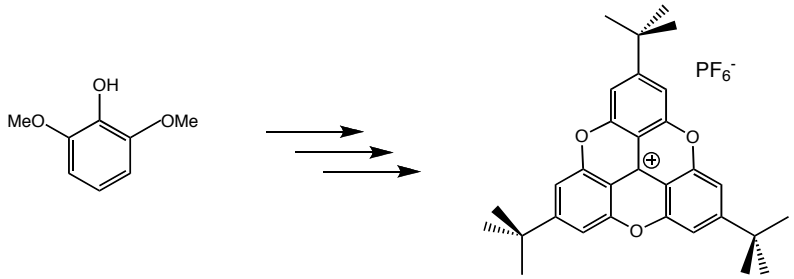

3.32

4.2.3 Synthesis of the *tert*-butyl Trioxatriangulene Building Blocks

Chapter 3 examined the synthesis of a variety of potential trioxatriangulene building blocks. In this project, two building blocks were chosen due to their facile, large-scale preparation and utility in further reaction conditions to generate a series of trioxatriangulene superstructures.

The first building block is the ethynylene species **3.43**. Starting with the organolithium trimethylsilylethynylene species and adding the *tert*-butyl trioxatriangulene cation **3.32** to the low temperature solution, the expected intermediate of building block **3.43** was produced. Under basic deprotection conditions, the desired ethynylene building block **3.43** was obtained in good yield (Scheme 4.2).

Scheme 4.2

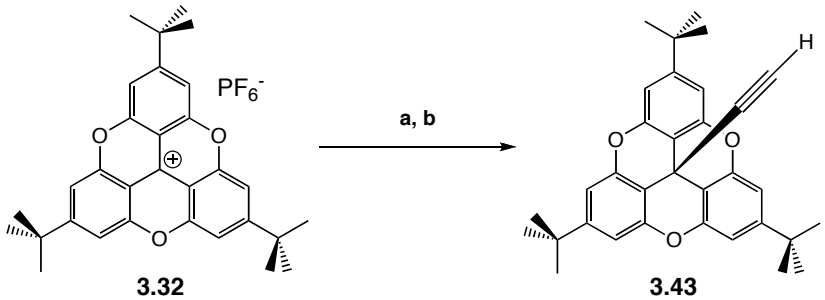

3.32 **3.43**

a. Ethynyltrimethylsilane, Bu^nLi, THF, 98% b. K_2CO_3, MeOH, THF, 98 %

The second building block is the iodophenylene species **3.47**. Starting with the organolithium diiodobenzene species and adding the *tert*-butyl trioxatriangulene cation **3.32** to the low temperature solution, the desired iodophenylene building block **3.47** was obtained in 98 % yield and *ca.* 750 mg (Scheme 4.3).

Scheme 4.3

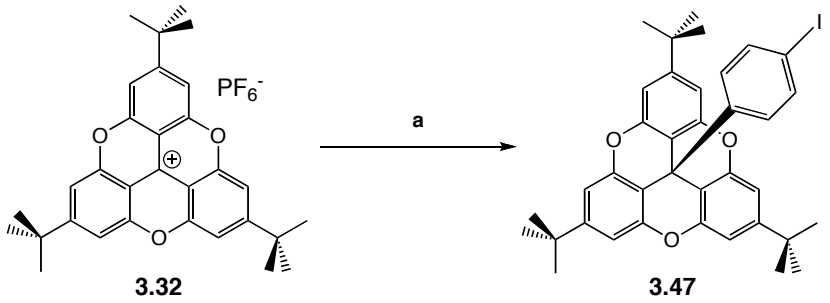

a. 1,4-Diiodobenzene, Bu^{n}Li, THF, 98 %

4.3 tert-butyl Trioxatriangulene Sandwich Structures

4.3.1 Introduction

The trioxatriangulene sandwich structures are the principal synthetic target in this project. A series of sandwich species were generated from common building TOTA blocks and a spacer (Reaction 1).

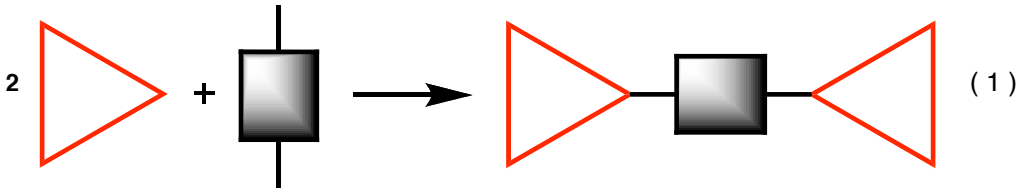

By generating a series of sandwich species with a combination of ethnylene and phenylene moieties the axial distance in the superstructure will be precisely controlled. The phenylene moiety is *ca.* 2.8 Å in length and the ethynylene moiety is *ca.* 1.2 Å in length, thus this will allow for the axis length to be precisely modulated, shielding the central region with an axis length ranging from 4.1 to 14.4 Å (Figure

4.7). Additionally, the superstructure series allows for insertion of well-known chromophores, *e.g. p*-terphenyl or tolan.

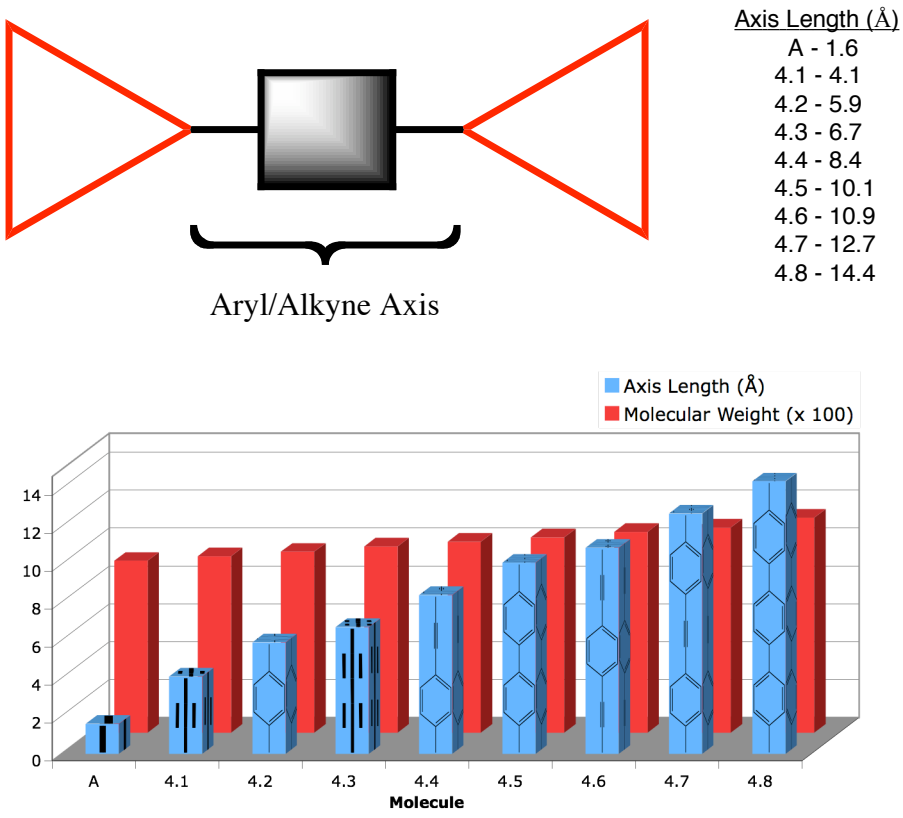

Figure 4.7 Basic sandwich superstructure with a *tert*-butyl TOTA molecule at each end of a well-defined axis.

4.3.2 *tert*-butyl TOTA Sandwich Structures in the Solid State

One objective of this project is to compare the solid-state packing characteristics across the series of TOTA compounds. In a simple discussion, one may generate some hypothetical examples of the solid-state characteristics (Figure 4.8): A, B, C or D. By precisely varying the axis length, and therefore the empty space created by the separation of the bulky TOTA molecules, several physical and geometric observables may be investigated. This pattern may be manifested in a perpendicular or parallel molecular arrangement. Additionally, guest molecules may

have a preference to reside in the spaces created by the TOTA superstructures. Also, in a simplified parallel geometric association there may a definable molecular offset in the lattice arrangement. Since there is a precise and incremental control of the axis length in the molecular series, it may ultimately be possible to predict a pattern in the crystal packing of the molecules, or more specifically, the unit cell type and symmetry.

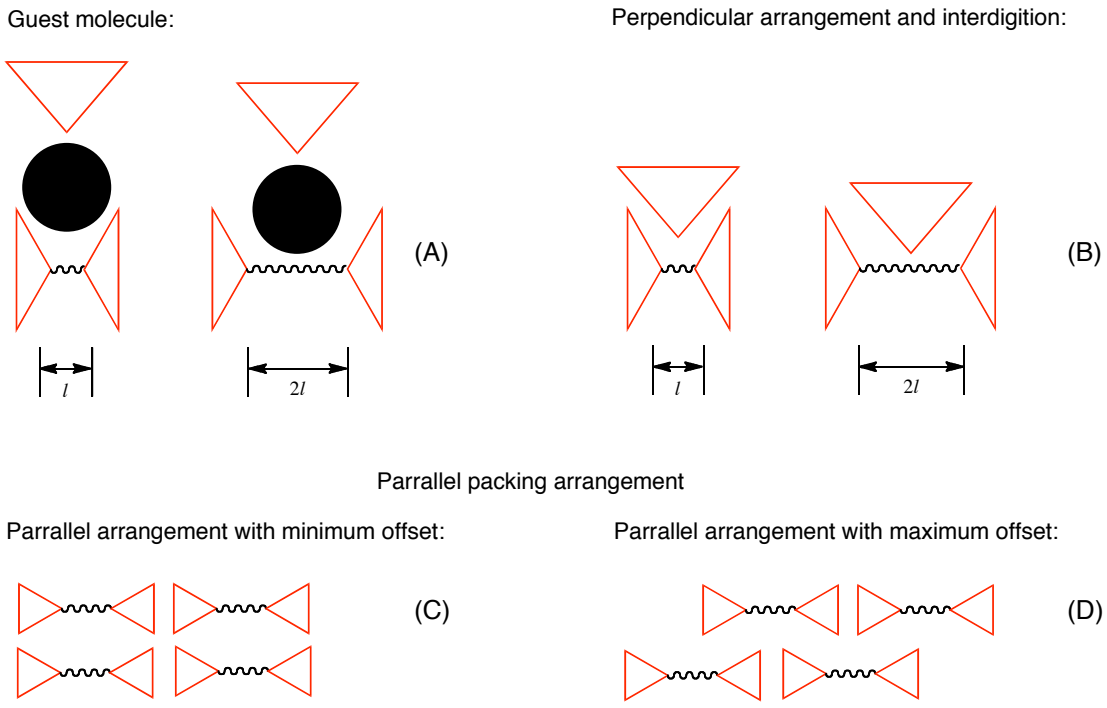

Figure 4.8 Schematic illustration of the *t*-butyl TOTA superstructures in the solid state with a short (*l*) and long (2*l*) central axis length.

4.3.3 Rotation Consideration of a Phenylene Moiety in the *tert*-butyl TOTA Sandwich Structures

A second objective of this investigation is to evaluate the energetic significance of rotational barriers through intermolecular or intramolecular solid-state interactions of the TOTA sandwich structures possessing a single phenylene group in the central axis. The rational design and construction of relatively simple artificial

rotary assemblies remains a challenge to chemists.[13] The space-filling model of the *t*-butyl TOTA sandwich demonstrates the extent to which the central phenylene ring is shielded from its surroundings (Figure 4.9). Although the energy barrier is expected to be quite low in solution phase and difficult to determine by variable temperature NMR, solid-state ^{13}C and ^{2}H NMR spectroscopy may enable elucidation of molecular dynamics for the central phenyl ring. The ethynyl-phenylene and the ethynyl-phenyl-ethynylene species, as well, would be expected to display some comparative rotational dynamics of the central phenylene ring (Figure 4.9).

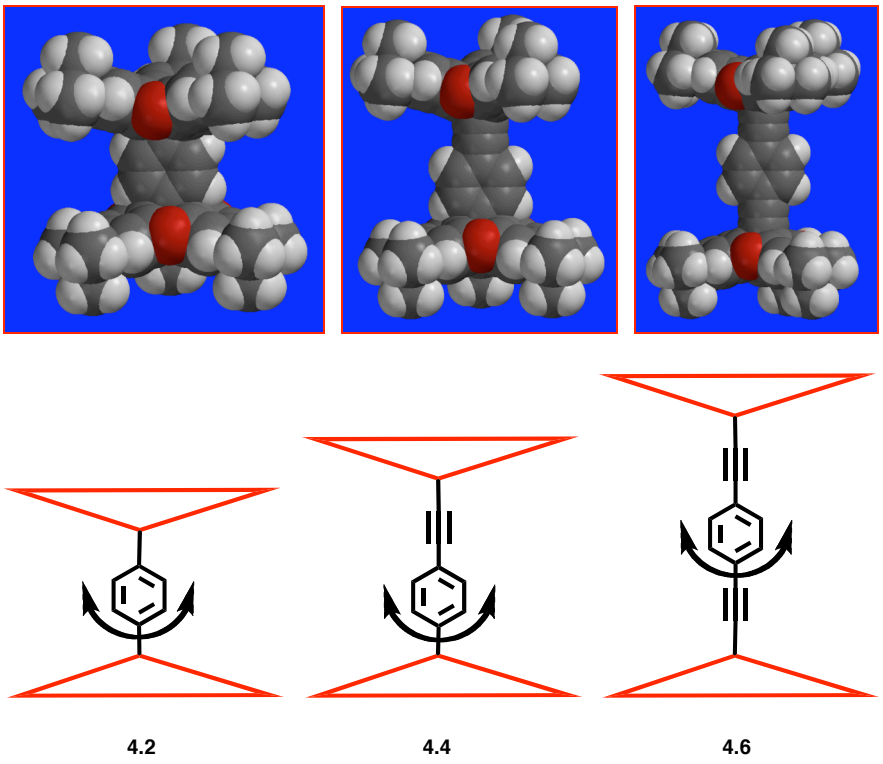

Figure 4.9 Space-filling models and illustration of the phenylene rotation for three of the *t*-butyl TOTA superstructures.

4.3.4 Retrosynthesis of the *tert*-butyl TOTA Sandwich Structures

The retrosynthesis of the *t*-butyl TOTA sandwich involves similar disconnections as that of the *t*-butyl TOTA building blocks (Figure 4.10). In each case, a bond between an aryl or alkyne bond and the central point of attachment must be broken. Experimentally, organometallation methodology or palladium cross-

coupling methodology will principally be used in the syntheses. The species with a central phenylene unit could be formed by the addition of two equivalents of a *t*-butyl TOTA building block cation and one equivalent of a 1,4-dihalobenzene. The symmetric species, diethynylene or biphenylene, can be generated from the homo-coupling two *t*-butyl TOTA building blocks. The asymmetric species will simply require one equivalent of each *t*-butyl TOTA building block. As the axis length is increased, the number of steps will likely also have to be increased. The tolan or terphenyl axis could come from different functionalized phenylene *t*-butyl TOTA building blocks and coupled together to generate the final sandwich species.

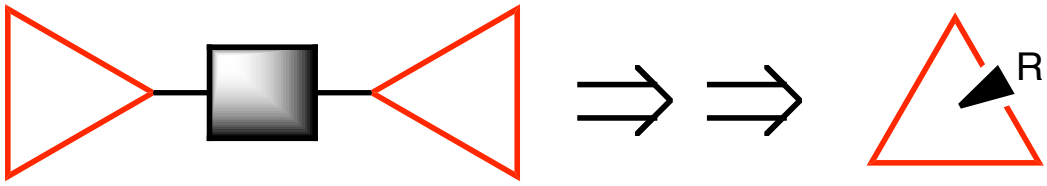

Figure 4.10 Retrosynthesis analysis for the *t*-butyl TOTA sandwich structures.

4.3.5 Synthesis of the Ethynylene Sandwich

Synthesis of the ethynylene sandwich **4.1** begins with the ethynylene building block **3.43**. Standard low-temperatures conditions generate the organolithium species and then the *t*-butyl TOTA cation **3.32** is added to the solution. The final product is obtained in moderately good yield (Scheme 4.4).

Scheme 4.4

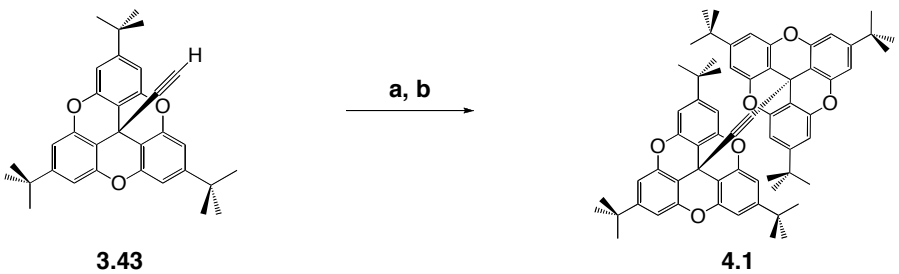

3.43 **4.1**

a. Bu^{n}Li, THF b. Compound 3.32, 75 %

The NMR spectroscopic analysis of this first species demonstrates the highly symmetrical nature of these sandwich compounds in solution. In the ^{1}H NMR spectrum only two singlets (δ 6.85 and δ 1.28 ppm) are observed that correspond to the two different protons on the TOTA moiety. In the ^{13}C NMR spectrum 8 resonance peaks for the molecule are observed.

4.3.6 Synthesis of the Phenylene Sandwich

Two routes have been explored to generate the phenylene sandwich **4.2**. Initially, it was considered that generation of the organolithium species of the phenyl building block **3.47** and addition of the *t*-butyl TOTA cation **3.32** would generate the desired species (Scheme 4.5, Reaction 1). Poor and unreliable yields encouraged an alternative route. The generation of the double organolithium dihalobenzene species with *t*-butyllithium[14] and addition of two equivalents of the *t*-butyl TOTA cation **3.32** should also generate the desired phenylene sandwich species (Scheme 4.5, Reaction 2). Indeed, the second route was found to be a reasonable method, eliminating one step and obtaining the desired product; although, unreliable yields were very low ranging from no detectable product to 26%.

Scheme 4.5

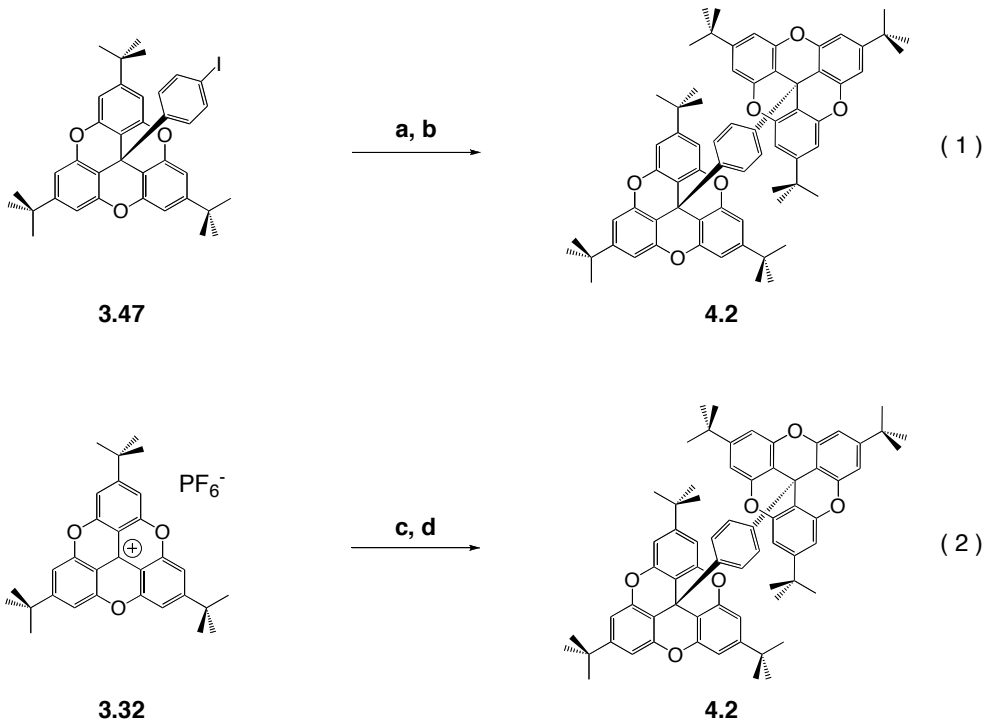

a. Bu^{n}Li, THF b. Compound 3.32, 12% c. 1,4-diiodobenzene, Bu^{t}Li (2 eq.), THF d. Compound 3.32 (2 eq.), 26%

4.3.6.1 Phenylene Sandwich Side Products

A number of side products and crystal structures resulted from the initial trials in the synthesis of the phenylene sandwich that demonstrates the reactivity of the cation. First, as expected, reduced material is frequently obtained after exposing the halophenyl building block to the halo-metal exchange conditions (Scheme 4.6, Reaction 1). Secondly, the alkylated species was also obtained due to excess *n*-butyllithium in the reaction mixture (Scheme 4.6, Reaction 2). A third side product obtained in one case was the propanone adduct (Scheme 4.6, Reaction 3). Presumably a trace amount of acetone was present from the rubber septa, which had been rinsed with acetone prior to the reaction.

Similar side products were obtained even when changing the alkyllithium regeants from ^{n}BuLi to ^{t}BuLi. In the last side product obtained after using ^{t}BuLi to

give the *t*-butyl adduct (Scheme 4.6, Reaction 4). The *t*-butyl species is interesting because it suggests the three-fold symmetric [2,2,2] bicyclo species could also be a reasonable synthetic target. Also, the single crystal X-ray structure revealed the C–C bond (sp^3-sp^3) from the central TOTA carbon to the tertiary carbon of the *t*-butyl moiety to be quite long, 1.589 Å.

Scheme 4.6

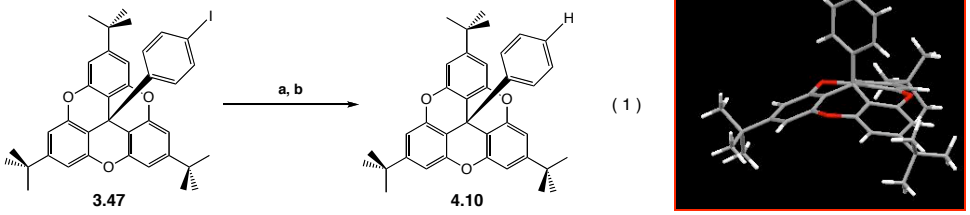

(1)

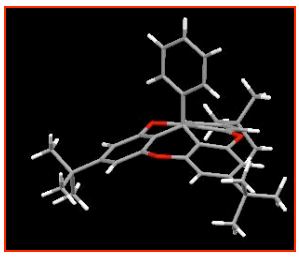

a. Bu^{n}Li, THF b. Compound 3.32, Aqueous workup, *ca.* 50%

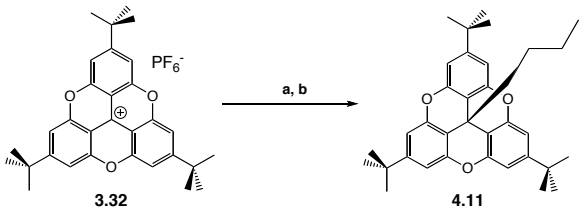

(2)

a. Compound 3.46, Bu^{n}Li, THF b. Compound 3.32, 2 equiv., *ca.* 25%

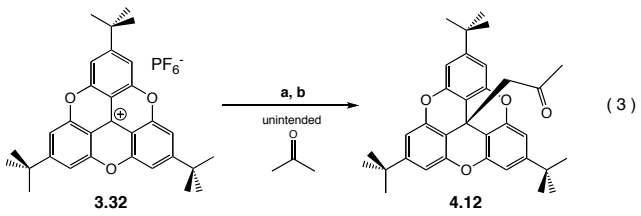

(3)

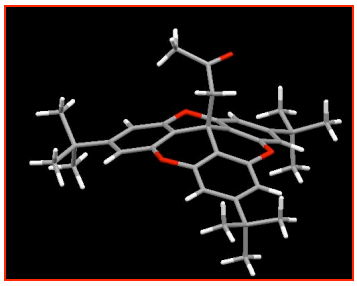

a. Compound 3.46, Bu^{t}Li, THF b. Compound 3.32, 1.5 equiv., *ca.* 50%

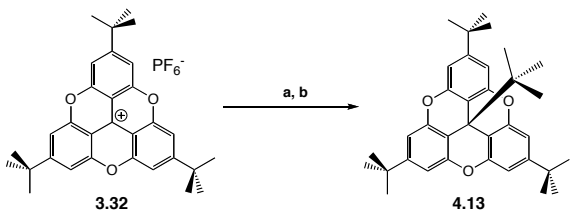

(4)

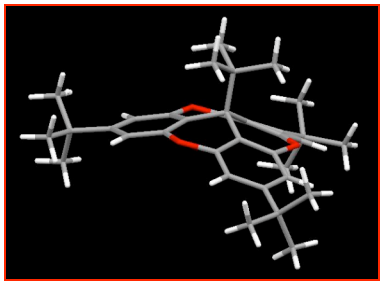

a. Compound 3.46, Bu^{t}Li, THF b. Compound 3.32, 2 equiv., *ca.* 25%

Table 4.1 Summary of Single Crystal X-ray Characteristics for **4.2** Side Products

Molecule	Formula	MW	Crystal System Space Group	Z	Packing Coefficient
4.10	$C_{37}H_{38}O_3$	531	Orthorhombic *Pbca*	8	0.85
4.11	$C_{35}H_{42}O_3$	511	Triclinic $P\bar{1}$	2	0.82
4.12	$C_{34}H_{38}O_4$	511	Monoclinic $P2_1$	4	0.83
4.13	$C_{35}H_{42}O_3$	511	Orthorhombic *Pnma*	4	0.87

4.3.7 Synthesis of the Diethynylene Sandwich

The diethynylene species **4.3** is made by direct homo-coupling of the ethynylene building block **3.43** under Eglington oxidative copper (II) conditions (Scheme 4.7).[15]

Scheme 4.7

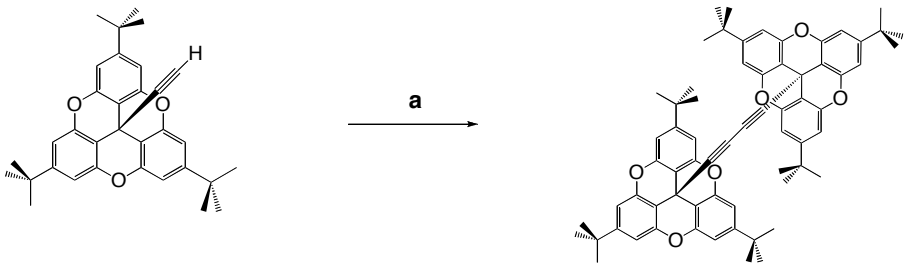

3.43 **4.3**

a. $Cu(OAc)_2 \cdot H_2O$, EtOH, 16 %

4.3.8 Synthesis of the Phenyl-Ethynylene Sandwich

Transition metal coupling methodology was used to prepare the asymmetric species **4.4**. Selective Sonogashira coupling[16] between the phenylene building block **3.47** and the ethynylene building block **3.43** generates the asymmetric species **4.4** (Scheme 4.8).

Scheme 4.8

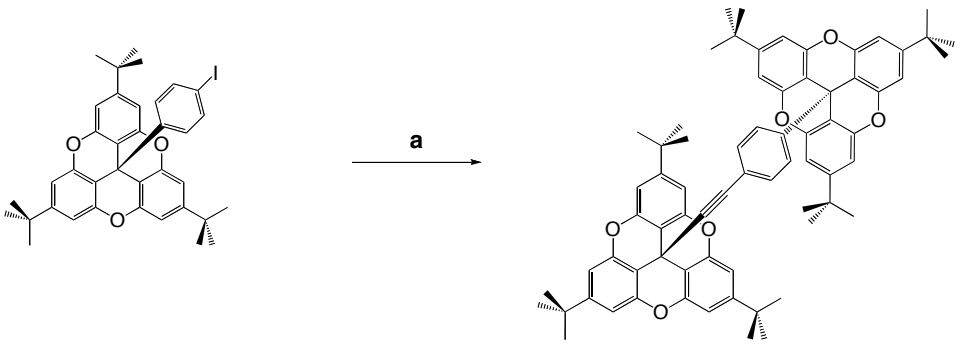

3.47 **4.4**

a. $Pd(PPh_3)_4$, CuI, Et_3N, Compound 3.43, 98%

4.3.9 Synthesis of the Biphenyl Sandwich

Several procedures where considered for the biphenyl sandwich **4.5**. Initially, it was thought homo-coupling the zincate of the phenylene building block **3.47** under Negishi conditions,[17] or preparing the borate species of the phenylene building block **3.47** and applying it to Suzuki conditions,[18] could make the desired product. It was also speculated that two equivalents of *n*-butyllithium and 4,4'-diiodobiphenyl would generated the desired organolithium species and the subsequent addition of the TOTA cation **3.32** would produce the desired sandwich species. Indeed, this last method was utilized and produced the biphenyl sandwich **4.5** in moderately good yield (Scheme 4.9).

Scheme 4.9

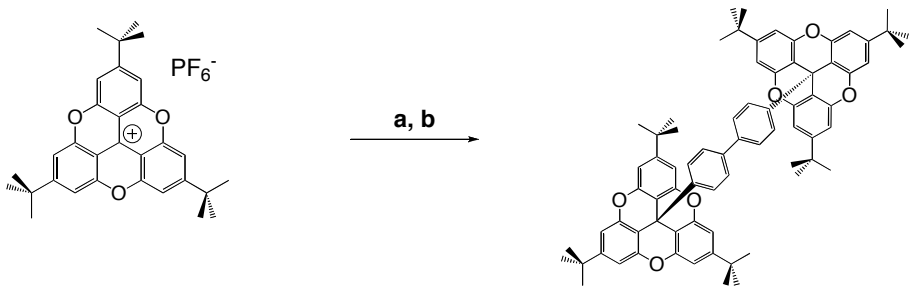

3.32 **4.5**

a. 4,4-Diiodobiphenyl, Bu^nLi (2 eq.), THF b. Compound 3.32 (2 eq.), 75%

4.3.10 Synthesis of the Ethynyl-Phenyl-Ethynylene Sandwich

Although the ethynyl-phenyl-ethynylene sandwich species could be prepared by a step-wise addition to the TOTA building block, it was determined a double cross-coupling of a dihalobenzene and TOTA building block **3.43** would be a desirable route. The ethynyl-phenyl-ethynylene sandwich **4.6** was generated with the Sonogashira reaction[16] of 1,4-diiodobenzene and two equivalents of the ethynylene TOTA building block **3.43** in a moderately good yield (Scheme 4.10).

Scheme 4.10

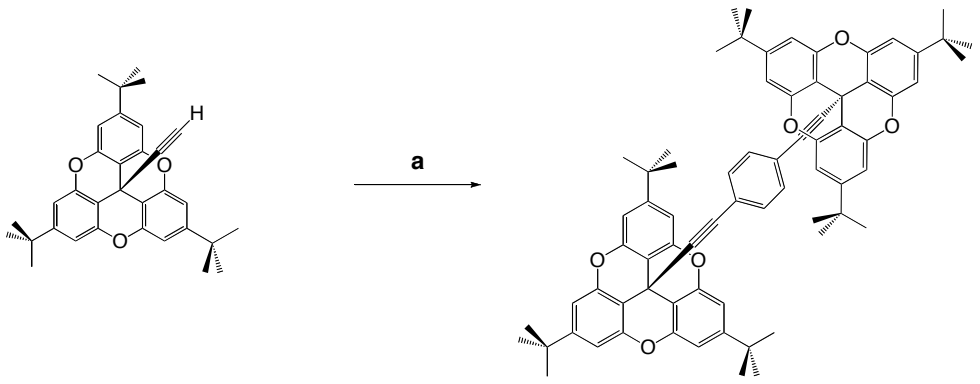

3.43 **4.6**

a. 1,4-Diiodobenzene (0.5 eq.), $Pd(PPh_3)_2Cl_2$, CuI, Et_3N, 78%

4.3.11 Synthesis of the Tolan Sandwich

In order to prepare the tolan sandwich species **4.7**, the phenylene TOTA building block was first modified. Under Sonogashira conditions,[16] ethynyltrimethylsilane was added to the phenylene TOTA building block **3.47** to generate **4.9a** and the TMS moiety was subsequently cleaved under basic conditions. Species **4.9b** was then cross-coupled to the phenylene TOTA building block **3.47** under Sonogashira conditions (Scheme 4.11).[16]

Scheme 4.11

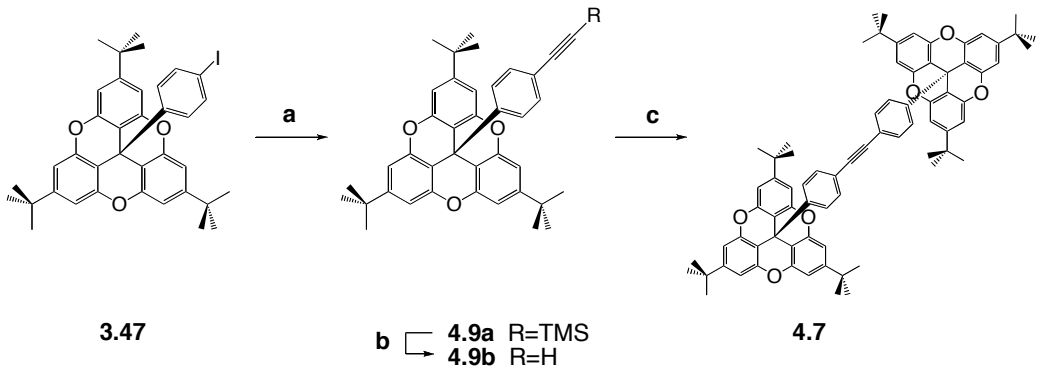

a. Ethynyltrimethylsilane, $Pd(PPh_3)_4$, CuI, Et_3N, 98% b. K_2CO_3, MeOH, THF, 94%
c. $Pd(PPh_3)_4$, CuI, Et_3N, Compound 3.47, 58%

4.3.12 Synthesis of the Terphenyl Sandwich

Preparation of the terphenyl sandwich species **4.8** was accomplished by converting the phenylene TOTA building block **3.47** to be converted into the boronic ester **3.51**.[19] Afterwards, two equivalents of **3.51** was combined with 1,4-diiodobenzene under Suzuki coupling conditions[18] to yield the terphenyl sandwich **4.8** (Scheme 4.12).

Scheme 4.12

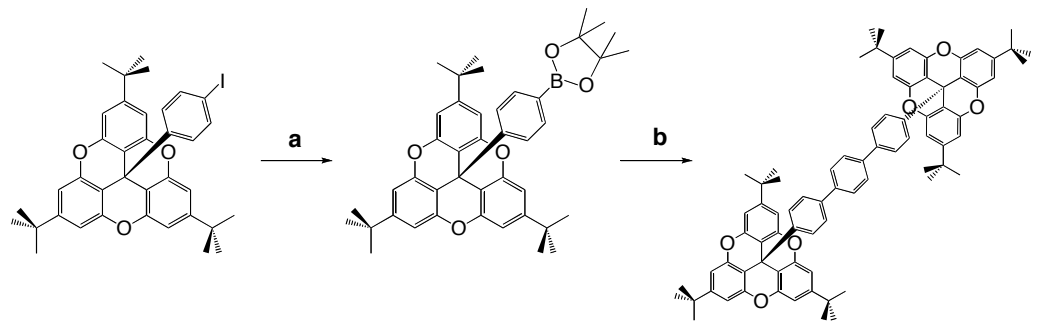

a. $(Me_4C_2O_2)B\text{-}B(O_2C_2Me_4)$, $PdCl_2(dppf)$, KOAc, DMSO, 40% b. 1,4-Diiodobenzene, $Pd(PPh_3)_4$, aq. Na_2CO_3, Toluene, 46%

Table 4.2 Synthetic Summary of the TOTA Sandwich Structures

Compound	Axis (-R-)	Reagents[b]	Conditions	Yield[a] (%)	Steps from **3.32**
4.1	-C≡C-	Bu^nLi, THF	1 h, -78 °C	91	5
4.2	-Ph-	Bu^nLi, THF	1 h, -78 °C	25	4
4.3	-C≡C-C≡C-	$CuSO_4$-H_2O, EtOH	16 h, Reflux	16	4
4.4	-Ph-C≡C-	$Pd(PPh_3)_4$, CuI, NEt_3	16 h, 80 °C	80	3
4.5	-Biphenyl-	4,4'-DIB, Bu^nLi, THF	1.5 h, -78 °C	58	2
4.6	-C≡C-Ph-C≡C-	1,4-DIB, $Pd(PPh_3)_4$, CuI, NEt_3	16 h, 80 °C	90	4
4.7	-Tolan-	$Pd(PPh_3)_4$, CuI, NEt_3	16 h, 80 °C	75	5
4.8	-Terphenyl-	1,4-DIB, $Pd(PPh_3)_4$, *aq*. Na_2CO_3, Toluene	16 h, 80 °C	46	4

[a] Conditions for final step to generate the superstructure.
[b] 4,4'-DIB = 4,4'-Diiodobiphenyl, 1,4-DIB = 1,4-Diiodobenzene

4.3.13 Solid-state Properties of *tert*-butyl TOTA Sandwich Structures

Single crystal X-ray structures were obtained for two of the *t*-butyl TOTA sandwich structures, **4.2** and **4.3**. Their molecular packing, basic unit cell and molecular geometries were investigated. A dynamic variable temperature X-ray study was also undertaken for the phenylene sandwich **4.2**. Powder samples of all of the sandwich species were investigated for unit cell parameters.

4.3.14 Single Crystal Structure of the Phenylene *tert*-butyl TOTA Sandwich 4.2

Slow evaporation from methylene chloride yielded crystals of **4.2** suitable for single crystal X-ray diffraction analysis. The compound crystallized in the cubic crystal system with the centre of the molecule sitting about a site of $\bar{3}$ symmetry. This crystallographic orientation means that only one sixth of the molecule is unique and the central benzene ring is threefold disordered (Figure 4.11), although, it was not

clear from the initial analysis if the disorder is static or dynamic. Residual electron density peaks suggested the presence of two disordered sites for solvent molecules. The crystal structure shows the two *t*-butyl TOTA moieties at the end of the structure with a 5.91 Å phenylene axis (C_q—C_q). The central carbon is nearly regular tetrahedral and the bond length from the central carbon to the *ipso* carbon on the central phenyl ring is quite long (1.55 Å, Figure 4.11). The depth of the molecular bowl was measured and found to be 1.55 Å (C_q to a plane made by the *pseudo-para* carbons of the trioxatriangulene). Also, the *t*-butyl TOTA moieties on the end of the molecule are oriented *anti* (180°) to each other. The compound was found to occupy the *Pa*3-*bar* space group, a cubic crystal system with 4 (Z) molecules per unit cell.

With regard to molecular packing, there appears to be no interdigitation between molecules thus leaving a significant void space around the central axis. With respect to the axis of the central molecule in the unit cell, the axes of the other molecules are approximately perpendicular (*ca*. 70°) and can be observed in Figure 4.13.

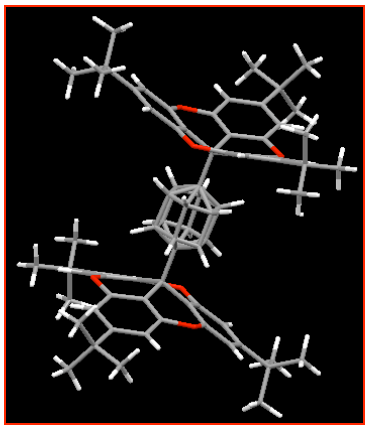

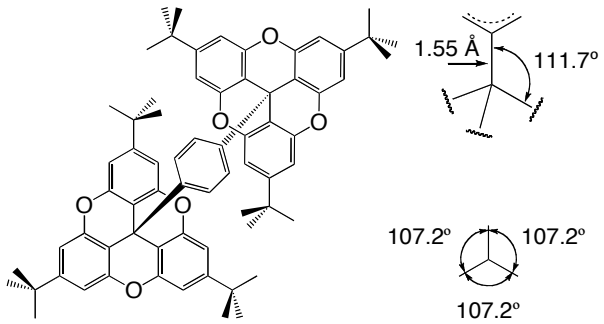

4.2

Figure 4.11 X-ray crystal structure of **4.2** at 160 K. Bond angles around the central carbon are also represented and the bond distance from the central quaternary carbon to the central phenyl ring.

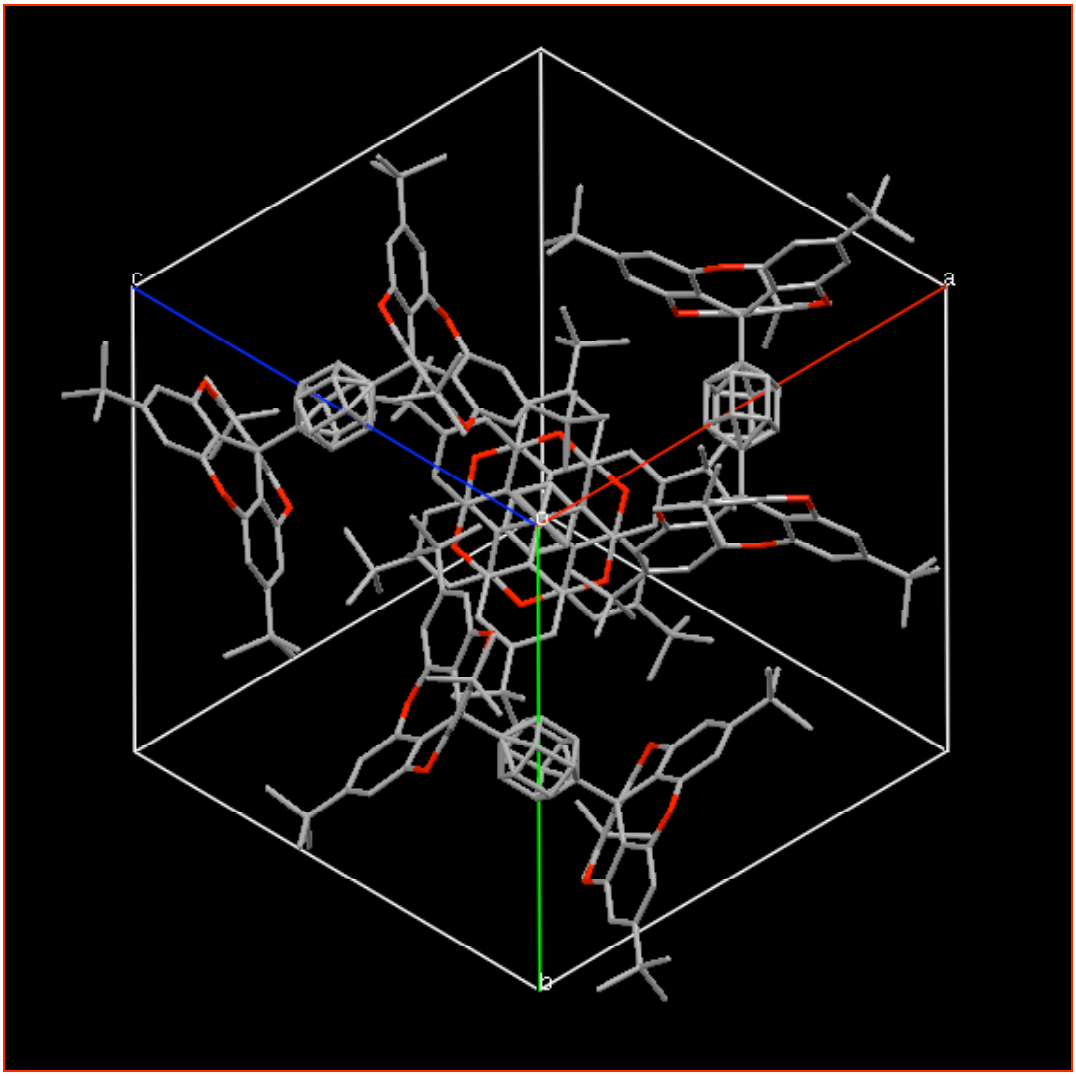

Figure 4.12 Section through the unit cell of **4.2** viewed looking down the six-fold axis of the cubic unit cell. The center of the three other molecules lie on the *a*, *b*, and *c* axis of the unit cell. Hydrogens have been omitted for clarity.

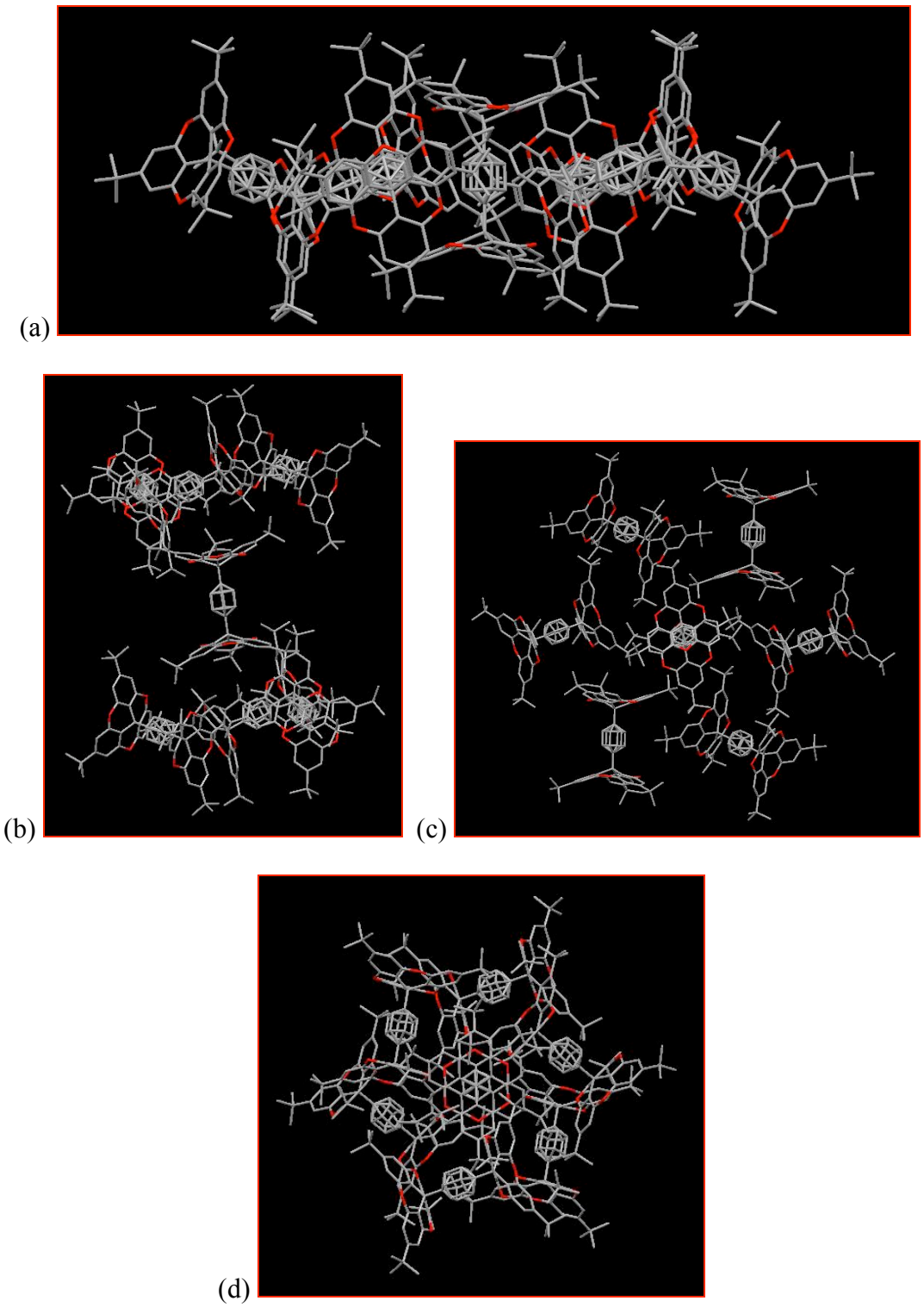

Figure 4.13 Several views of the molecular packing of the X-ray crystal structure of **4.2**: (a) Side view with six molecules radiating from the central molecule. (b) Side view with three molecules above and below the molecular bowls of the central molecule. (c) Axial view with six molecules radiating out from the central molecule. (d) Axial view with three molecules above and below the molecular bowls of the central molecule. Hydrogens have been omitted for clarity.

4.3.15 Variable Temperature Analysis of the Single Crystal of 4.2

Even though looking at an ORTEP drawing might give the impression of a static situation, the atoms in a crystal are not stationary. Anisotropic Gaussian displacement parameters (ADPs) obtained in a crystal structure solution provide information about the atoms displacement from its mean position. Although is not possible to make conclusions about atomic movement on the basis of ADPs alone, models have reproduced the correlated motions of groups of atoms from ADPs.[20]

Shortly after the discovery of X-ray diffraction in 1913, Debye[21] showed that increasing the temperature reduces the diffraction intensities, especially at large scattering angles, by increasing the extent of vibration of atoms about their average positions. Cruickshank 40 years later reported that anisotropic "vibration parameters" for aromatic systems could be interpreted in terms of molecular rigid-body motion[22] and thus be related to the spectroscopic and thermodynamic properties[23] of crystals. Since the pioneering work by Cruickshank, many crystallographers have made contributions toward the understanding of crystallographic ADPs and their utility in understanding molecular motions in crystals. In more recent years, Dunitz,[24,25] Schomaker,[24] Maverick,[26] Trueblood,[24,25,26] and Bürgi[27] have influenced the way chemists use crystallographic ADPs. Given the uncertainty of the static or dynamic three-fold disordered phenylene ring in the crystal structure of **4.2**, we decided to explore the use of X-ray ADPs to investigate the nature of the rotational potential in phenylene sandwich **4.2**.

Single-crystal diffraction data for the phenylene TOTA sandwich **4.2** were acquired from 100 to 298 K in 30-degree increments using the same crystal specimen. Initially, electron density two-dimensional contour maps taken through the plane of

atoms of interest (Scheme 4.13) show variations in the electron density about the central axis at 270 K and 100 K (Figures 4.14 and 4.15).

Scheme 4.13

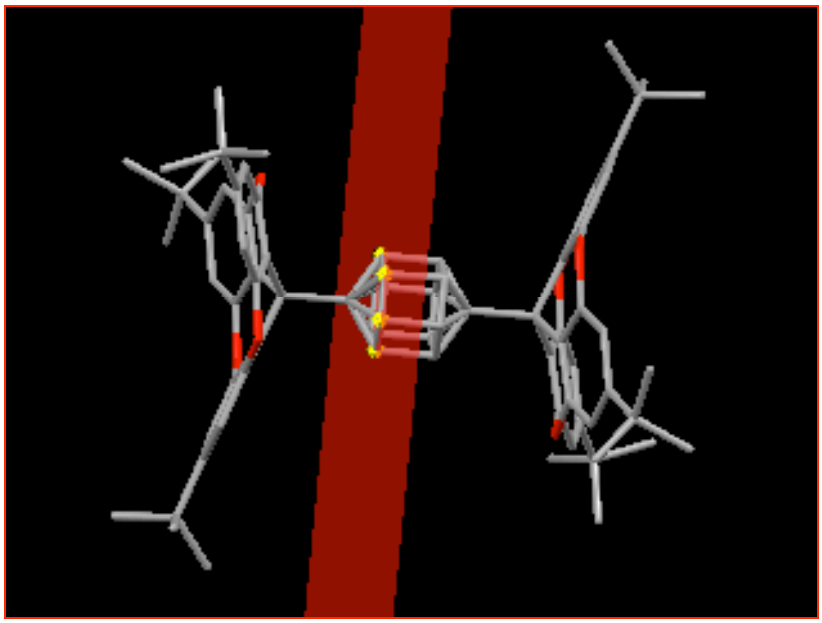

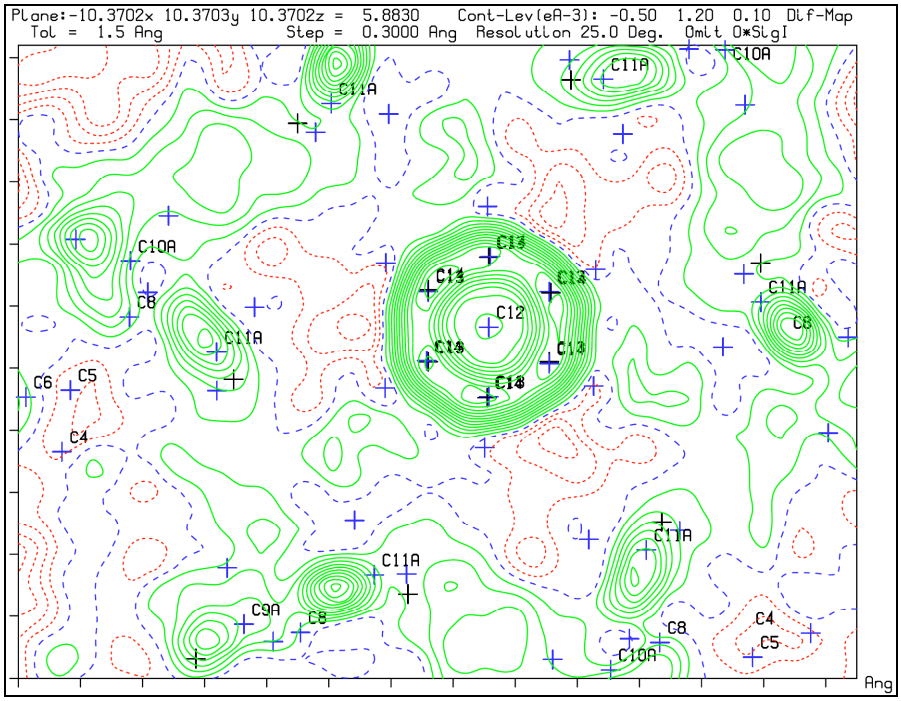

(a)

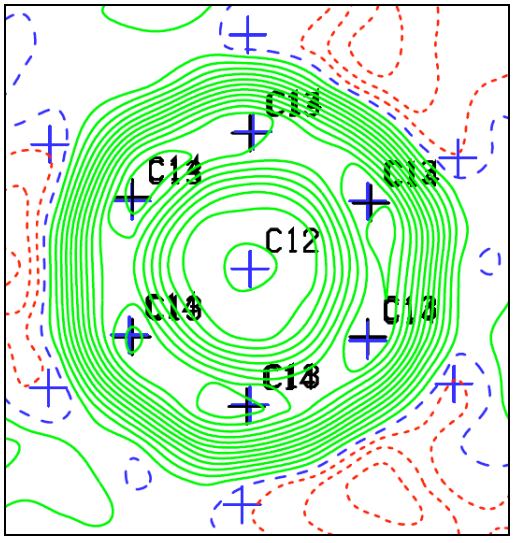

(b)

Figure 4.14 Electron density contour map of **4.2** at 270 K. The contour levels are drawn at intervals of 0.1 e A^{-3}.

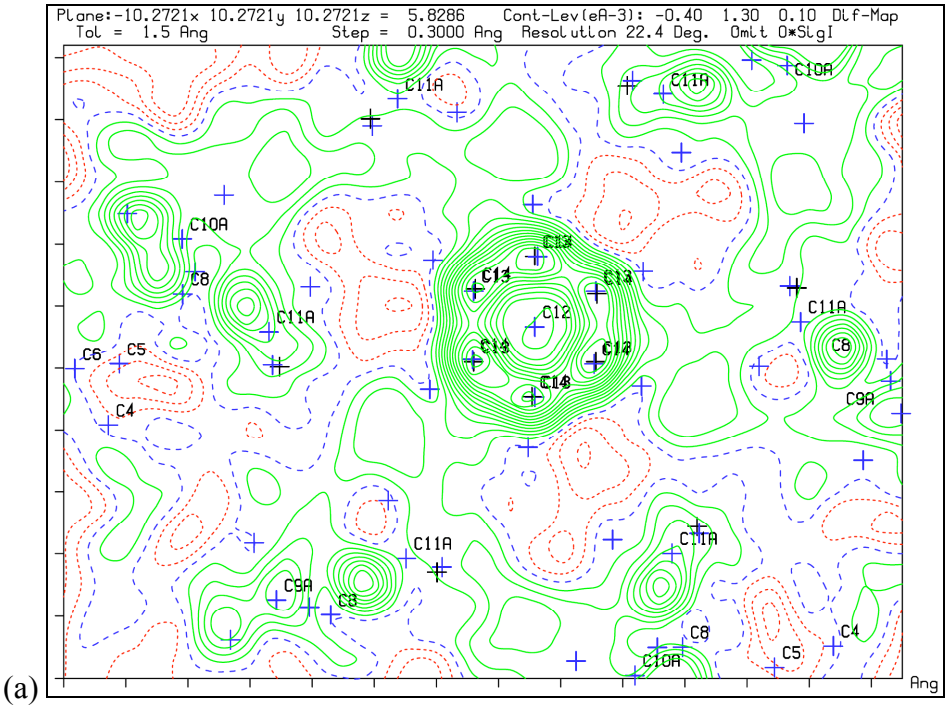

(a)

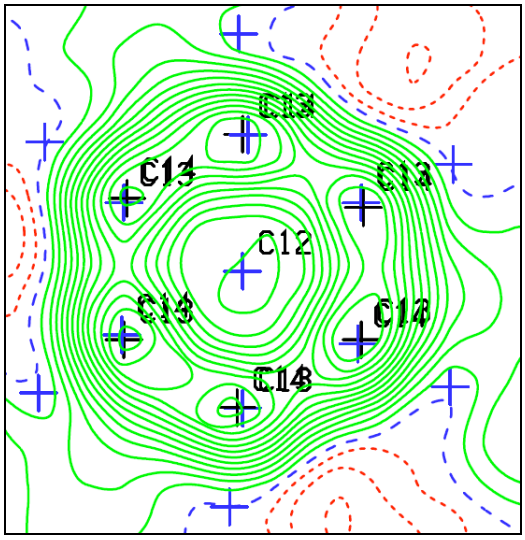

(b)

Figure 4.15 Electron density contour map of **4.2** at 100 K. The contour levels are drawn at intervals of 0.1 e A^{-3}.

Immediately one is drawn to the smear of electron density in the center of the contour map, Carbon-13 and Carbon-14 atoms of the central phenylene ring (Figures 4.14b and 4.15b). In Figures 4.14 and 4.15 the image is oriented looking down the three-fold axis, a cross section has been mapped showing the electron density in a

plane perpendicular to the three-fold and cutting through the *pseudo-ortho* atoms (C13 and C14) of the phenylene ring (Scheme 4.13). As the ring is three-fold disordered, this plane contains six atomic positions. The electron density from the *t*-butyls group is also observed, radiating out from the center torus.

In the 270 K measurement, the electron density appears generally smeared out into a torus, with only slight "bumps" at the positions where the atoms have been refined. At the lower temperature, 100 K, the "bumps" are slightly more defined, but the electron density is still quite significant around the torus. Carbon-12 is the pivot atom of the phenylene ring and is not in the presented plane.

The ADPs from the data sets are illustrated by ORTEP diagrams drawn at the 30% probability level with a view down the plane of the central phenylene ring in Figure 4.16. The size and direction of the elongated ellipsoid semi-major axes of the central phenylene carbons (C13 and C14) suggest that motion perpendicular to the principle plane of the phenylene unit may occur even at 100 K. As expected from an increase in thermal energy, from 100 K to 298 K, the phenylene carbon ellipsoids are more elongated (Figure 4.16).

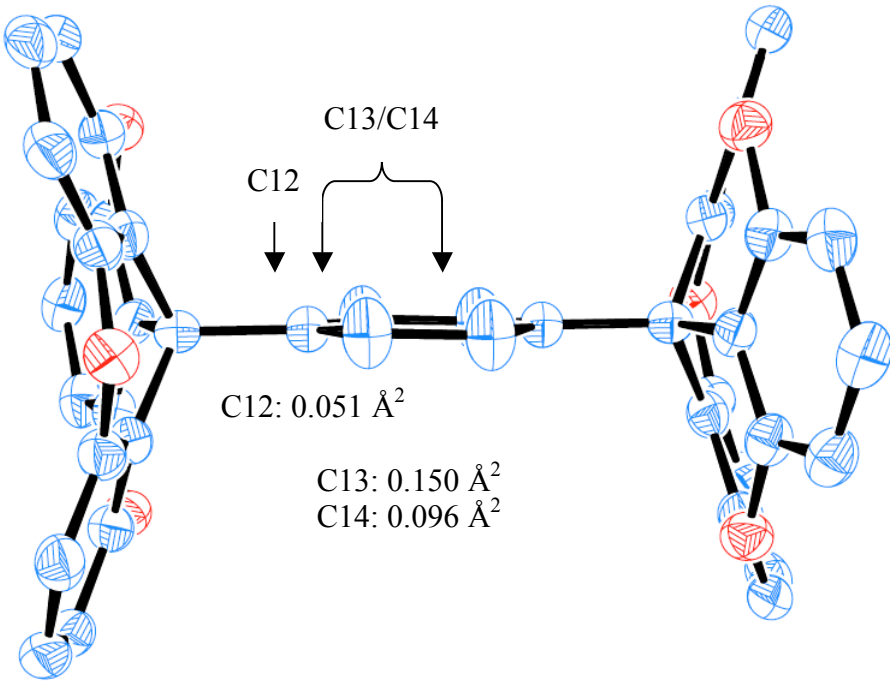
C13/C14
C12
C12: 0.051 Å^2
C13: 0.150 Å^2
C14: 0.096 Å^2

(a) 100 K

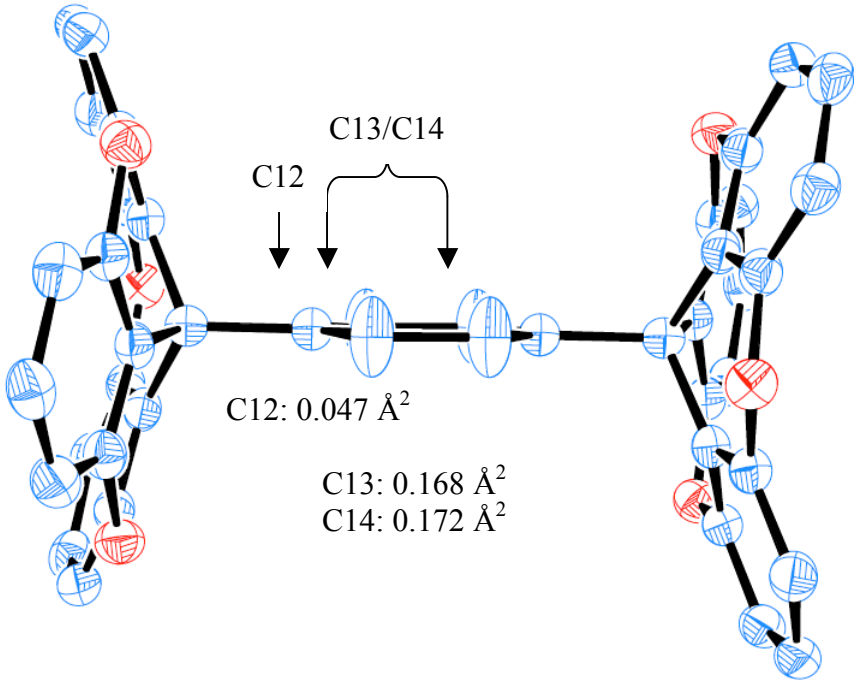
C13/C14
C12
C12: 0.047 Å^2
C13: 0.168 Å^2
C14: 0.172 Å^2

(b) 210 K

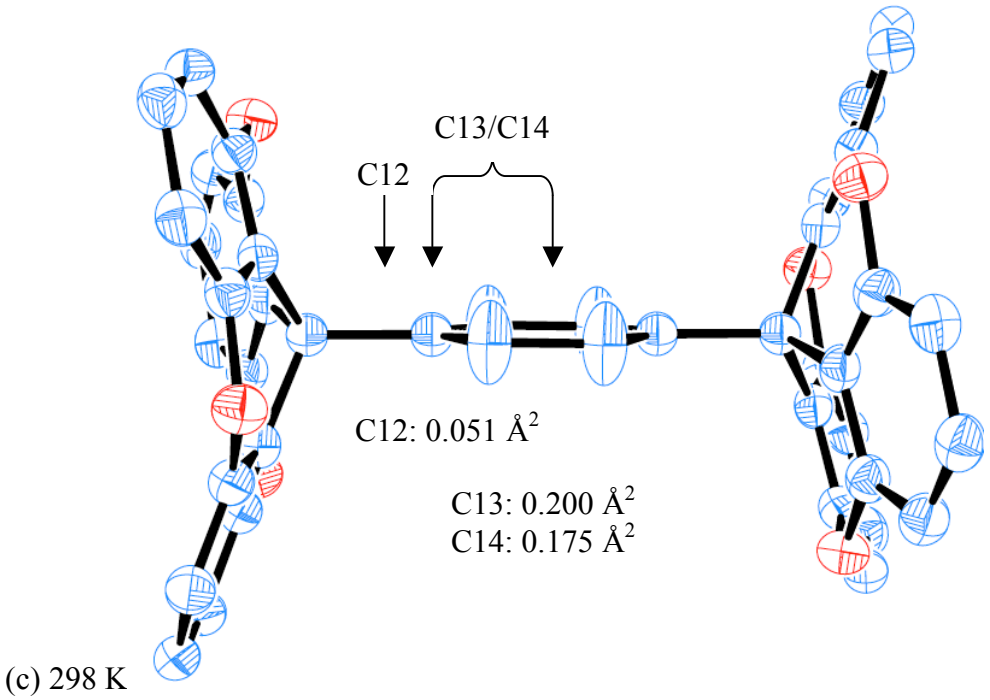

Figure 4.16 ORTEP displacement diagrams of the phenylene sandwich **4.2** from data taken at 100, 210, and 298 K, with ellipsoids drawn at the 30% probability level. Values for the principle mean square atomic displacement (U^2) of carbon atoms of the phenylene group about the long molecular axis are shown. Hydrogens and *t*-butyl groups have been omitted for clarity.

The data for the thermal evolution of the ADPs for the atoms of interest is also presented in Table 4.3. As expected there is a slight increase in the unit cell volume as the temperature increases. Also, C13 and C14 shown an increase in the semi-major axes (SMAs), first column for each atom, and the axis perpendicular to the plane of the of the central phenylene ring.

Table 4.3 Unit Cell Volumes and Principle Mean Square Atomic Displacement (U^2) of SMAs for **4.2**

Temp (K)	Unit Cell Volume(Å^3)	C12 – Pivot atom (Å^2)			C13 – Phenyl atom (Å^2)			C14 – Phenyl atom (Å^2)		
100	5632	0.0515	0.0515	0.0494	0.1500	0.0543	0.0285	0.0957	0.0725	0.0493
130	5650	0.0490	0.0490	0.0444	0.1449	0.0541	0.0367	0.1094	0.0691	0.0440
160	5669	0.0363	0.0363	0.0291	0.1694	0.0216	0.0160	0.1227	0.0506	0.0303
190	5709	0.0483	0.0483	0.0416	0.1653	0.0463	0.0373	0.1537	0.0601	0.0395
210	5731	0.0478	0.0478	0.0457	0.1676	0.0513	0.0256	0.1724	0.0408	0.0398
240	5764	0.0488	0.0488	0.0423	0.1898	0.0490	0.0265	0.1635	0.0538	0.0406
270	5795	0.0518	0.0518	0.0493	0.1915	0.0444	0.0333	0.2371	0.0461	0.0293
298	5826	0.0523	0.0523	0.0490	0.1996	0.0381	0.0337	0.1748	0.0679	0.0368

A graphical representation of the semi-major axes clearly shows some interesting trends. Carbon-12, the pivot atom, shows very little variation among the temperatures in the length of the semi-major axis, with each approximately 0.05 $Å^2$. Carbon-13 and Carbon-14 show clearly a different trend. First, looking at the axes parallel to the phenyl rings, a range similar to Carbon-12 axes is found, approximately 0.02-0.07 $Å^2$. However, the axes perpendicular to the phenyl ring are quite elongated at all temperatures and are approximately 0.1-0.2 $Å^2$. Also, from the graph (Figure 4.17), a slight increase in the longest semi-major axes (SMA1) is observed for Carbon-13 and Carbon-14, whereas Carbon-12 is relatively constant throughout the temperature measurements

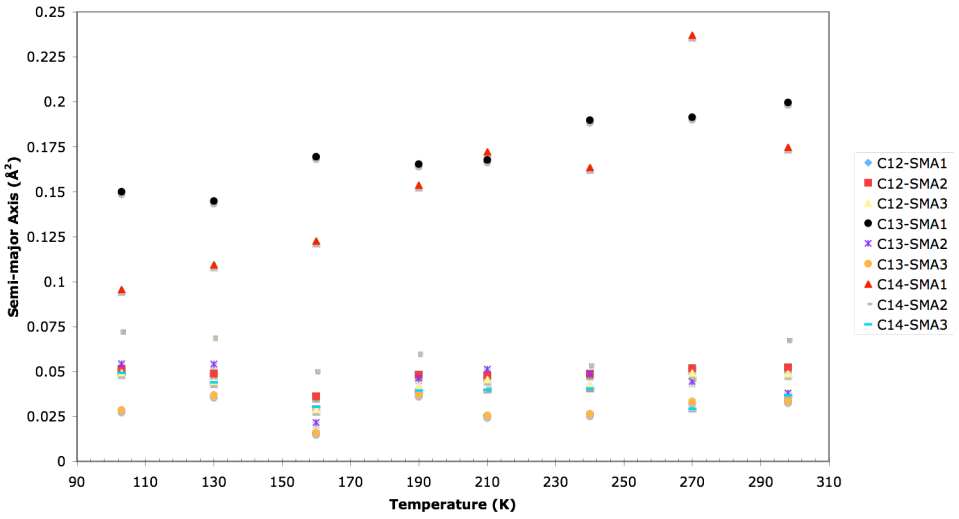

Figure 4.17 Graph depicting the semi-major axis versus temperature of the carbons in the central phenylene ring of **4.2**.

Because the SMA1 of C13 and C13 seemed to have a relatively wide range, refinement was done again with EADP restraint, averaging SMA1 of Carbon-13 and Carbon-14. Results showed no significant worsening of the model and the values were used to further evaluate the variable temperature measurements (Table 4.4).

Table 4.4 Refinement values with EADP restraint of **4.2**

Temp (K)	Without restraint (R-value)	SMA1 - C13 and C14 (max U^2 displacement)	With EADP restraint (R-value)
100	0.0988	0.124	0.0991
130	0.0970	0.125	0.0970
160	0.1024	0.141	0.1024
190	0.0871	0.156	0.0872
210	0.0781	0.165	0.0784
240	0.0746	0.173	0.0748
270	0.0773	0.193	0.0773
298	0.0775	0.185	0.0777

Again the values of the SMA1 for C13, C14 and C12 are graphically represented in Figure 4.18. While the similar trends are observed for the axes, there is a better linear agreement from the EADP restraint.

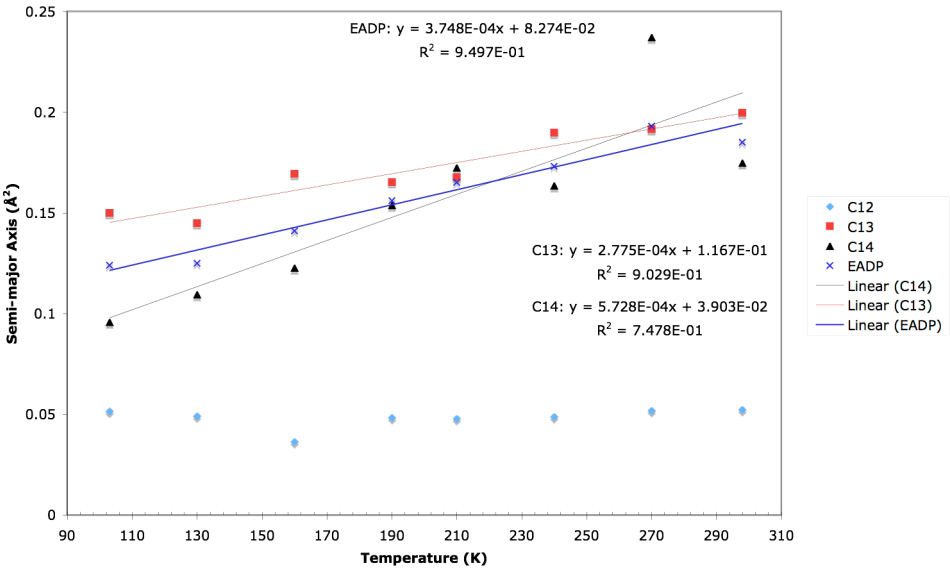

Figure 4.18 Graph depicting SMA1 versus temperature before and after refinement with EADP restraint of the carbons in the central phenylene ring of **4.2**.

It was further decided that the lattice motion in the direction perpendicular to the phenyl ring could be approximated from the Carbon-12 SMA1 (*ca*. 0.05 Å^2) and subtracted from the refined ADPs values for C13 and C14. The results are again graphically represented, with good linear correlation (Figure 4.19).

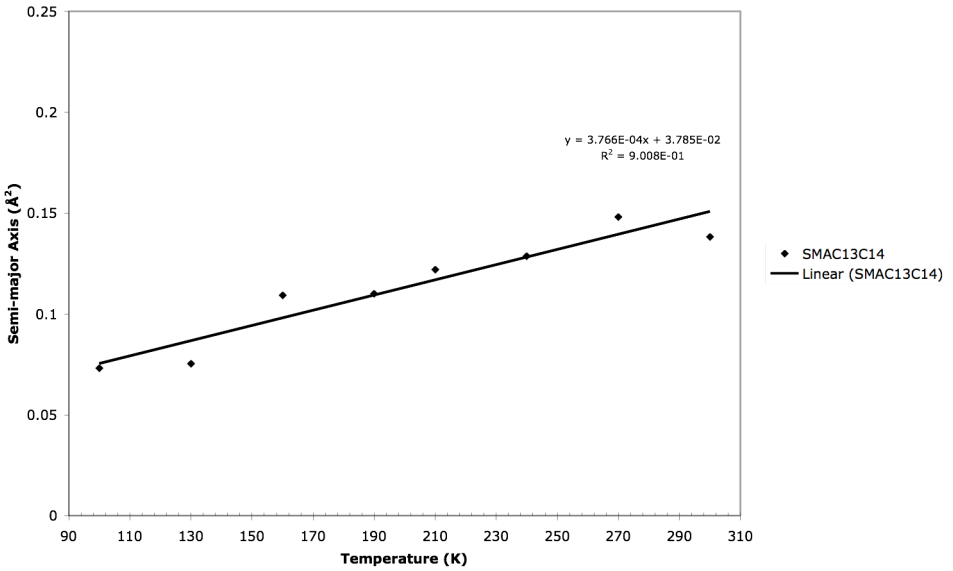

Figure 4.19 Graph depicting the semi-major axis (SMA1) for C13 and C14 versus temperature after subtraction of the lattice motion.

With this thermal motion data of the phenyl ellipsoids, it was then applied to the Maverick-Dunitz model.[28] The ADPs, or SMA1, of each Carbon-13 and -14 are analyzed to obtain the mean square amplitudes of vibration, $<\phi^2>$. A periodic sinusoidal potential for rotation is assumed about the six-fold axis:

$$V(\phi) = B(1-\cos n\phi)/2 \quad (4.1)$$

where B is the barrier to rotation and n = 6. A mean square amplitude of libration, $<\phi^2>$, of the central phenyl ring is obtained from the following expression:

$$\left\langle \phi^2 \right\rangle = \frac{\int_0^{\pi/n} \left(\phi^2\right) e^{\{-B(1-\cos n\phi)/2RT\}} d\phi}{\int_0^{\pi/n} e^{\{-B(1-\cos n\phi)/2RT\}} d\phi} \quad (4.2)$$

A plot was then generated by evaluation the definite integrals for various values of RT/B. This plot of $<\phi^2>$ as a function of RT/B for n = 6 is shown in Figure 4.20. The linear dependence for a classical harmonic oscillator (CHO) with the same quadratic force constant is also shown in Figure 4.20. At very low values of RT/B the Equation 4.2 does not hold and a quantum mechanical expression for $<\phi^2>$ must be considered.[20] There is also an upper limit where the curves cross that corresponds to a

constant probability of the rotation angle over the entire ϕ range. This upper limit was determined to be 250 deg^2 (or 220 K). Using the linear equation from Figure 4.19, ΔU = 3.766 e -10^{-4}T + 0.03785, ΔU (Å^2) was determined for 100 K, 150 K and 200 K. These values were then converted to amplitude of liberation (deg^2) to find the barrier to rotation value B from the Figure 4.20. Standard uncertainty (± s.u.) from variable temperature refinement X-ray data was carried through in the same manner for upper and lower energy barrier limits.

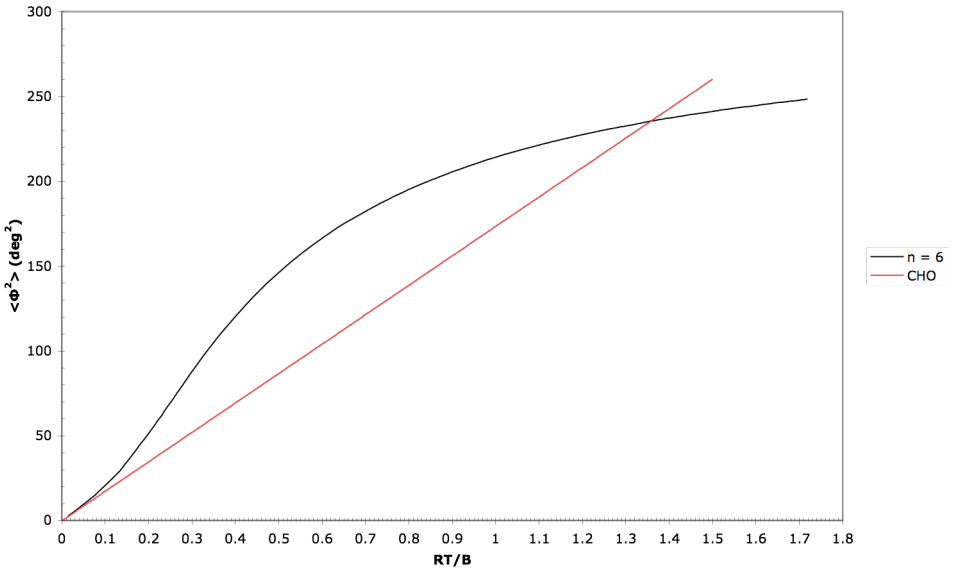

Figure 4.20 Variation of mean-square libration amplitude $<\phi^2>$ with RT/B for a six-fold (n = 6) periodic sinusoidal restricting potential with barrier height B. The red curve is for a classical harmonic oscillator (CHO) potential with the same quadratic force constant.

The calculated values for the barrier to rotation are given in Table 4.5. From this simple model of analysis of the ADPs for molecular motion in crystals, an average of 0.32 kcal/mol is calculated for the rotational barrier of the central phenylene ring in **4.2**. While other data is needed to support this result it is still believe that the disorder in the phenylene ring is due to dynamic and not vibration motion.

Table 4.5 Values for Barrier to Rotation for the Central Phenylene Ring in **4.2**

Temperature (K)	Lower limit	Middle Barrier (kcal/mol)	Upper limit	Energy Barrier (kcal/mol)
100	0.277	0.341	0.412	0.34 ± 0.07
150	0.266	0.347	0.431	0.35 ± 0.08
200	---[a]	0.266	0.364	0.27 + 0.10

[a] Value is outside predetermined range

4.3.16 Single Crystal Structure of the *tert*-butyl Diethynylene TOTA Sandwich 4.3

Slow evaporation of a methylene chloride solution of **4.3** yielded crystals suitable for X-ray diffraction analysis. The molecule sits about a site of $\bar{3}$ symmetry. The crystal structure shows the two *t*-butyl TOTA moieties at the end of the structure with a 6.72 Å diyne axis (C_q—C_q) and the acetylenic bonds in the central axis are linear (∠180.0°) (Figure 4.21). The central carbon is nearly tetrahedral. The depth of the molecular bowl was measured and found to be 1.47 Å (C_q to a plane made by the *pseudo-para* carbons of the trioxatriangulene). Also, the *t*-butyl TOTA moieties on the end of the molecule are oriented *anti* (180°), as observed with the phenylene sandwich **4.2** crystal structure. The compound was found to occupy the $Pa\bar{3}$ space group and possess a cubic crystal system with 4 (Z) molecules per unit cell with no observed solvent molecules.

With regard to molecular packing, there appears to be no interdigitation leaving a significant void around the central axis. With respect to the axis of the central molecules in the unit cell, the axes of the other molecules are approximately perpendicular (*ca*. 70°) and can be observed in Figure 4.23. The structure is isostructural with that of the previous phenylene sandwich **4.2** analogue.

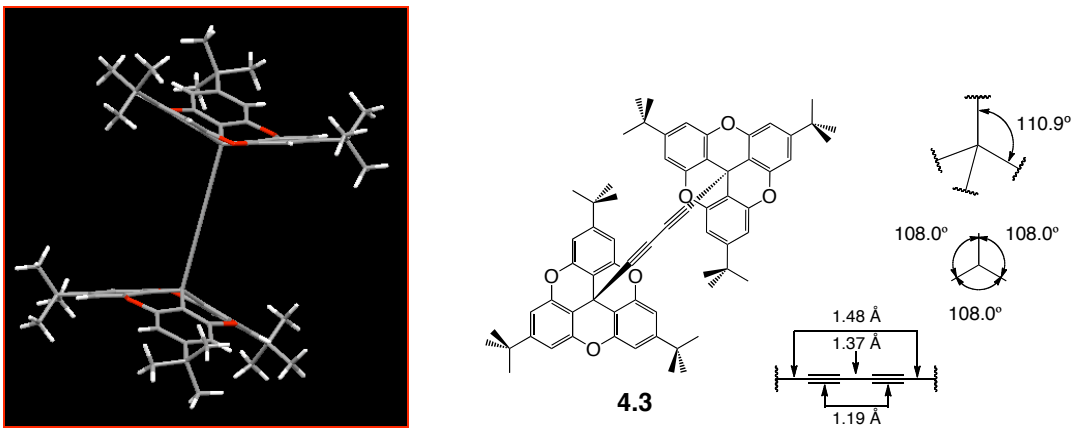

Figure 4.21 X-ray crystal structure of **4.3**. Bond angles of the central carbon and bond lengths of the diethynylene axis are also represented.

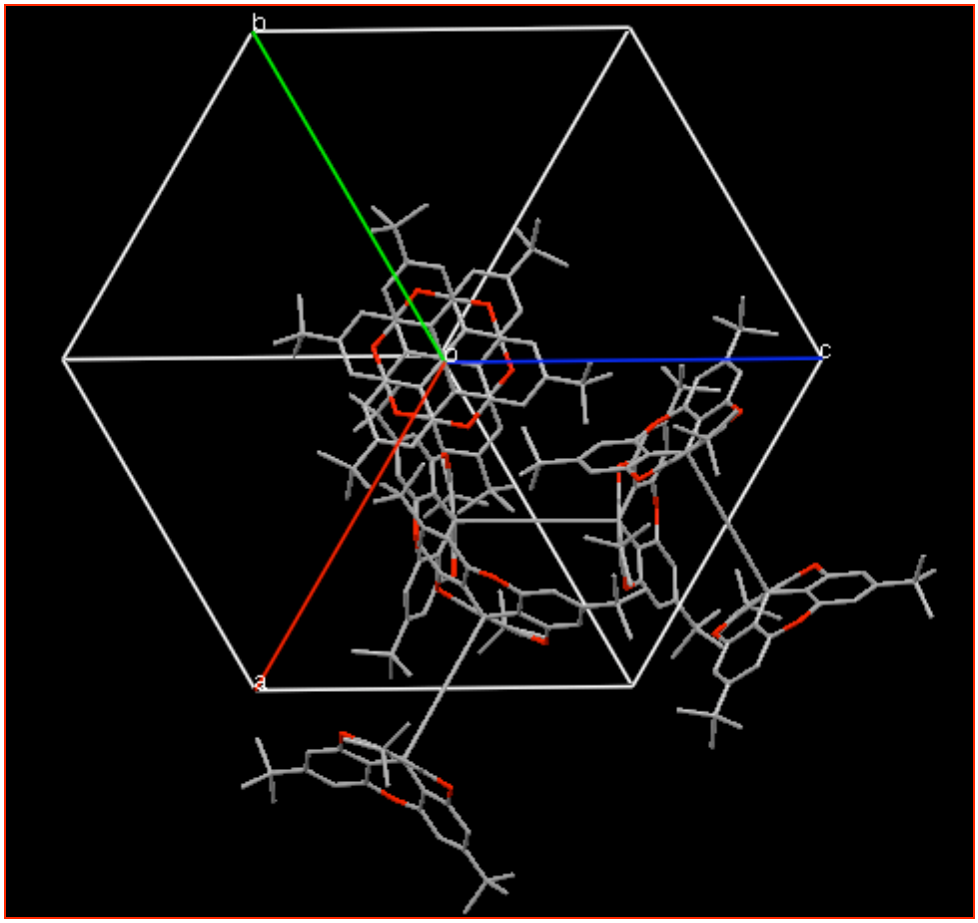

Figure 4.22 Axial view of the X-ray crystal structure of **4.3** looking down the six-fold axis of the cubic unit cell. The center of the three other molecules lie on the *a*, *b*, and *c* axis of the unit cell. Hydrogens have been omitted for clarity.

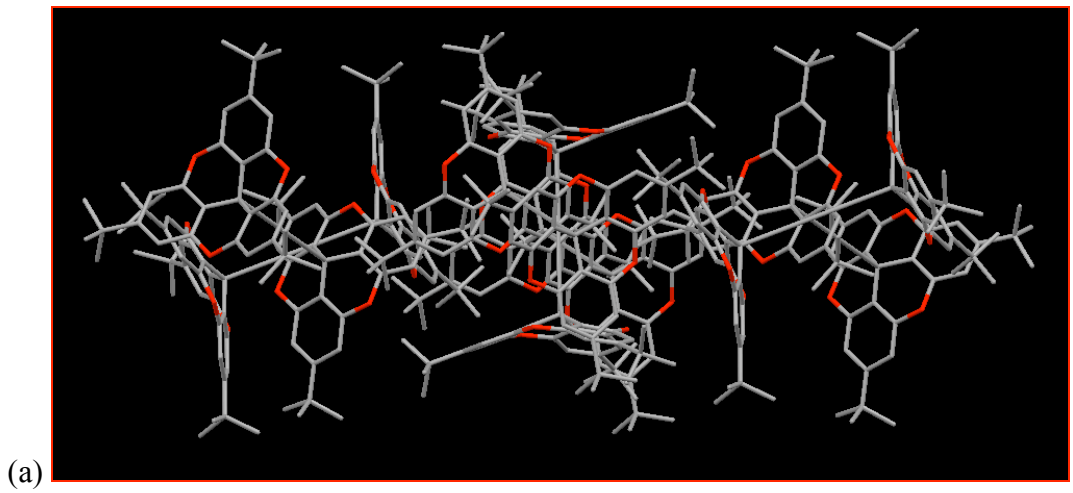

(a)

(b)

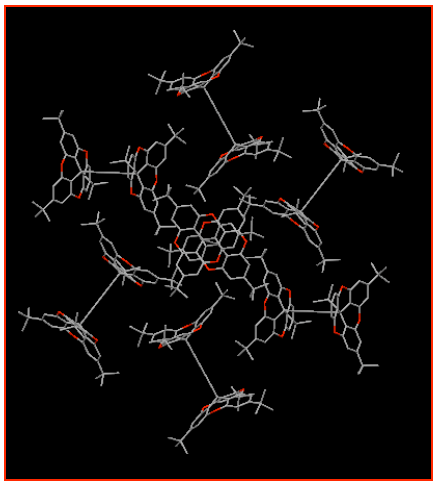

(c)

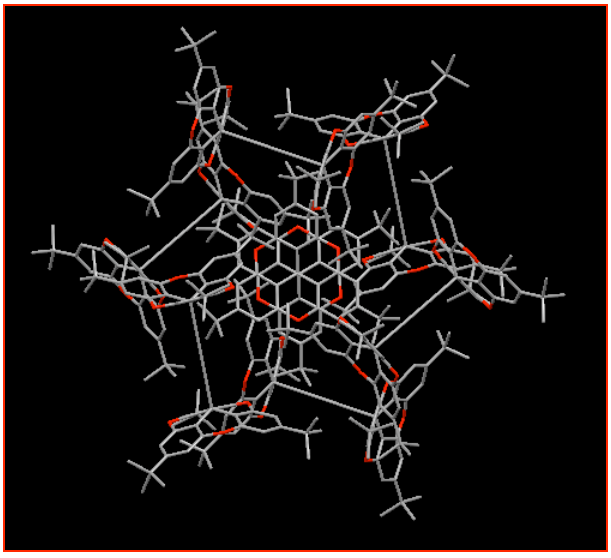

(d)

Figure 4.23 Several views of the molecular packing of the X-ray crystal structure of **4.3**: (a) Side view with six molecules radiating from the central molecule. (b) Side view with three molecules above and below the molecular bowls of the central molecule. (c) Axial view with six molecules radiating out from the central molecule. (d) Axial view with three molecules above and below the molecular bowls of the central molecule. Hydrogens have been omitted for clarity.

4.3.17 Solid-state Structures of the *tert*-butyl TOTA Sandwich Series

Although conditions have not yet been found to obtain quality single crystals of the *t*-butyl TOTA sandwich species, the solid material appears crystalline under a microscope. Initially, it can be claimed that there is some degree of control in the crystal system; in that, a *t*-butyl TOTA superstructure with an approximate 6 Å axis length results in a cubic unit cell system. These initial unit cell results for two compounds are surprising since cubic space groups are very rare among organic materials.[29] Also, the possibility of a mixed-order crystal from **4.2** and **4.3** is probable because of the isostructural nature of the two compounds in the solid state.

Since the remaining TOTA materials appear microcrystalline further analytical techniques may be used to obtain solid-state characteristics. Compounds **4.1** and **4.7** were submitted for low-resolution X-ray Powder Diffraction (XRPD) analysis and qualitatively exhibit a microcrystalline diffraction pattern. Therefore, the remaining samples may be good candidates for XRPD with a high-resolution synchrotron source followed by molecular modeling in order to determine the unit cell parameters (*a*, *b*, *c*, α, β, and γ) and molecular packing characteristics.[30]

Table 4.6 Summary of the Solid-state Characteristics from Single Crystal Analysis

Molecule	Formula	MW	Axis Length[a] (Å (X-ray))	Crystal System Space Group	Z	Packing Coefficient	mp (°C)[b]
4.1	$C_{64}H_{66}O_6$	931	4.10	---	-	---	> 350
4.2	$C_{68}H_{70}O_6$	983	5.87 (5.91)	Cubic $Pa\bar{3}$	4	0.79	> 350
4.3	$C_{66}H_{66}O_6$	955	6.67 (6.72)	Cubic $Pa\bar{3}$	4	0.76	> 350
4.4	$C_{70}H_{70}O_6$	1007	8.40	---	-	---	> 350
4.5	$C_{74}H_{74}O_6$	1059	10.14	---	-	---	> 350
4.6	$C_{72}H_{70}O_6$	1031	10.92	---	-	---	> 350
4.7	$C_{76}H_{74}O_6$	1083	12.68	---	-	---	> 350
4.8	$C_{80}H_{78}O_6$	1135	14.40	---	-	---	> 350

[a] Full geometry optimization calculations were carried out using the PM3 protocol and the TITAN program (Jaguar 3.5, Schrödinger, Inc., Portland, Oregon, 1998).

[b] Solid material maintains microcrystalline structure by visual observation to 350 °C during measurements.

4.3.18 Powder Diffraction Analysis of the *t*-butyl TOTA Sandwich Series

4.3.18.1 Introduction

In a single crystal diffraction experiment a suitably mounted crystal of a sample is illuminated with monochromatic beam of X-rays with a wavelength comparable to the interatomic separation in the crystal, *e.g.* a copper source produces X-rays with λ = 1.54 Å. X-rays are diffracted by the crystal in discrete direction in space and collected by a detector. From the direction of the diffracted X-rays, it is possible to determine the size and shape of the unit cell and with suitable data the identity and positions of atoms in the unit cell. Thus the definitive proof the crystal's chemical identity.

In a X-ray powder diffraction experiment, a large number of individual crystals, or the powder, are in the path of the incident X-rays and instead of spots, as seen with a single crystal experiment, rings of intensity are observed from the detector. The peak positions are determined by the size and shape of the unit cells of the sample with the Bragg equation (Equation 4.3).

$$n\lambda = 2d_{hkl}\sin\vartheta \quad (4.3)$$

In the powder diffraction experiment, the 3D information is compressed onto one dimension and the observation of diffracted intensity versus diffraction angle, 2θ, from which to deduce structural information.

When single crystal data is not available, or the molecular system does not form long-range order, X-ray powder diffraction offers the opportunity to elucidate the solid-state structure. If one has an approximate structural model it is possible to derive structural information similar to single crystal methods by a least squares refinement technique. Despite advances in recent years, solutions from powder diffraction remain a challenging and complex task.[31] We hope to determine phase

identification, unit cell parameters (*a*, *b*, *c*, α, β, and γ) and possible atomic coordinates of the *t*-butyl TOTA series that would lead to full structural Rietveld determination.[32]

4.3.18.2 Powder Diffraction Measurements

Using the single crystal data and assuming the same unit cell characteristics, one can simulate the expected powder diffraction and *hkl* peaks for the powder material.[33] The XRPD simulation from the single crystal data for **4.2** and **4.3** is shown in Figure 4.24. A list of the first ten *hkl* peaks for the simulation data is shown in Table 4.7 and 4.8.

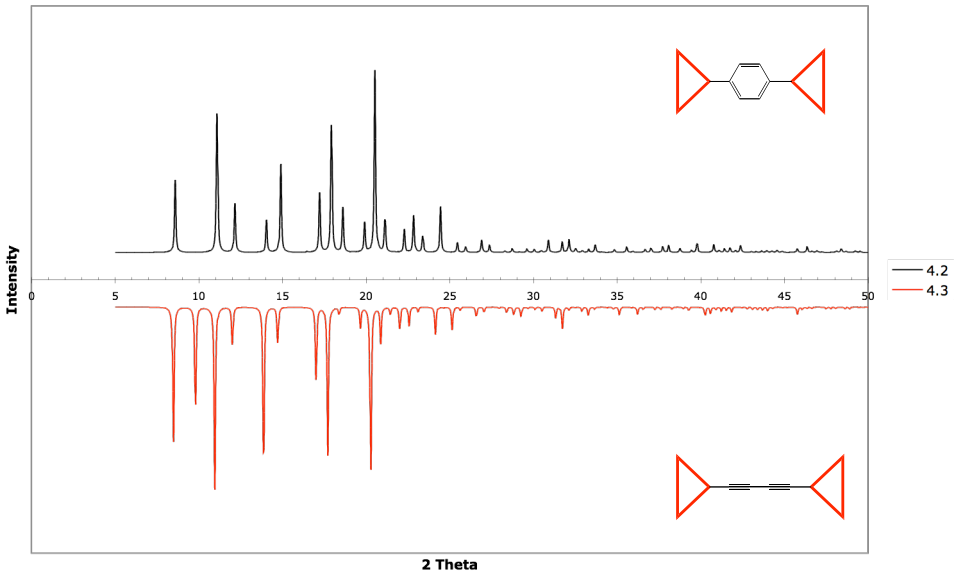

Figure 4.24 XRPD simulation from single crystal data for species **4.2** and **4.3**. Data indexed by CuKα (λ = 1.54056).

Table 4.7 Calculated *hkl* peaks for **4.2** - cubic unit cell with a = 17.83 Å

Peak	*h*	*k*	*l*	d_{hkl}	2 θ	Multiplicity
1	1	1	1	10.294	8.582	8
2	2	0	0	8.915	9.913	6
3	2	1	0	7.974	11.087	12
4	2	1	1	7.279	12.149	24
5	2	2	0	6.304	14.037	12
6	2	2	1	5.943	14.893	24
7	3	1	1	5.376	16.476	24
8	2	2	2	5.147	17.214	8
9	3	0	2	4.945	17.922	12
10	3	1	2	4.765	18.605	24

Table 4.8 Calculated *hkl* peaks for **4.3** - cubic unit cell with a = 18.05 Å

Peak	*h*	*k*	*l*	d_{hkl}	2 θ	Multiplicity
1	1	1	1	10.419	8.479	8
2	2	0	0	9.024	9.794	6
3	2	1	0	8.071	10.953	12
4	2	1	1	7.368	12.002	24
5	2	2	0	6.381	13.868	12
6	2	2	1	6.016	14.713	24
7	3	1	1	5.441	16.276	24
8	2	2	2	5.21	17.005	8
9	3	0	2	5.005	17.705	12
10	3	1	2	4.823	18.379	24

After purification, all of the samples were precipitated from methylene chloride as a white crystalline powder. Samples were then packed in a glass capillary tube and mounted with epoxy glue in a metal goniometer for synchrotron radiation measurements. Measurements were recorded with the Swiss Light Source at the Paul Scherrer Institute in Villigen, Switzerland. Samples were measured at 100, 200, and 300 K on the Material Sciences Beamline with a Mythen 2 microstrip detector (Figure 4.25).[34]

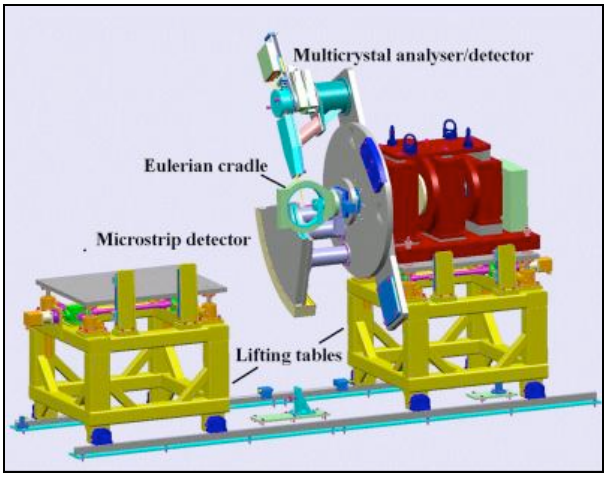

Figure 4.25 Schematic representation of the powder diffractometer station at the Paul Scherrer Institute.

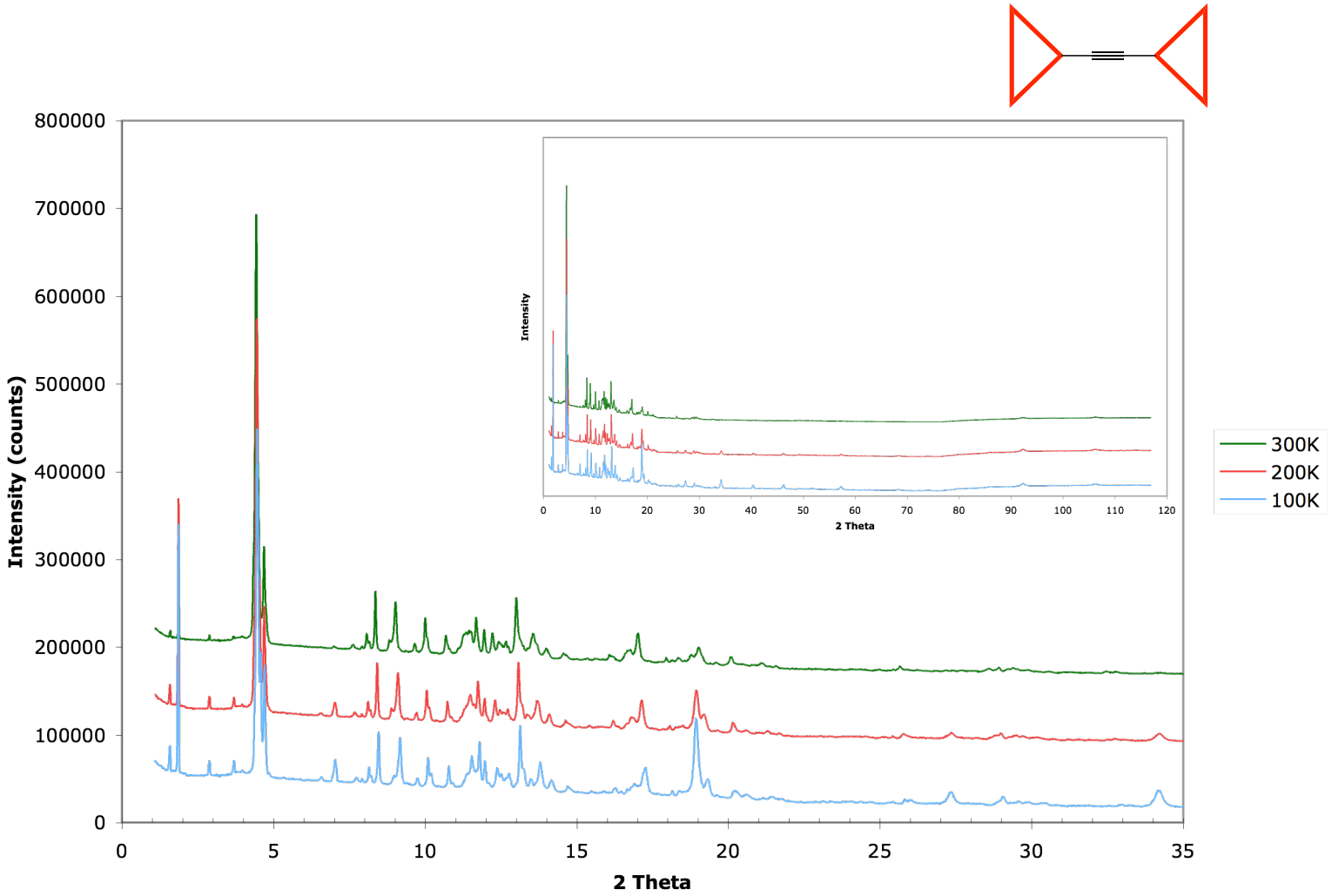

Figure 4.26 X-ray powder diffraction pattern for **4.1**. Measurements at 200 K and 300 K are offset with respect to intensity for clarity.

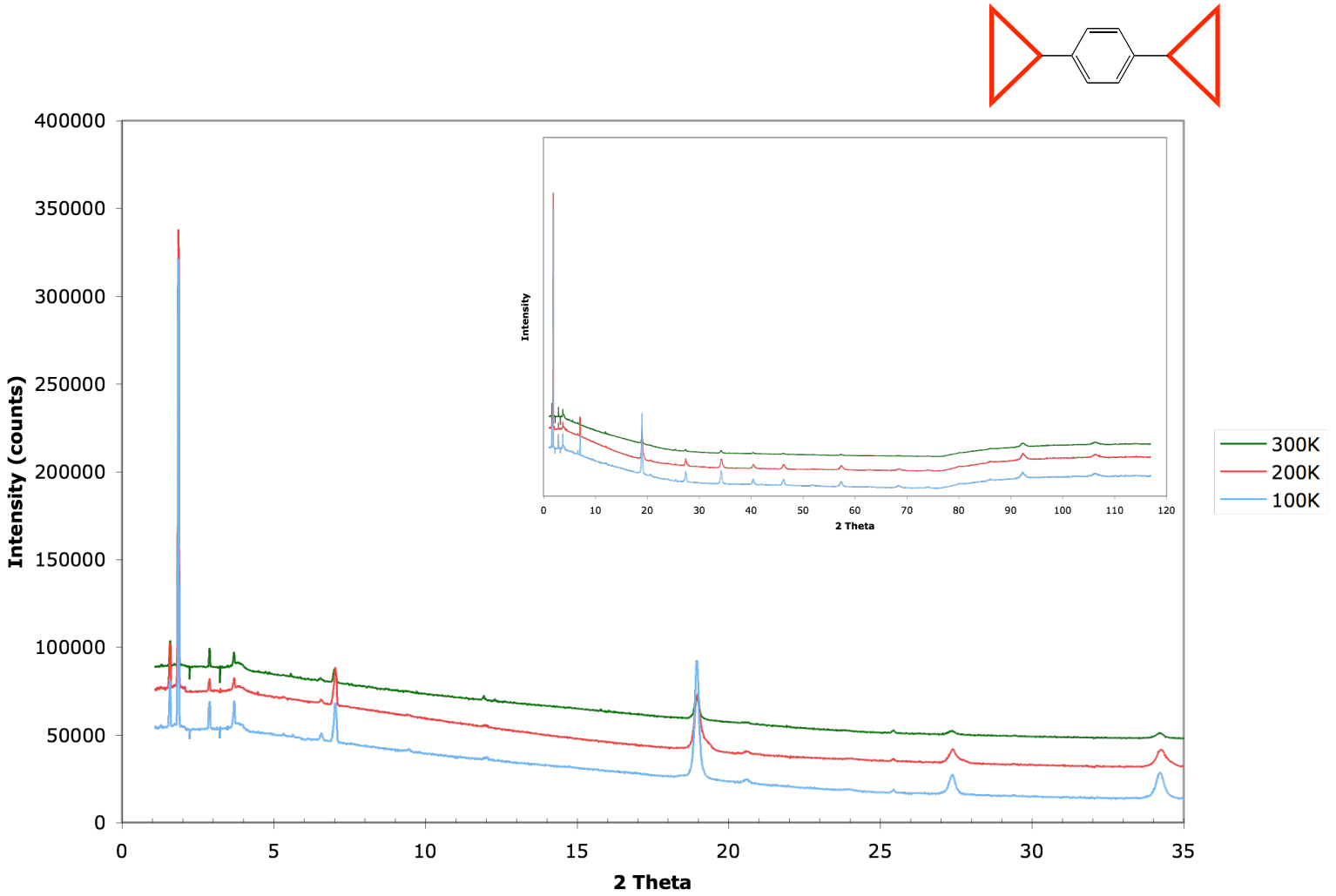

Figure 4.27 X-ray powder diffraction pattern for **4.2**. Measurements at 200 K and 300 K are offset with respect to intensity for clarity.

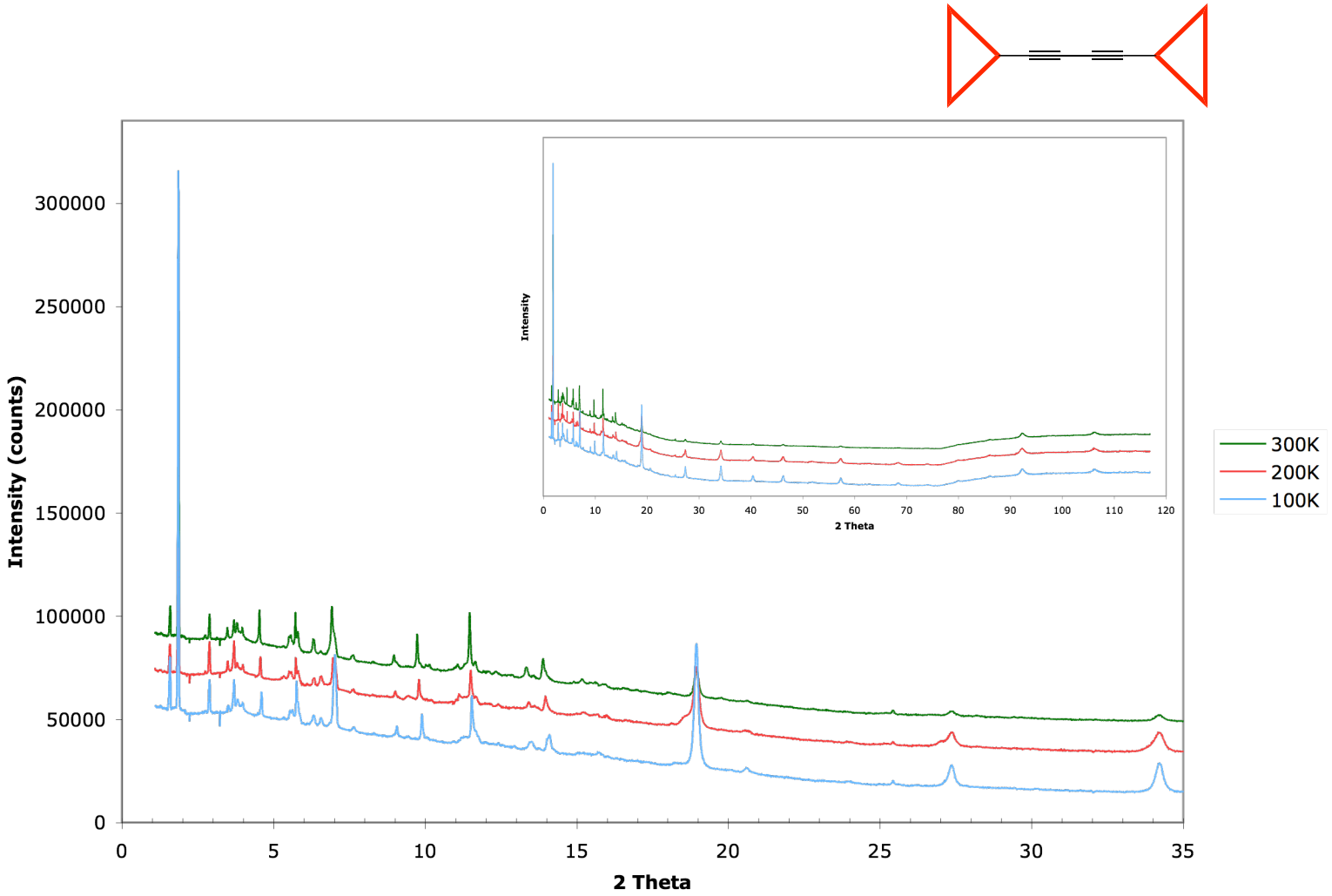

Figure 4.28 X-ray powder diffraction pattern for **4.3**. Measurements at 200 K and 300 K are offset with respect to intensity for clarity.

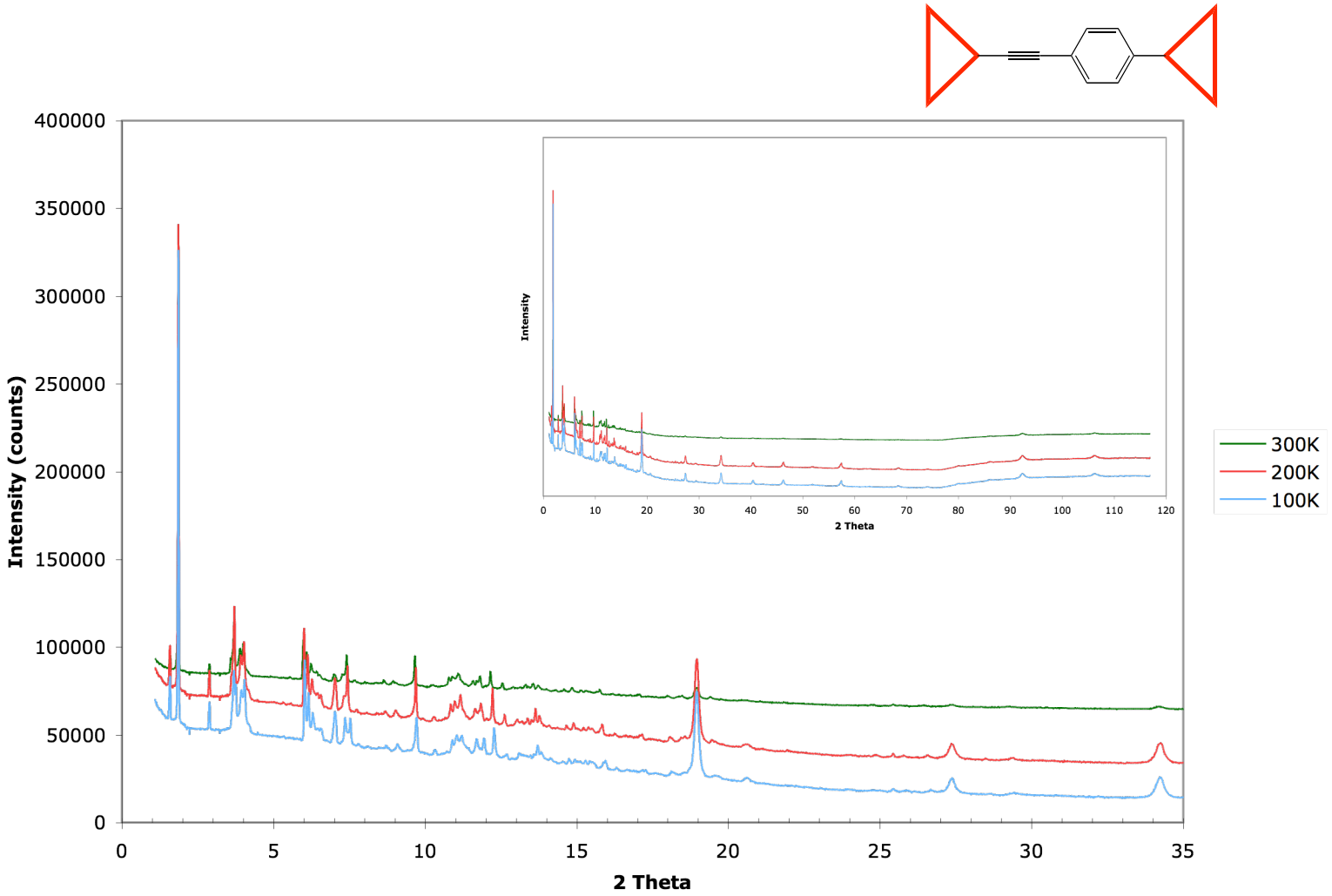

Figure 4.29 X-ray powder diffraction pattern for **4.4**. Measurements at 200 K and 300 K are offset with respect to intensity for clarity.

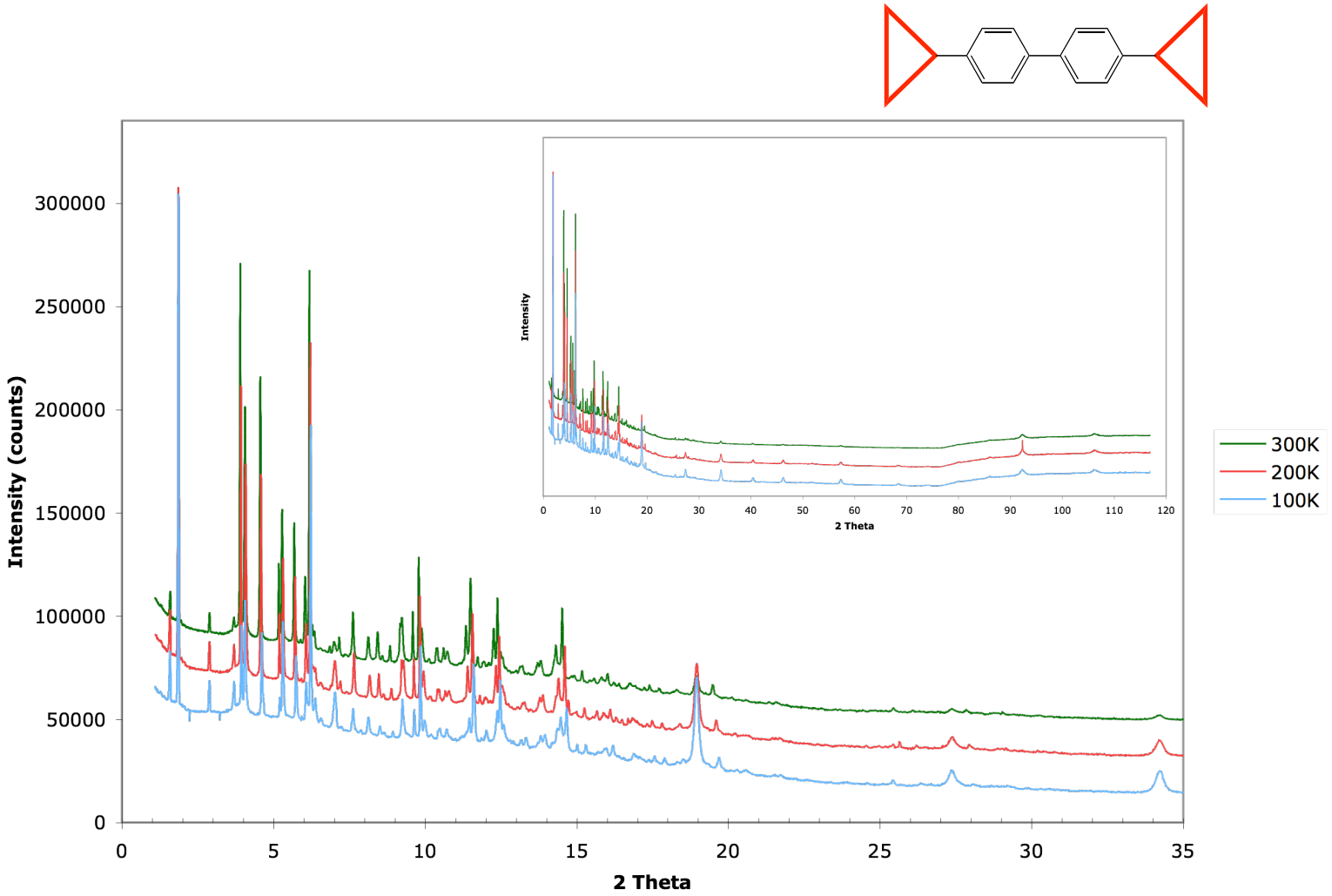

Figure 4.30 X-ray powder diffraction pattern for **4.5**. Measurements at 200 K and 300 K are offset with respect to intensity for clarity.

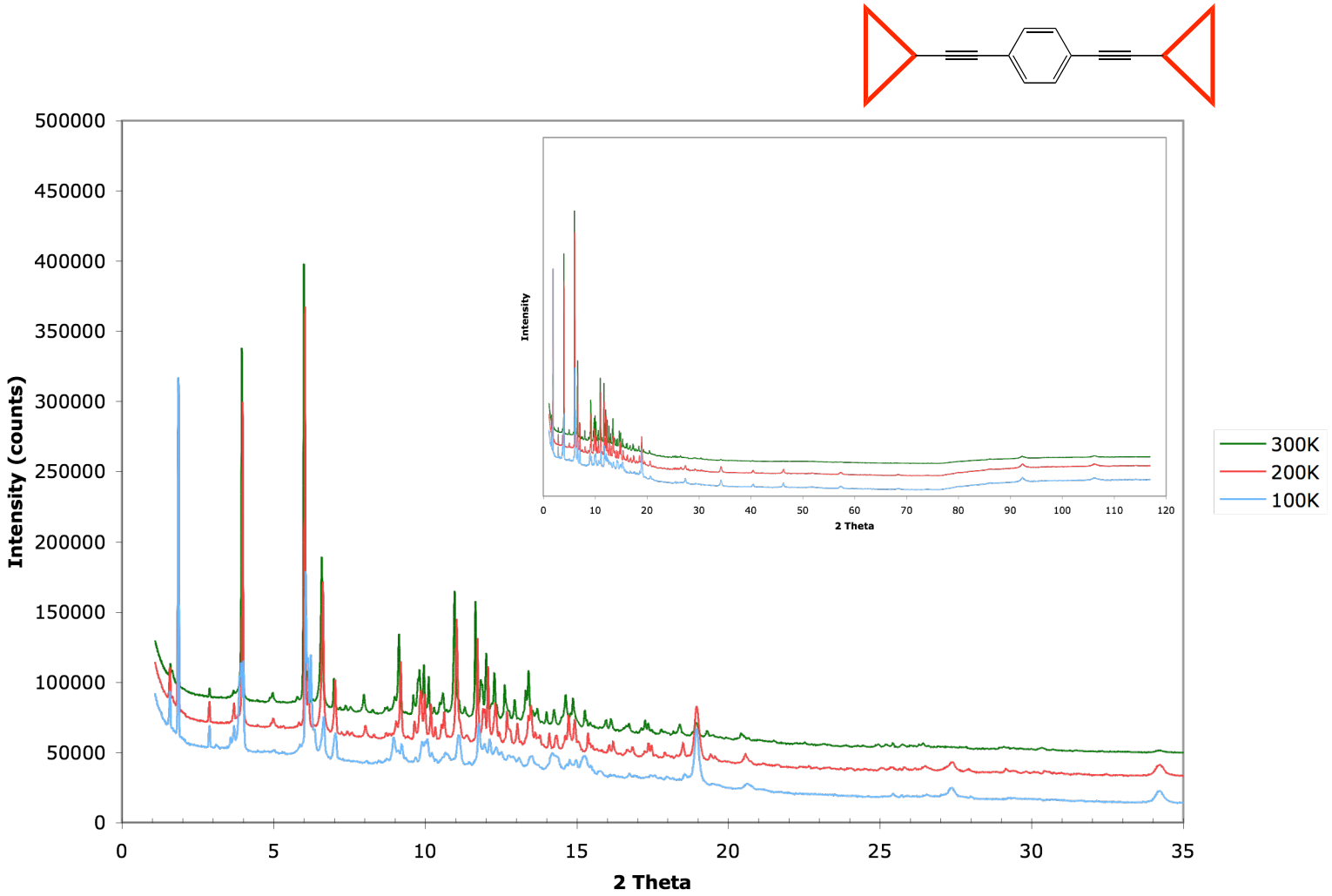

Figure 4.31 X-ray powder diffraction pattern for **4.6**. Measurements at 200 K and 300 K are offset with respect to intensity for clarity.

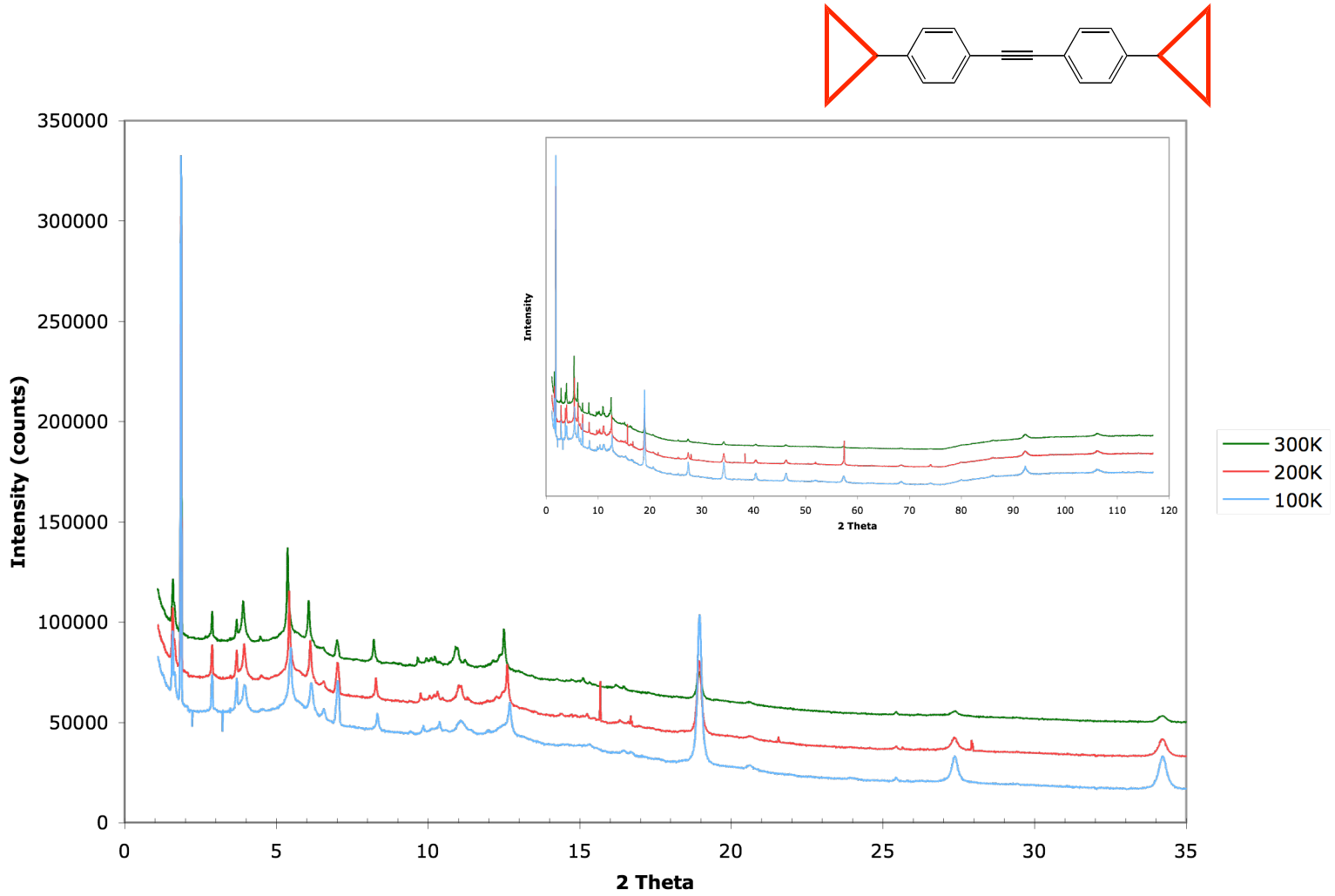

Figure 4.32 X-ray powder diffraction pattern for **4.7**. Measurements at 200 K and 300 K are offset with respect to intensity for clarity.

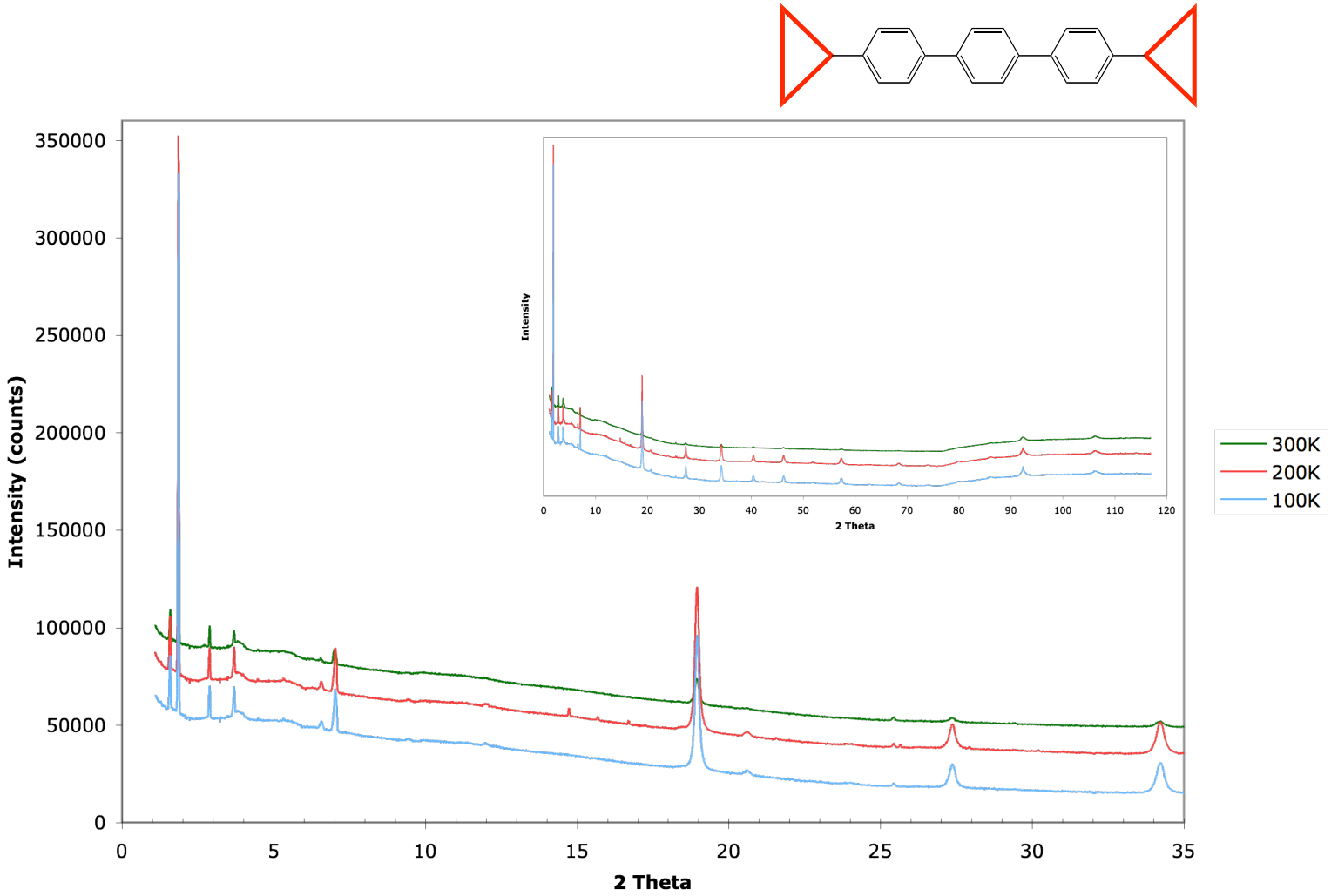

Figure 4.33 X-ray powder diffraction pattern for **4.8**. Measurements at 200 K and 300 K are offset with respect to intensity for clarity.

X-ray powder diffraction patterns at three temperatures for the series of compounds are shown in Figures 4.26 through 4.33. With deceasing temperature, there is an expected increase in the diffraction peak intensity but no apparent phase transition in the material. Initially, one observes a high baseline between the 0 and 20 2θ region in most of the samples that suggest some amorphous material in the sample. Diffraction patterns from compounds **4.2** and **4.3** are of immediate interest in order to compare to simulated XRPD data (Figure 4.24). The samples contain 5 to 20 peaks between the 0 and 20 2θ region, which may be sufficient for indexing the unit cell parameters (20 peaks in this region is considered the minimum). Another initial observation is the lack of diffraction peaks in sample **4.8** and a high baseline suggestive of a substantial amount of amorphous material. Lastly, samples **4.1** and **4.4** to **4.7** contain a number of peaks between the 0 and 20 2θ region, which suggest the possibility of indexing the samples for unit cell parameters.

In order to closely compare samples **4.2** and **4.3** the simulated data was superimposed on the experimental data for the 0 to 20 2θ region (Figures 4.34 and 4.35). In this 0 to 20 2θ region, there is an overlap of some peaks but sample **4.2** has too few peaks for indexing purposes. Initially, there does not seem to be a strong correlation between the simulation data for samples **4.2** and **4.3** and the acquired powder diffraction data.

Another concern was observed when comparing the diffraction patterns of all of the samples. Some 2θ diffraction peaks appear at the exact same location throughout 2θ in every sample (Figures 4.36, 4.37 and 4.38), which suggest that some diffraction peaks were not from the sample in the capillary tube or a common impurity. The suspected artifact peaks (APs) are tabulated in Table 4.9.

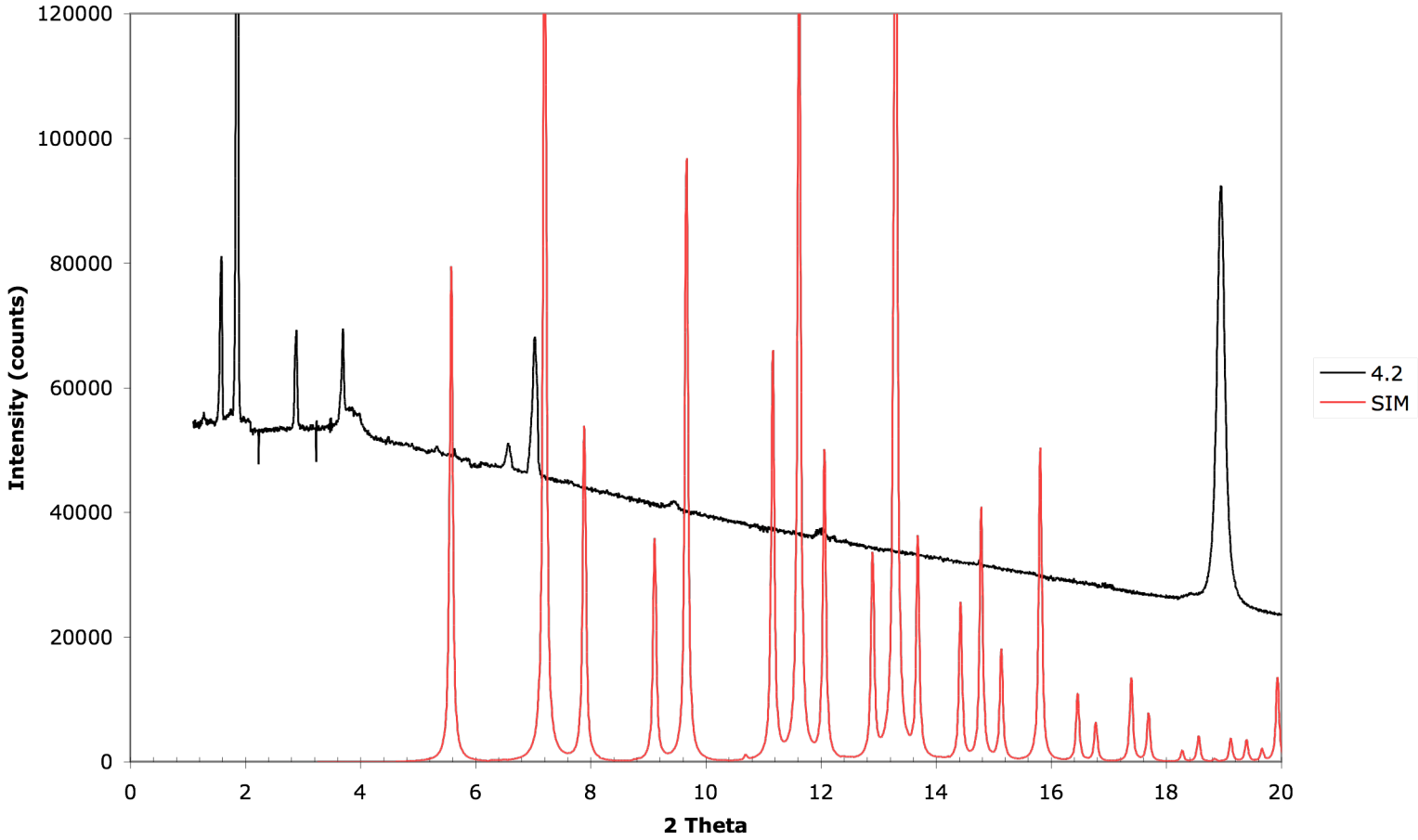

Figure 4.34 X-ray powder diffraction pattern of **4.2** with simulated pattern superimposed. Simulation has been converted to synchrotron wavelength (1.000992 nm). Only displaying diffraction pattern up to 20 *2θ*.

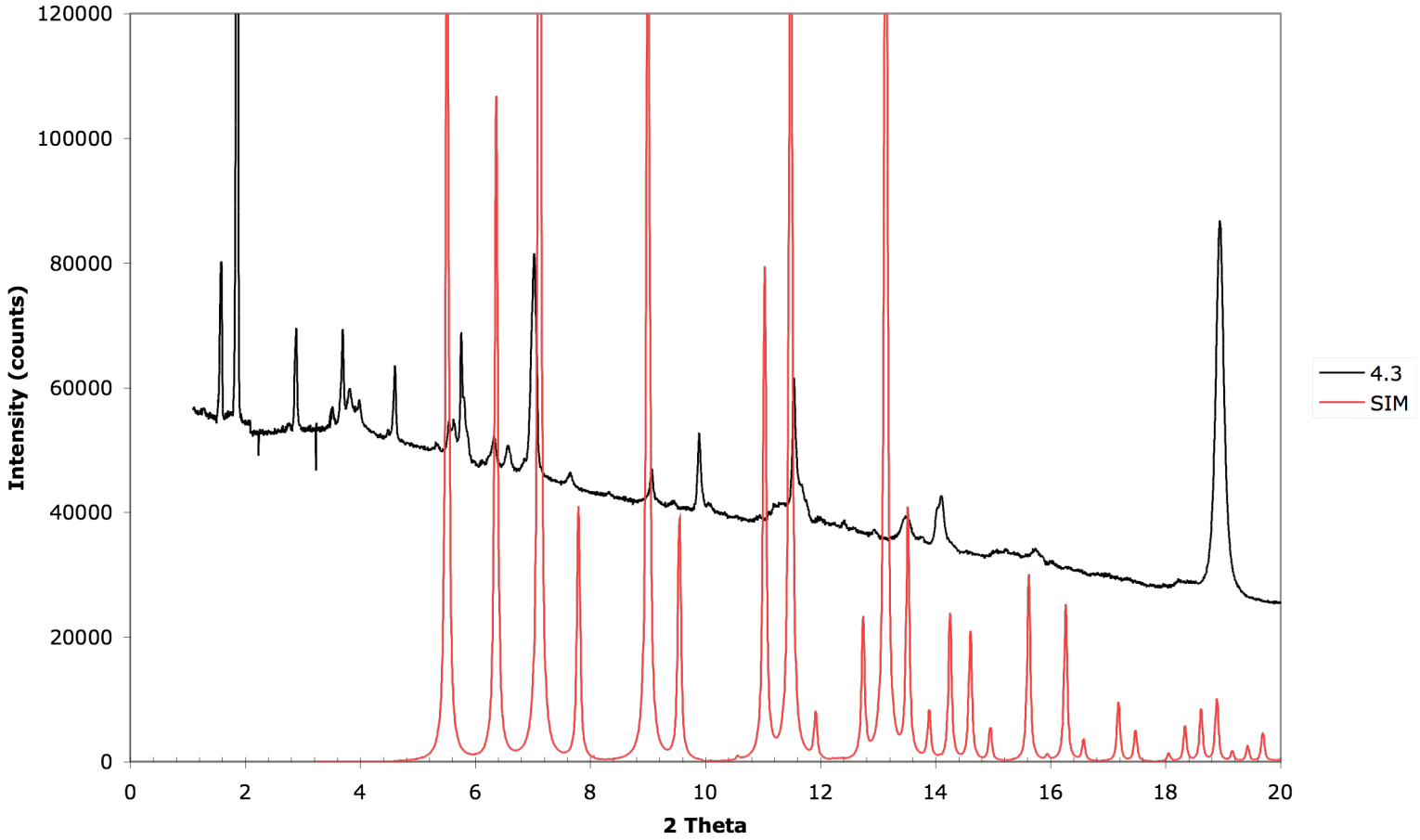

Figure 4.35 X-ray powder diffraction pattern of **4.3** with simulated pattern superimposed. Simulation has been converted to synchrotron wavelength (1.000992 nm). Only displaying diffraction pattern up to 20 *2θ*.

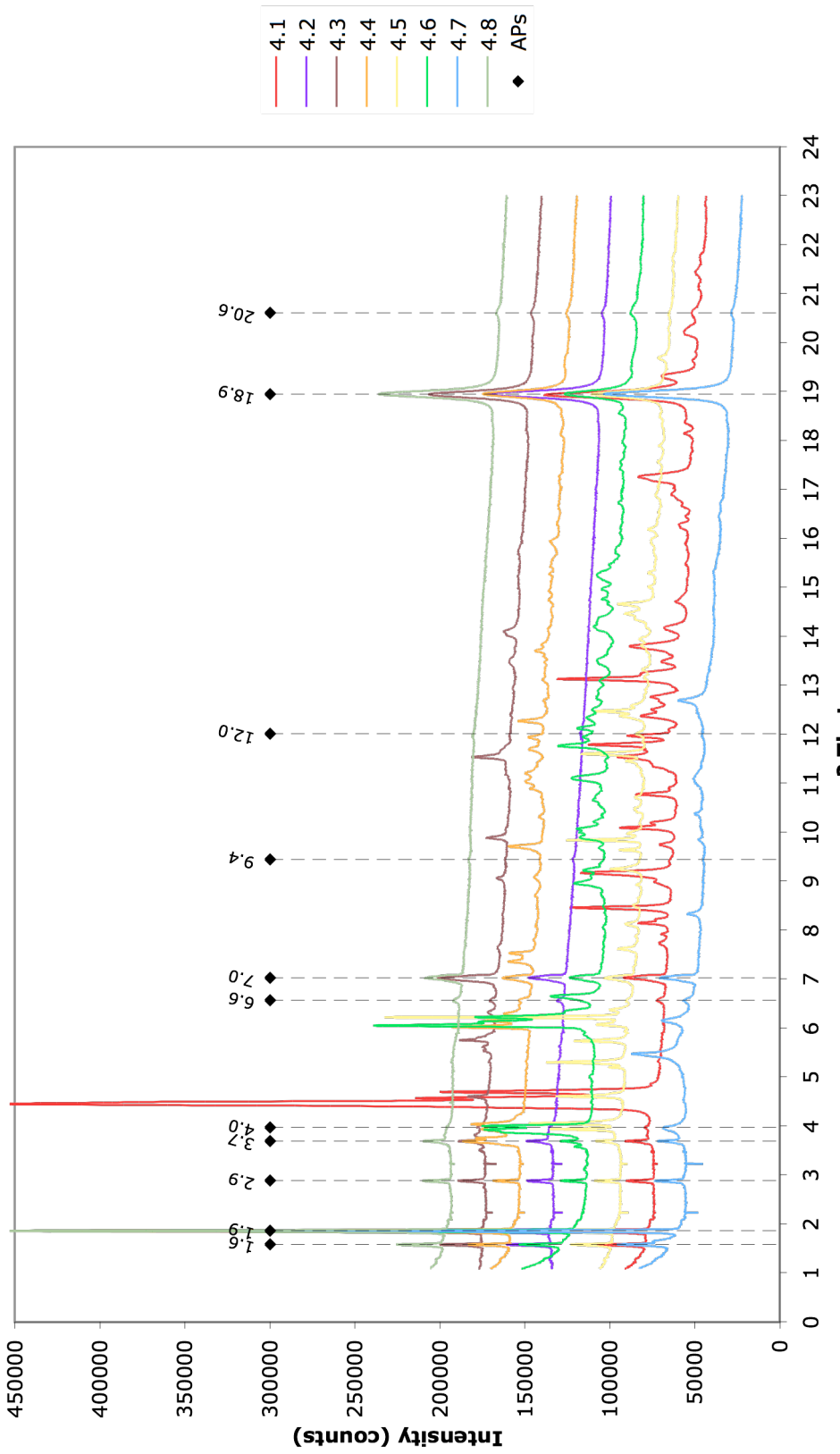

Figure 4.36 Combined synchrotron diffraction data at 100 K (0 – 23 2θ) and identified artifact peaks (APs). Measurements are offset with respect to intensity for clarity.

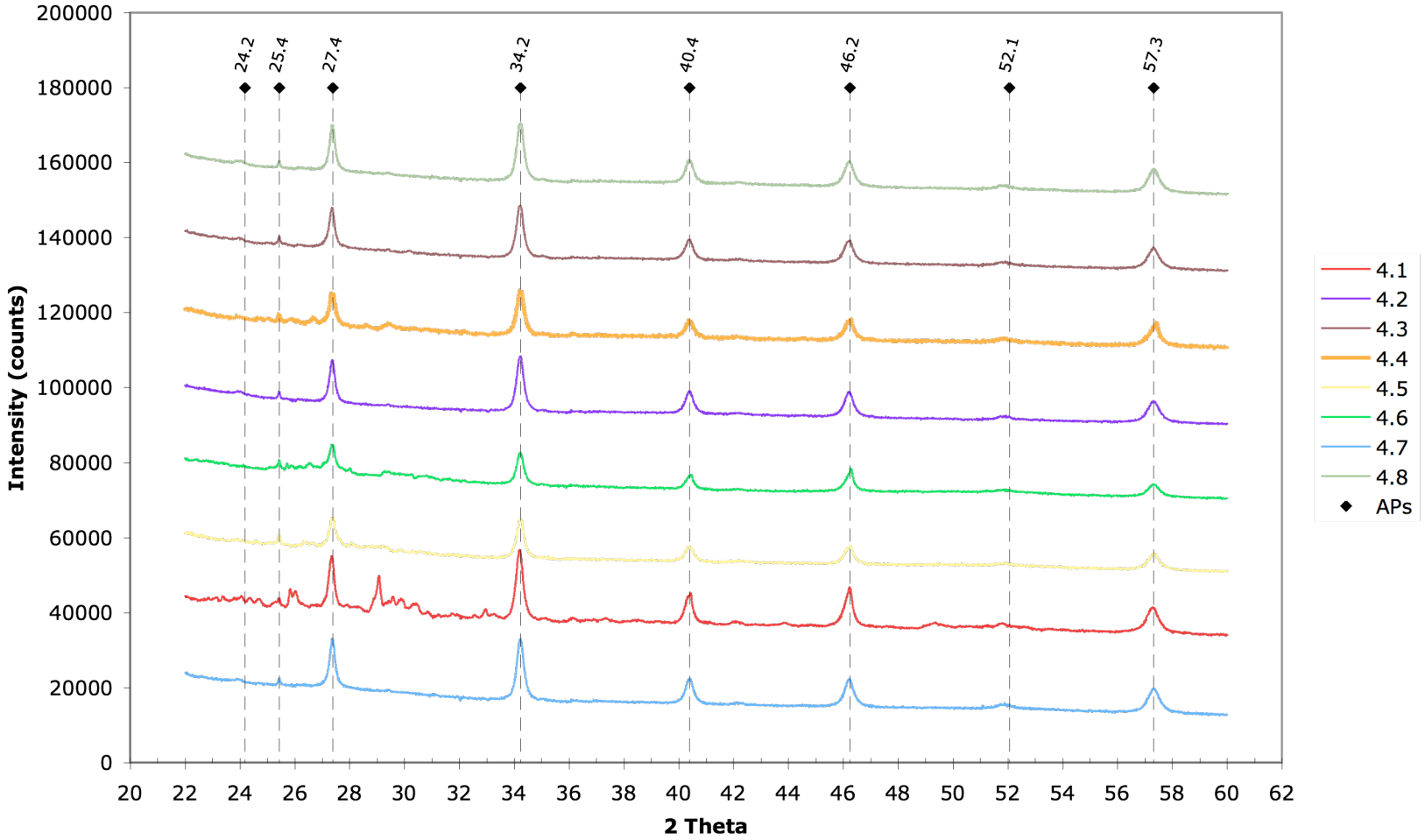

Figure 4.37 Combined synchrotron diffraction data at 100 K (22 – 60 *2θ*) and identified artifact peaks (APs). Measurements are offset with respect to intensity for clarity.

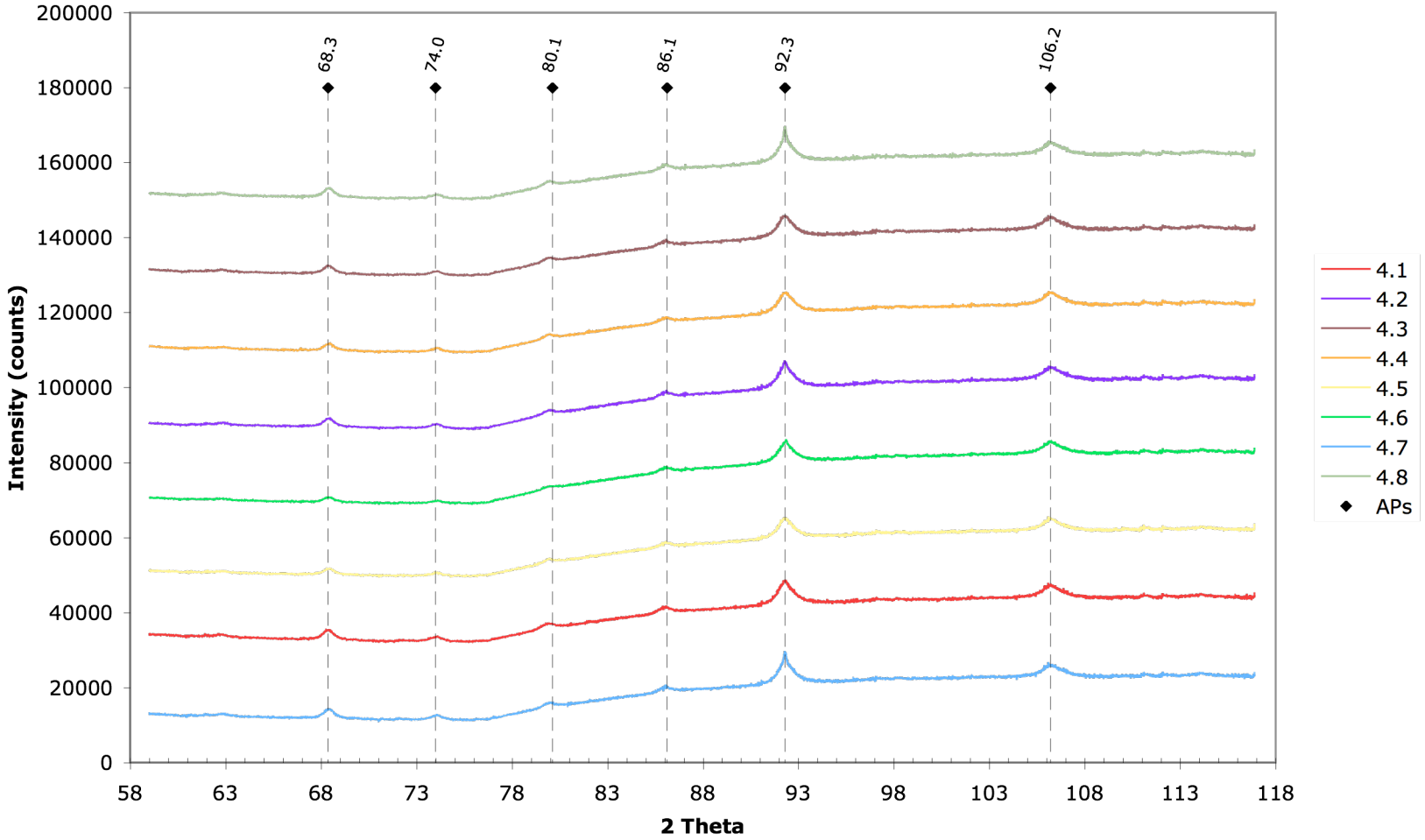

Figure 4.38 Combined synchrotron diffraction data at 100K (58 – 120 2θ) and identified artifact peaks (APs). Measurements are offset with respect to intensity for clarity.

Table 4.9 Artifact Peaks from Synchrotron Diffraction Data (100 K)

2 Theta	Intensity – **4.2**	Intensity – **4.7**	Intensity – **4.8**	Peak Shape
1.6	81096	95843	85467	sharp
1.9	317283	329990	329486	sharp
2.9	68905	73978	70256	sharp
3.7	69472	72292	70000	sharp
4.0	55740	68683	56197	shoulder
6.6	51171	56935	52079	sharp
7.0	68066	70645	68161	sharp
9.4	41930	44964	43395	broad
12.0	37574	45978	40804	broad
18.9	92335	103839	95865	sharp
20.6	24739	28767	26797	broad
24.2	18514	21592	19843	broad
25.4	18988	22582	20492	sharp
27.4	27336	32793	29986	sharp
34.2	28605	33214	30623	sharp
40.4	19146	22247	20684	sharp
46.2	18926	22069	20296	sharp
52.1	12276	15734	13527	broad
57.3	16613	19796	18493	sharp
68.3	11875	14474	13178	broad
74.0	10445	12651	11418	broad
80.1	14098	15764	14984	broad
86.1	18538	19851	19066	broad
92.3	27122	29683	29776	sharp
106.2	25795	26409	25334	broad

In an attempt to determine the basic unit cell parameters from the X-ray powder diffraction data, a hypothesis was proposed in which there may be a relation between the *t*-butyl TOTA molecular structure and the unit cell properties. The two solved single crystal X-ray structures, **4.2** and **4.3**, required that there be a center of inversion in order for the cubic unit cell solution. All of the other *t*-butyl TOTA structures, except **4.4**, meet the criteria that a center of inversion also exists in the *t*-butyl TOTA molecular structure. Furthermore, there may be a relation between the length of the molecule and the length of the unit cell parameter, *a*. Assuming the other structures, except **4.4**, also exist in a cubic unit cell, *hkl* peak patterns were generated for the powder samples to test this hypothesis (Table 4.10).

Table 4.10 Calculated Parameter, *a*, and Unit Cell Volume for a Cubic Unit Cell

Molecule	Formula	MW	Overall Length of Molecule[a] (Å)	Unit Cell Length (*a*)[b,c]	Unit Cell Volume (Å^3)[c]
4.1	$C_{64}H_{66}O_6$	931	12.55	15.01	3382
4.2	$C_{68}H_{70}O_6$	983	14.83	17.83	5668
4.3	$C_{66}H_{66}O_6$	955	15.17	18.05	5877
4.5	$C_{74}H_{74}O_6$	1059	19.05	22.78	11827
4.6	$C_{72}H_{70}O_6$	1031	19.37	23.16	12429
4.7	$C_{76}H_{74}O_6$	1083	21.59	25.83	17233
4.8	$C_{80}H_{78}O_6$	1135	23.32	27.89	21692

[a] Overall length was calculated by the following: Overall length = Axis length + 2·(TOTA bowl depth + an approximation for the vdW radius of the *t*-butyl groups)

[b] Unit cell length determined by the average of the ratio of molecule length (**4.2** and **4.3**) to (*a*) = 0.84

[c] Unit cell lengths and unit cell volumes for **4.2** and **4.3** are from experimental data

Using the unit cell parameter, *a*, and the assumption that the other compounds also have a cubic unit cell solution, the hypothetical *hkl* peak patterns were determined for the 0 to 20 2θ region.[35] The predicted positions of the *hkl* peaks were then superimposed on the experimental data (Figures 4.39 to 4.43). In comparing the simulation and experimental data, there does not seem to be a strong correlation between the location of the simulated peaks and experimental peaks. Also, the high baseline at the low angles of 2θ due may obscure the full analysis of the powder diffraction data.

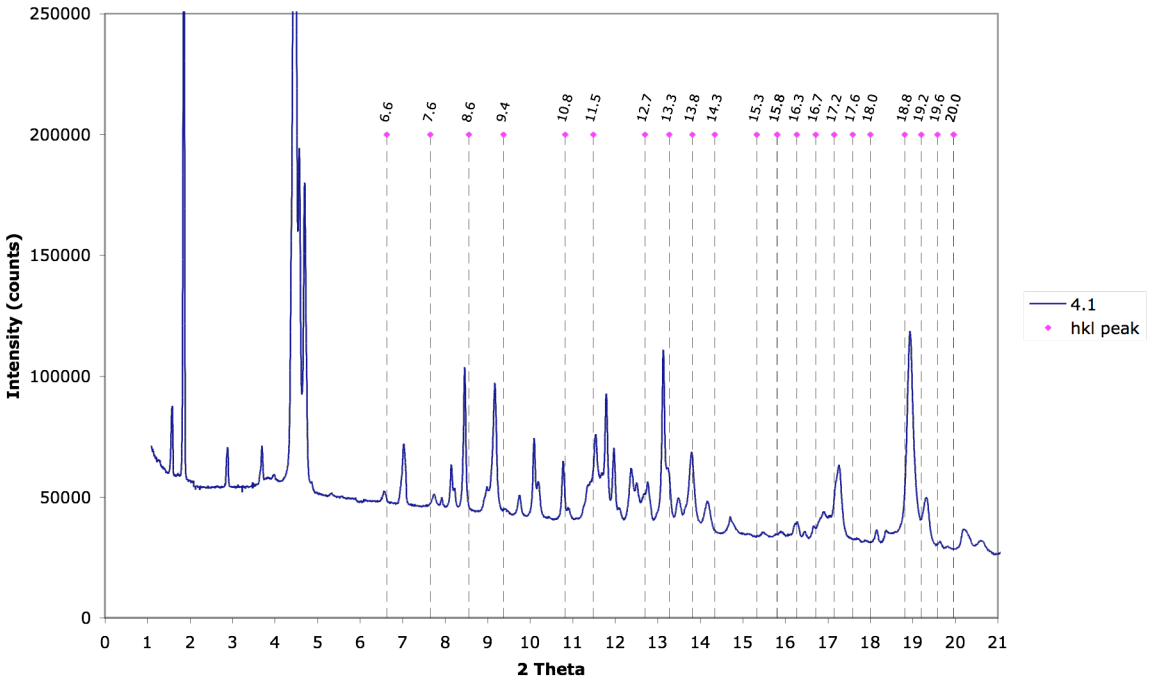

Figure 4.39 X-ray powder diffraction pattern of **4.1** at 100 K with predicted location of *hkl* peaks for a = 15.01 Å.

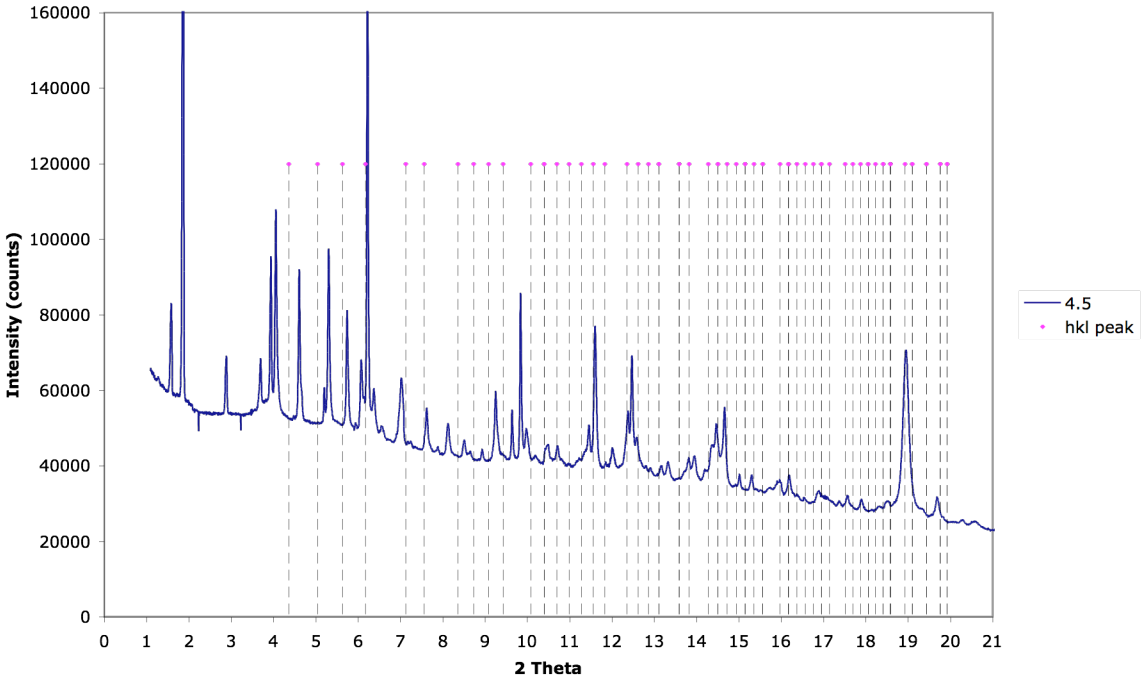

Figure 4.40 X-ray powder diffraction pattern of **4.5** at 100 K with predicted location of *hkl* peaks for a = 22.78 Å.

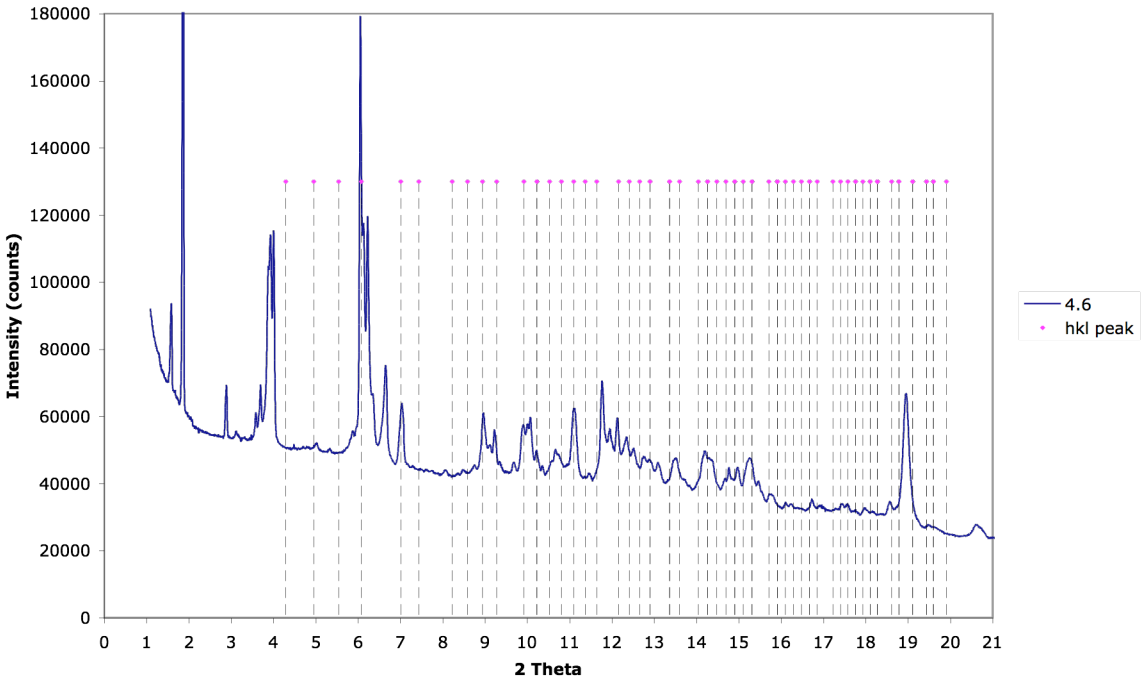

Figure 4.41 X-ray powder diffraction pattern of **4.6** at 100 K with predicted location of *hkl* peaks for a = 23.16 Å.

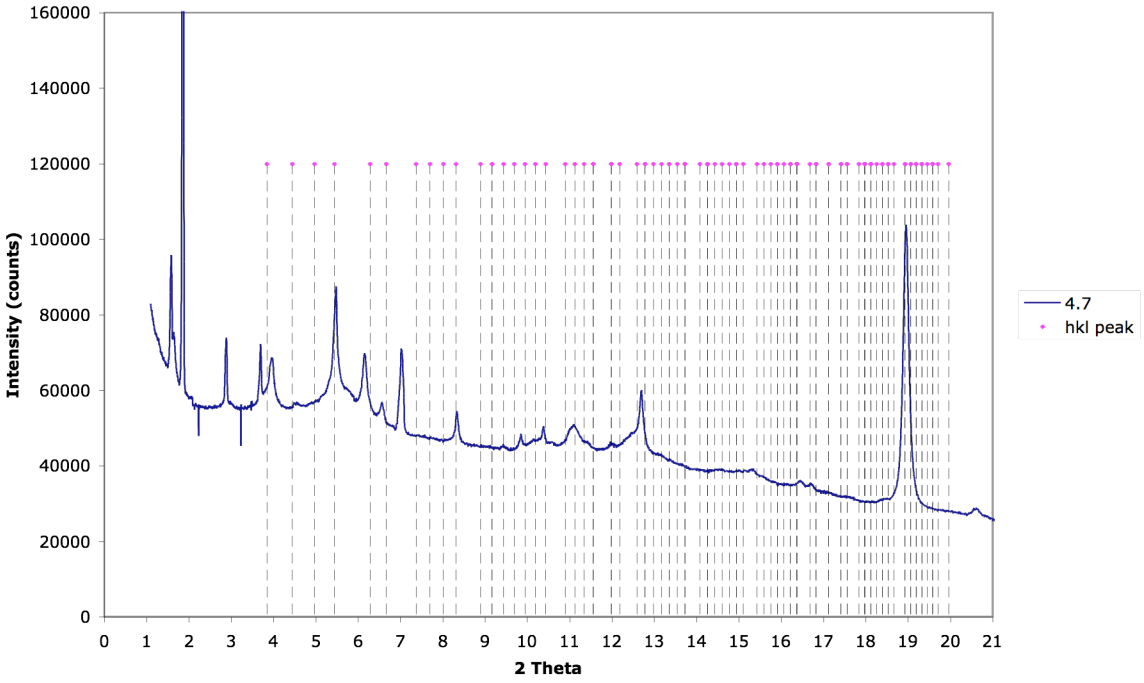

Figure 4.42 X-ray powder diffraction pattern of **4.7** at 100 K with predicted location of *hkl* peaks for a = 25.83 Å.

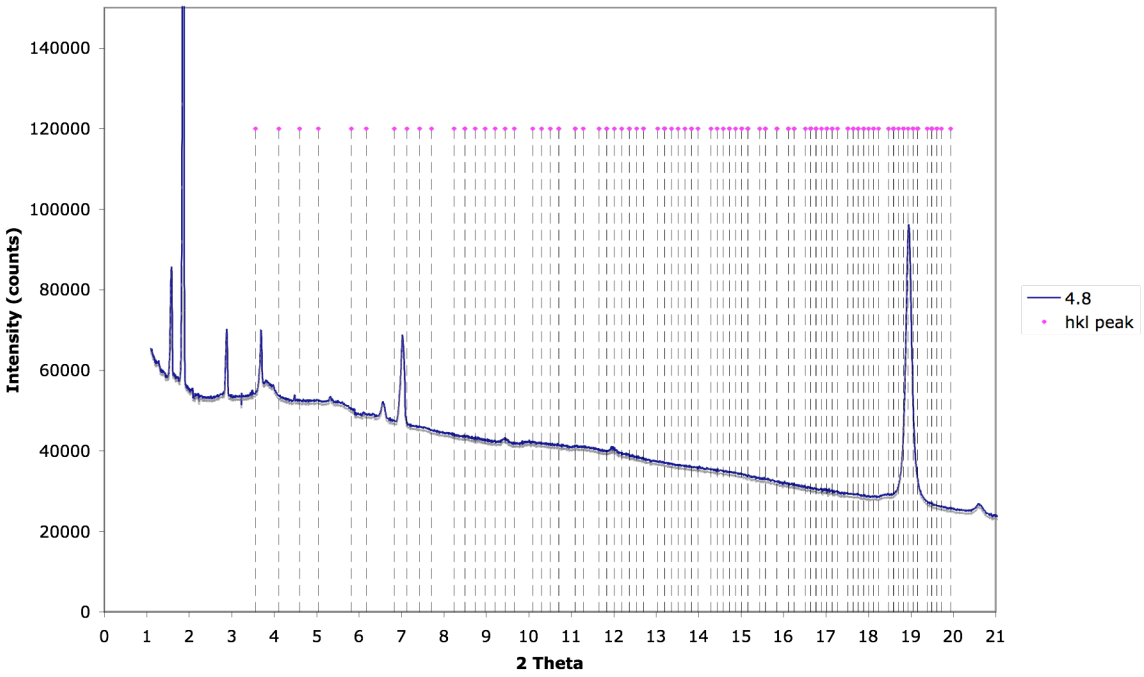

Figure 4.43 X-ray powder diffraction pattern of **4.8** at 100 K with predicted location of *hkl* peaks for a = 27.89 Å.

Unfortunately, the estimation of the unit cell parameter, a, did not produce any definitive conclusions in simulating the powder diffraction data. Further attempts were utilized with computer programs to search for solutions to indexing the powder diffraction data. First, the *CMPR* program was used to observe small changes in the predicted unit cell parameter, a.[36] Because there may be a slight variation of a from the calculated value, the *CMPR* program allows one to vary the unit cell length parameter, *e.g.* a, by ± 10 %, repositioning a predicted peak. This variation in the unit cell parameter a also did not produce any strong correlations between predicted *hkl* peaks location and the experimental powder diffraction data. Consideration was also given to other unit cells, such as monoclinic or orthorhombic, which are commonly occurring unit cells with an approximate 90º angle (α, β, and γ) and $a \approx b \approx c$. Again, no solutions were found that correlated the simulated data and the experimental powder diffraction data. A second program, *TOPAS*, was also utilized to search for

solutions to the unit cell parameters.[37] *TOPAS* was used in two ways to search for a solution. The first required the peaks in the experimental data to be identified and then an algorithm was used to search for probable solutions. Again, no correlations were found with this method. A second algorithm in *TOPAS* was also utilized that allowed one to input unit cell parameters (*e.g.* unit cell type) and probable solutions were generated with regard to unit cell volume. In this case, no strong correlations were found between the predicted solutions and the powder diffraction experimental data. At this point, a solution to the powder diffraction data cannot be ruled out and may require some further diffraction experiments.

Since definite artifacts peaks were discovered in the synchrotron powder diffraction data, a second powder sample was submitted to the Paul Scherrer Institute for analysis. The sample **4.1** was again packed in a glass capillary tube but for this experiment it was mounted in the goniometer with a soft wax material (a mounting epoxy glue was used in the first experiments). Results from the second synchrotron powder diffraction experiment are given in Figure 4.44. The powder diffraction spectrum of this sample contains the previously observed peaks for the compound **4.1** but none of the identified artifacts peaks are observed in the spectrum. Presumably the artifact peaks are a result of scattering from epoxy glue material previously used to mount the samples in the goniometer.

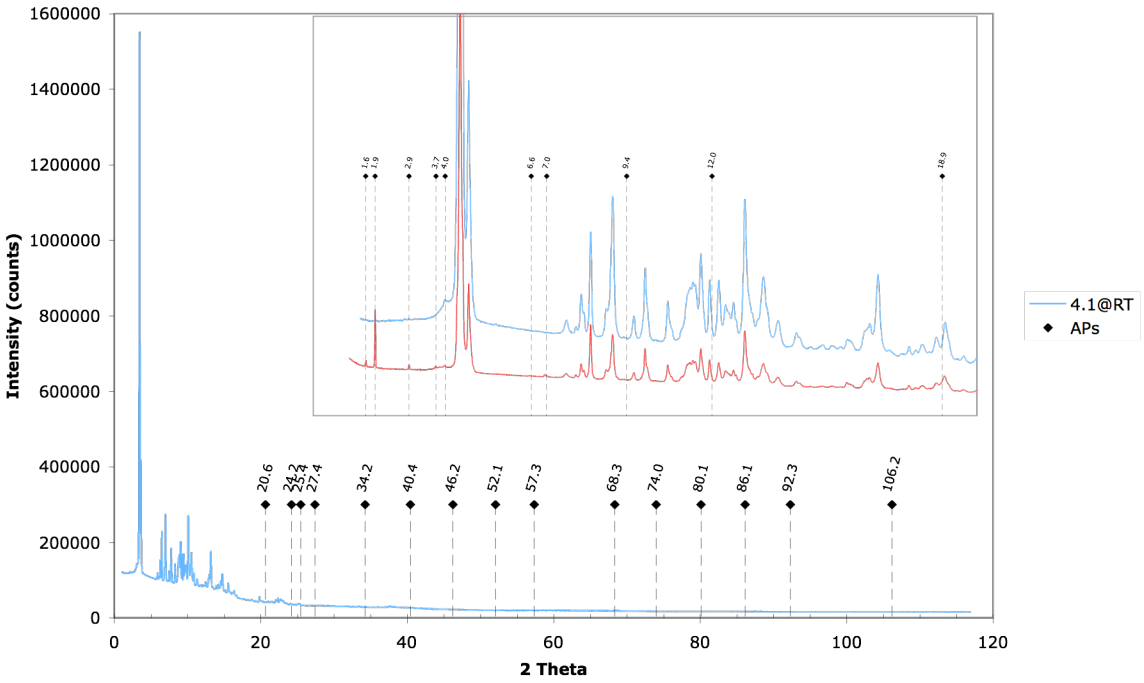

Figure 4.44 Repeated synchrotron powder diffraction measurement at the PSI of **4.1** at 16 eV and 300 K. Previous measurement shown in inset and in red. Positions of artifacts peaks (APs) are also shown.

4.4 Physical Properties

4.4.1 Introduction

The physical properties of a representative group of the *t*-butyl TOTA compounds were investigated. Studies included photophysical and solid-state NMR measurements. The goal of the photophysical measurements was to compare the spectra for the series of *t*-butyl TOTA superstructures as the central axis length is varied and compare two of the structures with those of the parent tolan and *p*-terphenyl molecules. Solid-state NMR measurements were conducted in order to determine dynamics with respect to the rotational barrier of the central spindle in the solid phase.

4.4.2 Photophysical Processes

Photophysical measurement techniques, absorption and luminescence, provide some important physical characteristics of the substance being studied. One photophysical parameter is the efficiency of the fluorescence process, or quantum yield. Quantum yield is not only a physical characteristic of a substance in specified conditions, but it is ultimately part of the calculation of quenching-rate constants, energy transfer, lasing ability, and radiative and nonraditive rate constants, from which the whole photophysical behavior of the substance can be deduced.[38]

When molecules absorb a photon of light, an electron is excited from a low energy orbital (Ψ) into an unoccupied higher energy orbital (Ψ^*); typically from the highest occupied molecular orbital (HOMO) into the lowest unoccupied orbital (LUMO) (Figure 4.45).[39] There are at least two possible excited electronic states, depending on the configuration of the electrons. When the spins of the two electrons are paired (antiparallel), the new excited state is called a *singlet state* (Figure 4.45a). When the two spins are unpaired (parallel), the excited state is called a *triplet state*. The initial, ground state configuration is also a singlet state and written as S_0.[40] The lowest energy excited singlet state is indicated as S_1. The lowest energy excited triplet state is T_1. The photophysical processes of absorption (excitation) and emission (fluorescence and phosphorescence) can be individually visualized (Figure 4.45) but are more concisely described in a Jablonksi diagram (Figure 4.46).[41]

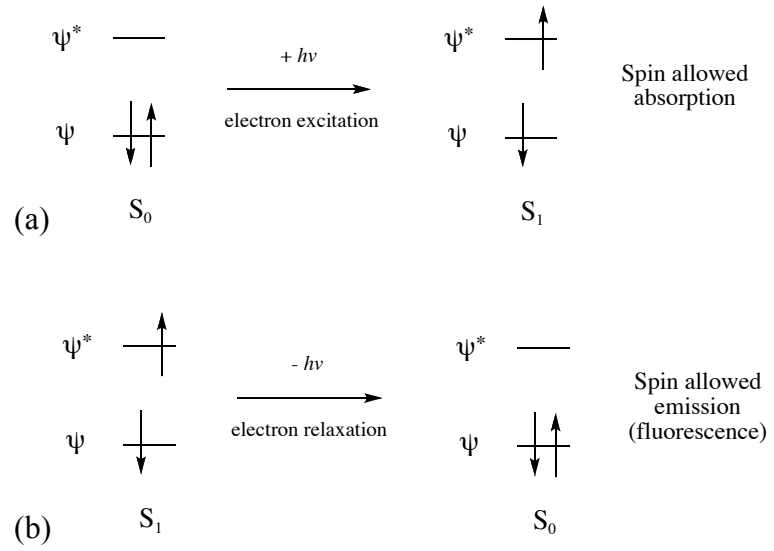

Figure 4.45 Orbital level energy diagram of allowed absorption, (a), and allowed emission, (b), processes.

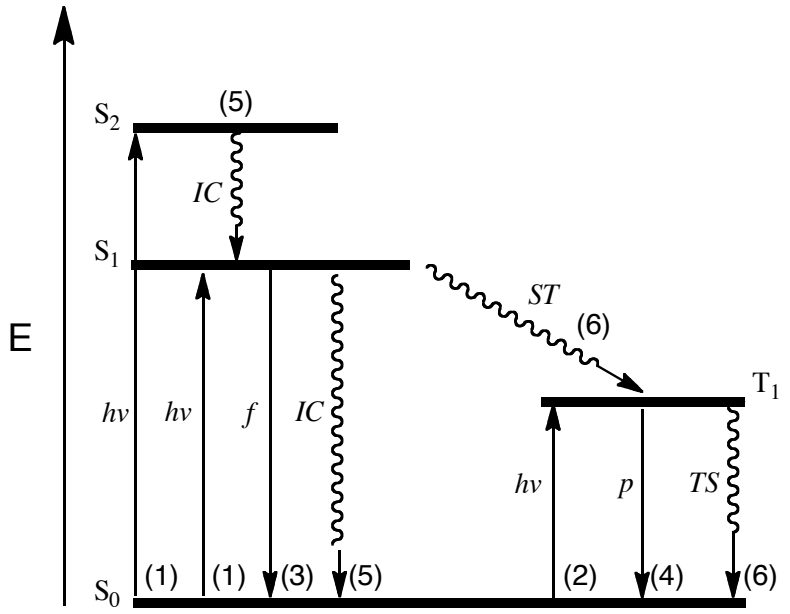

Figure 4.46 A Jablonski energy state diagram illustrating photophysical transitions.[39]

A photophysical process is any transition that interconverts between excited states and the ground state or between excited states,[39] and may be categorized as radiative or non-radiative processes. Transitions between states of different spin require electron spin inversion and are called "forbidden." The important photophysical radiative processes are:[39] (1) "Allowed" absorption from the singlet ground state to a singlet excited state; typically $S_0 \rightarrow S_1$, experimentally quantified by the extinction coefficient ε; (2) "Forbidden" absorption from the singlet ground state

to a triplet excited state; typically $S_0 \rightarrow T_1$, also experimentally quantified by the extinction coefficient ε; (3) Fluorescence: "Allowed" emission from a singlet excited state to the ground state, typically $S_1 \rightarrow S_0$, described by the fluorescence rate constant k_f; (4) Phosphorescence: "Forbidden" emission from a triplet excited state to the ground state, typically $T_1 \rightarrow S_0$, described by the phosphorescence rate constant k_p. Electrons may be excited into any of the higher level excited states (S_2, S_3…; T_2, T_3…) but usually only transitions into S_1 and S_2 are observed. Based on these observations, Kasha postulated that fluorescence occurs from the S_1 state, and phosphorescence from the T_1 state, regardless of into which level the initial excitation took place.[42]

The important photophysical non-radiative processes are:[42] (5) Internal Conversion: "Allowed" nonradiative transitions between states of the same spin; *e.g.*, $S_2 \rightarrow S_1$ or $S_1 \rightarrow S_0$, described by the rate constant k_{IC}; (6) Intersystem Crossing: "Forbidden" non-radiative transitions between states of different spin; *e.g.*, $S_1 \rightarrow T_1$ or $T_1 \rightarrow S_0$, characterized by the rate constants k_{ST} and k_{TS}.

The efficiency of a photophysical process is described by its quantum yield (Φ), which is simply the number of photophysical events per number of absorbed photons (Equation 4.4).

$$\Phi = \frac{number\ of\ events}{number\ of\ photons\ absorbed} \quad (4.4)$$

The fluorescence quantum yield, Φ_f, is then the ratio of the number of photons emitted (from S_1) to the number of photons absorbed. Non-radiative processes, governed by the rate constants k_{IC} and k_{ST}, depopulate the excited state, competitive with fluorescence, so the fluorescent quantum yield can be viewed as:

$$\Phi_f = \frac{k_f}{k_{IC} + k_{ST} + k_f} = k_f \tau_f \quad (4.5)$$

where the observed fluorescence lifetime, τ_f, equals $(k_{IC} + k_{ST})^{-1}$.

The phosphorescence quantum yield, Φ_p, is the number of photons emitted (from T_1) per photons absorbed and in terms of competing processes. Typically, fluorescence is fast ($\tau_f \sim 10^{-10}$ - 10^{-7} sec) and phosphorescence lifetimes are relatively long ($\tau_p \sim 10^{-6}$ - 1 sec).[39] The sum of radiative and non-radiative (Φ_{NR}) quantum yields is the total quantum yield (Φ_T) and equals unity, by definition (Equation 4.6).

$$\Phi_f + \Phi_p + \sum \Phi_{NR} = 1 \quad (4.6)$$

If the simplified Jablonski diagram (Figure 4.46) were sufficient, the excitation and relaxation of an electron by a single photon of the appropriate energy ($\Delta E = h\nu$) would result in spectra of "sharp" transition lines (Figure 4.47a). This is not the usual case and only the spectra of atoms in the gas phase exhibit distinct, well-defined transitions. The electronic states of molecules are affected by the motions (vibrations, rotations, etc.) of the nuclei relative to each other. Transitions between the vibrational levels of electronic states in molecules can sometimes be observed in the gas phase at low pressures (Figure 4.47b). In solution, these vibrational levels are often partially or completely unresolved and broad bands corresponding to an average of the vibrational levels of the two electronic states in a transition are observed (Figure 4.47c).

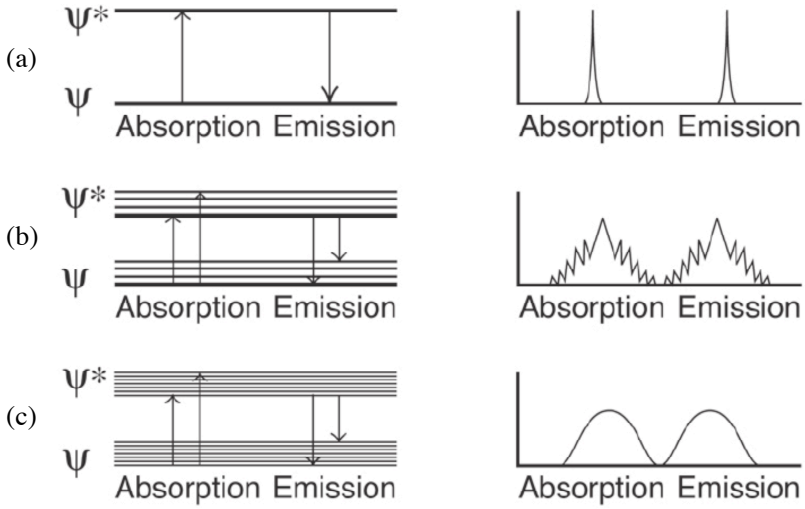

Figure 4.47 (a) Sharp absorption and emission spectra from gas phase atoms; (b) absorption and emission spectra with vibrational structure from molecules in the gas phase; and (c) broad, structureless absorption and emission from molecules in solution.[39]

The relative intensity of a given transition indicates its probability and is governed by the Franck-Condon principle.[43] As the time required for the absorption (or emission) of a photon of light is very fast (10^{-15} sec) compared to the speed of nuclear motion (10^{-13} sec), the principle states that, during an electronic transition, the nuclei remain fixed in space. After the transition, the molecule is in a new energetic state and the nuclei can relax (through vibrations, rotations, etc.) into their new equilibrium positions. The status of nuclei is indicated by vertical lines, representing the primary electronic transitions, connecting two potential energy surfaces (Figure 4.48).

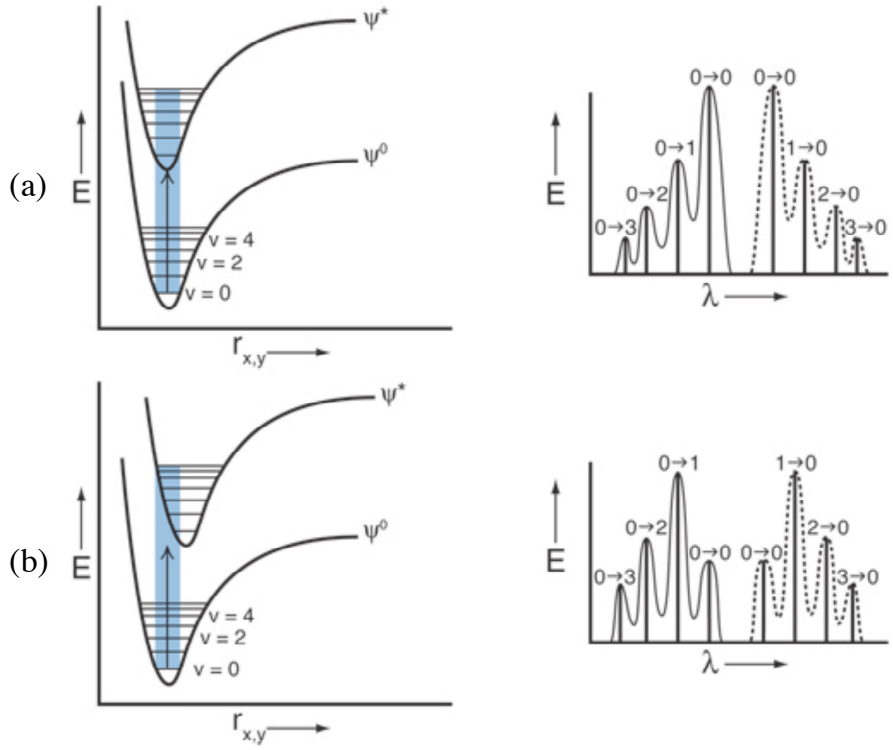

Figure 4.48 The Franck Condon principle. Potential energy curves and absorption (solid) and emission (dotted) spectra for transitions with (a) similar and (b) different excited state geometries. Shaded regions on the potential energy surfaces represent Franck-Condon overlap and correspond to spectral transitions with large intensity.[39]

At room temperature, most molecules exist in the ground vibronic state (Ψ^0, $v = 0$) and vertical excitation occurs primarily into the $v = 0$ and $v = 1$ vibrational levels of the excited state Ψ^* (Figure 4.48a). This state occurs when the equilibrium bonding and geometries in Ψ^0 and Ψ^* are similar, *e.g.*, rigid aromatic hydrocarbons. When the equilibrium bonding and geometries of Ψ^0 and Ψ^* are not similar, the potential energy curve of Ψ^* is displaced relative to Ψ^0 and vertical excitation occurs into the higher vibrational levels of Ψ^* (Figure 4.48b).

The Franck-Condon principle holds true for emission as well and when the emissive excited state is the same as the absorptive excited state, the absorption and emission spectra will be mirror images (Figure 4.48); however, due to vibrational loss of energy, emissive processes shift to longer wavelengths (*red-shift*). This is called

the Stokes shift after Irish physicist George G. Stokes, who first observed this difference in 1852.[44]

4.4.3 Photophysics of the *tert*-butyl TOTA Sandwich Series

In addition to the characterization of the series of *t*-butyl TOTA compounds, the insertion of an aromatic chromophore into the *t*-butyl TOTA scaffold may have some practical applications. In conductive oligo(phenylene ethynylene)s (OPEs) it has been shown that changes in the local environment, *i.e.* intermolecular interactions in a self-assembled monolayer,[45] can have a profound effect on conductance and electronic properties.

The absorbance and emission spectra were measured for a select group of the *t*-butyl TOTA compounds that were synthesized. The *t*-butyl TOTA compounds measured were the simple ethynylene sandwich **4.1**, the phenylene sandwich **4.2**, the ethynyl-phenylene sandwich **4.4**, the biphenyl sandwich **4.5**, the ethynyl-phenyl-ethynylene **4.6**, the tolan sandwich **4.7**, and the *p*-terphenyl sandwich **4.8**. The results of the last two compounds were compared to their parent compounds, which are well-known luminescent species.

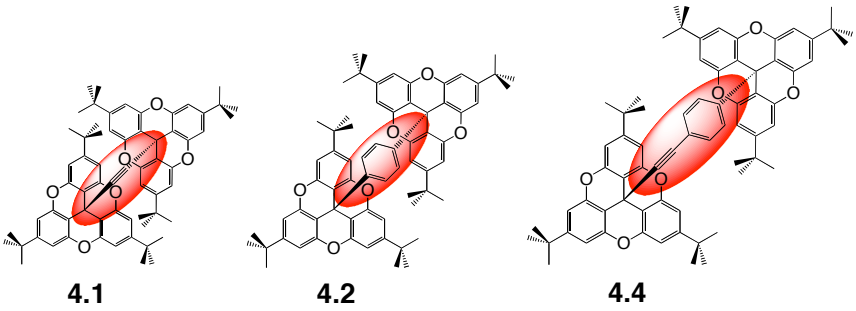

4.1 **4.2** **4.4**

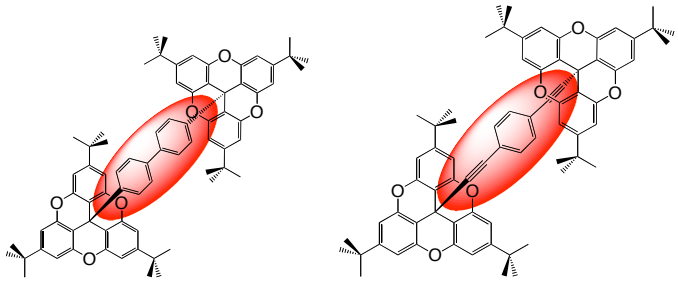

4.5 **4.6**

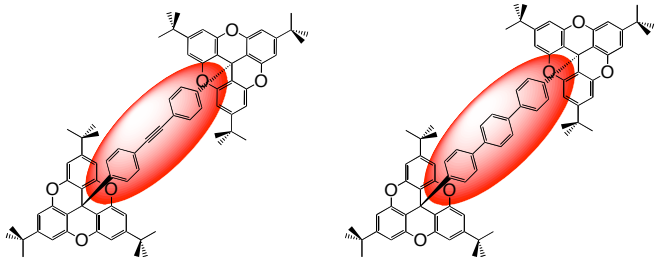

4.7 **4.8**

The absorbance spectra for the seven *t*-butyl TOTA compounds have similar broad shape at the maximum absorption (Figure 4.49) at the near UV region and are most likely π → π* absorptions in view of the large absorption coefficient. In general absorption of the sandwich structures is *red-shifted* as the length of the central axis increases. With regard to the larger chromophores, the tolan sandwich **4.7** maintains similar absorption characteristics, with two large absorption peaks, to its parent but there is a significant *red-shift* of about 40 nm (Figure 4.51). In the case of the terphenyl sandwich **4.8**, there does not appear to be a *red-shift* (Figure 4.52), however the absorption is significantly quenched (Table 4.11).

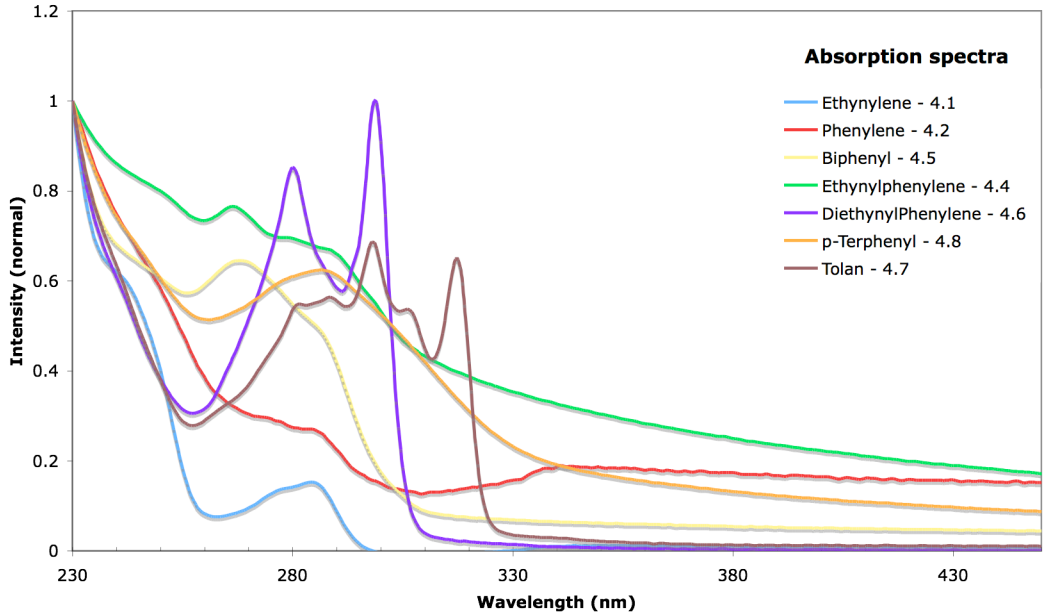

Figure 4.49 Normalized absorption spectra of the *t*-butyl TOTA sandwich compounds in ethanol at room temperature.

The emission spectra, quantum yields (Φ_f), and lifetimes (τ) were measured for the *t*-butyl TOTA compounds in ethanol at room temperature. The emission spectra were obtained by exciting with a wavelength found at the absorption maximum. The emission spectra are similar in shape for all of the compounds, with 2 – 3 maximum peaks in each spectrum (Figure 4.50). Across the series, there is a slight variation in quantum yield and lifetime, with the highest quantum yield associated with the tolan sandwich **4.7** and longest lifetime found for the terphenyl sandwich **4.8**. Quantum yield and lifetime were not obtained for compound **4.1** due to weak emission. In general, the quantum yields are less than unity and lifetimes range from 1 - 2 ns.

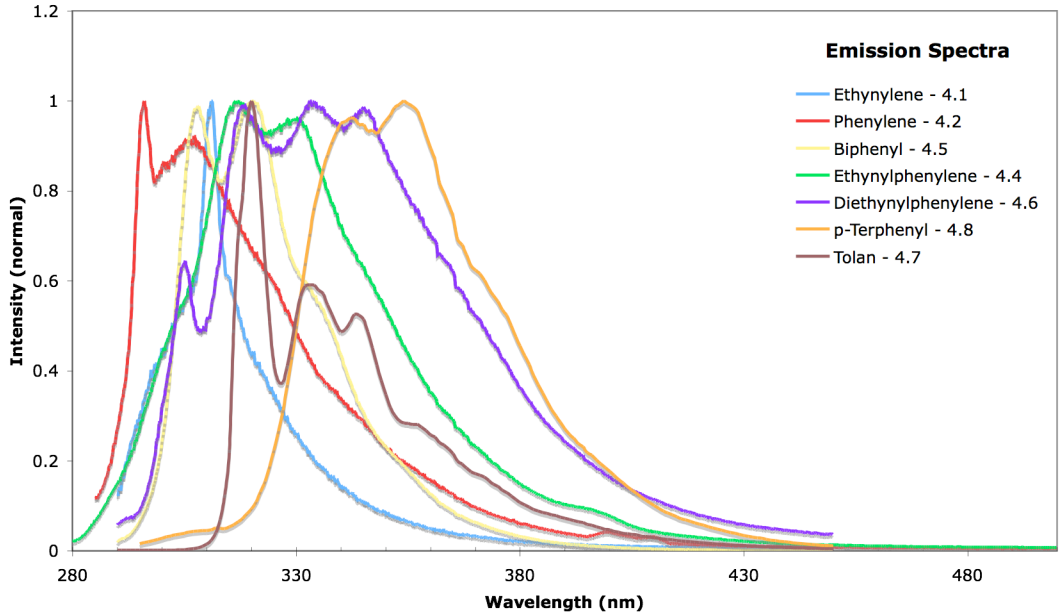

Figure 4.50 Normalized emission spectra of the *t*-butyl TOTA sandwich compounds in ethanol at room temperature.

The *t*-butyl TOTA sandwich compound **4.2** and the phenylene adduct **4.10** photophysics has some interesting aspects to its parent species, benzene. Both show broad absorption in the violet region and, as reported for substituted benzenes, a slight shift to lower frequency from the benzene absorption of 260 nm.[46] In the case of the "xylene effect",[47] *ortho* and *para* phenylene substituents enhance Φ_f. An "∝-substitution effect"[48] has also been described where alkyl substituents on the ∝-carbon to a benzene ring result in a reduction of the Φ_f. In the *t*-butyl TOTA structures, **4.2** was found to have a Φ_f of 0.042 and **4.10** a Φ_f of 0.145 and a relationship with the xylene or ∝-substitution effect appears not to be represented in these cases.

For comparison, the parent compounds for **4.7** and **4.8** were also measured under the same conditions. The measured quantum yield and lifetime of the parent *p*-terphenyl was similar to the values determined for the *t*-butyl TOTA terphenyl

sandwich **4.8**, and maintains very good luminescent properties in the *t*-butyl TOTA scaffold (Table 4.11). However, there was a much larger difference in the quantum yield and lifetime for the parent tolan *versus* the *t*-butyl TOTA tolan sandwich **4.7**. Also, in comparison to the parent species, the emission spectra have a similar shape but both the *t*-butyl TOTA tolan sandwich **4.7** (Figure 4.51) and the *t*-butyl TOTA terphenyl sandwich **4.8** are slightly *red-shifted* (Figure 4.52). In general, the incorporation of a chromophore in the *t*-butyl TOTA scaffold appears to not bring about large changes to the electronic spectrum of the aromatic chromophore core. However, there does appear to be a dependence on fluorescence quantum yield. The variation in the quantum yield may be attributed to the fact that the *t*-butyl TOTA scaffold prevents π–π stacking for occurring between the aromatic cores.[49]

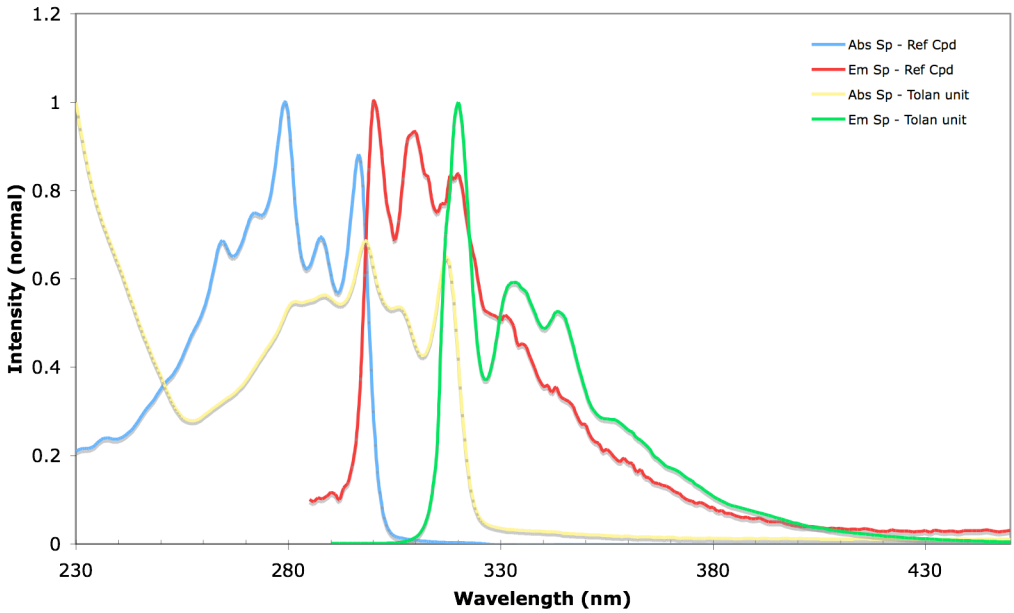

Figure 4.51 Normalized absorption and emission spectra of tolan and tolan moiety in *t*-butyl TOTA compound **4.7** in ethanol at room temperature.

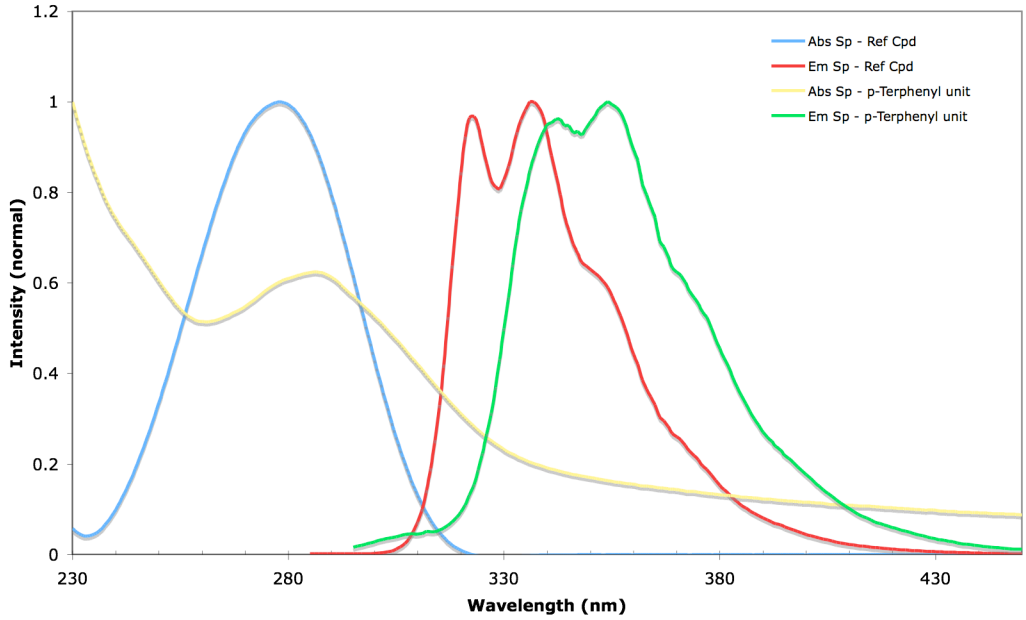

Figure 4.52 Normalized absorption and emission spectra of *p*-terphenyl and terphenyl moiety in *t*-butyl TOTA compound **4.8** in ethanol at room temperature.

Table 4.11 Absorption and Emission Data, Quantum Yields and Lifetimes for the TOTA series[a]

Compound	λ_{max} (nm)	ε (M^{-1} cm^{-1})	λ_{em} (nm)	Quantum Yield (Φ_f)	Lifetime (τ, ns)
Ethynylene - **4.1**	284	8570	312	---	---
Phenylene - **4.2**	284	2700	296	0.042	1.40
Phenylene-TOTA - **4.10**	284	4180	307	0.145	2.0
Ethynylphenylene - **4.4**	267	38730	318	0.040	0.76
Biphenyl - **4.5**	268	24300	320	0.456	2.20
Diethynylphenylene - **4.6**	299	68700	306	0.0498	6.0
Diphenylethynyl - **4.7** (Tolan)	298	46300	320	0.350	1.56
Tolan[50]	279	27560	302	0.0034	< 1.0
Tolan	270	30900	309	0.022	---
p-Terphenyl - **4.8**	287	41000	354	0.646	1.71
p-Terphenyl[51]	276	33800	337	0.930	0.95
p-Terphenyl	278	32140	336	0.980	1.48

[a] All measurements performed in ethanol at room temperature.

4.4.4 Solid-state NMR: A Dynamic Study

4.4.4.1 Introduction

In the study of molecular motions, NMR spectroscopy has become the preferred instrument by chemists. Dynamic motions can be studied in the solution phase, however, solid-state NMR offers many attractive aspects to detect and quantify molecular motion in the solid state. Two solid-state NMR techniques will be considered in this project. The first technique will be solid-state NMR by cross polarization magic angle spin (CPMAS) and the second technique will be quadrupolar ^{2}H NMR spectroscopy.[52]

4.4.4.2 ^{13}C NMR Solid-state Spectroscopy

^{13}C CPMAS NMR spectroscopy is a cross polarization technique that involves the transfer of magnetization from abundant, sensitive ^{1}H nuclei to less sensitive, dilute nuclei, such as ^{13}C. The experimental procedure requires high power ^{1}H decoupling and fast sample spinning (5-20 kHz) at the magic angle (54.7°) to remove line broadening from anisotropic interactions mediated by the external magnetic field.[53] Although resolution and line widths in the solid state are not as good as in solution, chemical shifts determined by CPMAS are comparable.

An additional technique known as dipolar dephasing (DD), or non-quaternary signal suppression (NQS), can be used in sequence with CPMAS to confirm molecular motion.[54] The CPMAS-DD experiment requires turning off the high power ^{1}H decoupler immediately after cross polarization and before signal acquisition. Dipole-dipole interactions of C–H groups that are part of highly mobile substituents or molecules can be diminished by dynamic averaging, resulting in a persistence of the corresponding signals after the DD pulses. Thus solid-state ^{13}C CPMAS-DD signals of highly mobile methyl groups and rapidly rotating molecules can be

detected. Furthermore, it can be expected that highly dynamic rotators will present signals that remain after the CPMAS-DD pulse sequence, whilst the signals corresponding to the 'stationary' stator should disappear by virtue of strong dipole-dipole interactions.

Rotators with atoms occupying two or more magnetically non-equivalent positions may experience a dynamic process where these atoms jump from site to site. The rate of exchange (k) between sites is governed by the energy barriers along the rotational profile and by the sample temperature. Variations in the spectrum as a function of temperature provide information on the exchange rate within certain dynamic windows (Figure 4.53).

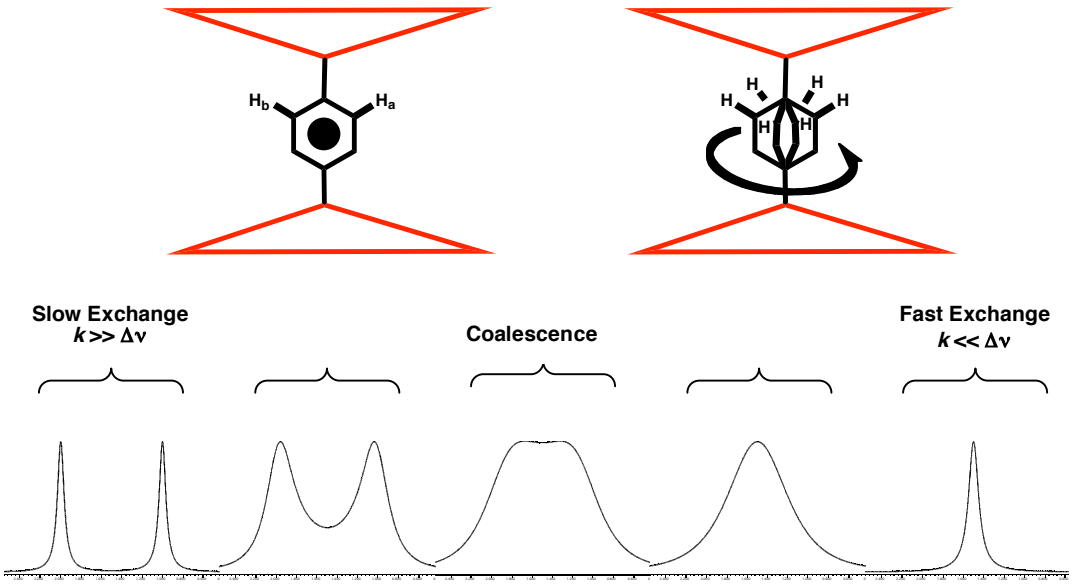

Figure 4.53 Hypothetical changes in simulated spectra as a result of dynamic motion of a phenylene unit in a TOTA superstructure. The correlation time at the coalescence temperature (T_c) is given by: $\tau_c = 2^{1/2}/(\pi\Delta\nu)$.

4.4.4.3 Quadrupolar ^{2}H NMR Solid-state Spectroscopy

Another useful solid-state technique is deuterium (^{2}H) NMR to study molecular order and dynamics.[55] Deuterium has a nuclear spin $I = 1$ and most of the NMR properties in the solid state are dictated by quadrupolar interactions with the

electric field gradient tensor. The use of ^{2}H isotopically labeled positions makes ^{2}H NMR a very sensitive probe for molecular dynamics in the solid state. In a powder sample the molecules will be oriented in all possible values of the orientation angle ß, angle that C–^{2}H bond makes with respect to the external field. The corresponding spectrum consists of a collection of doublets from C–^{2}H bonds in all possible orientations, which give rise to a broad symmetric spectrum, characterized by two maxima and two shoulders (Figure 4.54). With the spin-echo pulse sequence, systematic variations in the powder pattern occur when the C–^{2}H bonds experience dynamic exchange between sites that have different $\Delta\nu$ values. The internal dynamics of substituents and full body molecular reorientations result in the dynamic averaging of the magnetic interactions for different molecular orientations. Spectral lineshapes can be analyzed in terms of dynamic models that consider the types and rates of motion.[56]

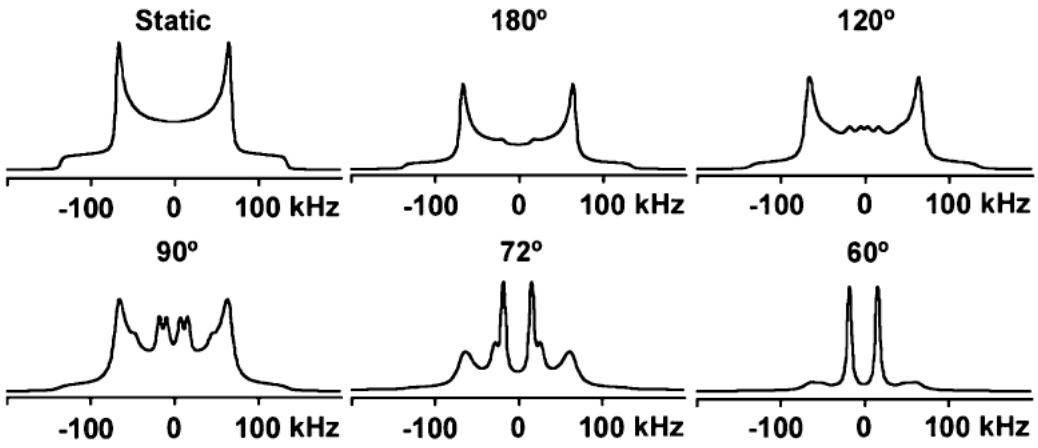

Figure 4.54 Pake powder pattern from simulated ^{2}H NMR line shapes for a static rotator, and for rotator undergoing angular displacements with an exchange rate of 10^5 s^{-1}.

4.4.4.4 Current Work

In light of the disordered phenylene ring seen in the crystal structure of *t*-butyl TOTA **4.2** (Figure 4.11) and the work of the Garcia-Garibay group with crystalline

rotors,[57] the solid-state dynamic properties of the *t*-butyl TOTA sandwich compound was considered with a phenylene moiety. As previously described, a series of aryl alkyne molecular rotors with the goal of designing crystalline molecular machines was prepared in the Garcia-Garibay group. Solid-state rotational barriers were determined for these compounds using ^{13}C CPMAS and ^{2}H NMR methods. Rotational dynamics of these systems found the barrier to rotation to be about 8.0 kcal/mol at 300 K.[58] If the phenylene *t*-butyl TOTA species **4.2** is found to have a measurable dynamic component, one might expect the rotational barrier to be less than 8.0 kcal/mol and influenced by packing characteristics in the solid state. The same NMR spectroscopic methods should be applicable in this case with *t*-butyl TOTA **4.2** to determine the rotational barriers in the solid phase.

Also in the work of Garcia-Garibay, it was determined that interdigitation of adjacent molecules was the primary cause for a rotational barrier. Therefore, it is postulated with varying axis length of the *t*-butyl TOTA series the problem of interdigitation could be explored and leading potentially to a "free" molecular rotor of the phenylene rotator in the solid state.

In order to examine the dynamics of the central phenylene ring in the *t*-butyl TOTA scaffold, the compound was prepared with a central deuterium labeled phenyl ring. A sample of the deuterated phenylene species (**4.2**-d_4) was submitted to the solid-state NMR group at the ETH, Zürich, Switzerland. Figure 4.55 is the initial spectrum obtained from ^{2}H NMR measurements.

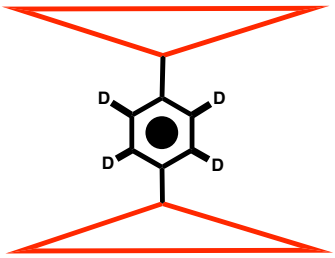

4.2-d_4

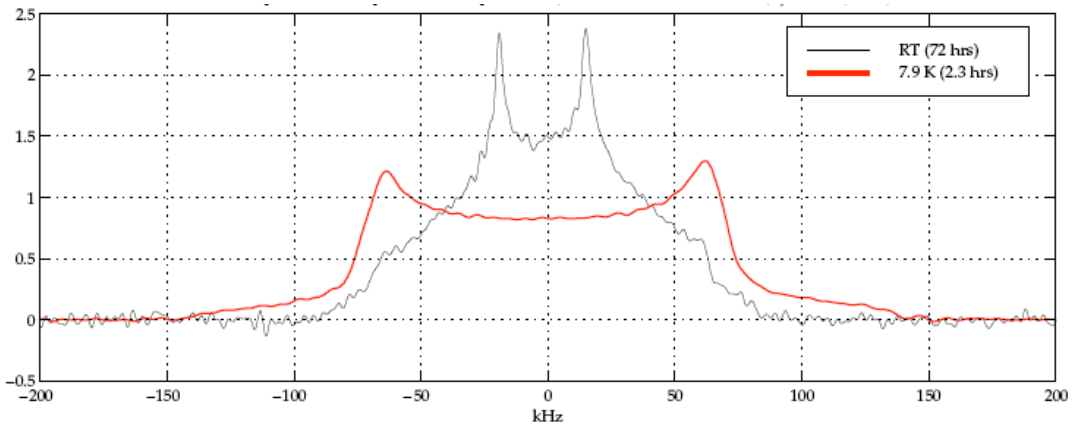

Figure 4.55 Solid-state ^{2}H NMR spectrum for sandwich *t*-butyl TOTA species **4.2**-d_4 acquired at room temperature and 8 K.

The characteristic Pake pattern is observed with two maxima and two shoulders in the measurements at room temperature and 8 K. The two distinct peaks indicate that there are two quadrupole couplings and the two are not quite equivalent. The observed separation in the doublet splitting observed for the deuterium atom reflects the degree of rotational freedom of the deuterium atom in the molecule. One might speculate that the room temperature measurement represents the "fast" exchange regime and when the sample is cooled down to 8 K the spectrum represents the "slow" exchange regime.

In conclusion, the shape and breath of these spectra seem to exclude the presence of a rigid phenylene in the *t*-butyl TOTA scaffold, although the angle of the "jumps" about the axis is not clear and will require more measurements. Also, line shape simulation in the intermediate exchange regime will require the input of several parameters to obtain dynamic data.[56] Preferably measurements taken at several

intermediate temperatures should help to elucidate the energetics of the system as determined by Arrhenius analysis of the exchange rate versus temperature.

4.5 Conclusions

A series of unique *t*-butyl TOTA superstructures have been prepared. The project design principle is based on the transmission of the molecular structure to other fundamental properties; in this case, predominantly order and dynamics. Furthermore, this investigation has relied on a rage of techniques that include current organic synthetic methodology, X-ray crystallography, and NMR spectroscopy. Although a complete conclusion cannot be given, initial results are promising in that molecular structure may lead to the control of order in the solid state and axial dynamic properties. In addition to the already completed crystallographic and spectroscopic analysis, efforts are ongoing concerning solid-state NMR experiments to evaluate the significance of the intermolecular interactions and axial dynamics. Also, a complete crystallographic analysis of the *t*-butyl TOTA series will be beneficial. The photophysical properties of this series of aryl alkynes *t*-butyl TOTA species were also examined and compared to the parent species, exhibiting similar electronic features.

The structural elaboration of these compounds has led to interesting crystal lattice structures and potential artificial molecular rotor species. With further crystal structure determination, the list of structural motifs to control packing order may be expanded. Also, introduction of a higher symmetry or an asymmetric species into the molecular axis of these molecules is synthetically feasible and allows for further dynamic investigations. Comparison of energy barriers among the series of compounds and computational studies may improve our understanding of the relationship between intermolecular dynamics and rotational barriers. A “free” rotor

sequestered from its surroundings is an attractive synthetic target, with potential applications in the field of molecular machines.

4.6 Experimental

Materials and Methods

^{1}H NMR and ^{13}C NMR were recorded on *Bruker* AV-300, AV-400, and AV-500 MHz spectrometers and were referenced to residual solvent peak: chloroform (^{1}H NMR: 7.26 ppm; ^{13}C NMR: 77.00 ppm) or acetone (^{1}H NMR: 2.05 ppm; ^{13}C NMR: 29.84 ppm). All experiments were carried out under a nitrogen or normal atmosphere in reagent grade solvents unless otherwise noted. Dry solvents were obtained from a *MBraun Solvent Purification System*. Commercial chemicals were used as supplied by *Sigma-Aldrich*, *Fluka* or *Acrõs Chemical Co*. *n*-Butyllithium and *t*-buytllithium reagents were titrated with Diphenylacetic acid prior to use to determine the concentration of the alkyl lithium solution. Palladium catalysts were prepared according to procedure or obtained from *Strem Chemicals, Inc*. An ammonia gas cylinder was obtained from *PANGAS*. Column chromatography was performed on silica gel (*Zeochem C-Gel*: C-560; 40-60 μm). Melting points are uncorrected and were recorded on a *Mel-Temp Laboratory Device*.

All photophysical spectra were recorded in spectroscopic grade dichloromethane and ethanol and are uncorrected. 2,5-diphenyloxazole (DPO) was used as the quantum yield standard for all samples. UV-Vis absorption spectra were recorded on *Perkin-Elmer UV/Vis/NIR Lambda 19* spectrometer at concentrations of *ca*. 10^{-5} M. Emission measurements were made using an *Edinburgh Instruments FLS920P* combined steady state, fluorescence and phosphorescence spectrometer. Emission and excitation spectra were collected using a Xe900 450 W steady state xenon arc lamp. Mass spectrometry was done by the Laboratory for Mass Spectrometry, Institute of Organic Chemistry, University of Zürich.

Single Crystal X-ray Diffraction Methods

All single crystal X-ray measurements and variable temperature measurements for compounds **3.32**, **3.40**, **3.41**, **3.44**, **3.45**, **4.2**, **4.3**, **4.10**, **4.11**, **4.12** and **4.13** were made by the X-ray Crystallography Facility, Institute of Organic Chemistry, University of Zurich, on a *Nonius KappaCCD* area-detector diffractometer[59] using graphite-monochromated Mo Kα radiation (λ = 0.71073 Å) and an *Oxford Cryosystems Cryostream 700* cooler. Data reduction was performed with *HKL Denzo and Scalepack*.[60] The intensities were corrected for Lorentz and polarization effects, but not for absorption. The structures were solved by direct methods using *SIR92*,[61] which revealed the positions of all non-hydrogen atoms. The non-hydrogen atoms were refined anisotropically. All of the H-atoms were placed in geometrically calculated positions and refined using a riding model where each H-atom was assigned a fixed isotropic displacement parameter with a value equal to $1.2U_{eq}$ of its parent atom ($1.5U_{eq}$ for the methyl groups). Refinement of the structure was carried out on F^2 by using full-matrix least-squares procedures, which minimized the function $\Sigma w(F_o^2 - F_c^2)^2$. The weighting scheme was based on counting statistics and included a factor to downweight the intense reflections. Neutral atom scattering factors for non-hydrogen atoms were taken from *Maslen, Fox and O'Keefe*[62] and the scattering factors for H-atoms were taken from *Stewart, Davidson and Simpson*.[63] Anomalous dispersion effects were included in F_c;[64] the values for f' and f'' were those of *Creagh and McAuley*.[65] The values of the mass attenuation coefficients are those of *Creagh and Hubbel*.[66] All calculations were performed using the *SHELXL97* program[67] and figures were produced with *ORTEPII*.[68]

Powder Diffraction Measurements

Powder diffraction measurements were carried out at the Paul Scherrer Institute/Swiss Light Source in Villigen, Switzerland. Samples were measured at the Materials Science X04SA beamline. The powder diffractometer was equipped with the second generation Mythen 2 microstrip detector covering an angular range of 120°.[34] Samples were prepared, mounted and sealed in glass capillary tubes. Temperatures were maintained with Oxford Instruments LN2 Cryojet.

The PSI/SLS results of the refinement with silicon (NIST 640c) from measurements made in May 2008:

λ = 1.000992 ± 0.000025 Å
E = 12.385714 ± 0.000309 KeV
2θ-Offset = + 0.007458 ± 0.000017 degree

The PSI/SLS results of the refinement with silicon (NIST 640c) from measurements made in June 2008:

λ = 0.776369 ± 0.000030 Å
E = 15.969209 ± 0.000620 KeV
2θ-Offset = + 0.002353 ± 0.000025 degree

4-*tert*-butyl-2,6-dimethoxyphenol (3.33)

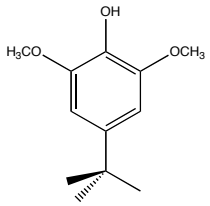

A solution of 2,6-dimethoxyphenol (77 g, 0.53 mol) in CH_3SO_3H (115 mL) was warmed under reflux conditions to 40 °C. *t*-BuOH (155 mL, 1.59 mol) was added slowly, keeping the temperature between 50-55 °C. After the addition, the temperature was kept at 50 °C for approximately 2 hours, then allowed to come to room temperature overnight. The reaction mixture was poured onto *ca*. 500 g ice, and then extracted with diethyl ether (3 x 100 mL). The organic phases were combined and washed with water (3 x 100 mL), saturated aqueous $NaHCO_3$ (2 x 250 mL), and again water (2 x 50 mL), dried with $MgSO_4$, and concentrated on the rotary evaporator to yield a yellow oil (*ca*. 190 ml) that was used directly in the next reaction. ^{1}H NMR (300 MHz, $CDCl_3$, TMS) δ_H 6.61 (2H, s, Ar*H*), 5.37 (1H, s, O*H*), 3.89 (6H, s, OCH_3), 1.31 (9H, s, C(CH_3)$_3$). Mass Spectrometry (GC) *m/z*: M^+ 210 ($C_{12}H_{18}O_3$).

Diethyl-4-*tert*-butyl-2,6-dimethoxyphenyl phosphate (3.34)

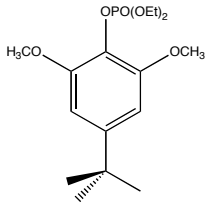

The product **3.33** (0.53 mol) was dissolved in diethyl phosphite (82 mL, 0.64 mol) and CCl_4 (75 mL) at 0 °C under nitrogen atmosphere. After about 10 minutes of stirring, triethylamine (96 mL, 0.69 mol) was added gradually, maintaining the temperature below 10 °C. This addition was done over a period of 4 hours, and then

the reaction mixture was allowed to come to room temperature and stirred overnight. The reaction mixture was concentrated, and dissolved in a mixture of diethyl ether (400 mL) and water (400 mL). The aqueous and organic phases were separated, and the aqueous phase was washed again with diethyl ether (20 mL). The combined organic phases were washed with water (100 mL), 1M HCl (2 x 75 mL), water (100 mL), 4M NaOH (2 x 75 mL), and water (100 mL), dried with $MgSO_4$, and evaporated to dryness to give a yellow solid. Recrystallization from hexane yielded 140 g (76%) of off-white flakes: mp = 75 °C; ^{1}H NMR (300 MHz, $CDCl_3$, TMS) δ_H 6.59 (2H, s, Ar*H*), 4.31 (4H, q, *J* = 7.10 Hz, POC*H*$_2$CH$_3$), 3.86 (6H, s, OC*H*$_3$), 1.38 (6H, td, *J* = 7.10 Hz, POCH$_2$C*H*$_3$), 1.30[9H, s, C(C*H*$_3$)$_3$]; ^{13}C{^{1}H} NMR (75.5 MHz, $CDCl_3$, TMS) δ_C 151.6, 148.8, 127.9, 103.0, 64.6, 56.5, 35.4, 31.8, 16.5; Mass Spectrometry (GC) *m/z*: M^+ 346 ($C_{16}H_{27}O_6P$).

1-*tert*-butyl-2,5-dimethoxybenzene (3.35)

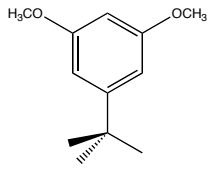

Compound **3.34** (140 g, 0.4 mol) was dissolved in a 1:5 mixture of dry THF (50 mL) and dry diethyl ether (250 mL). Ammonia (*ca.* 500 mL) was condensed using a dry ice / ethanol bath, and lithium metal (4 g, 0.57 mol) was added slowly to prepare the dark blue solution. The starting material **3.34** in THF/Et_2O was then added drop wise over 2 hours. During this addition, additional lithium metal (2.4 g, 0.35 mol) was added to the solution to maintain its dark blue colour. After the completion of the addition, the reaction mixture was stirred for one hour, followed by slow quenching with saturated aqueous NH_4Cl (*ca.* 100 mL). The cooling bath was removed, and the reaction mixture was allowed to stir overnight at room temperature,

allowing for the evaporation of the ammonia through the appropriate outflow apparatus. The reaction mixture was washed with diethyl ether (2 x 400 mL). The organic phase was then washed with water (100 mL), 2M NaOH (2 x 200 mL), and water (2 x 100 mL), followed by drying over K_2CO_3 and concentrated by rotary evaporation. The product was recrystallized from hexane yielding 95 g (98 %) of white crystals: mp = 50 °C; ^{1}H NMR (300 MHz, $CDCl_3$, TMS) δ_H 6.54 (2H, d, J = 2.2 Hz), 6.31 (1H, t, J = 2.2 Hz), 3.80 (6H, s, OCH_3), 1.30 (9H, s, C(CH_3)$_3$); ^{13}C{^{1}H} NMR (75.5 MHz, $CDCl_3$, TMS) δ_C 160.5, 153.9, 104.1, 96.8, 55.2, 35.0, 31.3; Mass Spectrometry (GC) *m/z*: M^+ 194 ($C_{12}H_{18}O_2$).

2-bromo-5-*tert*-butyl-1,3-dimethoxybenzene (3.36)

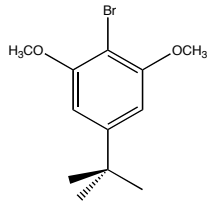

Compound **3.35** (95 g, 0.4 mol) was dissolved in 600 mL CCl_4 at 0 °C, and Br_2 (21 mL, 0.4 mol) in 110 mL CCl_4 was added drop wise over 2 hours to give a cloudy red solution. After addition, the reaction mixture was stirred for 1.5 hours at 0 °C. The product was concentrated and recrystallized from hexane to yield 104 g (95%) of a crystalline product: mp = 120 °C; ^{1}H NMR (300 MHz, $CDCl_3$, TMS) δ_H 6.60 (2H, s, Ar*H*), 3.91 (6H, s, OCH_3), 1.33 (9H, s, C(CH_3)$_3$); ^{13}C{^{1}H} NMR (75.5 MHz, $CDCl_3$, TMS) δ_C 154.9, 150.5, 100.7, 96.3, 54.7, 33.5, 29.6; Mass Spectrometry (GC) *m/z*: M^+ 272 (one peak in the correct isotopic ratio for a mono-brominated compound, $C_{12}H_{17}BrO_2$).

tris(4-*tert*-butyl-2,6-dimethoxyphenyl)methanol (3.37)

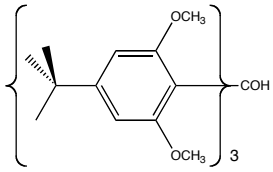

Compound **3.36** (8.0 g, 29.4 mmol) was added to a mixture of 50 mL dry toluene and 60 mL dry THF. Bu^{t}Li (39 mL, 58.8 mmol) was added slowly, maintaining the temperature below – 60 °C. After the addition, the reaction mixture was stirred for 1 hour at – 78 °C, followed by the drop wise addition of diethyl carbonate (1.2 mL, 9.8 mmol) in 15 mL of dry THF. The reaction mixture was then allowed to come to room temperature, generating a bright green solution, followed by reflux for 2 days. The transparent brown reaction mixture was then cooled to RT and quenched with 30 mL of technical grade ethanol. The reaction mixture was washed with 100 mL diethyl ether and then the organic phase was washed with water (100 mL). The aqueous layers were washed with diethyl ether (30 mL), and then the combined organic phases were washed once again with water, followed by drying over $MgSO_4$ and removal of the solvent by rotary evaporation. Recrystallization from hexane gave compound **3.37** (3.41 g, 57 %) as a fine, white solid: mp = 176 °C; ^{1}H NMR (300 MHz, $CDCl_3$, TMS) δ_H 6.72 (1H, s, O*H*), 6.49 (6H, s, Ar*H*), 3.39 (18H, s, OCH_3), 1.27 (27H, s, C(CH_3)$_3$); ^{13}C{^{1}H} NMR (75.5 MHz, $CDCl_3$, TMS) δ_C 158.2, 149.2, 125.9, 124.9, 104.2, 56.6, 34.6, 31.3; UV-Vis (CH_3CH_2OH) λ_{max} (log ε) nm: 225 (4.88), 276 (3.84), 282 (3.48).

2,6,10-tri-*tert*-butyl-12c-ethoxy-4,8,12-trioxa-4,8,12,12c-tetrahydrodibenzo[*cd,mn*]pyrene (3.39)

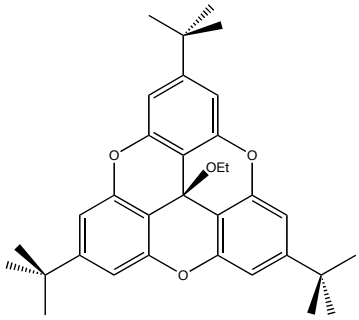

A mixture of compound **3.37** (8.2 g, 13.5 mmol) in water (600 mL) was treated with concentrated HCl (20 mL) and the blue solution was refluxed for 4 hours. The reaction mixture was filtered and the filter cake was washed several times with water until the crude off-white xanthon **3.38** was obtained. After drying, the crude material **3.38** (9.2 g, 13.5 mmol) was mixed with excess pyridine hydrochloride (15 g, 133 mol) and heated under a reflux condenser to 150 °C for 2 hours. The reaction mixture changed colour from dark purple to a reddish orange. The reaction mixture was cooled and poured into water (50 mL). This solution was filtered, and the filter cake washed with water, 2M HCl, and water again. The filtrate was treated with 2M NaOH until the solution was basic to litmus paper and a white precipitate appeared. The pasty precipitate was collected by filtration and dissolved in technical grade ethanol under reflux. Upon cooling, the final product precipitated and was collected by filtration as a white powder (3.51 g, 52% yield): mp > 230 °C; ^{1}H NMR (300 MHz, $CDCl_3$, TMS) δ_H 7.06 (6H, s, Ar*H*), 3.13 (2H, q, OCH_2CH_3), 1.35 (27H, s, $C(CH_3)_3$), 0.92 (3H, q, OCH_2CH_3); $^{13}C\{^{1}H\}$ NMR (75.5 MHz, $CDCl_3$, TMS) δ_C 154.0, 153.0, 125.9, 108.4, 106.9, 56.9, 35.3, 31.4, 15.3.

2,6,10-tri-*tert*-butyl-4,8,12-trioxa-4,8,12,12c-tetrahydrodibenzo[*cd,mn*]pyrenium hexafluorophosphate (3.32)

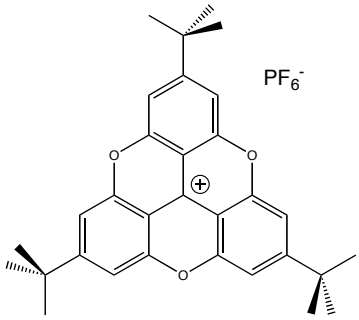

Aqueous 65% HPF_6 (0.89 mL, 7.05 mmol) was added drop wise to a solution of **3.39** (3.51 g, 7.05 mmol) in diethyl ether (400 mL) at 0 °C. The formation of a bright yellow precipitate was seen immediately. The reaction mixture was stirred at 0 °C for 1 hour, filtered, washed with cold diethyl ether, and dried under vacuum to give 4.0 g (95%) of the yellow product **3.32** as a fine yellow powder: mp > 300 °C. ^{1}H NMR (300 MHz, $CDCl_3$, TMS) δ_H 7.67 (6H, s, Ar*H*); 1.50 (27H, s, C(C*H*$_3$)$_3$). ^{13}C{^{1}H} NMR ($CDCl_3$) δ_c 169.7, 153.5, 142.3, 110.1, 103.8, 37.8, 31.5. UV-Vis (CH_3CH_2OH) λ_{max} (log ε) nm: 215 (4.74), 285 (3.94), 350 (3.67), 442 (3.51). Mass Spectrometry (ESI) *m/z*: M^+ 453.3 ($C_{31}H_{33}O_3^+$).

2,6,10-tri-*tert*-butyl-4,8,12-trioxa-4,8,12,12c-tetrahydrodibenzo[*cd,mn*]pyrene (3.40)

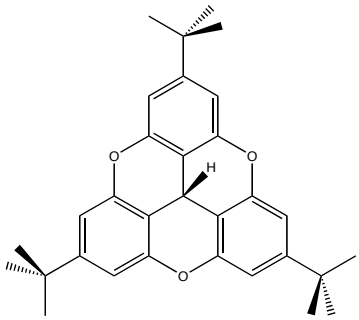

$NaBH_4$ (187 mg, 4.95 mmol) was added to a solution of compound **3.32** (200 mg, 0.33 mmol) in 20 mL DME. The reaction mixture changed from yellow to

colourless during the additional 1 hour at reflux. The reaction was cooled to room temperature, poured into ice (*ca*. 200 g) and diethyl ether (100 mL) was added. The organic phase was extracted with water (2 x 50 mL), dried (Na_2SO_4) and evaporated to dryness. Recrystallisation from ethyl acetate produced 135 mg (91%) clear crystals suitable for X-ray diffraction: mp = 255 °C; ^{1}H NMR (400 MHz, $CDCl_3$, TMS) δ_H 6.96 (6H, s, Ar*H*), 4.75 (1H, s, 12c-*H*), 1.33 [27H, s, C(C*H*$_3$)$_3$]; ^{13}C{^{1}H} NMR (75.5 MHz, $CDCl_3$, TMS) δ_c 152.8, 152.7, 108.4, 106.8, 35.0, 31.3, 20.2. UV-Vis (CH_3CH_2OH) λ_{max} (log ε) nm: 212 (4.73), 280 (3.62). Mass Spectrometry (ESI) *m/z*: M^+ 453.3 ($C_{31}H_{33}O_3^+$).

2,6,10-tri-*tert*-butyl-12c-methyl-4,8,12-trioxa-4,8,12,12c-tetrahydrodibenzo[*cd,mn*]pyrene (3.41)

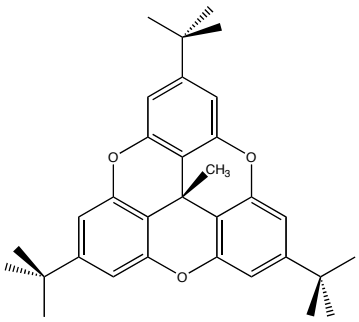

A solution of compound **3.32** (204 mg, 0.34 mmol) in 20 mL dry THF was cooled to – 78 °C under nitrogen atmosphere. CuI (126 mg, 0.66 mmol) was added to the solution. After 10 minutes of stirring, 1.6 M MeLi (1.2 mL, 1.9 mmol) was slowly added. The reaction mixture changed colour from yellow to green. The mixture was stirred for 1 hour at – 78 °C. The temperature was allowed to reach room temperature followed by the addition of 10 mL saturated aqueous NH_4Cl to quench the reaction mixture. The aqueous phase was extracted with $CHCl_3$ (2 x 25 mL) and the combined organic phases were washed with water (2 x 25 mL), dried

(Na_2SO_4) and evaporated to give a clear oil. The crude product was purified by column chromatography with silica gel (R_f = 0.4) with hexane as the eluent to yield 178 mg (98%) of a white powder. Recrystallization from ethyl acetate produced clear crystals suitable for X-ray diffraction: mp > 300 °C. ^{1}H NMR (300 MHz, $CDCl_3$, TMS) δ_H 6.96 (6H, s, Ar*H*), 1.53 (3H, s, C*H*$_3$), 1.32 [27H, s, C(C*H*$_3$)$_3$]; ^{13}C{^{1}H} NMR (75.5 MHz, $CDCl_3$, TMS) δ_c 152.3, 152.1, 112.4, 108.4, 35.0, 31.8, 31.5, 22.6; Mass Spectrometry (ESI) *m/z*: $(M+H)^+$ 469.2 ($C_{32}H_{36}O_3^+$).

2,6,10-tri-*tert*-butyl-12c-((trimethylsilyl)ethynyl)-4,8,12-trioxa-4,8,12,12c-tetrahydrodibenzo[*cd,mn*]pyrene (3.42)

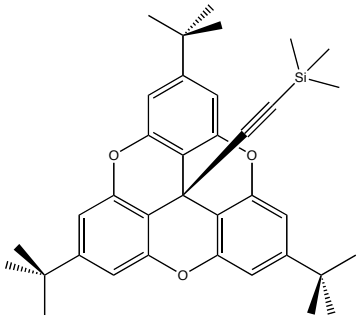

An oven-dried 100 mL flask containing a Teflon stir bar and nitrogen atmosphere was charged with ethynyltrimethylsilane (0.53 mL, 3.76 mmol) and 5 mL dry THF. The solution was subsequently cooled to – 78 °C with a dry ice/acetone bath and Bu^{n}Li (1.6 mL, 3.76 mmol) was added drop wise with a disposable syringe. The solution was stirred for 45 minutes. In a second dry 100 mL flask, compound **3.32** (750 mg, 1.25 mmol) was dissolved in 10 mL dry THF and cooled to – 78 °C with a dry ice/acetone bath. This solution was then transfer with a stainless steel cannula to the ethynyltrimethylsilane solution and allowed to stir for 45 minutes. The reaction mixture was allowed to warm to 0 °C and quenched with 10 mL saturated aqueous NH_4Cl. The layers were separated and the aqueous layer washed three times

with Et_2O. The organic layers were combined, dried ($MgSO_4$) and the solvent removed by rotary evaporation. The desired product was purified by chromatography on silica gel (R_f = 0.3), with hexane as the eluent, to yield 700 mg (98%) of white powder: mp = 300 °C ^{1}H NMR (300 MHz, $CDCl_3$) δ_H 7.00 (6H, s, Ar*H*), 1.34 [27H, s, C(C*H*$_3$)$_3$], 0.01 [9H, s, Si(C*H*$_3$)$_3$]; $^{13}C\{^1H\}$ NMR (75.5 MHz, $CDCl_3$) δ_c 153.1, 152.3, 109.1, 105.7, 87.6, 35.2, 31.4, 22.7, 14.2, 0.00. Mass Spectrometry (ESI): $(M+Na)^+$ 573.3 ($C_{36}H_{42}O_3SiNa^+$).

2,6,10-tri-*tert*-butyl-12c-(ethynyl)-4,8,12-trioxa-4,8,12,12c-tetrahydrodibenzo[*cd,mn*]pyrene (3.43)

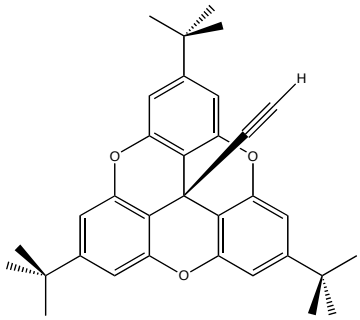

To a solution of **3.42** (700 mg, 1.25 mmol) in 20 mL methanol / 30 mL THF was added potassium carbonate (900 mg, 7.0 mmol) and the mixture was stirred at room temperature for 16 hours. Diethyl ether was added to the reaction mixture, which was then transferred to a separatory funnel. The organic phase was washed twice with water, and then dried over magnesium sulfate. The solvent was evaporated under reduced pressure. The desired product was purified by column chromatography on silica gel (R_f = 0.6), with 8:2 hexane/dichloromethane as the eluent, to yield 520 mg (79%) of white powder: mp = 338 °C; ^{1}H NMR (400 MHz, $CDCl_3$, TMS) δ_H 7.02 (6H, s, Ar*H*), 2.41(1H, s, CC*H*), 1.33 [27H, s, C(C*H*$_3$)$_3$]; $^{13}C\{^1H\}$ NMR (100.6 MHz,

$CDCl_3$, TMS) δ_c 153.6, 152.3, 109.1, 108.2, 84.9, 71.9, 35.2, 31.3, 21.6; Mass Spectrometry (ESI): $(M+Na)^+$ 501.3 ($C_{33}H_{34}O_3Na^+$).

2,6,10-tri-*tert*-butyl-12c-(ethynylphenyl)-4,8,12-trioxa-4,8,12,12c-tetrahydrodibenzo[*cd,mn*]pyrene (3.44)

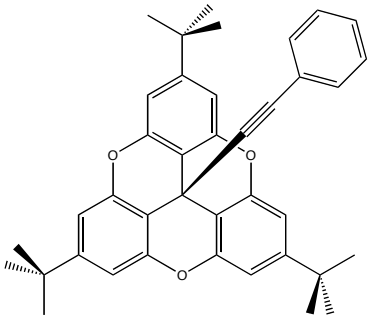

An oven-dried 100 mL flask containing a stir bar and nitrogen atmosphere was charged with phenylacetylene (0.11 mL, 1.02 mmol) and 5 ml dry THF. The solution was subsequently cooled to – 78 °C with a dry ice/acetone bath and Bu^{n}Li (0.40 mL, 1.02 mmol) was added drop wise with a disposable syringe. The solution was stirred for 45 minutes. In a second dried 100 mL flask, compound **3.32** (200 mg, 0.34 mmol) was dissolved in 10 mL dry THF and cooled to – 78 °C with a dry ice/acetone bath. This solution was then transfer with a stainless steel cannula tube to the phenylacetylene solution and allowed to stir for 45 minutes. The reaction mixture was allowed to warm to 0 °C and quenched with 10 mL saturated aqueous NH_4Cl. The layers were separated and the aqueous layer washed three times with Et_2O. The organic layers were combined, dried ($MgSO_4$) and the solvent removed by rotary evaporation. The desired product was purified by column chromatography on silica gel (R_f = 0.3), with hexane as the eluent, to yield 150 mg (80%) of white powder. ^{1}H NMR (300 MHz, $CDCl_3$, TMS) δ_H 7.30-7.11 (5H, m, Ph*H*), 7.02 (6H, s, Ar*H*), 1.34 [27H, s, C(C*H*$_3$)$_3$]; $^{13}C\{^1H\}$ NMR (75.5 MHz, $CDCl_3$, TMS) δ_c 153.1, 152.2, 131.7,

128.0, 127.8, 122.6, 108.9, 108.7, 90.4, 83.4, 35.1, 31.3, 22.2. Mass Spectrometry (ESI): $(M+Na)^+$ 577.3 ($C_{39}H_{38}O_3Na^+$).

2,6,10-tri-*tert*-butyl-12c-(ethynyl-3-pyridyl)-4,8,12-trioxa-4,8,12,12c-tetrahydrodibenzo[*cd,mn*]pyrene (3.45)

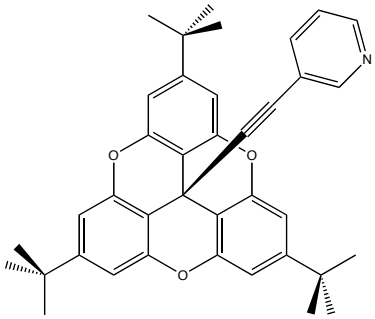

An oven-dried 100 mL flask containing a stir bar and nitrogen atmosphere was charged with 3-ethynylpyridine (105 mg, 1.02 mmol) and 5 ml dry THF. The solution was subsequently cooled to – 78 °C with a dry ice/acetone bath and Bu^nLi (0.44 mL, 1.02 mmol) was added drop wise with a disposable syringe. The solution was stirred for 45 minutes. In a second dry 100 mL flask, compound **3.32** (200 mg, 0.34 mmol) was dissolved in 10 mL dry THF and cooled to – 78 °C with a dry ice/acetone bath. This solution was then transfer with a stainless steel cannula tube to the 3-ethynylpyridine solution and allow to stir for 45 minutes. The reaction mixture was allowed to warm to 0 °C and quenched with 10 mL saturated aqueous NH_4Cl. The layers were separated and the aqueous layer washed three times with Et_2O. The organic layers were combined, dried ($MgSO_4$) and the solvent removed by rotary evaporation. The desired product was purified by column chromatography on silica gel (R_f = 0.6), with 4:1 ethyl acetate/hexane as the eluent, to yield 110 mg (58%) of white powder. ^1H NMR (300 MHz, $CDCl_3$, TMS) δ_H 8.46, 8.38, 7.54 and 7.08 (4H, m, Pyr*H*), 7.04 (6H, s, Ar*H*), 1.35 [27H, s, $C(CH_3)_3$]; $^{13}C\{^1H\}$ NMR (75.5 MHz,

$CDCl_3$, TMS) δ_c 153.3, 153.0, 152.2, 149.4, 139.7, 123.4, 116.5, 108.9, 108.7, 94.3, 66.8, 35.1, 31.3, 22.2. Mass Spectrometry (ESI): $(M+H)^+$ 556.4 ($C_{38}H_{37}NO_3^+$).

2,6,10-tri-*tert*-butyl-12c-(4-bromophenyl)-4,8,12-trioxa-4,8,12,12c-tetrahydrodibenzo[*cd,mn*]pyrene (3.46)

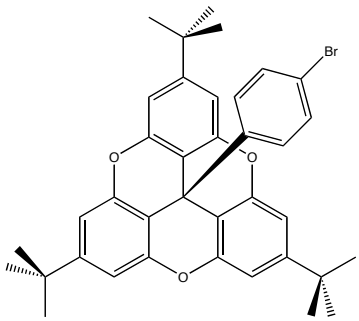

Compound **3.32** (500 mg, 0.82 mmol) was put in a oven dried 100 mL flask, dissolved in 10 mL dry THF and cooled to -78 °C with a dry ice/acetone bath. In a second oven dried flask 1,4-dibromobenzene (580 mg, 2.46 mmol) was dissolved in 10 mL dry THF at –78 °C. Nitrogen atmosphere was maintained in both flasks. Bu^nLi (1.1 mL, 2.46 mmol) was added drop wise to the dibromobenzene solution over a period of 10 minutes. This solution was allowed to stir for 45 minutes. The solution of **3.32** in THF was then transferred by a stainless steel cannula to the lithiated dibromobenzene solution. The bright yellow color of the cation solution immediately disappeared upon its cannulation. After 45 minutes of stirring, the solution was allowed to warm to 0 °C with an ice bath. The reaction was quenched with 10 mL saturated aqueous NH_4Cl and diethyl ether (10 mL) was added. The aqueous layer was collected and then washed again with diethyl ether (10 mL). The organic layers were then collected, dried over $MgSO_4$, and concentrated to give a white powder. The desired product was purified by column chromatography on silica gel (R_f = 0.2) with hexane as the eluent, and it was collected and concentrated (450

mg) in 90% yield: mp = 275 °C. ^{1}H NMR (300 MHz, $CDCl_3$, TMS) δ_H 7.28 (2H, d, Ar*H*, *J* = 8.0 Hz), 6.95 (2H, d, Ar*H*, *J* = 8.0 Hz), 7.00 (6H, s, Ar*H*), 1.33 [27H, s, C(C*H*$_3$)$_3$]; ^{13}C{^{1}H} NMR (75.5 MHz, $CDCl_3$, TMS) δ_c 153.1, 152.5, 145.4, 131.8, 127.7, 120.9, 111.4, 108.9, 35.2, 31.4, 15.3; Mass Spectrometry (ESI): $(M+H)^+$ 609.4 (in correct isotopic ratio, $C_{37}H_{37}BrO_3^+$).

2,6,10-tri-*tert*-butyl-12c-(4-iodophenyl)-4,8,12-trioxa-4,8,12,12c-tetrahydrodibenzo[*cd,mn*]pyrene (3.47)

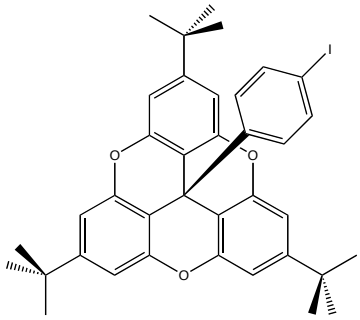

Compound **3.32** (600 mg, 1.0 mmol) was put in a oven dried 100 mL flask, dissolved in 10 mL dry THF and cooled to -78 °C with a dry ice/acetone bath. In a second oven dried flask 1,4-diiodobenzene (993 mg, 3.0 mmol) was dissolved in 7 mL dry THF at –78 °C. A nitrogen atmosphere was maintained in both flasks. Bu^{n}Li (1.25 mL, 3.0 mmol) was added drop wise to the diiodobenzene solution over a period of 10 minutes. This solution was then stirred for 45 minutes. The solution of **3.32** in THF was transferred by a stainless steel cannula to the lithiated diiodobenzene solution. The bright yellow color of the cation solution immediately disappeared upon its cannulation. After 45 minutes of stirring, the solution was allowed to warm to 0 °C with an ice bath. The reaction was quenched with 10 mL saturated aqueous NH_4Cl and diethyl ether (10 mL) was added. The aqueous layer was collected and then washed again with diethyl ether (10 mL). The organic layers were then

collected, dried over $MgSO_4$, and concentrated to give a white powder. The desired product was purified by column chromatography on silica gel (R_f = 0.4) with hexane as the eluent, and it was collected and concentrated (600 mg) in 98% yield. mp = 275 – 278 °C. ^{1}H NMR (400 MHz, $CDCl_3$, TMS) δ_H 7.49 (2H, d, Ar*H*, *J* = 8.0 Hz), 7.00 (6H, s, Ar*H*), 6.82 (2H, d, Ar*H*, *J* = 8.0 Hz), 1.33 (27H, s, C(C*H*$_3$)$_3$). ^{13}C{^{1}H} NMR (100.6 MHz, $CDCl_3$, TMS) δ_c 152.5, 152.1, 146.2, 137.8, 128.0, 120.9, 111.3, 108.9, 35.2, 31.4, 22.6. Mass Spectrometry (ESI): $(M+Na)^+$ 679.2 (in correct isotopic ratio, $C_{37}H_{37}IO_3Na^+$).

2,6,10-tri-*tert*-butyl-12c-(4-methoxyphenyl)-4,8,12-trioxa-4,8,12,12c-tetrahydrodibenzo[*cd,mn*]pyrene (3.48)

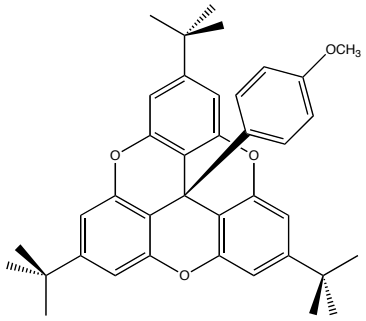

Compound **3.32** (200 mg, 0.34 mmol) was put in a oven dried 100 mL flask, dissolved in 10 mL dry THF and cooled to -78 °C with a dry ice/acetone bath. In a second oven dried flask 4-bromoanisole (0.13 mL, 1.02 mmol) was dissolved in 10 mL dry THF at –78 °C. A nitrogen atmosphere was maintained in both flasks. Bu^{n}Li (0.40 mL, 1.02 mmol) was added drop wise to the 4-bromoanisole solution over a period of 10 minutes. This solution was then stirred for 45 minutes. The solution of **3.32** in THF was then transferred by a stainless steel cannula to the lithiated 4-bromoanisole solution. The bright yellow color of the cation solution immediately disappeared upon cannulation into the 4-bromoanisole solution. After 45 minutes of

stirring, the reaction flask was allowed to warm to 0 °C with an ice bath. The reaction was quenched with 10 mL saturated aqueous NH_4Cl and diethyl ether (10 mL) was added. The aqueous layer was collected and then washed again with diethyl ether (10 mL). The organic layers were then collected, dried over $MgSO_4$, and concentrated to give a white powder. The desired product was purified by column chromatography on silica gel (R_f = 0.1) with hexane as the eluent, and it was collected and concentrated (190 mg) in 98% yield. ^{1}H NMR (300 MHz, $CDCl_3$, TMS) δ_H 7.03 (2H, d, Ar*H*, *J* = 9.0 Hz), 6.71 (2H, d, Ar*H*, *J* = 9.0 Hz), 7.03 (6H, s, Ar*H*), 3.67 (3H, s, OC*H*$_3$), 1.34 [27H, s, C(C*H*$_3$)$_3$]; ^{13}C{^{1}H} NMR (75.5 MHz, $CDCl_3$, TMS) δ_c 157.6, 153.1, 152.5, 142.3, 126.1, 113.9, 111.4, 108.9, 55.9, 45.7, 35.2, 31.4; Mass Spectrometry (ESI): $(M+Na)^+$ 583.3 ($C_{38}H_{40}O_4Na^+$).

2,6,10-tri-*tert*-butyl-12c-(4-hydroxyphenyl)-4,8,12-trioxa-4,8,12,12c-tetrahydrodibenzo[*cd,mn*]pyrene (3.49)

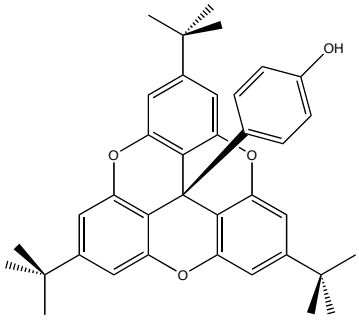

To a solution of **3.48** (130 mg, 0.23 mmol) in 5 mL methylene chloride at –78 °C was slowly added boron tribromide (0.35 mL, 3.7 mmol) by disposable syringe. The reaction mixture was stirred for 16 hours and warmed to room temperature. Water was slowly added to the reaction mixture at 0 °C and the contents were transferred to a separatory funnel. The organic phase was washed twice with water and dried over magnesium sulfate. The solvent was evaporated under reduced

pressure. The desired product was purified by column chromatography on silica gel (R_f = 0.3), with 10:1 hexane/dichloromethane as the eluent, to yield 90 mg (70%) of white powder; ^{1}H NMR (300 MHz, $CDCl_3$, TMS) δ_H 7.00 (6H, s, Ar*H*), 6.93 (2H, d, Ar*H*, *J* = 9.0 Hz), 6.62 (2H, d, Ar*H*, *J* = 9.0 Hz), 1.33 [27H, s, C(C*H*$_3$)$_3$], no phenyl-O*H* resonance signal observed; ^{13}C{^{1}H} NMR (75.5 MHz, $CDCl_3$, TMS) δ_c 155.4, 153.4, 152.3, 142.6, 126.5, 115.5, 111.6, 109.2, 40.7, 35.3, 31.1.

2,6,10-tri-*tert*-butyl-12c-(4- Trifluoromethanesulfonate phenyl)-4,8,12-trioxa-4,8,12,12c-tetrahydrodibenzo[*cd,mn*]pyrene (3.50)

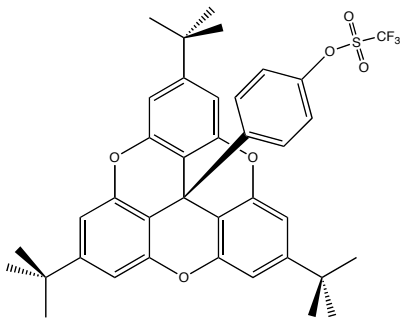

To a solution of **3.49** (90 mg, 0.16 mmol) and pyridine (5 mL) in 5 mL methylene chloride at –78°C was slowly added triflic anhydride (0.05 mL, 0.32 mmol) by disposable syringe. The reaction mixture was stirred for 18 hours at room temperature, and then water was added. The solution was transferred to a separatory funnel, methylene chloride was added, and the phases were separated. The organic phase was washed twice with water, and then dried over magnesium sulfate. Solvent was evaporated under reduced pressure. The desired product was purified by column chromatography on silica gel (R_f = 0.6) with 8:2 hexane/dichloromethane as the eluent, to yield 70 mg (65%) of white powder; ^{1}H NMR (300 MHz, $CDCl_3$, TMS) δ_H 7.14 (2H, d, Ar*H*, *J* = 9.0 Hz), 7.03 (2H, d, Ar*H*, *J* = 9.0 Hz), 7.02 (6H, s, Ar*H*), 1.33 [27H, s, C(C*H*$_3$)$_3$]; ^{13}C{^{1}H} NMR (75.5 MHz, $CDCl_3$, TMS) δ_c 153.1, 152.5, 148.7,

142.6, 126.5, 117.9, 115.5, 111.4, 108.9, 38.7, 35.2, 31.4; Mass Spectrometry (ESI): $(M+Na)^+$ 701.4 ($C_{38}H_{37}F_3O_6SNa^+$).

2,6,10-tri-*tert*-butyl-12c-(4-boronic esterphenyl)-4,8,12-trioxa-4,8,12,12c-tetrahydrodibenzo[*cd,mn*]pyrene (3.51)

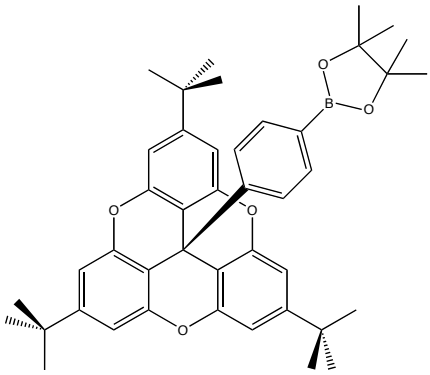

A 100 mL flask was charged with compound **3.47** (250 mg, 0.38 mmol), diboronic acid ($(Me_4C_2O_2)BB(O_2C_2Me_4)$) (120 mg, 0.42 mmol), KOAc (112 mg, 1.14 mmol), and palladium dichloride(dppf) (8 mg, 0.011 mmol) in 6 mL DMSO. Under a nitrogen atmosphere, the reaction mixture was heated to 75 °C and stirred at this temperature for 24 hours. The reaction mixture was allowed to cool to room temperature, and then diluted with methylene chloride. The mixture was transferred to a separatory funnel, washed twice with water, and dried over magnesium sulfate. The solvent mixture was evaporated under reduced pressure. The crude product was purified by column chromatography on silica (R_f = 0.2) with 2:1 hexane/dichloromethane as the eluent to yield 100 mg (40%) of a white powder. ^{1}H NMR (400 MHz, $CDCl_3$, TMS) δ_H 7.62 (2H, d, Ar*H, J* = 8.0 Hz), 7.08 (2H, d, Ar*H, J* = 8.0 Hz), 6.99 (6H, s, Ar*H*), 1.32 [27H, s, C(C*H*$_3$)$_3$], 1.24 (12H, s, C(C*H*$_3$)$_2$); ^{13}C{^{1}H} NMR (100.6 MHz, $CDCl_3$, TMS) δ_c 152.9, 152.6, 149.3, 135.3, 125.2, 111.6, 108.8, 83.6, 35.2, 32.4, 31.4, 24.7, 14.1. Mass Spectrometry (ESI): $(M+Na)^+$ 679.6 ($C_{43}H_{49}BO_5Na^+$).

2,6,10-tri-*tert*-butyl-12c-(4-trimethylstannanephenyl)-4,8,12-trioxa-4,8,12,12c-tetrahydrodibenzo[*cd,mn*]pyrene (3.52)

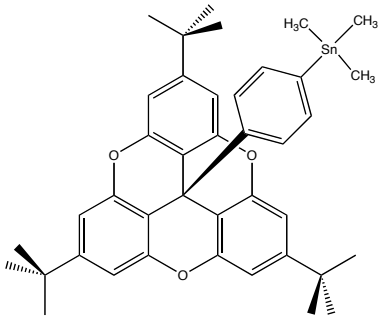

A 100 mL flask was charged with compound **3.46** (135 mg, 0.22 mmol), hexamethylditin ($Me_3SnSnMe_3$) (110 mg, 0.33 mmol), and palladium tetrakis(triphenylphosphine) (12 mg, 0.01 mmol) in 10 mL dry THF. Under a nitrogen atmosphere, the reaction mixture was heated to 75 °C and stirred at this temperature for 48 hours. The reaction mixture was allowed to cool to room temperature and the solvent was evaporated under reduced pressure leaving a brown solid. The crude product was purified by column chromatography on silica ($R_f = 0.4$) with hexane as the eluent to yield 60 mg (41%) of a white powder. ^{1}H NMR (300 MHz, $CDCl_3$, TMS) δ_H 7.32 (2H, d, Ar*H, J* = 8.0 Hz), 7.17 (2H, d, Ar*H, J* = 8.0 Hz), 7.00 (6H, s, Ar*H*), 1.32 [27H, s, C(C*H*$_3$)$_3$], 0.16 (9H, s, Sn(C*H*$_3$)$_3$); ^{13}C{^{1}H} NMR (100.6 MHz, $CDCl_3$, TMS) δ_c 152.9, 152.6, 149.7, 144.5, 136.1, 124.9, 111.6, 108.8, 35.2, 31.4, 24.7, -8.8. Mass Spectrometry (ESI): $(M+Na)^+$ 717.4.6 ($C_{40}H_{46}SnO_3Na^+$).

2,6,10-tri-*tert*-butyl-12c-(4-trimethylsilylethynylphenyl)-4,8,12-trioxa-4,8,12,12c-tetrahydrodibenzo[*cd,mn*]pyrene (4.9a)

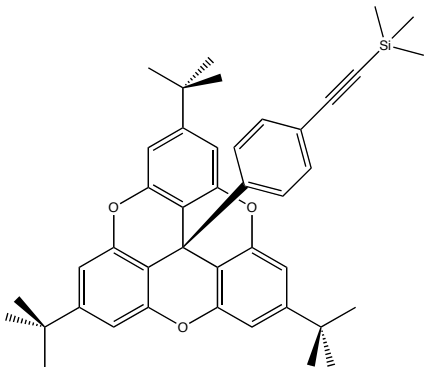

A solution of **3.47** (330 mg, 0.50 mmol), ethynyltrimethylsilane (0.08 mL, 0.55 mmol), copper iodide (8 mg, 0.04 mmol), and palladium tetrakis(triphenylphosphine) (23 mg, 0.02 mmol) in 10 mL triethylamine was heated in a sealed flask to 75 °C and stirred at this temperature for 18 hours. The reaction mixture was allowed to cool to room temperature, and then diluted with methylene chloride. The reaction mixture was transferred to a separatory funnel, washed twice with water, and dried over magnesium sulfate. The solvent was evaporated under reduced pressure. The desired product was purified by column chromatography on silica gel (R_f = 0.3) with hexane as the eluent to yield 325 mg (98%) of a white powder. ^{1}H NMR (400 MHz, $CDCl_3$) δ_H 7.24 (2H, d, Ar*H*, *J* = 8.0 Hz), 7.00 (2H, d, Ar*H*, *J* = 8.0 Hz), 7.00 (6H, s, Ar*H*), 1.33 [27H, s, C(C*H*$_3$)$_3$], 0.01 [9H, s, Si(C*H*$_3$)$_3$]; ^{13}C NMR (100.6 MHz, $CDCl_3$) δ_c 153.1, 152.6, 146.6, 132.4, 125.8, 121.9, 111.5, 109.0, 104.9, 94.3, 35.2, 31.4, 14.2, 0.00. Mass Spectrometry (ESI): M^+ 629.4 ($C_{42}H_{46}O_3Si^+$).

2,6,10-tri-*tert*-butyl-12c-(4-ethynylphenyl)-4,8,12-trioxa-4,8,12,12c-tetrahydrodibenzo[*cd,mn*]pyrene (4.9b)

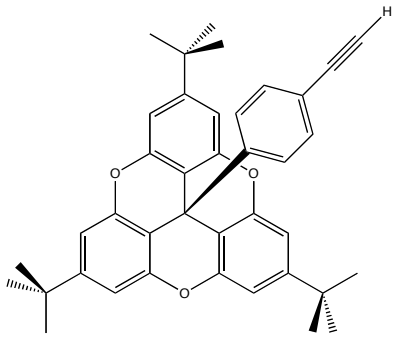

To a solution of **4.9a** (325 mg, 0.52 mmol) in 10 mL methanol / 20 mL THF was added potassium carbonate (440 mg, 2.6 mmol) and the mixture was stirred at room temperature for 12 hours. Diethyl ether was added to the reaction mixture, which was then transferred to a separatory funnel. The organic phase was washed twice with water, and then dried over magnesium sulfate. The solvent was evaporated under reduced pressure. The desired product was purified by column chromatography on silica gel (R_f = 0.3) with 9:1 hexane/dichloromethane as the eluent to yield 270 mg (94%) of a white powder. ^{1}H NMR (400 MHz, $CDCl_3$, TMS) δ_H 7.22 (2H, d, Ar*H*, *J* = 8.0 Hz), 6.97 (2H, d, Ar*H*, *J* = 8.0 Hz), 6.94 (6H, s, Ar*H*), 2.87 (1H, s, CC*H*), 1.25 [27H, s, C(CH_3)$_3$]; ^{13}C NMR (100.6 MHz, $CDCl_3$, TMS) δ_c 153.6, 153.1, 147.5, 133.1, 126.4, 121.3, 111.9, 109.4, 83.9, 68.5, 35.7, 31.9, 26.1. Mass Spectrometry (ESI): $(M+Na)^+$ 577.3 ($C_{39}H_{38}O_3Na^+$).

Bis[2,6,10-tri-*tert*-butyl-4,8,12-trioxa-4,8,12,12c-tetrahydrodibenzo[*cd,mn*]pyrene] ethynylene (4.1)

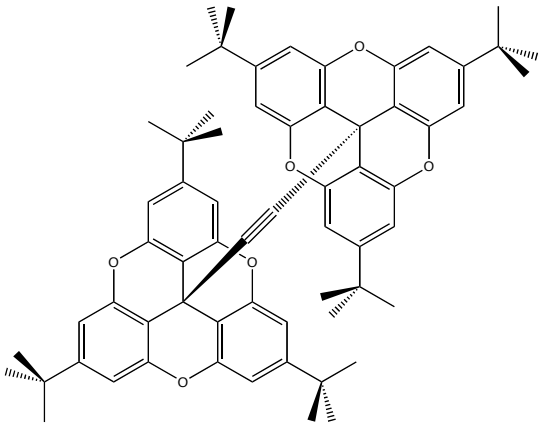

An oven dried 100 mL flask under nitrogen atmosphere and Teflon stir bar was charged with **3.43** (510mg, 1.07 mmol) and dissolved in 10 mL dry THF. After cooling to – 78 °C, Bu^{n}Li (0.45 mL, 1.07 mmol) was added drop wise. The solution was allowed to stir for 45 minutes. A second oven dried 100 mL flask under nitrogen atmosphere and Teflon stir bar was charged with the trioxatriangulene cation **3.32** (640 mg, 1.07 mmol) and dissolved in 10 mL dry THF and cooled to – 78 °C. The cation **3.32** solution was then transferred with a stainless steel cannula to the first flask and allowed to stir for 45 minutes. Afterwards, the solution was allowed to warm to 0 °C and quenched with saturated aqueous NH_4Cl solution. The organic and aqueous phases were separated and the aqueous phase washed three times with Et_2O. The combined organic phase was dried ($MgSO_4$) and the solvent removed by rotary evaporation. The desired product was purified by column chromatography on silica gel (R_f = 0.4) with 9:1 hexane/dichloromethane as the eluent to yield 750 mg (75%) of a white solid: mp > 350 °C; ^{1}H NMR(400 MHz, $CDCl_3$, TMS) δ_H 6.85 (6H, s, Ar*H*), 1.28 [27H, s, C(C*H*$_3$)$_3$]; ^{13}C{^{1}H} NMR (100.6 MHz, $CDCl_3$, TMS) δ_c 152.9, 152.1, 108.6, 108.5, 85.4, 35.1, 31.3, 22.0; Mass Spectrometry (ESI): $(M+Na)^+$ 953.6 ($C_{64}H_{66}O_6Na^+$). UV-Vis (CH_3CH_2OH): λ_{max}, nm (log ε): 284 (3.93). λ_{em}: 311 nm.

1,4-bis[2,6,10-tri-*tert*-butyl-4,8,12-trioxa-4,8,12,12c-tetrahydrodibenzo[*cd,mn*]pyrene] phenylene (4.2)

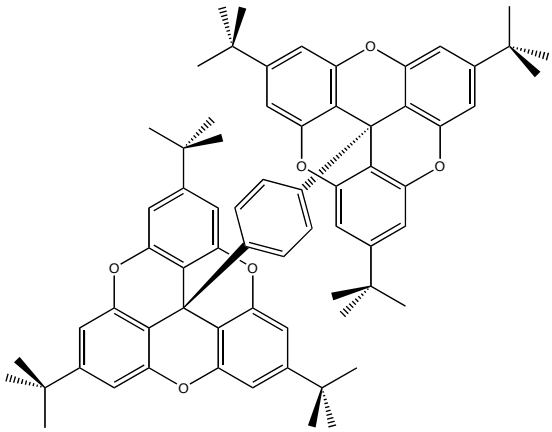

An oven dried 100 mL flask with a tefon stir bar and nitrogen atmosphere was charged with 1,4-diiodobenzene (138 mg, 0.42 mmol) and dissolved in 8 mL dry THF. After cooling to – 78 °C, Bu^tLi (1.1 mL, 1.68 mmol) was added drop wise. The solution was allowed to stir for 45 minutes. A second oven dried 100 mL flask under nitrogen atmosphere and Teflon stir bar was charged with the trioxatriangulene cation **3.32** (500 mg, 0.84 mmol) and dissolved in 10 mL dry THF and cooled to – 78 °C. The cation **3.32** solution was then transferred with a stainless steel cannula to the first flask and allowed to stir for 45 minutes. Afterwards, the solution was allowed to warm to 0 °C and quenched with saturated aqueous NH_4Cl solution. The organic and aqueous phases were separated and the aqueous phase washed three times with Et_2O. The combined organic phase was dried ($MgSO_4$) and the solvent removed by rotary evaporation. The desired product was purified by column chromatography on silica gel (R_f = 0.5) with 9:1 hexane/dichloromethane to yield 110 mg (26%) of a white solid: mp > 350 °C; ^{1}H NMR (400 MHz, $CDCl_3$, TMS) δ_H 6.92 (6H, s, Ar*H*), 6.87 (4H, s, Ar*H*), 1.28 [27H, s, C(C*H*$_3$)$_3$]; $^{13}C\{^1H\}$ NMR (100.6 MHz, $CDCl_3$, TMS) δ_c 153.6, 152.5, 126.3, 111.8, 108.9, 35.1, 31.3, 22.7, 14.1; Mass Spectrometry (ESI):

$(M+Na)^+$ 1005.7 ($C_{68}H_{70}O_6^+$). UV-Vis (CH_3CH_2OH): λ_{max}, nm (log ε): 284 (3.93). λ_{em}: 310 nm.

Bis[2,6,10-tri-*tert*-butyl-4,8,12-trioxa-4,8,12,12c-tetrahydrodibenzo[*cd,mn*]pyrene] diethynylene (4.3)

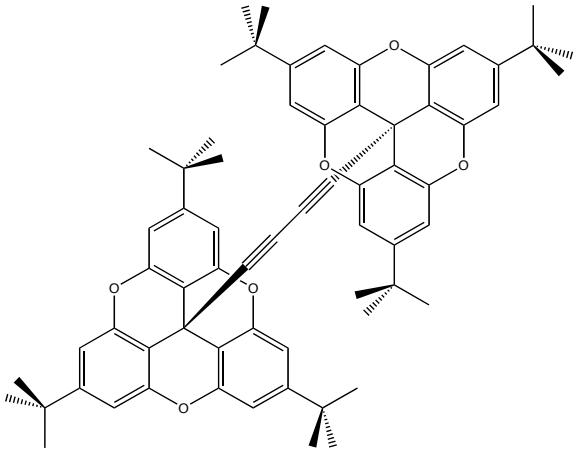

A solution of **3.43** (300 mg, 0.63 mmol) and copper acetate monohydrate (1250 mg, 6.3 mmol) in ethanol (100 mL) was heated to reflux. The reaction mixture was stirred at this temperature for 48 hours, then allowed to cool and diluted with methylene chloride. The mixture was transferred into a separatory funnel and washed twice with water, then dried over magnesium sulfate. Solvent was evaporated under reduced pressure. The desired product was purified by column chromatography on silica gel (R_f = 0.5) with 9:1 methylene chloride: hexanes as the eluent to yield 45 mg (16%) of a white solid: mp > 350 °C; ^{1}H NMR (400 MHz, $CDCl_3$, TMS) δ_H 6.92 (6H, s, Ar*H*), 1.28 [27H, s, C(C*H*$_3$)$_3$]; ^{13}C{^{1}H} NMR (100.6 MHz, $CDCl_3$, TMS) δ_C 152.9, 152.1, 108.6, 108.5, 81.0, 63.8, 35.2, 31.3, 21.8; Mass Spectrometry (ESI): $(M+Na)^+$ 977.6 ($C_{66}H_{66}O_6Na^+$). UV-Vis (CH_3CH_2OH): λ_{max}, nm (log ε): 289 (4.03). λ_{em}: 311 nm.

1,4-Bis[2,6,10-tri-*tert*-butyl-4,8,12-trioxa-4,8,12,12c-tetrahydrodibenzo[*cd,mn*]pyrene] ethynylphenylene (4.4)

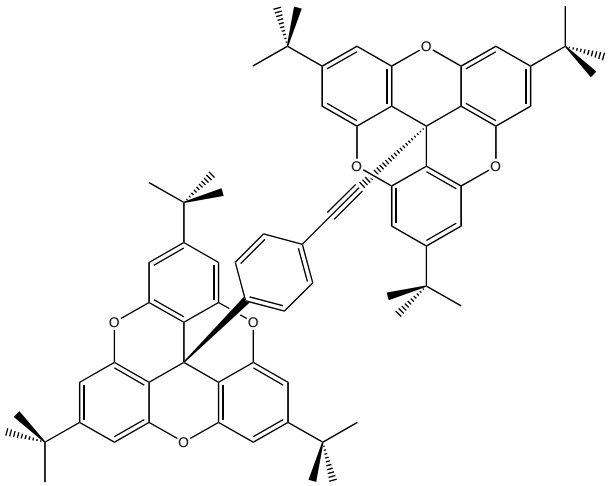

A solution of **3.47** (154 mg, 0.23 mmol), **3.43** (110 mg 0.23 mmol), copper iodide (4 mg, 0.018 mmol), and palladium tetrakis(triphenylphosphine) (11 mg, 0.009 mmol) in 10 mL triethylamine was heated to 80 °C and stirred at this temperature for 48 hours. The reaction mixture was allowed to cool to room temperature, then diluted with dichloromethane. The mixture was transferred to a separatory funnel, washed twice with water, and then dried over magnesium sulfate. Solvent was evaporated under reduced pressure. The desired product was purified by column chromatography on silica gel (R_f = 0.2) on silica with hexane as the eluent to yield 226 mg (98%) of a white solid: mp > 350 °C; ^{1}H NMR (400 MHz, $CDCl_3$, TMS) δ_H 7.04 (2H, d, Ar*H*, *J* = 8.0 Hz), 6.86 (2H, d, Ar*H*, *J* = 8.0 Hz), 6.96 (6H, s, Ar*H*), 6.94 (6H, s, Ar*H*), 1.30 [27H, s, C(C*H*$_3$)$_3$], 1.29 [27H, s, C(C*H*$_3$)$_3$]; ^{13}C NMR (75.5 MHz, $CDCl_3$, TMS) δ_c 153.1, 152.9, 152.4, 152.2, 132.1, 125.5, 121.3, 111.3, 109.0, 108.9, 108.8, 108.7, 90.9, 83.5, 35.2, 35.1, 31.3, 31.2, 22.7, 14.1; Mass Spectrometry (ESI): $(M+Na)^+$ 1029.7 ($C_{70}H_{70}O_6Na^+$). UV-Vis (CH_3CH_2OH): λ_{max}, nm (log ε): 267 (4.59). λ_{em}: 318 nm.

4,4'-Bis[2,6,10-tri-*tert*-butyl-4,8,12-trioxa-4,8,12,12c-tetrahydrodibenzo[*cd,mn*]pyrene] biphenylene (4.5)

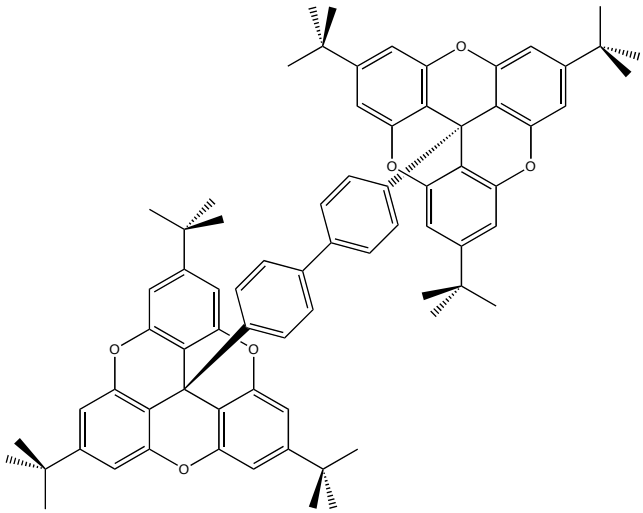

An oven dried 100 mL flask with a tefon stir bar and under nitrogen was charged with 4,4'-diiodobiphenyl (80 mg, 0.17 mmol) and dissolved in 5 mL dry THF. After cooling to – 78 °C, Bu^nLi (0.14 mL, 0.34 mmol) was added drop wise. The solution was allowed to stir for 45 minutes. A second oven dried 100 mL flask under nitrogen atmosphere and Teflon stir bar was charged with the trioxatriangulene cation **3.32** (200 mg, 0.33 mmol) and dissolved in 5 mL dry THF and cooled to – 78 °C. The cation **3.32** solution was then transferred with a stainless steel cannula to the first flask and allowed to stir for 45 minutes. Afterwards, the solution was allowed to warm to 0 °C and quenched with saturated aqueous NH_4Cl solution. The organic and aqueous phases were separated and the aqueous phase washed three times with Et_2O. The combined organic phase was dried ($MgSO_4$) and the solvent removed by rotary evaporation. The desired product was purified by column chromatography on silica gel (R_f = 0.1) with hexane as the eluent to yield 135 mg (75%) of a white solid: mp > 350 °C; ^{1}H NMR (400 MHz, $CDCl_3$, TMS) δ_H 7.23 (2H, d, Ar*H*, *J* = 8.0 Hz), 7.05 (2H, d, Ar*H*, *J* = 8.0 Hz), 7.00 (6H, s, Ar*H*), 1.31 [27H, s, C(CH_3)$_3$]; ^{13}C NMR (100.6 MHz, $CDCl_3$, TMS) δ_c 152.8, 152.6, 145.1, 139.3, 127.4, 126.2, 111.9, 108.9, 35.2,

31.4, 14.1; Mass Spectrometry (ESI): $(M+Na)^+$ 1081.6 ($C_{74}H_{74}O_6Na^+$). UV-Vis (CH_3CH_2OH): λ_{max}, nm (log ε): 268 (4.39). λ_{em}: 320 nm.

1,4-Bis[2,6,10-tri-*tert*-butyl-12c-Ethynyl-4,8,12-trioxa-4,8,12,12c-tetrahydrodibenzo[*cd,mn*]pyrene] phenylene (4.6)

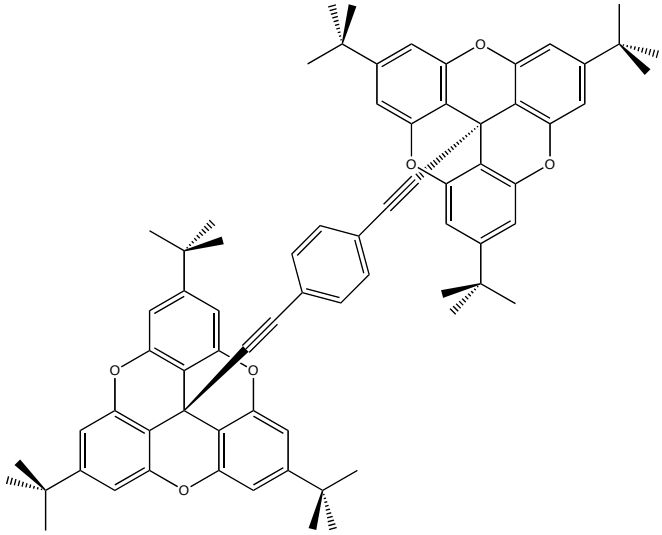

A solution of 1,4-diiodobenzene (69 mg, 0.20 mmol), **3.43** (200 mg 0.42 mmol), copper iodide (6 mg, 0.029 mmol), and palladium tetrakis(triphenylphosphine) (40 mg, 0.060 mmol) in 5 mL triethylamine was heated to 80 °C and stirred at this temperature for 48 hours. The reaction mixture was allowed to cool to room temperature, and then diluted with dichloromethane. The mixture was transferred to a separatory funnel, washed twice with water, and dried over magnesium sulfate. The solvent was evaporated under reduced pressure. The desired product was purified by column chromatography on silica gel (R_f = 0.5) with 8:2 hexane/dichloromethane as the eluent to yield 160 mg (78%) of a white solid: mp > 350 °C; ^{1}H NMR (400 MHz, $CDCl_3$, TMS) δ_H 7.07 (4H, s, Ar*H*), 6.99 (6H, s, Ar*H*), 1.32 [27H, s, C(C*H*$_3$)$_3$]; ^{13}C NMR (75.5 MHz, $CDCl_3$, TMS) δ_c 153.3, 152.3, 131.4, 122.4, 109.1, 108.7, 91.9, 83.1, 35.2, 31.3, 22.4; Mass Spectrometry (ESI): $(M+Na)^+$

1053.6 ($C_{72}H_{70}O_6Na^+$). UV-Vis (CH_3CH_2OH): λ_{max}, nm (log ε): 299 (4.84). λ_{em}: 334 nm.

Bis[2,6,10-tri-*tert*-butyl-12c-(4-Phenylene)-4,8,12-trioxa-4,8,12,12c-tetrahydrodibenzo[*cd,mn*]pyrene] ethynylene (4.7)

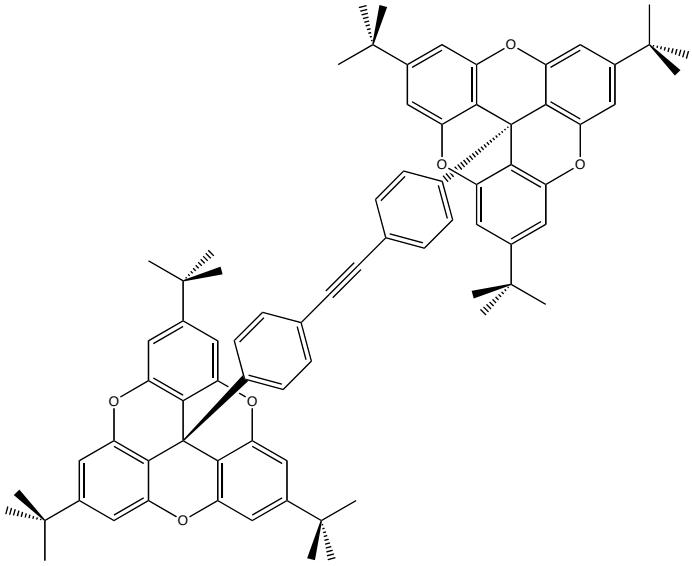

A solution of **3.47** (92 mg, 0.14 mmol), **4.9b** (80 mg 0.14 mmol), copper iodide (3 mg, 0.012 mmol), and palladium tetrakis(triphenylphosphine) (7 mg, 0.006 mmol) in 7 mL triethylamine was heated to 80 °C and stirred at this temperature for 48 hours. The reaction mixture was allowed to cool to room temperature, and then diluted with dichloromethane. The reaction mixture was transferred to a separatory funnel, washed twice with water, and dried over magnesium sulfate. The solvent was evaporated under reduced pressure. The desired product was purified by column chromatography on silica gel (R_f = 0.2) with 9:1 hexane/dichloromethane as the eluent to yield 50 mg (33%) of a white solid: mp > 350 °C; ^{1}H NMR (400 MHz, $CDCl_3$, TMS) δ_H 7.23 (4H, d, Ar*H*, *J* = 8.0 Hz), 7.01 (4H, d, Ar*H*, *J* = 8.0 Hz), 6.99 (6H, s, Ar*H*), 1.32 [27H, s, C(C*H*$_3$)$_3$]; ^{13}C NMR (100.6 MHz, $CDCl_3$, TMS) δ_c 153.0, 152.5, 146.3, 132.0, 125.8, 121.9, 111.4, 108.9, 89.1, 35.2, 31.4, No quaternary

carbon observed; Mass Spectrometry (ESI): $(M+Na)^+$ 1105.8 ($C_{76}H_{74}O_6Na^+$). UV-Vis (CH_3CH_2OH): λ_{max}, nm (log ε): 298 (4.67). λ_{em}: 320 nm.

1,4-Bis[2,6,10-tri-*tert*-butyl-4,8,12-trioxa-4,8,12,12c-tetrahydrodibenzo[*cd,mn*]pyrene] terphenylene (4.8)

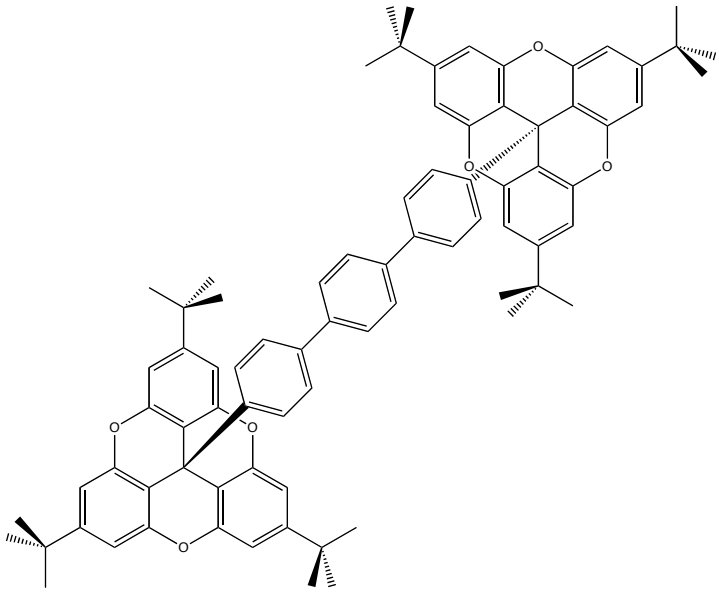

A solution of 1,4-diiodobenzene (25 mg, 0.076 mmol), **3.51** (100 mg 0.15 mmol), 4 mL 2M aqueous Na_2CO_3, and palladium tetrakis(triphenylphosphine) (18 mg, 0.015 mmol) in 6 mL toluene was heated to 80 °C and stirred at this temperature for 48 hours. The reaction mixture was allowed to cool to room temperature, and then diluted with dichloromethane. The mixture was transferred to a separatory funnel, washed twice with water, and dried over magnesium sulfate. The solvent was evaporated under reduced pressure. The desired product was purified by column chromatography on silica gel (R_f = 0.6) with 8:2 hexane/dichloromethane as the eluent to yield 40 mg (46%) of a white solid: mp > 350 °C; ^{1}H NMR (400 MHz, $CDCl_3$, TMS) δ_H 7.42 (4H, s, Ar*H*), 7.38 (4H, d, Ar*H*, *J* = 8.0 Hz), 7.13 (4H, d, Ar*H*, *J* = 8.0 Hz), 7.01 (6H, s, Ar*H*), 1.33 [27H, s, C(C*H*$_3$)$_3$] ; ^{13}C NMR (100.6 MHz, $CDCl_3$, TMS) δ_c 152.9, 152.6, 128.7, 127.5, 127.4, 127.2, 127.0, 126.3, 111.8, 109.0,

35.2, 31.4, 14.1; Mass Spectrometry (ESI): $(M+Na)^+$ 1158.6 ($C_{80}H_{78}O_6Na^+$). UV-Vis (CH_3CH_2OH): λ_{max}, nm (log ε): 287 (4.61). λ_{em}: 354 nm.

Table 4.12 Crystallographic Data for **3.32**

Crystallised from	CH_2Cl_2
Empirical formula	$C_{31.5}H_{34}ClF_6O_3P$
Formula weight [g mol^{-1}]	641.03
Crystal colour, habit	orange, prism
Crystal dimensions [mm]	0.08 × 0.10 × 0.20
Temperature [K]	160(1)
Crystal system	monoclinic
Space group	$P2_1/c$ (#14)
Z	8
Reflections for cell determination	76104
2θ range for cell determination [°]	4 – 52
Unit cell parameters a [Å]	17.9017(3)
b [Å]	18.7130(3)
c [Å]	17.9089(2)
α [°]	90
β [°]	92.349(1)
γ [°]	90
V [Å^3]	5994.3(2)
$F(000)$	2664
D_x [g cm^{-3}]	1.420
μ(Mo $K\alpha$) [mm^{-1}]	0.250
Scan type	ω
$2\theta_{(max)}$ [°]	52
Total reflections measured	63464
Symmetry independent reflections	11772
R_{int}	0.076
Reflections with $I > 2\sigma(I)$	7510
Reflections used in refinement	11772
Parameters refined	784
Final $R(F)$ [$I > 2\sigma(I)$ reflections]	0.0680
$wR(F^2)$ (all data)	0.2149
Weights: $w = [\sigma^2(F_o^2) + (0.1159P)^2 + 5.3545P]^{-1}$ where $P = (F_o^2 + 2F_c^2)/3$	
Goodness of fit	1.024
Final Δ_{max}/σ	0.001
$\Delta\rho$ (max; min) [e Å^{-3}]	0.67; -1.19
$\sigma(d_{(C-C)})$ [Å]	0.004 – 0.006

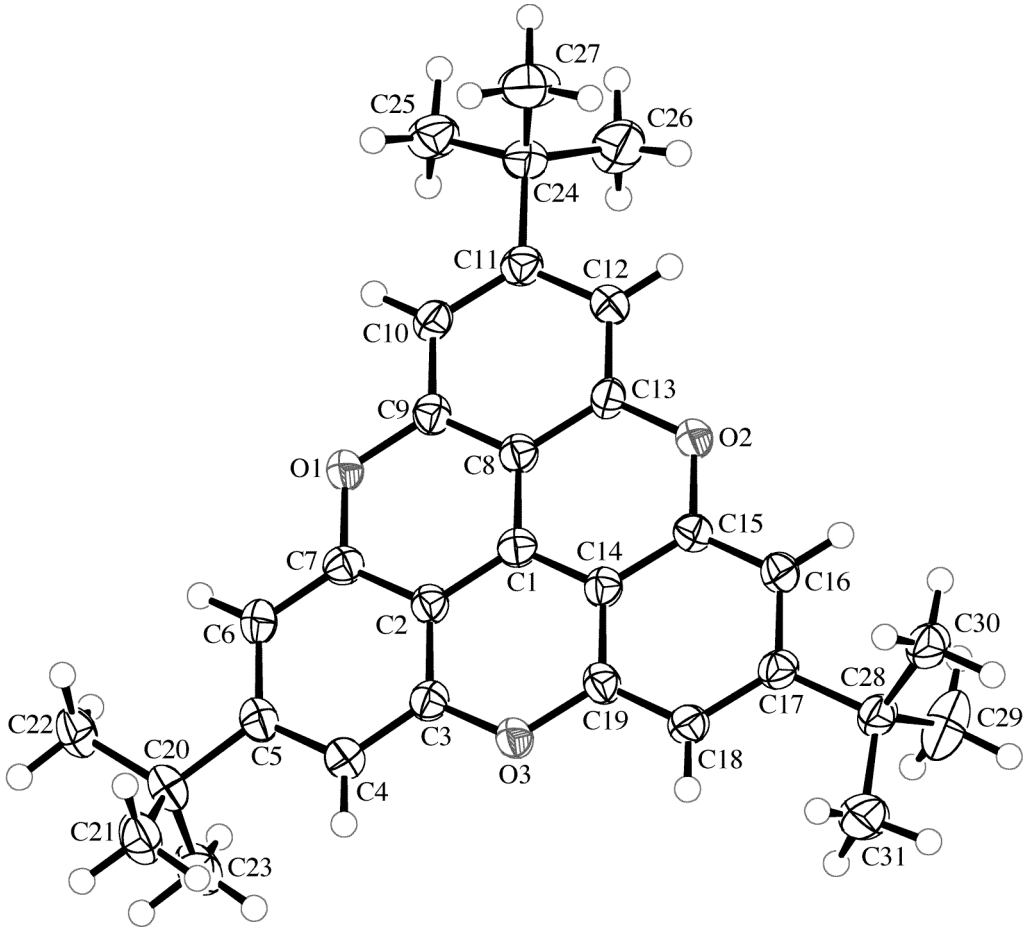
C27
C25
C26
C24
C11
C12
C10
C13
C9
O2
O1
C8
C15
C7
C14
C16
C1
C6
C2
C30
C28
C22
C20
C5
C3
C19
C17
C29
C18
O3
C4
C21
C23
C31

Table 4.13 Crystallographic Data for **3.40**

Crystallised from	EtOAc
Empirical formula	$C_{31}H_{34}O_3$
Formula weight [g mol^{-1}]	454.61
Crystal colour, habit	colourless, prism
Crystal dimensions [mm]	0.22 × 0.25 × 0.32
Temperature [K]	160(1)
Crystal system	cubic
Space group	$I\bar{4}3d$ (#220)
Z	16
Reflections for cell determination	1442
2θ range for cell determination [°]	4 – 60
Unit cell parameters a [Å]	21.5432(4)
b [Å]	21.5432(4)
c [Å]	21.5432(4)
α [°]	90
β [°]	90
γ [°]	90
V [Å^3]	9998.4(3)
F(000)	3904
D_x [g cm^{-3}]	1.208
μ(Mo $K\alpha$) [mm^{-1}]	0.0759
Scan type	ϕ and ω
$2\theta_{(max)}$ [°]	60
Total reflections measured	29471
Symmetry independent reflections	1314
R_{int}	0.085
Reflections with $I > 2\sigma(I)$	1046
Reflections used in refinement	1314
Parameters refined; restraints	138; 36
Final $R(F)$ [$I > 2\sigma(I)$ reflections]	0.0503
$wR(F^2)$ (all data)	0.1265
Weights: $w = [\sigma^2(F_o^2) + (0.068P)^2 + 0.3776P]^{-1}$ where $P = (F_o^2 + 2F_c^2)/3$	
Goodness of fit	1.057
Final Δ_{max}/σ	0.001
$\Delta\rho$ (max; min) [e Å^{-3}]	0.19; -0.19
$\sigma(d_{(C-C)})$ [Å]	0.002 – 0.006

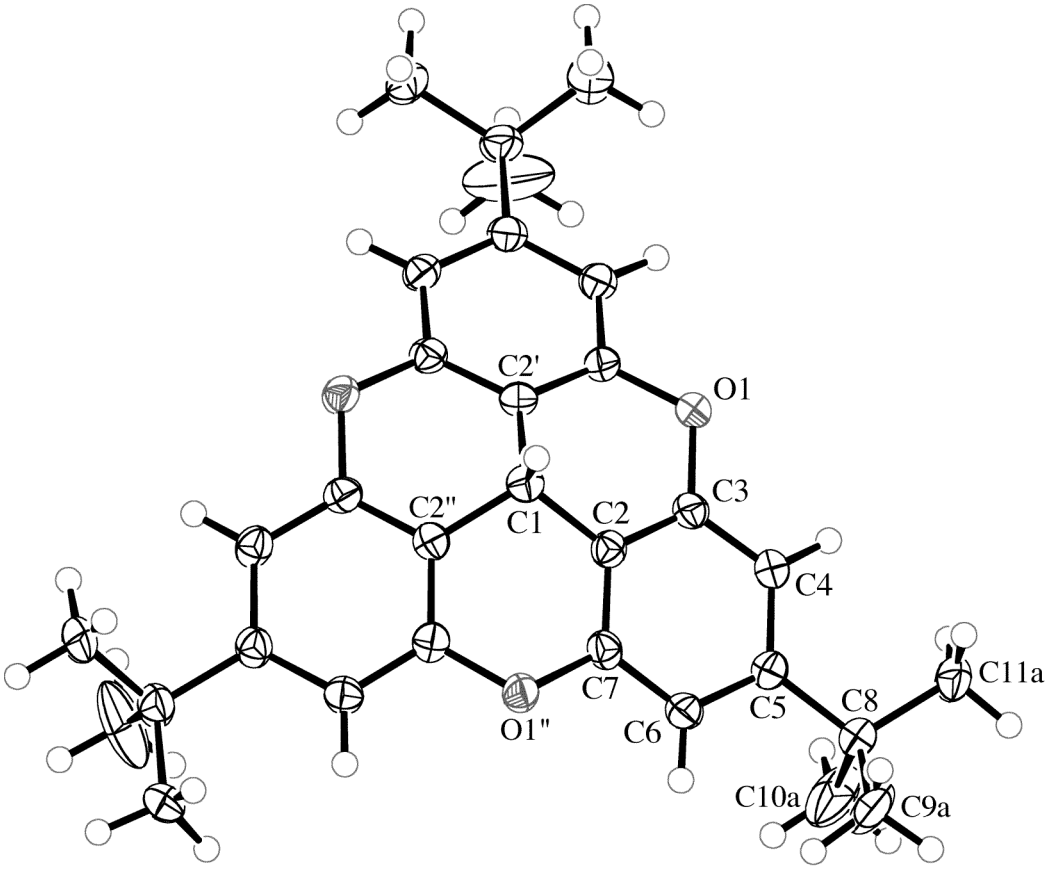
C2'
O1
C2"
C1
C2
C3
C4
C7
C5
C8
C11a
O1"
C6
C10a
C9a

Table 4.14 Crystallographic Data for **3.41**

Crystallised from	CH_2Cl_2 / hexane
Empirical formula	$C_{32}H_{36}O_3$
Formula weight [g mol^{-1}]	468.63
Crystal colour, habit	colourless, prism
Crystal dimensions [mm]	0.15 × 0.15 × 0.32
Temperature [K]	160(1)
Crystal system	orthorhombic
Space group	*Pnma* (#62)
Z	4
Reflections for cell determination	2643
2θ range for cell determination [°]	4 – 50
Unit cell parameters a [Å]	12.5333(6)
b [Å]	17.2238(9)
c [Å]	12.1265(5)
α [°]	90
β [°]	90
γ [°]	90
V [Å^3]	2617.8(2)
F(000)	1008
D_x [g cm^{-3}]	1.189
μ(Mo $K\alpha$) [mm^{-1}]	0.0745
Scan type	ω
$2\theta_{(max)}$ [°]	50
Total reflections measured	25620
Symmetry independent reflections	2398
R_{int}	0.106
Reflections with $I > 2\sigma(I)$	1590
Reflections used in refinement	2396
Parameters refined; restraints	205; 48
Final $R(F)$ [$I > 2\sigma(I)$ reflections]	0.0608
$wR(F^2)$ (all data)	0.1616
Weights: $w = [\sigma^2(F_o^2) + (0.0806P)^2 + 0.213P]^{-1}$ where $P = (F_o^2 + 2F_c^2)/3$	
Goodness of fit	1.070
Secondary extinction coefficient	0.031(3)
Final Δ_{max}/σ	0.001
$\Delta\rho$ (max; min) [e Å^{-3}]	0.41; -0.25
$\sigma(d_{(C-C)})$ [Å]	0.003 – 0.004

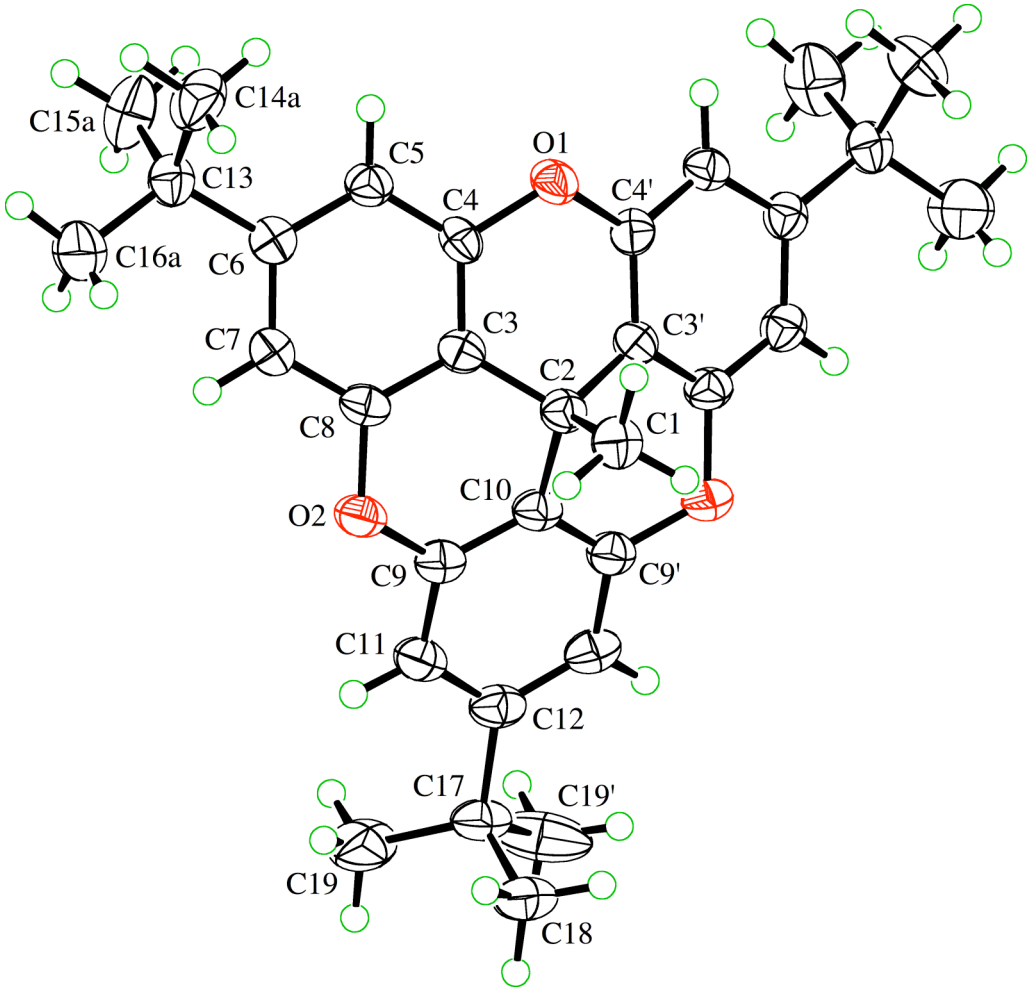
C14a
C15a
C13
C5
O1
C4
C4'
C16a
C6
C3
C3'
C7
C2
C8
C1
C10
O2
C9
C9'
C11
C12
C17
C19'
C19
C18

Table 4.15 Crystallographic Data for **3.44**

Crystallised from	hexane
Empirical formula	$C_{39}H_{38}O_3$
Formula weight [g mol^{-1}]	554.73
Crystal colour, habit	colourless, prism
Crystal dimensions [mm]	0.15 × 0.25 × 0.28
Temperature [K]	160(1)
Crystal system	monoclinic
Space group	$P2_1/n$ (#14)
Z	4
Reflections for cell determination	9231
2θ range for cell determination [°]	4 – 60
Unit cell parameters a [Å]	14.1508(3)
b [Å]	14.4737(4)
c [Å]	14.9128(3)
α [°]	90
β [°]	90.974(1)
γ [°]	90
V [Å^3]	3053.9(1)
F(000)	1184
D_x [g cm^{-3}]	1.206
μ(Mo $K\alpha$) [mm^{-1}]	0.0745
Scan type	ϕ and ω
$2\theta_{(max)}$ [°]	60
Total reflections measured	80120
Symmetry independent reflections	8917
R_{int}	0.109
Reflections with $I > 2\sigma(I)$	4806
Reflections used in refinement	8917
Parameters refined	389
Final $R(F)$ [$I > 2\sigma(I)$ reflections]	0.0606
$wR(F^2)$ (all data)	0.1658
Weights: $w = [\sigma^2(F_o^2) + (0.0777P)^2]^{-1}$ where $P = (F_o^2 + 2F_c^2)/3$	
Goodness of fit	1.014
Secondary extinction coefficient	0.036(2)
Final Δ_{max}/σ	0.001
$\Delta\rho$ (max; min) [e Å^{-3}]	0.35; -0.28
$\sigma(d_{(C-C)})$ [Å]	0.002 – 0.003

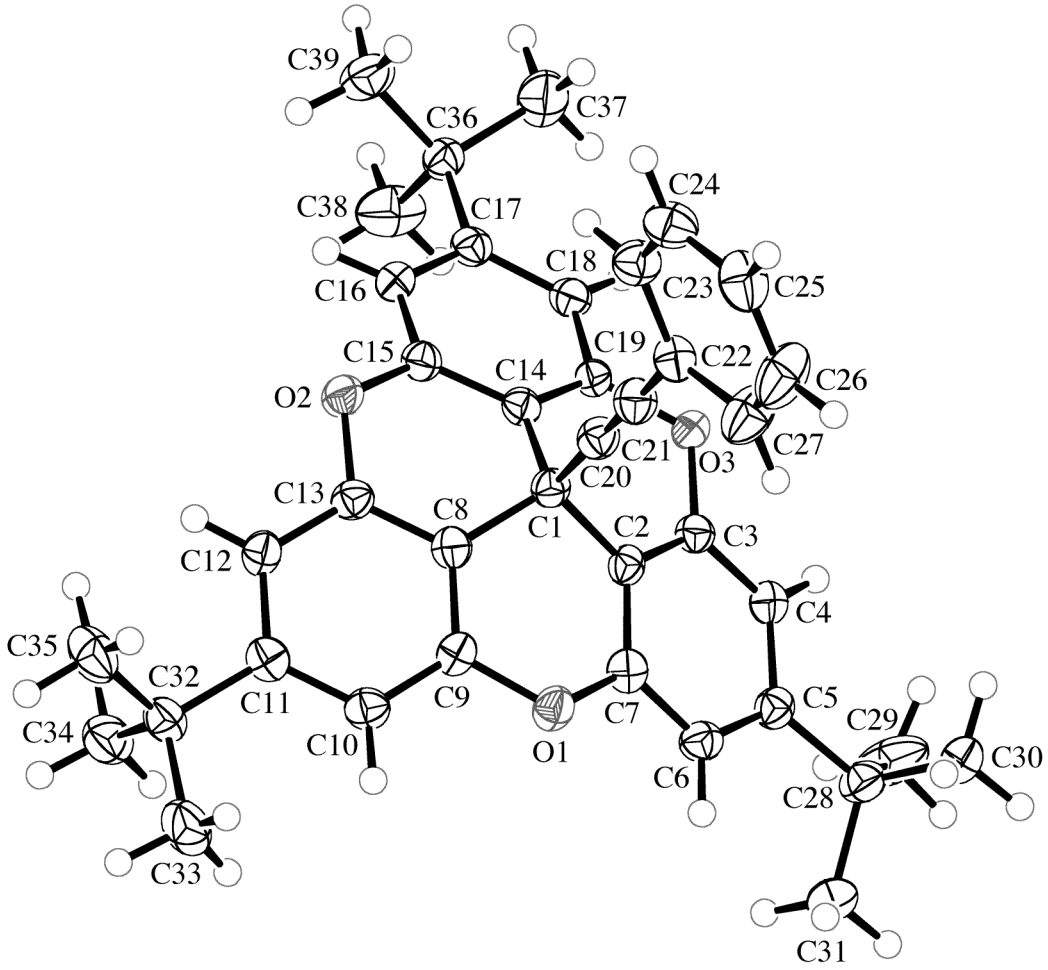
C39
C36
C37
C38
C17
C24
C18
C16
C23
C25
C15
C19
C22
C26
C14
O2
C21
C27
O3
C20
C13
C8
C1
C2
C3
C12
C4
C35
C32
C11
C9
C7
C5
C29
C34
C10
O1
C6
C30
C28
C33
C31

Table 4.16 Crystallographic Data for **3.45**

Crystallised from	hexane / EtOAc
Empirical formula	$C_{38}H_{37}NO_3$
Formula weight [g mol^{-1}]	555.71
Crystal colour, habit	yellow, plate
Crystal dimensions [mm]	0.08 × 0.15 × 0.23
Temperature [K]	160(1)
Crystal system	monoclinic
Space group	$P2_1/n$ (#14)
Z	4
Reflections for cell determination	5504
2θ range for cell determination [°]	4 – 50
Unit cell parameters a [Å]	14.1297(1)
b [Å]	14.4666(2)
c [Å]	14.8410(1)
α [°]	90
β [°]	90.4463(6)
γ [°]	90
V [Å^3]	3033.54(5)
$F(000)$	1184
D_x [g cm^{-3}]	1.217
μ(Mo $K\alpha$) [mm^{-1}]	0.0760
Scan type	ω
$2\theta_{(max)}$ [°]	50
Total reflections measured	39968
Symmetry independent reflections	5318
R_{int}	0.058
Reflections with $I > 2\sigma(I)$	4461
Reflections used in refinement	5316
Parameters refined	389
Final $R(F)$ [$I > 2\sigma(I)$ reflections]	0.0492
$wR(F^2)$ (all data)	0.1293
Weights: $w = [\sigma^2(F_o^2) + (0.0579P)^2 + 1.3274P]^{-1}$ where $P = (F_o^2 + 2F_c^2)/3$	
Goodness of fit	1.071
Secondary extinction coefficient	0.059(3)
Final Δ_{max}/σ	0.001
$\Delta\rho$ (max; min) [e Å^{-3}]	0.45; -0.27
$\sigma(d_{(C-C)})$ [Å]	0.002 – 0.003

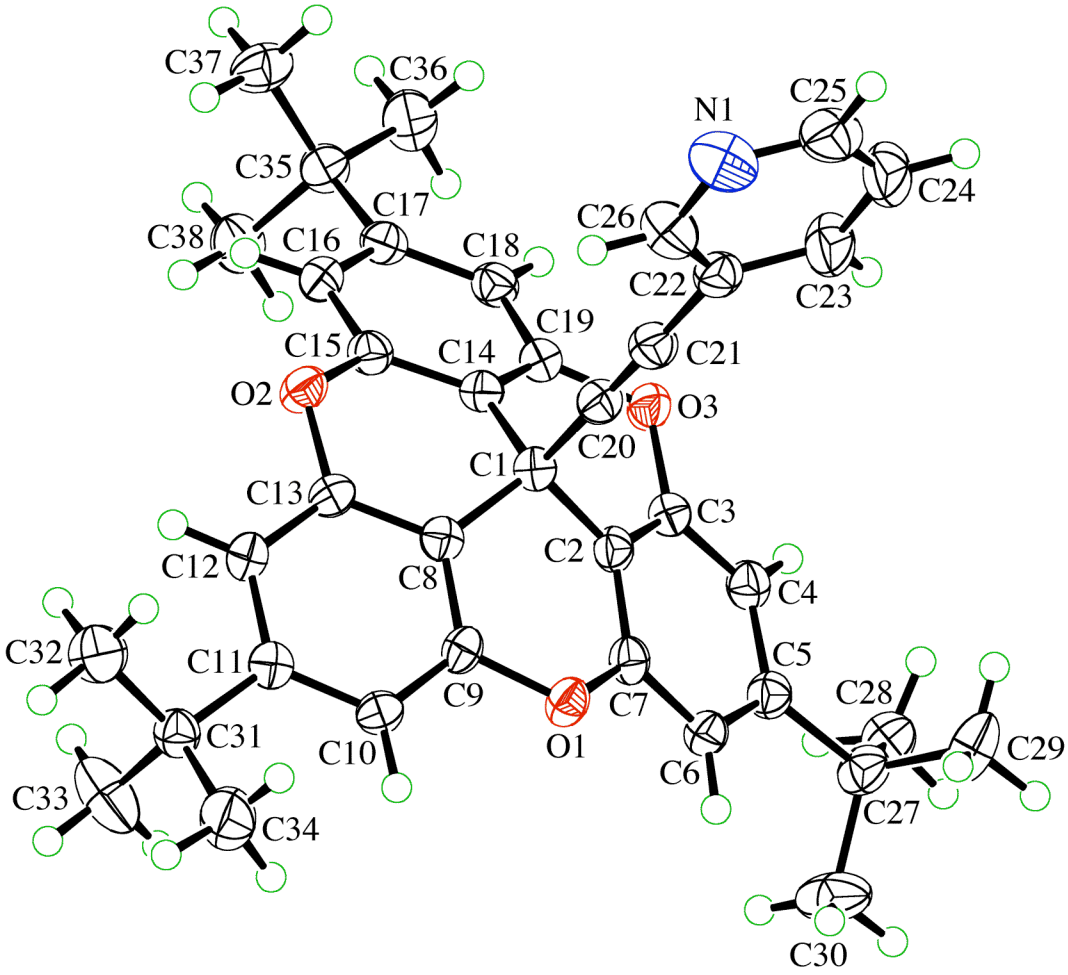
C37
C36
C35
C17
C38
C16
C18
C19
C15
C14
C21
O2
O3
C20
C1
C13
C3
C12
C8
C2
C4
C32
C11
C9
C7
C5
C28
C31
C10
O1
C6
C29
C33
C34
C27
C30
N1
C25
C24
C26
C22
C23

Table 4.17 Crystallographic Data for **4.2**

Crystallised from	CH_2Cl_2
Empirical formula	$C_{68}H_{78}O_{10}$
Formula weight [g mol^{-1}]	1055.35
Crystal colour, habit	orange, prism
Crystal dimensions [mm]	0.15 × 0.17 × 0.25
Temperature [K]	160(1)
Crystal system	cubic
Space group	$Pa\bar{3}$ (#205)
Z	4
Reflections for cell determination	1856
2θ range for cell determination [°]	4 – 50
Unit cell parameters a [Å]	17.8302(9)
b [Å]	17.8302(9)
c [Å]	17.8302(9)
α [°]	90
β [°]	90
γ [°]	90
V [Å^3]	5668.5(5)
F(000)	2264
D_x [g cm^{-3}]	1.237
μ(Mo $K\alpha$) [mm^{-1}]	0.0814
Scan type	ω
$2\theta_{(max)}$ [°]	50
Total reflections measured	18143
Symmetry independent reflections	1676
R_{int}	0.113
Reflections with $I > 2\sigma(I)$	1032
Reflections used in refinement	1676
Parameters refined; restraints	176; 78
Final $R(F)$ [$I > 2\sigma(I)$ reflections]	0.1028
$wR(F^2)$ (all data)	0.3320
Weights: $w = [\sigma^2(F_o^2) + (0.1638P)^2 + 9.0606P]^{-1}$ where $P = (F_o^2 + 2F_c^2)/3$	
Goodness of fit	1.098
Final Δ_{max}/σ	0.001
$\Delta\rho$ (max; min) [e Å^{-3}]	0.73; -0.32
$\sigma(d_{(C-C)})$ [Å]	0.005 – 0.002

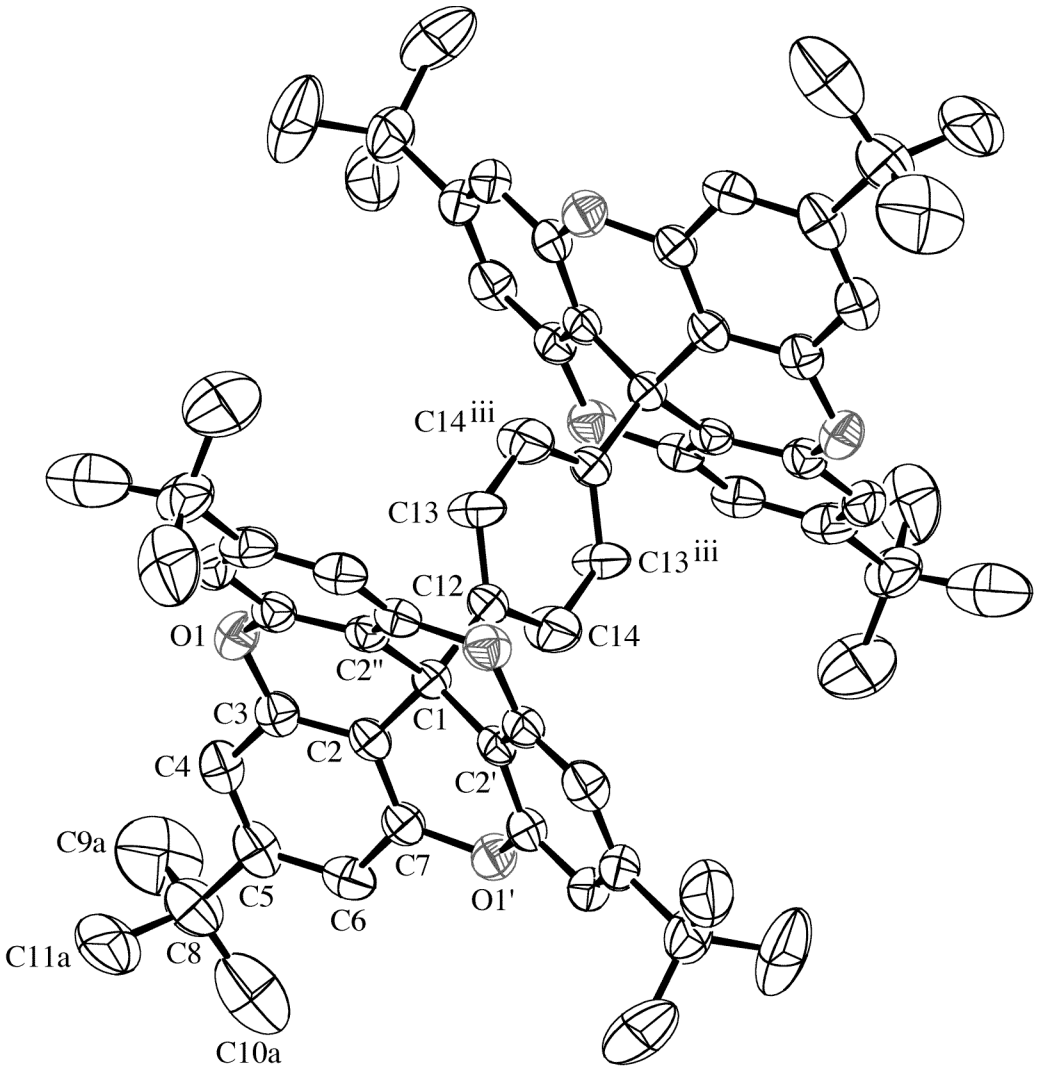
C14iii
C13
C13iii
C12
C14
O1
C2"
C1
C3
C2
C4
C2'
C9a
C7
C5
O1'
C6
C11a
C8
C10a

Table 4.18 Crystallographic Data for **4.3**

Crystallised from	CH_2Cl_2
Empirical formula	$C_{66}H_{66}O_6$
Formula weight [g mol^{-1}]	955.24
Crystal colour, habit	colourless, prism
Crystal dimensions [mm]	0.17 × 0.22 × 0.25
Temperature [K]	160(1)
Crystal system	cubic
Space group	$Pa\bar{3}$ (#205)
Z	4
Reflections for cell determination	1907
2θ range for cell determination [°]	4 – 50
Unit cell parameters a [Å]	18.047(1)
b [Å]	18.047(1)
c [Å]	18.047(1)
α [°]	90
β [°]	90
γ [°]	90
V [Å^3]	5877.7(6)
F(000)	2040
D_x [g cm^{-3}]	1.079
μ(Mo $K\alpha$) [mm^{-1}]	0.0676
Scan type	ω
$2\theta_{(max)}$ [°]	50
Total reflections measured	31032
Symmetry independent reflections	1742
R_{int}	0.121
Reflections with $I > 2\sigma(I)$	1075
Reflections used in refinement	1742
Parameters refined; restraints	144; 48
Final $R(F)$ [$I > 2\sigma(I)$ reflections]	0.0654
$wR(F^2)$ (all data)	0.1868
Weights: $w = [\sigma^2(F_o^2) + (0.1081P)^2 + 0.1454P]^{-1}$ where $P = (F_o^2 + 2F_c^2)/3$	
Goodness of fit	1.018
Final Δ_{max}/σ	0.001
$\Delta\rho$ (max; min) [e Å^{-3}]	0.33; -0.22
$\sigma(d_{(C-C)})$ [Å]	0.003 – 0.006

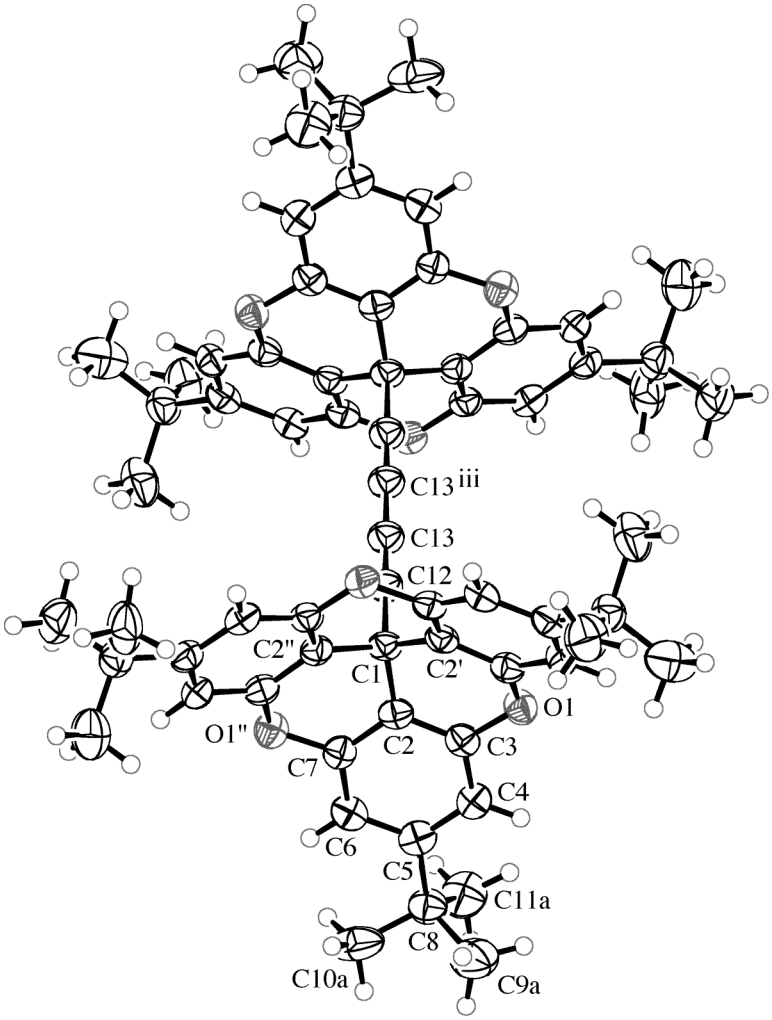
C13iii
C13
C12
C2"
C1
C2'
O1
O1"
C7
C2
C3
C4
C6
C5
C11a
C8
C10a
C9a

Table 4.19 Crystallographic Data for **4.10**

Crystallised from	hexane
Empirical formula	$C_{37}H_{38}O_3$
Formula weight [g mol^{-1}]	530.70
Crystal colour, habit	colourless, prism
Crystal dimensions [mm]	0.30 × 0.32 × 0.38
Temperature [K]	160(1)
Crystal system	orthorhombic
Space group	*Pbca* (#61)
Z	8
Reflections for cell determination	7178
2θ range for cell determination [°]	4 – 55
Unit cell parameters a [Å]	17.8568(3)
b [Å]	17.9448(3)
c [Å]	17.9868(3)
α [°]	90
β [°]	90
γ [°]	90
V [Å^3]	5763.6(2)
F(000)	2272
D_x [g cm^{-3}]	1.223
μ(Mo $K\alpha$) [mm^{-1}]	0.0758
Scan type	ϕ and ω
$2\theta_{(max)}$ [°]	55
Total reflections measured	78427
Symmetry independent reflections	6580
R_{int}	0.095
Reflections with $I > 2\sigma(I)$	4758
Reflections used in refinement	6580
Parameters refined	371
Final $R(F)$ [$I > 2\sigma(I)$ reflections]	0.0544
$wR(F^2)$ (all data)	0.1461
Weights: $w = [\sigma^2(F_o^2) + (0.0694P)^2 + 1.9396P]^{-1}$ where $P = (F_o^2 + 2F_c^2)/3$	
Goodness of fit	1.043
Secondary extinction coefficient	0.0105(7)
Final Δ_{max}/σ	0.001
$\Delta\rho$ (max; min) [e Å^{-3}]	0.49; -0.35
$\sigma(d_{(C-C)})$ [Å]	0.002 – 0.003

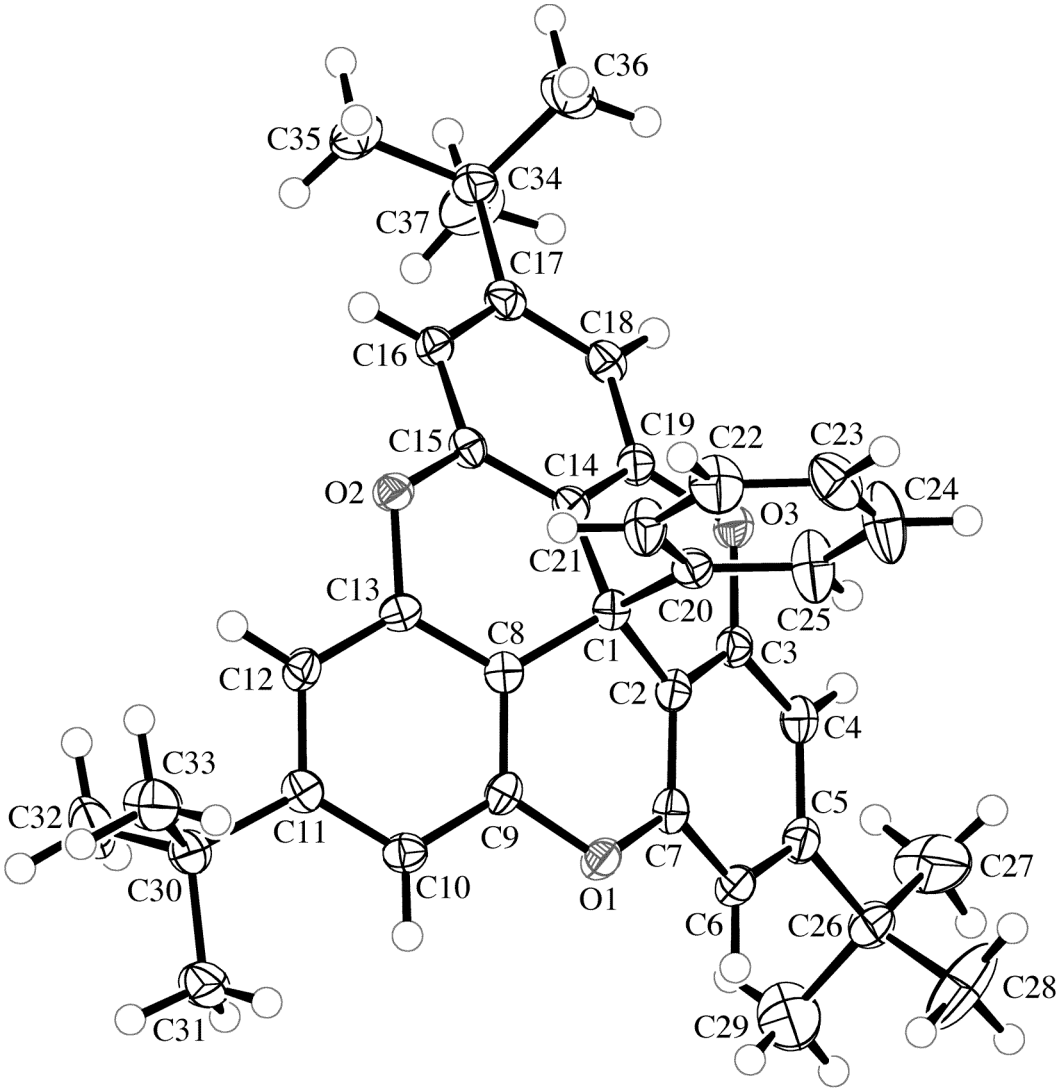
C36
C35
C34
C37
C17
C18
C16
C19
C22
C23
C15
C14
O2
O3
C24
C21
C13
C20
C25
C8
C1
C3
C12
C2
C4
C33
C32
C11
C9
C7
C5
C27
C30
C10
O1
C6
C26
C28
C31
C29

Table 4.20 Crystallographic Data for **4.11**

Crystallised from	hexane
Empirical formula	$C_{73}H_{91}O_6$
Formula weight [g mol^{-1}]	1064.5
Crystal colour, habit	colourless, prism
Crystal dimensions [mm]	0.15 × 0.25 × 0.35
Temperature [K]	160(1)
Crystal system	triclinic
Space group	$P\bar{1}$ (#2)
Z	2
Reflections for cell determination	10711
2θ range for cell determination [°]	4 – 50
Unit cell parameters a [Å]	12.3113(5)
b [Å]	16.5656(8)
c [Å]	16.9350(8)
α [°]	108.290(3)
β [°]	106.408(3)
γ [°]	90.520(3)
V [Å^3]	3127.6(3)
F(000)	1154
D_x [g cm^{-3}]	1.130
μ(Mo $K\alpha$) [mm^{-1}]	0.0697
Scan type	ω
$2\theta_{(max)}$ [°]	50
Total reflections measured	39474
Symmetry independent reflections	11010
R_{int}	0.067
Reflections with $I > 2\sigma(I)$	8160
Reflections used in refinement	11010
Parameters refined; restraints	795; 109
Final $R(F)$ [$I > 2\sigma(I)$ reflections]	0.0664
$wR(F^2)$ (all data)	0.1809
Weights: $w = [\sigma^2(F_o^2) + (0.0778P)^2 + 2.0142P]^{-1}$ where $P = (F_o^2 + 2F_c^2)/3$	
Goodness of fit	1.068
Secondary extinction coefficient	0.048(3)
Final Δ_{max}/σ	0.001
$\Delta\rho$ (max; min) [e Å^{-3}]	0.86; -0.36
$\sigma(d_{(C-C)})$ [Å]	0.003 – 0.004

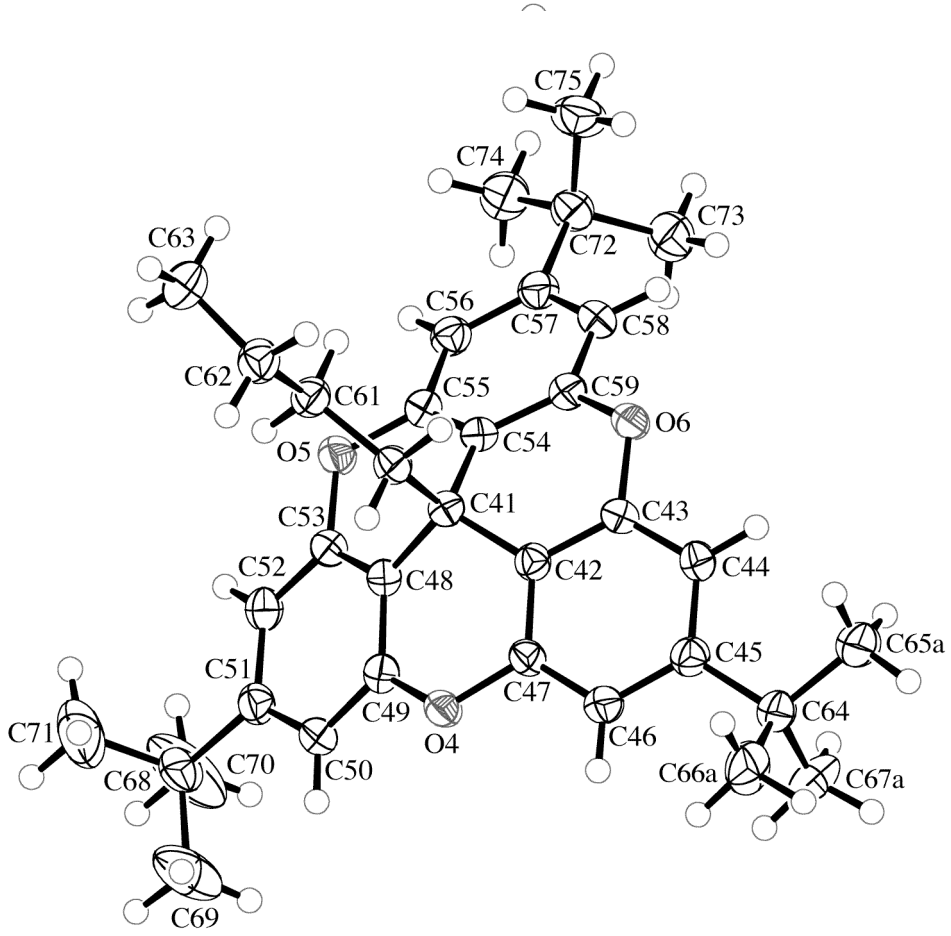
C75
C74
C73
C72
C63
C56
C57
C58
C62
C61
C55
C59
O6
O5
C54
C53
C41
C43
C52
C48
C42
C44
C51
C45
C65a
C49
C47
C64
C71
O4
C46
C68
C70
C50
C66a
C67a
C69

Table 4.21 Crystallographic Data for **4.12**

Crystallised from	hexane
Empirical formula	$C_{34}H_{38}O_4$
Formula weight [g mol^{-1}]	510.67
Crystal colour, habit	pale-yellow, prism
Crystal dimensions [mm]	0.20 × 0.25 × 0.28
Temperature [K]	160(1)
Crystal system	monoclinic
Space group	$P2_1$ (#4)
Z	4
Reflections for cell determination	6744
2θ range for cell determination [°]	4 – 55
Unit cell parameters a [Å]	10.8643(1)
b [Å]	12.4412(2)
c [Å]	20.9445(2)
α [°]	90
β [°]	91.1860(8)
γ [°]	90
V [Å^3]	2830.35(6)
$F(000)$	1096
D_x [g cm^{-3}]	1.198
μ(Mo $K\alpha$) [mm^{-1}]	0.0769
Scan type	ϕ and ω
$2\theta_{(max)}$ [°]	55
Total reflections measured	60992
Symmetry independent reflections	6778
R_{int}	0.076
Reflections with $I > 2\sigma(I)$	5663
Reflections used in refinement	6778
Parameters refined; restraints	706; 1
Final $R(F)$ [$I > 2\sigma(I)$ reflections]	0.0523
$wR(F^2)$ (all data)	0.1354
Weights: $w = [\sigma^2(F_o^2) + (0.0744P)^2 + 0.6803P]^{-1}$ where $P = (F_o^2 + 2F_c^2)/3$	
Goodness of fit	1.036
Secondary extinction coefficient	0.024(2)
Final Δ_{max}/σ	0.001
$\Delta\rho$ (max; min) [e Å^{-3}]	0.35; -0.36
$\sigma(d_{(C-C)})$ [Å]	0.004 – 0.006

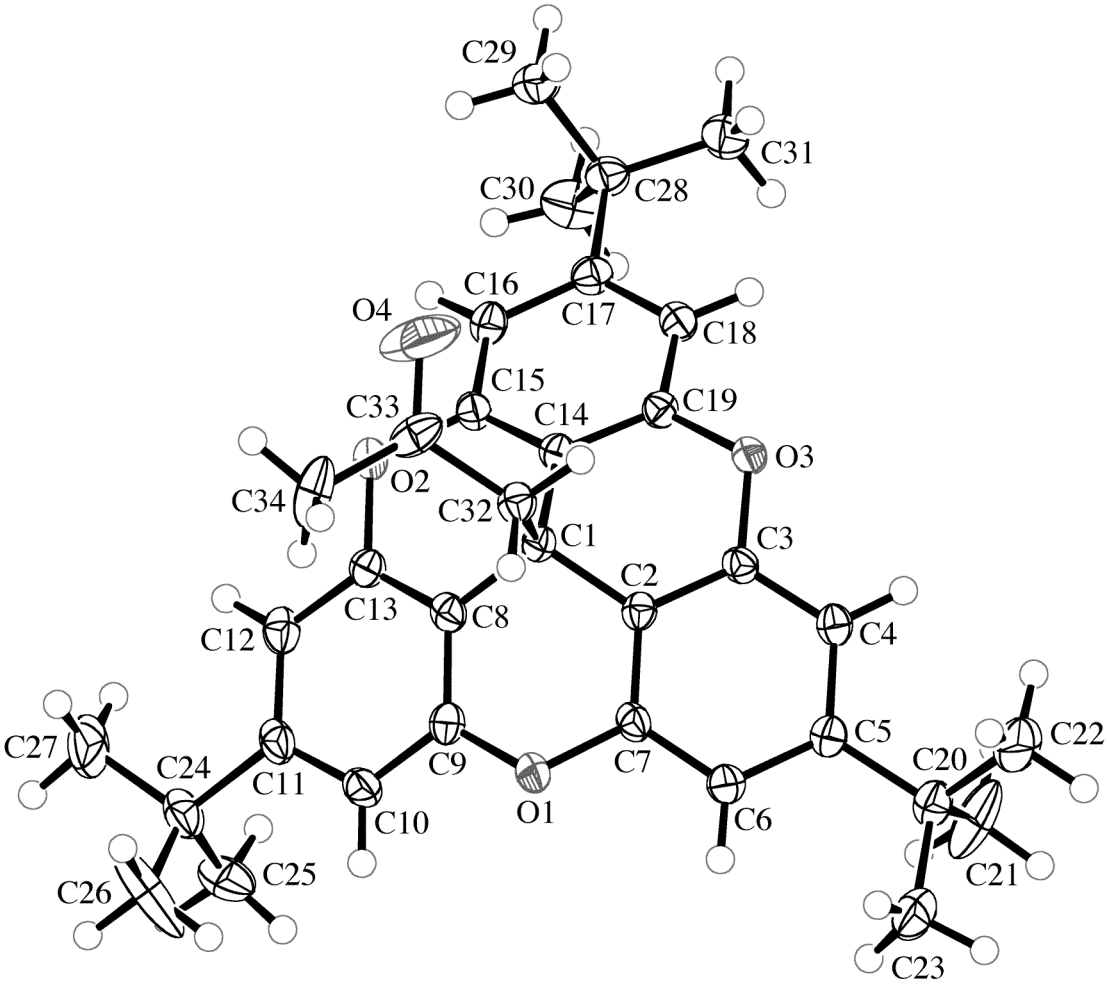
C29
C31
C30
C28
C16
O4
C17
C18
C15
C33
C14
C19
O2
O3
C34
C32
C1
C3
C2
C13
C8
C12
C4
C27
C24
C11
C9
C7
C5
C22
C20
C10
O1
C6
C25
C21
C26
C23

Table 4.22 Crystallographic Data for **4.13**

Crystallised from	hexane / CH_2Cl_2
Empirical formula	$C_{35}H_{42}O_3$
Formula weight [g mol^{-1}]	510.71
Crystal colour, habit	yellow, prism
Crystal dimensions [mm]	0.28 × 0.28 × 0.30
Temperature [K]	160(1)
Crystal system	orthorhombic
Space group	*Pnma* (#62)
Z	4
Reflections for cell determination	2819
2θ range for cell determination [°]	4 – 50
Unit cell parameters a [Å]	12.0236(7)
b [Å]	19.615(1)
c [Å]	12.2362(8)
α [°]	90
β [°]	90
γ [°]	90
V [Å^3]	2885.8(3)
F(000)	1104
D_x [g cm^{-3}]	1.175
μ(Mo $K\alpha$) [mm^{-1}]	0.0728
Scan type	ϕ and ω
$2\theta_{(max)}$ [°]	50
Total reflections measured	27486
Symmetry independent reflections	2619
R_{int}	0.125
Reflections with $I > 2\sigma(I)$	1389
Reflections used in refinement	2619
Parameters refined; restraints	243; 133
Final $R(F)$ [$I > 2\sigma(I)$ reflections]	0.0807
$wR(F^2)$ (all data)	0.2445
Weights: $w = [\sigma^2(F_o^2) + (0.1126P)^2 + 1.1672P]^{-1}$ where $P = (F_o^2 + 2F_c^2)/3$	
Goodness of fit	1.066
Final Δ_{max}/σ	0.001
$\Delta\rho$ (max; min) [e Å^{-3}]	0.31; -0.35
$\sigma(d_{(C-C)})$ [Å] 0.004 – 0.007	

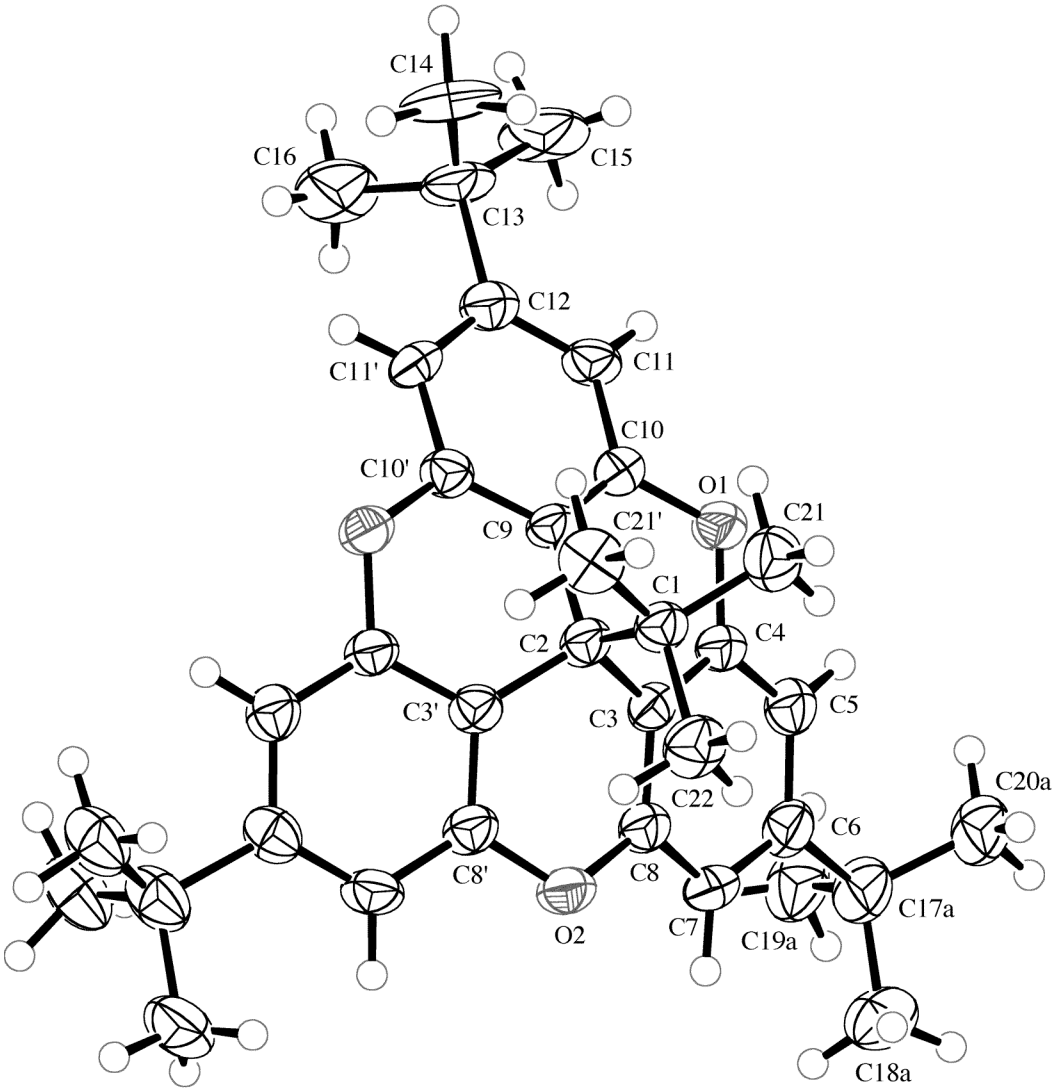
C14
C16
C15
C13
C12
C11'
C11
C10
C10'
O1
C21
C9
C21'
C1
C2
C4
C3'
C3
C5
C22
C20a
C6
C8'
C8
O2
C7
C19a
C17a
C18a

Summary of unit cell parameters and standard uncertainties from refinement with EADP restraint – 4.2 (100 – 298 K)

```
TITL SG0702_100

 CELL  0.71073 17.7918 17.7918 17.7918 90.0000 90.0000 90.0000
 ZERR  4 0.0009 0.0009 0.0009 0.0000 0.0000 0.0000
 LATT 1
 SYMM .50+X, .50-Y,    -Z
 SYMM    -X, .50+Y, .50-Z
 SYMM .50-X,    -Y, .50+Z
 SYMM    +Z,    +X,    +Y
 SYMM .50+Z, .50-X,    -Y
 SYMM    -Z, .50+X, .50-Y
 SYMM .50-Z,    -X, .50+Y
 SYMM    +Y,    +Z,    +X
 SYMM .50+Y, .50-Z,    -X
 SYMM    -Y, .50+Z, .50-X
 SYMM .50-Y,    -Z, .50+X
 SFAC C H O
 UNIT   272   312    40

 V =     5631.96     F(000) =    2264.0     Mu =   0.08 mm-1      Cell Wt =     4221.22    Rho =  1.245

SG0702_100

 ATOM           x         y         z          sof         U11       U22       U33       U23       U13       U12       Ueq

C12          0.04572  -0.04572   0.45428     0.33333     0.05116   0.05116   0.05116  -0.00152   0.00152   0.00152   0.05116
    0.00547   0.00031   0.00031   0.00031     0.00000     0.00257   0.00257   0.00257   0.00278   0.00278   0.00278   0.00257

 C13         -0.02826  -0.03774   0.44244     0.33333     0.04855   0.09539   0.08206  -0.03388  -0.01094   0.00048   0.07533
   0.04165   0.00125   0.00333   0.00266     0.00000     0.01156   0.01036   0.01963   0.01221   0.01145   0.01708   0.00537

 C14          0.07463  -0.01068   0.51297     0.33333     0.04855   0.09539   0.08206  -0.03388  -0.01094   0.00048   0.07533
   0.04262   0.00134   0.00327   0.00255     0.00000     0.01156   0.01036   0.01963   0.01221   0.01145   0.01708   0.00537
```

```
TITL SG0702 130

 CELL  0.71073 17.8110 17.8110 17.8110 90.0000 90.0000 90.0000
 ZERR  4 0.0009 0.0009 0.0009 0.0000 0.0000 0.0000
 LATT 1
 SYMM .50+X, .50-Y,    -Z
 SYMM    -X, .50+Y, .50-Z
 SYMM .50-X,    -Y, .50+Z
 SYMM    +Z,    +X,    +Y
 SYMM .50+Z, .50-X,    -Y
 SYMM    -Z, .50+X, .50-Y
 SYMM .50-Z,    -X, .50+Y
 SYMM    +Y,    +Z,    +X
 SYMM .50+Y, .50-Z,    -X
 SYMM    -Y, .50+Z, .50-X
 SYMM .50-Y,    -Z, .50+X
 SFAC C H O
 UNIT   272   312    40

 V =     5650.21     F(000) =    2264.0     Mu =   0.08 mm-1      Cell Wt =     4221.22    Rho =  1.241

C12         0.04573  -0.04573   0.45427     0.33333     0.04764   0.04764   0.04764  -0.00159   0.00159   0.00159    0.04764
  0.00414   0.00023   0.00023   0.00023     0.00000     0.00179   0.00179   0.00179   0.00185   0.00185   0.00185    0.00179

 C13        -0.02767  -0.03550   0.44019     0.33333     0.05808   0.09959   0.06957  -0.03179  -0.01659   0.01189    0.07575
   0.03214   0.00101   0.00196   0.00152     0.00000     0.00893   0.00883   0.01090   0.00716   0.00650   0.01105    0.00370

 C14         0.07365  -0.01189   0.51511     0.33333     0.05808   0.09959   0.06957  -0.03179  -0.01659   0.01189    0.07575
   0.03281   0.00106   0.00195   0.00146     0.00000     0.00893   0.00883   0.01090   0.00716   0.00650   0.01105    0.00370
```

TITL JRN II 215 (SG0702A) 160

```
 CELL  0.71073 17.8302 17.8302 17.8302 90.0000 90.0000 90.0000
 ZERR  4 0.0009 0.0009 0.0009 0.0000 0.0000 0.0000
 LATT 1
 SYMM .50+X, .50-Y,    -Z
 SYMM    -X, .50+Y, .50-Z
 SYMM .50-X,    -Y, .50+Z
 SYMM    +Z,    +X,    +Y
 SYMM .50+Z, .50-X,    -Y
 SYMM    -Z, .50+X, .50-Y
 SYMM .50-Z,    -X, .50+Y
 SYMM    +Y,    +Z,    +X
 SYMM .50+Y, .50-Z,    -X
 SYMM    -Y, .50+Z, .50-X
 SYMM .50-Y,    -Z, .50+X
 SFAC C H O
 UNIT   272   312    40

 V =     5668.51     F(000) =    2264.0     Mu =   0.08 mm-1      Cell Wt =     4221.22    Rho =  1.237

C12         0.04570  -0.04570   0.45430     0.33333     0.03381   0.03381   0.03381  -0.00220   0.00220   0.00220    0.03381
  0.00441   0.00025   0.00025   0.00025     0.00000     0.00185   0.00185   0.00185   0.00193   0.00193   0.00193    0.00185

 C13        -0.02813  -0.03620   0.44242     0.33333     0.03463   0.10232   0.06427  -0.05175  -0.01309   0.00890    0.06707
   0.03622   0.00107   0.00279   0.00209     0.00000     0.00830   0.01010   0.01335   0.00942   0.00768   0.01197    0.00463

 C14         0.07342  -0.00960   0.51424     0.33333     0.03463   0.10232   0.06427  -0.05175  -0.01309   0.00890    0.06707
   0.03611   0.00108   0.00275   0.00204     0.00000     0.00830   0.01010   0.01335   0.00942   0.00768   0.01197    0.00463
```

```
TITL SG0702 190

 CELL  0.71073 17.8722 17.8722 17.8722 90.0000 90.0000 90.0000
 ZERR  4 0.0009 0.0009 0.0009 0.0000 0.0000 0.0000
 LATT 1
 SYMM .50+X, .50-Y,    -Z
 SYMM    -X, .50+Y, .50-Z
 SYMM .50-X,    -Y, .50+Z
 SYMM    +Z,    +X,    +Y
 SYMM .50+Z, .50-X,    -Y
 SYMM    -Z, .50+X, .50-Y
 SYMM .50-Z,    -X, .50+Y
 SYMM    +Y,    +Z,    +X
 SYMM .50+Y, .50-Z,    -X
 SYMM    -Y, .50+Z, .50-X
 SYMM .50-Y,    -Z, .50+X
 SFAC C H O
 UNIT   272   312    40

 V =     5708.66     F(000) =    2264.0     Mu =   0.08 mm-1      Cell Wt =     4221.22    Rho =  1.228

C12         0.04546  -0.04546   0.45454     0.33333     0.04595   0.04595   0.04595  -0.00227   0.00227   0.00227    0.04595
  0.00390   0.00022   0.00022   0.00022     0.00000     0.00168   0.00168   0.00168   0.00175   0.00175   0.00175    0.00168

 C13        -0.02691  -0.03491   0.44093     0.33333     0.05131   0.12144   0.07506  -0.04636  -0.01897   0.01654    0.08260
   0.04034   0.00114   0.00293   0.00203     0.00000     0.00893   0.01036   0.01187   0.00848   0.00691   0.01268    0.00441

 C14         0.07277  -0.01251   0.51456     0.33333     0.05131   0.12144   0.07506  -0.04636  -0.01897   0.01654    0.08260
   0.03963   0.00115   0.00290   0.00200     0.00000     0.00893   0.01036   0.01187   0.00848   0.00691   0.01268    0.00441
```

```
TITL SG0702 210

 CELL  0.71073 17.8959 17.8959 17.8959 90.0000 90.0000 90.0000
 ZERR  4 0.0009 0.0009 0.0009 0.0000 0.0000 0.0000
 LATT 1
 SYMM .50+X, .50-Y,    -Z
 SYMM    -X, .50+Y, .50-Z
 SYMM .50-X,    -Y, .50+Z
 SYMM    +Z,    +X,    +Y
 SYMM .50+Z, .50-X,    -Y
 SYMM    -Z, .50+X, .50-Y
 SYMM .50-Z,    -X, .50+Y
 SYMM    +Y,    +Z,    +X
 SYMM .50+Y, .50-Z,    -X
 SYMM    -Y, .50+Z, .50-X
 SYMM .50-Y,    -Z, .50+X
 SFAC C H O
 UNIT   272   312    40

 V =     5731.40     F(000) =    2264.0     Mu =   0.08 mm-1      Cell Wt =     4221.22    Rho =  1.223

C12         0.04555  -0.04555   0.45445     0.33333     0.04714   0.04714   0.04714  -0.00093   0.00093   0.00093    0.04714
  0.00415   0.00023   0.00023   0.00023     0.00000     0.00188   0.00188   0.00188   0.00201   0.00201   0.00201    0.00188

 C13        -0.02573  -0.03203   0.43907     0.33333     0.05510   0.12208   0.06972  -0.05133  -0.02538   0.02573    0.08230
   0.05585   0.00167   0.00390   0.00260     0.00000     0.01218   0.01121   0.01340   0.00986   0.00700   0.01519    0.00502

 C14         0.07185  -0.01456   0.51663     0.33333     0.05510   0.12208   0.06972  -0.05133  -0.02538   0.02573    0.08230
   0.05394   0.00162   0.00381   0.00256     0.00000     0.01218   0.01121   0.01340   0.00986   0.00700   0.01519    0.00502
```

```
TITL SG0702 240

 CELL  0.71073 17.9295 17.9295 17.9295 90.0000 90.0000 90.0000
 ZERR  4 0.0009 0.0009 0.0009 0.0000 0.0000 0.0000
 LATT 1
 SYMM .50+X, .50-Y,    -Z
 SYMM    -X, .50+Y, .50-Z
 SYMM .50-X,    -Y, .50+Z
 SYMM    +Z,    +X,    +Y
 SYMM .50+Z, .50-X,    -Y
 SYMM    -Z, .50+X, .50-Y
 SYMM .50-Z,    -X, .50+Y
 SYMM    +Y,    +Z,    +X
 SYMM .50+Y, .50-Z,    -X
 SYMM    -Y, .50+Z, .50-X
 SYMM .50-Y,    -Z, .50+X
 SFAC C H O
 UNIT   272   312    40

 V =     5763.74     F(000) =    2264.0     Mu =   0.08 mm-1      Cell Wt =     4221.22    Rho =  1.216

C12         0.04543  -0.04543   0.45457     0.33333     0.04696   0.04696   0.04696  -0.00272   0.00272   0.00272    0.04696
  0.00392   0.00022   0.00022   0.00022     0.00000     0.00179   0.00179   0.00179   0.00191   0.00191   0.00191    0.00179

 C13        -0.02727  -0.03471   0.44104     0.33333     0.05059   0.12926   0.08058  -0.05637  -0.02133   0.02030    0.08681
   0.05202   0.00145   0.00422   0.00292     0.00000     0.01038   0.01164   0.01433   0.01045   0.00841   0.01536    0.00521

 C14         0.07212  -0.01209   0.51398     0.33333     0.05059   0.12926   0.08058  -0.05637  -0.02133   0.02030    0.08681
   0.05001   0.00140   0.00421   0.00296     0.00000     0.01038   0.01164   0.01433   0.01045   0.00841   0.01536    0.00521
```

```
TITL SG0702 270

 CELL  0.71073 17.9618 17.9618 17.9618 90.0000 90.0000 90.0000
 ZERR  4 0.0009 0.0009 0.0009 0.0000 0.0000 0.0000
 LATT 1
 SYMM .50+X, .50-Y,    -Z
 SYMM    -X, .50+Y, .50-Z
 SYMM .50-X,    -Y, .50+Z
 SYMM    +Z,    +X,    +Y
 SYMM .50+Z, .50-X,    -Y
 SYMM    -Z, .50+X, .50-Y
 SYMM .50-Z,    -X, .50+Y
 SYMM    +Y,    +Z,    +X
 SYMM .50+Y, .50-Z,    -X
 SYMM    -Y, .50+Z, .50-X
 SYMM .50-Y,    -Z, .50+X
 SFAC C H O
 UNIT   272   312    40

 V =     5794.95     F(000) =    2264.0     Mu =   0.08 mm-1      Cell Wt =     4221.22    Rho =  1.210

C12         0.04554  -0.04554   0.45446     0.33333     0.05116   0.05116   0.05116  -0.00085   0.00085   0.00085    0.05116
  0.00350   0.00019   0.00019   0.00019     0.00000     0.00152   0.00152   0.00152   0.00158   0.00158   0.00158    0.00152

 C13        -0.02695  -0.03399   0.43993     0.33333     0.04755   0.13718   0.09099  -0.06750  -0.02314   0.02353    0.09191
   0.03822   0.00113   0.00297   0.00216     0.00000     0.00721   0.00970   0.01179   0.00938   0.00555   0.00960    0.00488

 C14         0.07210  -0.01296   0.51510     0.33333     0.04755   0.13718   0.09099  -0.06750  -0.02314   0.02353    0.09191
   0.03687   0.00110   0.00297   0.00217     0.00000     0.00721   0.00970   0.01179   0.00938   0.00555   0.00960    0.00488
```

```
TITL SG0702 298

 CELL  0.71073 17.9939 17.9939 17.9939 90.0000 90.0000 90.0000
 ZERR  4 0.0009 0.0009 0.0009 0.0000 0.0000 0.0000
 LATT 1
 SYMM .50+X, .50-Y,    -Z
 SYMM    -X, .50+Y, .50-Z
 SYMM .50-X,    -Y, .50+Z
 SYMM    +Z,    +X,    +Y
 SYMM .50+Z, .50-X,    -Y
 SYMM    -Z, .50+X, .50-Y
 SYMM .50-Z,    -X, .50+Y
 SYMM    +Y,    +Z,    +X
 SYMM .50+Y, .50-Z,    -X
 SYMM    -Y, .50+Z, .50-X
 SYMM .50-Y,    -Z, .50+X
 SFAC C H O
 UNIT   272   312    40

 V =     5826.07     F(000) =    2264.0     Mu =   0.08 mm-1      Cell Wt =     4221.22    Rho =  1.203

C12         0.04518  -0.04518   0.45482     0.33333     0.05133   0.05133   0.05133  -0.00140   0.00140   0.00140    0.05133
  0.00361   0.00020   0.00020   0.00020     0.00000     0.00159   0.00159   0.00159   0.00168   0.00168   0.00168    0.00159

 C13        -0.02427  -0.02682   0.43702     0.33333     0.05759   0.13627   0.07856  -0.05172  -0.03000   0.03753    0.09081
   0.05441   0.00160   0.00335   0.00210     0.00000     0.01000   0.01000   0.01138   0.01000   0.00483   0.01095    0.00475

 C14         0.06946  -0.01881   0.51892     0.33333     0.05759   0.13627   0.07856  -0.05172  -0.03000   0.03753    0.09081
   0.05267   0.00156   0.00331   0.00209     0.00000     0.01000   0.01000   0.01138   0.01000   0.00483   0.01095    0.00475
```

4.7 References:

[1] Dunitz, J.D. *Pure Appl. Chem.* **1991**, *63*, 177-185.

[2] Schmidt, G.M.J. *Pure Appl. Chem.* **1971**, *27*, 647-678.

[3] Kitaigorodskii, A.I. *Organic Chemcal Crystallography*. Consultants Bureau: New York, 1961.

[4] Etter, M.C. *Acc. Chem. Res.* **1990**, *23*, 120-126.

[5] Lincoln Logs™ are a trademark of Hasbro, Inc, Rhode Island, U.S.A. A children's wood construction set.

[6] (a) Robertson, J.M.; Woodward, I. *Proc. R. Soc. A,* **1938**, *164*, 436-446. (b) Liberles, A.; Matlosz, B. *J. Org. Chem.* **1971**, *36*, 2710-2713.

[7] Bedard, T.C.; Moore, J.S. *J. Am. Chem. Soc.* **1995**, *117*, 10662-10671.

[8] (a) Toyota, S.; Yamamori, T.; Asakura, M.; Oki, M. *Bull. Chem. Soc. Jpn.* **2000**, *73*, 205-213. (b) Toyota, S.; Yamamori, T.; Makino, T.; Oki, M. *Bull. Chem. Soc. Jpn.* **2000**, *73*, 2591-2597. (c) Toyota, S.; Yamamori, T.; Makino, T. *Tetrahedron*, **2001**, *57*, 3521-3528. (d) Toyota, S.; Iida, T.; Kunizane, C.; Tanifuji, N.; Yoshida, Y. *Org. Biomol. Chem.* **2003**, *1*, 2298-2302. (e) Toyota, S.; Yanagihara, T.; Yoshida, Y.; Goichi, M. *Bull. Chem. Soc. Jpn.* **2005**, *78*, 1351-1353.

[9] Stupp, S.I. *Chem. Rev.* **2005**, *105*, 1023-1024.

[10] Lofthagen, M.; VernonClark, R.; Baldridge, K.K.; Siegel, J.S. *J. Org. Chem.* **1992**, *57*, 61-69.

[11] (a) Krebs, F.C.; Larsen, P.S.; Larsen, J.; Jacobsen, C.S.; Boutton, C.; Thorup, N. *J. Am. Chem. Soc.* **1997**, *119*, 1208-1216. (b) Laursen, B.W.; Krebs, F.C.; Nielsen, M.F.; Bechgaard, K.; Christensen, J.B.; Harrit, N. *J. Am. Chem. Soc.* **1998**, *120*, 12255-12263. (c) Madsen, G.K.H.; Krebs, F.C.; Lebech, B.; Larsen, F.K. *Chem. Eur.*

J. **2000**, *6*, 1797-1804. (d) Laursen, B.W.; Krebs, F.C. *Chem. Eur. J*. **2001**, *7*, 1773-1783.

[12] (a) Faldt, A.; Krebs, F.C.; Thorup, N. *J. Chem. Soc., Perkin Trans. 2*, **1997**, 2219-2227. (b) Peters, N. J. Synthesis and Properties of Ortho-Bridged Triarylmethyl Compounds. Ph.D. Dissertation, University of Illinois, Urbana-Champaign, IL, 1980.

[13] Kottas, G.S.; Clarke, L.I.; Horinek, D.; Michl, J. *Chem. Rev*. **2005**, *105*, 1281-1376.

[14] Buchwald, S.L.; Lucas, E.A.; Dewan, J.C. *J. Am. Chem. Soc*. **1987**, *109*, 4396-4397.

[15] Eglinton, G.; Galbraith, A.R. *J. Chem. Soc*. **1959**, 889-896.

[16] (a) Sonogashira, K.; Tohda, Y.; Hagihara, N. *Tetrahedron Lett*. **1975**, *16*, 4467-4470. (b) Venkataramana, G.; Sankararaman, S. *Org. Lett*. **2006**, *8*, 2739-2742.

[17] Negishi, E.-I. *Acc. Chem. Res*. **1982**, *15,* 340-348.

[18] Unrau, C.M.; Campbell, M.G.; Snieckus, V. *Tetrahedron Lett*. **1992**, *33*, 2773-2776.

[19] Ishiyama, T.; Murata, M.; Miyaura, N. *J. Org. Chem*. **1995**, *60*, 7508-7510.

[20] Trueblood, K.N.; Dunitz, J.D. *Acta Cryst*. **1983**, *B39*, 120-133.

[21] Debye, P. *Verh. Dtsch. Phys. Ges*. **1913**, *15*, 738-752.

[22] Cruickshank, D. W. J. *Acta Crystallogr*. **1956**, *9*, 754-756.

[23] Cruickshank, D. W. J. *Acta Crystallogr*. **1956**, *9*, 1005-1011.

[24] (a) Dunitz, J. D.; Schomaker, V.; Trueblood, K. N. *J. Phys. Chem*. **1988**, *92*, 856-867. (b) Schomaker, V.; Trueblood, K. N. *Acta Crystallogr*. **1998**, *B54*, 507-514.

[25] Dunitz, J. D.; Maverick, E. F.; Trueblood, K. N. *Angew. Chem., Int. Ed. Engl*. **1988**, *27*, 880-895.

[26] Maverick, E. F.; Knobler, C. B.; Khan, S. I.; Canary, J. W.; Dicker, I. B.;

Trueblood, K. N. *Helv. Chim. Acta* **2003**, *86*, 1309-1319.

[27] Bürgi, H.-B.; Capelli, S. C. *Helv. Chim. Acta* **2003**, *86*, 1625-1640.

[28] Maverick, E. F.: Dunitz, J. D. *Mol. Phys.* **1987**, *62*, 451-459.

[29] Mighell, A.D.; Rodgers, J.R. *Acta Cryst.* **1980**, *A36*, 321-326.

[30] David, W.I.F.; Shankland, K. *Acta Cryst.* **2008**, *A64*, 52-64.

[31] (a) Altomare, A.; Caliandro, R. Giacovazzo, C. Moliterni, A.G.G., Rizzi, R. *J. Appl. Crystallogr.*, **2003**, *36*, 230-238. (b) Harris, K.D.M.; Tremayne, M.; Kariuki, B.M. *Angew Chem. Int. Ed.*, **2001**, *40*, 1626-1651. (c) Harris, K.D.M.; Cheung, E.Y. *Chem. Soc. Rev.*, **2004**, *33*, 526-538.

[32] (a) *The Rietveld Method*, ed. R. A. Young, Oxford University Press, Oxford, UK, 1995. (b) Rietveld, H.M. *J. Appl. Crystallogr.* **1969**, *2*, 65-71.

[33] The computer program *Mercury CSD 2.0* was used for this simulation: Macrae, C. F.; Bruno, I. J.; Chisholm, J. A.; Edgington, P. R.; McCabe, P.; Pidcock, E.; Rodriguez-Monge, L.; Taylor, R.; van de Streek, J.; Wood, P. A. *J. Appl. Cryst.*, **2008**, *41*, 466-470.

[34] (a) Schmitt, B.; Brönnimann, Ch.; Eikenberry, E.F.; Gozzo, F.; Hörmann, C.; Horisberger, R.; Patterson, B. *Nucl. Instrum. Meth. A*, **2003**, *501*, 267-272. (b) Gozzo, F.; Schmitt, B.; Bortolamedi, Th.; Giannini, C.; Guagliardi, A.; Lange, M.; Meister, D.; Maden, D.; Willmott, P.; Patterson, B.D. *J. Alloy Compd.*, **2004**, *362*, 206-217.

[35] The computer program *Indx* was used to generate the *hkl* peaks: LMGP-SuiteSuite of Programs for the interpretation of X-ray Experiments, by Jean Laugier and Bernard Bochu, ENSP/Laboratoire des matériaux et du génie physique, Grenoble, France. WWW: http://www.inpg.fr/LMGP and http://www.ccp14.ac.uk/tutorial/lmgp/.

[36] The computer program *CMPR* was used to analyze the diffraction data: Toby, B.H. *J. Appl. Cryst*. **2005**, *38*, 1040-1041.

[37] The computer program *TOPAS* was used to evaluate diffraction data: Bruker AXS GmbH, Östliche Rheinbrückenstrasse 50, D-76181 Karlsruhe, Germany. Also, see ref.: Coelho, A. A. *J. Appl. Cryst*. **2003**, *36*, 86-95.

[38] Lanzani, G. *Photophysics of Molecular Materials*. Wiley-VCH Verlag GmbH: Weinheim, 2006.

[39] Valeur, B. *Molecular Fluorescence: Principles and Applications*. Wiley-VCH Verlag GmbH: Weinheim, 2001, pp 20-30.

[40] Molecules that possess a triplet ground state, e.g., molecular oxygen, are the exception and not common.

[41] Jablonski, A. *Z. Physik* **1935**, *94*, 38.

[42] Kasha, M. *Faraday Discuss*. **1950**, *9*, 14-19.

[43] Atkins P. W.; Friedman R. S. *Molecular Quantum Mechanics*. Oxford University Press: Oxford, 1997.

[44] Stokes, G. G. *Mathematical and Physical Papers*; Cambridge University Press: Cambridge, 1880-1905; Vol. I-V.

[45] Selzer, Y.; Cai, L.; Cabassi, M.A.; Yao, Y.; Tour, J.M.; Mayer, T.S.; Allara, D.L. *Nano Lett*. **2005**, *5*, 61-65.

[46] Petruska, J. *J. Chem. Phys*. **1961**, *34*, 1120-1136.

[47] (a) Berenfel'd, V.M.; Krongauz, V.A. *Theor. Exp. Chem. USSR*, **1967**, *3*, 63. (b) Berlman, I.B. *Handbook of Fluorescence Spectra of Aromatic Molecules*. Academic Press: New York, 1971.

[48] Froehlich, P.M.; Morrison, H.A. *J. Phys. Chem*. **1972**, *76*, 3566-3570.

[49] Masuo, S.; Yoshikawa, H.; Asahi, T.; Masuhara, H.; Sato, T.; Jiang, D.-H.; Aida, T. *J. Phys. Chem. B*, **2003**, *107*, 2471-2479.

[50] (a) Du, H.; Fuh, R. A.; Li, J.; Corkan, A.; Lindsey, J. S. *Photochem. Photobiol.* **1998**, *68*, 141-142. (b) Ferrante, C.; Kensy, U.; Dick, B. *J. Phys. Chem.* **1993**, *97*, 13457-13463.

[51] (a) Du, H.; Fuh, R. A.; Li, J.; Corkan, A.; Lindsey, J. S. *Photochem. Photobiol.* **1998**, *68*, 141-142. (b) Berlman, I.B. *Handbook of Fluorescence Spectra of Aromatic Molecules.* Academic Press: New York, 1971. (c) Pavlopoulos, T. G.; Hammond, P. R. *J. Am. Chem. Soc.* **1974**, *96*, 6568-6579.

[52] Fyfe, C.A. *Solid state NMR for Chemists*. C.F.C. Press: Guelph, Ontario, Canada, 1983.

[53] (a) Pines, A.; Gibby, M.G.; Waugh, J.S. *J. Chem. Phys.* **1973**, *59*, 569-590. (b) Taylor, R.E. *Concepts Magn. Reson., Pt. A*, **2004**, *22*, 37-49.

[54] Alemany, L.B.; Grant, D.M.; Alger, T.D.; Pugmire, R.J. *J. Am. Chem. Soc.* **1983**, *105*, 6697-6704.

[55] Mantsch, H.H.; Saito, H.; Smith, I.C.P. *Progr. NMR Spect.* **1977**, *11*, 211-272.

[56] Greenfield, M.S.; Ronemus, A.D.; Vold, R.L.; Vold, R.R.; Ellis, P.D.; Raidy, T.E. *J. Magn. Reson.* **1987**, *72*, 89-107.

[57] Khuong, T.-A.V.; Nuñez, J.E.; Godinez, C.E.; Garcia-Garibay, M.A. *Acc. Chem. Res.* **2006**, *39*, 413-422.

[58] Khuong, T-A. V.; Dang, H.; Jarowski, P.D.; Maverik, E.F.; Garcia-Garibay, M.A. *J. Am. Chem. Soc.* **2007**, *129*, 839-845.

[59] Hooft, R. *KappaCCD Collect Software*, Nonius BV, Delft, The Netherlands, 1999.

[60] Otwinowski, Z.; Minor, W. In *Methods in Enzymology*, Vol. 276, *Macromolecular Crystallography*, Part A, Eds. C.W. Carter Jr., R.M. Sweet, Academic Press, New York, 1997, pp. 307-326.

[61] Altomare, A.; Cascarano, G.; Giacovazzo, C.; Guagliardi, A.; Burla, M.C.; Polidori, G.; Camalli, M. *SIR92*, *J. Appl. Crystallogr.* **1994**, *27*, 435.

[62] Maslen, E.N.; Fox, A.G.; O'Keefe, M.A., in 'International Tables for Crystallography', Ed. A.J.C. Wilson, Kluwer Academic Publishers, Dordrecht, 1992, Vol. C, Table 6.1.1.1, pp. 477-486.

[63] Stewart, R.F.; Davidson, E.R.; Simpson, W.T. *J. Chem. Phys.* **1965**, *42*, 3175-3187.

[64] Ibers, J.A.; Hamilton, W.C. *Acta Crystallogr.* **1964**, *17*, 781-782.

[65] Creagh, D.C.; McAuley, W.J. In 'International Tables for Crystallography', Ed. A.J.C. Wilson, Kluwer Academic Publishers, Dordrecht, 1992, Vol. C, Table 4.2.6.8, pp. 219-222.

[66] Creagh, D.C.; Hubbel, J.H. In 'International Tables for Crystallography', Ed. A.J.C. Wilson, Kluwer Academic Publishers, Dordrecht, 1992, Vol. C, Table 4.2.4.3, pp. 200-206.

[67] Sheldrick, G.M. *SHELXL97, Program for the Refinement of Crystal Structures*, University of Göttingen, Germany, 1997.

[68] Johnson, C.K. *ORTEPII*, Report ORNL-5138, Oak Ridge National Laboratory, Oak Ridge, Tennessee, 1976.